



*Signalling from Endosomes in Neurodevelopment and
Neurodegenerative Disorders*

Dissertation

for the award of the degree
“Doctor rerum naturalium”
(Dr. rer. nat.)
of the Georg-August-Universität Göttingen

within the doctoral program *IMPRS for Neuroscience*
of the Georg-August University School of Science (GAUSS)

submitted by
Ronja Markworth

born in
Henstedt-Ulzburg, Germany

Göttingen 2021

Thesis Committee

Reviewer: Dr. Katja Burk

Clinic for Neurology, University Medical Center Göttingen

Second Reviewer: Prof. Dr. Silvio O. Rizzoli

Department of Neuro- and Sensory Physiology, University Medical Center Göttingen

Prof. Dr. Reinhard Jahn

Department of Neurobiology, Max-Planck Institute for Biophysical Chemistry, Göttingen

Members of the Examination Board

First Reviewer: **Dr. Katja Burk**

Clinic for Neurology, University Medical Center Göttingen

Second Reviewer: **Prof. Dr. Silvio O. Rizzoli**

Department of Neuro- and Sensory Physiology, University Medical Center
Göttingen

Further members of the Examination Board:

Prof. Dr. Reinhard Jahn

Department of Neurobiology, Max-Planck Institute for Biophysical Chemistry, Göttingen

Prof. Dr. Peter Schu

Department of Cellular Biochemistry, University Medical Center Göttingen

Prof. Dr. Carolin Wichmann

Institute for Auditory Neuroscience & InnerEarLab, University Medical Center Göttingen)

Prof. Dr. Thomas Dresbach

Dept. of Anatomy and Embryology, University Medical Center Göttingen

Date of the oral examination: 20.09.2021

DECLARATION

I hereby declare that this thesis entitled "*Signalling from Endosomes in Neurodevelopment and Neurodegenerative Disorders*" was written by me with no other sources and aids than quoted.

Ronja Markworth
July 28th, 2021, Göttingen, Germany

“Wenn man erstmal drin ist, ist es schön.“

Waltraut Oetjen

TABLE OF CONTENTS

ABSTRACT	7
1 INTRODUCTION	8
1.1 NEURODEVELOPMENT.....	8
1.2 NEUROTROPHIC FACTORS.....	9
1.3 NEUROTROPHIC RECEPTORS.....	10
1.4 NEUROTROPHIC SIGNALLING FOR SURVIVAL.....	10
1.5 NEUROTROPHIC SIGNALLING FOR GROWTH.....	11
1.6 RECEPTOR TRAFFICKING.....	12
1.7 THE NATURE OF THE SIGNALLING ENDOSOME.....	12
1.8 RECEPTOR SIGNALLING DEPENDS ON ITS LOCATION.....	13
1.9 HELD UP IN TRAFFIC - DEFECTS IN THE TRAFFICKING MACHINERY IN CHARCOT-MARIE-TOOTH DISEASE.....	15
2 SENSORY AXON GROWTH REQUIRES SPATIOTEMPORAL INTEGRATION OF CASR AND TRKB SIGNALING	52
2.1 ABSTRACT.....	54
2.2 INTRODUCTION.....	54
2.3 MATERIALS AND METHODS.....	55
2.4 RESULTS.....	57
2.5 DISCUSSION.....	68
2.6 REFERENCES.....	71
3 TUBULAR MICRODOMAINS OF RAB7-ENDOSOMES RETRIEVE TRKA, A MECHANISM DISRUPTED IN CHARCOT-MARIE-TOOTH 2B	73
3.1 ABSTRACT.....	75
3.2 INTRODUCTION.....	76
3.3 RESULTS.....	77
3.4 DISCUSSION.....	91
3.5 MATERIAL AND METHODS.....	94
3.6 REFERENCES.....	102
3.7 SUPPLEMENTARY DATA.....	106
4 DISCUSSION	111
4.1 SIGNAL INTEGRATION.....	111
4.1.1 <i>Signalling Nodes</i>	111
4.2 THE ENDOSOMAL SYSTEM AS A SIGNAL DIVERSIFIER.....	112
4.2.1 <i>Receptor localization to distinct endosomal populations</i>	112
4.2.2 <i>Receptor signalling from distinct subcellular locations</i>	113
4.2.3 <i>Receptor re-routing</i>	114
4.2.4 <i>Endosomal regulation of local translation</i>	115
4.2.5 <i>Signalling insulation by location</i>	115
4.2.6 <i>Endosomal signalling of Trk receptors</i>	115
4.2.7 <i>Retrieval of Trk receptors</i>	116
4.3 DIVERSITY OF RAB-GTPASES.....	117
4.4 THE ENDOSOMAL SYSTEM IN A DISEASE CONTEXT.....	117
4.5 CONCLUSION.....	118

5	REFERENCES	119
	LIST OF ABBREVIATIONS	125
	ACKNOWLEDGEMENTS	127

ABSTRACT

The nervous system is developed under the regulation of growth and guidance cues. This process is highly dynamic and tightly regulated by the composition, concentration and timely presence of different signalling molecules. whose interactions result in a variety of responses that are complex and specific. For these few, general signalling molecules to elicit so many differential responses, their signals must be integrated and a level of intracellular control for signal integration and differentiation must be in place. The endosomal system with its different organelles characterized by distinct sets of proteins associated is the ideal platform to implement signal diversity. In this thesis I investigate how the endosomal system regulates receptor signalling in axonal growth and degeneration.

In the first chapter I give an introduction into the mechanisms of neurodevelopment and signalling of neurotrophic factors, as well as the endosomal system and its involvement in neurodegenerative disorders.

In chapter two I present my first project, in which we investigated the principle of signal integration during neurodevelopment. We show that two unrelated receptors, stimulated by two different ligands localize to the same endosomes and spatiotemporally integrate their signal on a shared signalling node to induce neuronal growth.

In chapter three I present my second project, in which we have shown that a neurotrophic receptor is retrieved from vacuolar late endosomes by tubular microdomains, thus enabling proper signalling in sensory neurons. We also show how this mechanism is disrupted in neurodegenerative disorder Charcot-Marie-Tooth 2B.

In chapter four I discuss how both of these studies highlight the importance of receptor signalling from endosomes and the receptor's location being tightly controlled. I present other studies that contribute to the image of the endosomal system as a regulator of intracellular signalling and point out caveats in the interpretation of such results.

1 INTRODUCTION

Neuronal cells are characterized by their long processes and axons that can stretch over a meter in length. This highly polar structure allows fast communication between neurons over a long distance. However, this long, polarized structure can provide challenges for intra-neuronal signalling. In my doctoral thesis, I am looking at the endosomal system as an intracellular signalling platform. In my first project I investigate intracellular signalling during development, which allows neurons to grow over such long distances and provides regulatory mechanisms for survival. In my second project, I discuss intracellular signalling in mature sensory neurons and how disruption in receptor retrieval leads to Charcot-Marie-Tooth disease 2B (CMT2B).

1.1 NEURODEVELOPMENT

The nervous system is composed of the central nervous system (CNS), the peripheral nervous system (PNS) and the enteric nervous system (ENS). Since most of my work was conducted in the PNS, I will give an introduction below.

The PNS hosts the somatic and the autonomic systems, with the somatic system including sensory neurons and axons of motoneurons. The PNS is derived from neural crest cells as well as placodes, ectodermal swellings of the cranial region. During the final stages of neurulation the neural crest is formed from the margins of the neural folds, derived of the ectoderm. Neural crest cells separate and are not part of the neural tube - instead they migrate away upon neural tube closure (Burk, 2009; Pla and Monsoro-Burq, 2018).

Placode development is a tightly regulated process conserved across vertebrates. Bone Morphogenetic Protein (BMP), Fibroblast growth factor (FGF) and WNT signalling initiate interactions between neuronal and non-neuronal ectoderm at the border of the neural fold during early gastrulation. This border region between neuronal and non-neuronal cells is then further divided into subpopulations of neural crest and pre-placodal progenitors. Neural crest cells will develop on to form sensory and secretory cells of the PNS as well as cartilage, bone, smooth muscle and mesenchymal cells. On the other hand, pre-placodal cells will give rise to the sensory organs of the head. Based on their place of origin, cranial placodes are grouped into anterior, posterior and intermediate placodes. In my first study, we are looking at neurons of the nodose ganglia, which are derived from the posterior placode. The posterior placodes host the otic, lateral line and epibranchial placodes and the epibranchial placodes develop into the sensory neurons of the geniculate, petrosal and nodose ganglia (Jidigam and Gunhaga, 2013). The nodose ganglia are comprised of visceral sensory afferents. The precursors of the third epibranchial placode are specified to differentiate into nodose neurons by E2.5 (Vogel and Davies, 1991). Upon arrival of sensory neuronal progenitor cells to their ganglia, they differentiate into post-mitotic neurons that grow axons to innervate their targets.

Studies on cranial sensory neurons of different ganglia of the chick have shown that these neurons have an innate growth rate that is correlative to the distance of their target tissue. This innate growth rate is also observed when grown as isolated cells *in vitro* (Davies, 1989). Nodose neurons that have the longest distance to cover to their target tissue grow the fastest, whereas vestibular neurons with the shortest distance grow the slowest. Interestingly, the neurons' dependence on neurotrophic factors for survival also mirrored the time of arrival of their axons to the target tissue area.

Not only placode-derived neurons but the entire nervous system relies on a mechanism called axon guidance to ensure correct target innervation. Axonal growth and pathfinding are guided by the growth cone, a structure at the distal end of the axon. The growth cone is made up of actin filaments, adhesion molecules and expresses axon guidance receptors on its surface. An interaction between all these proteins ensures the mechanisms of axon guidance, while the growth cone is extending. While axon guidance receptors provide either an attractive or a repulsive response to or away from intermediate guideposts, fine extensions within the growth cone called filopodia are able to initiate movement of the growth cone. This includes a so-called “growth-cone collapse” in response to repulsive guidance cues and subsequent re-extension and growth-cone turning (Lowery and Vactor, 2009). Adhesion molecules are released and re-attached to the surface to provide flexibility and stability. With microtubules extending forward during this process, the axon navigates through the environment and eventually innervates its respective target. While these mechanisms sound relatively straight forward, they come with challenges. Guidance proteins (both ligands and receptors) can act as both, attractive and repulsive mediators, depending on neuronal subtypes, ligands binding to several receptors or co-receptors involved (Dudanova and Klein, 2013). One of the studies of my doctoral thesis sheds light on these regulatory mechanisms (see Chapter 2).

1.2 NEUROTROPHIC FACTORS

Since the model-receptors of my work are tropomyosin receptor kinase (Trk) A and B, I am giving an introduction into neurotrophins and their receptors. The discovery of neurotrophic factors dates back to early experiments from Hamburger, where they observed that the removal of a limb bud in a chick embryo led to fewer sensory and motoneurons in the spinal cord, whereas an increase was observed upon transplantation of an extra limb bud (Hamburger, 1934; Hamburger, 1939). Levi-Montalcini confirmed these results and proposed a target-derived signal that ensures neuronal survival (Levi-Montalcini and Levi, 1942). After the observation that implanted tumor cells in the hind limb region increased innervating sensory ganglia in size without affecting motoneurons, Levi-Montalcini and Cohen isolated the factor now known as neurotrophic growth factor (NGF) (Cohen et al., 1954). Further, when antibodies against NGF were administered into newborn rodents, there was almost a complete loss of sympathetic ganglia (Levi-Montalcini and Booker, 1960). Conversely, neuronal survival of rat superior cervical ganglion improved upon exogenous supply of NGF after surgical removal of their targets (Hendry and Campbell, 1976). Based on these experiments the neurotrophic factor hypothesis was postulated, stating that neurons compete for a limited amount of neurotrophins for survival and undergo apoptosis when they do not find enough (Barde, 1989; Levi-Montalcini, 1987; Purves, 1980).

The discovery of NGF marked the starting point for the neurotrophic family, which includes NGF, brain derived neurotrophic factor (BDNF), neurotrophin (NT) NT3-5 as well as NT6-7, that are only found in fish (Barde, 1990). NGF has been shown crucial for the survival and maintenance of sympathetic neurons, motoneurons and pain-responsive sensory neurons (Crowley et al., 1994). BDNF, on the other hand, promotes the survival of placode-derived vestibular, petrosal and nodose neurons *in vitro*, as well as the survival of early sensory neurons of the dorsal root ganglia (DRG) (Davies et al., 1986; Lindsay et al., 1985a; Lindsay et al., 1985b).

1.3 NEUROTROPHIC RECEPTORS

There are two types of neurotrophic receptors, TrkA, B and C and low-affinity neurotrophin receptor p75^{NTR}. Trks are high affinity receptors binding to specific neurotrophins. TrkA is the receptor for NGF, TrkB for BDNF and NT4, whereas TrkC is the preferential receptor for NT3 (Skaper, 2018). Neurotrophins bind their receptors via the extracellular N-terminal of Trks. Trks span the plasma membrane once and have an intracellular carboxy terminal, containing a tyrosine kinase domain with multiple tyrosine residues that are phosphorylated upon receptor activation. Upon activation, receptors dimerize and auto-phosphorylate their tyrosine residues. Subsequently, tyrosine residues recruit and function as docking sites for cytoplasmic adaptors and enzymes (Skaper, 2018).

The second type is p75^{NTR}, which is part of the Tumor necrosis factor (TNF) receptor superfamily and binds all neurotrophins equally. Its expression is upregulated after neuronal injury and its signalling contributes to axonal degeneration and dysfunction due to injury or cellular stress. However, it can also act as a co-receptor and potentiate NGF/TrkA signalling at suboptimal concentrations and promote retrograde transport of neurotrophins (Skaper, 2018).

Neurotrophic factors and receptors are critical for neuronal survival in early development, which has been shown by several knockout experiments. In mice lacking NGF or TrkA, sympathetic neurons, pain- and temperature-sensitive sensory neurons are lost (Crowley et al., 1994; Henderson et al., 1994; Smeyne et al., 1994). On the other hand, mice overexpressing NGF in their skin show an increase of sympathetic and sensory neurons in the PNS (Albers et al., 1994). *BDNF*^{-/-} mice die perinatally and show severe reduction in some cranial and spinal sensory neuron populations (Jones et al., 1994), whereas *TrkB*^{-/-} mice show a loss of the DRG, trigeminal and nodose neurons (Klein et al., 1993). Overexpression of BDNF in epithelial cells does not change trigeminal or DRG neurons but increases neurons of the nodose ganglion (LeMaster et al., 1999). Further, *TrkC*^{-/-} mice reveal a decrease of myelinated axons with a loss of a DRG neuron-derived subpopulation (Klein et al., 1994). Lastly, TrkA interference in the soma leads to apoptosis (Ye et al., 2003).

1.4 NEUROTROPHIC SIGNALLING FOR SURVIVAL

Interestingly, NGF synthesis in the target tissue is timed to the arrival of innervating axons (Davies et al., 1987), supporting the neurotrophic hypothesis. The neurotrophic factor hypothesis describes a time of naturally occurring apoptosis due to a limited amount of expressed survival signalling molecules during development of the nervous system, when neurons extend axons to innervate their target tissue. Upon arrival naturally occurring cell death ensures the amount of surviving neurons to match the target circuitry (Barde, 1989; Oppenheim, 1989; Purves, 1980). After this phase of apoptosis, the surviving neurons experience a phase of growth and spreading of neuronal processes and synaptogenesis.

Interestingly, after differentiation from their precursors when axons start to grow, several populations of neurons are independent of neurotrophins for survival. For example, chicken placode-derived cranial sensory neurons are independent of BDNF at earliest stages, whereas neurons of the embryonic mouse trigeminal ganglion are independent of NGF for survival before they innervate their targets (Buchman and Davies, 1993; Vogel and Davies, 1991). Chicken placode-derived cranial neurons are a particularly nice model to study this early neurotrophin independence since these ganglia are readily accessible for *in vitro* cultures. Neurons of the chick vestibular,

petrosal and nodose ganglia are neurotrophin-independent for survival *in vitro* after differentiation from progenitors and remain neurotrophin-independent throughout the axonal growth period. These neurons become neurotrophin-dependent upon innervation of their peripheral target field. Importantly, neurons from different ganglia reach their target fields at different times and thus develop their dependence on neurotrophic support for survival at different times as well (Davies, 1989). Neurons with distant targets, like the nodose ganglion, innervate their targets later and thus become neurotrophic-dependent at a later time point compared to neurons from ganglia with closer targets, like the vestibular ganglion (Vogel and Davies, 1991).

The majority of placode-derived neurons depend on BDNF for survival upon innervation of their target fields (Davies, 1989; Vogel and Davies, 1991). From the time point when axons reach the vicinity of the target fields, neurons start to express TrkB. As mentioned, vestibular neurons express TrkB the earliest, late innervating nodose neurons express TrkB the latest (Robinson et al., 1996). This observation indicates that expression of neurotrophic receptors and dependence on survival is a tightly temporally regulated process. Interestingly, the expression of neurotrophic factors in the target fields, though only occurring upon innervation, does not seem dependent on the innervation. NGF mRNA is expressed on time in chick embryo hindlimb buds even without the innervation of any axons (Rohrer et al., 1988), showing that the target tissue does not depend on axonal innervation to release neurotrophic factors. When signalling for survival, Trk activation leads to phosphoinositide 3-kinase (PI3K) and Mitogen-Activated Protein Kinase (MAPK) activation (Kuruvilla 2000, Watson 2001, Ye 2003) and a competitive survival feedback loop grants the survival of neurons upon target innervation. Neurons that express TrkA respond to NGF signalling by further increasing their Trk expression (Ascaño et al., 2009; Deppmann et al., 2008). This feedback-loop leads to the transcription of anti-apoptotic factors and pro-survival genes.

1.5 NEUROTROPHIC SIGNALLING FOR GROWTH

Since neurotrophins can regulate neuronal survival and neurite growth, the distinction between both regulating processes requires an experimental setting that blocks apoptosis. Mice lacking proapoptotic protein Bax helped to resolve this issue. No developmental neuronal cell death was observed in *Bax*^{-/-} mice, showing that Bax is a critical regulator of neuronal apoptosis (White et al., 1998). Therefore, these mice allow the study of neurotrophic influence on axonal outgrowth independently of neuronal survival. Both, NGF and NT3 have been shown to be important for sympathetic neurites to elongate and branch *in vitro*, showing defects upon antibody treatment and tyrosine kinase inhibitor (Orlke et al., 2001). *BAX*^{-/-}; *NT3*^{-/-} mice showed decreased axon extension before target innervation and *BAX*^{-/-}; *NGF*^{-/-} mice showed normal proximal axonal extension for some sympathetic subpopulations and defective arborization of all (Glebova and Ginty, 2004; Kuruvilla et al., 2004; Patel et al., 2003). Further, these mice revealed decreased numbers of sensory neurons positive for TrkA in the epidermis of their hindlimbs, indicating that NGF/TrkA signalling is required for axonal growth and terminal arborization (Patel et al., 2000). These experiments- in addition to the observation that sensory neurons turn towards the source of NGF *in vitro*- indicate that neurotrophins regulate neurite outgrowth and innervation.

Upon innervation, sympathetic neurons arborize and become reliant on target-derived NGF for survival (Glebova and Ginty, 2004; Kuruvilla et al., 2004; Patel et al., 2000).

Neurotrophic Trk receptors dimerize upon ligand binding and phosphorylate tyrosine residues. As a result, adaptor proteins, including Src homology and collagen homology (Shc) and Fibroblast growth factor receptor substrate 2 (FRS2), bind these residues, therefore linking activated Trk

receptors to these important signalling pathways: Ras-extracellular signal-regulated kinase (ERK), PI3K/Akt and Protein kinase C (PKC) (Harrington and Ginty, 2013; Reichardt, 2006). The Ras-ERK pathway promotes neuronal differentiation and neurite outgrowth. PI3K/Akt promotes neuronal survival and growth and PKC is involved in regulating synaptic plasticity (Reichardt, 2006).

1.6 RECEPTOR TRAFFICKING

Since neurons have such polar morphology, neurotrophic signalling faces the challenge of transferring the signal from the activated receptor at the tip of the neurite to the soma, covering a significant distance.

The first evidence pointing into the direction of Trk being transported in neurons stems from 1974, where Hendry et al. show that radiolabeled neurotrophins injected into the iris of mice ended in the soma of neurons located in the superior cervical ganglion (Hendry et al., 1974). Since then, many lines of evidence have supported the theory of Trk signalling by a retrogradely transported signalling organelle. Since this first observation, activated pTrk has been observed to be transported retrogradely in rat sciatic nerves *in vivo* (Bhattacharyya et al., 1997; Ehlers et al., 1995). Using Campenot chambers, retrograde axonal trafficking was shown *in vitro*. Campenot chambers are microfluidic chambers that allow the differential treatment of neuronal axons and cell bodies (Campenot, 1977). With the use of these chambers, pTrk was shown to accumulate in the soma upon stimulation with NGF at axon terminals. As a negative control, NGF coupled to beads that prevented endocytosis was not able to induce a response when administered to the nerve terminals, proposing that NGF internalization lead to the trafficking of the activated receptor to the soma (Riccio et al., 1997). Using biochemistry, Tsui-Pierchala succeeded to show that NGF and TrkA are retrogradely co-transported in sympathetic neurons and that the increase in pTrkA at the soma observed after NGF stimulation stemmed from retrogradely trafficked TrkA originating in the axon terminals (Tsui-Pierchala and Ginty, 1999). Further, disrupted Trk kinase activity or disrupted microtubule integrity disturbs retrograde transport of TrkB in sensory neurons and disrupted Cyclic AMP-responsive element-binding protein (CREB) phosphorylation *in vitro*. Here, TrkB was found in the soma with its ligand in a ligand-receptor complex by co-precipitation (Watson et al., 1999). The transport is facilitated by minus-end directed motor protein dynein that is shown to interact with Trks by immunoprecipitation (Yano et al., 2001). By now, retrograde transport of Trks together with their ligands has been confirmed by live cell imaging indicating that pTrk regulates the transport of its signalling endosome by direct signal interaction (Jullien et al., 2003; Nomura et al., 2011).

1.7 THE NATURE OF THE SIGNALLING ENDOSOME

The characterization of the vesicular organelles that transport Trk to the soma and allow its signalling has been shown to be trickier. Grimes et al. were the first to address this question and showed the internalization of TrkA into small and larger intracellular organelles in response to NGF. Fractionation experiments showed that TrkA is associated with NGF, tyrosine phosphorylated and associated with its downstream binding partner Phospholipase C (PLC)- γ 1 (Grimes et al., 1996; Grimes et al., 1997).

In electron microscopy (EM) studies, Trk and neurotrophins have been shown in vesicular organelles (Bhattacharyya et al., 2002; Sandow et al., 2000). However, the static nature of EM as well as the difficulty to properly stain for markers have made the identification of these organelles challenging. The organelles involved have been described as heterogenous vesicles and multi-

vesicular bodies (MVBs) (Bhattacharyya et al., 2002; Sandow et al., 2000). Howe et al. were the first to isolate possible signalling endosomes. These endosomes were clathrin-coated vesicles containing the activated receptor and several downstream signalling molecules able to phosphorylate Elk (Howe et al., 2001). These biochemically isolated NGF/TrkA containing vesicles were shown to be positive for Rab5, a GTPase that marks early endosomes (Delcroix et al., 2003). However, while Deinhardt et al. also showed that TrkB localizes to Rab5-positive endosomes, only Rab7-positive late endosomes were reported to traffic TrkB to the soma. The authors further show that, while Rab5 was found to be essential for the trafficking of Trk to the soma, Rab5 was stationary itself. Rab7-positive endosomes, however, were also shown to be essential for Trk transport and were observed to move to the soma in the same organelle as Trk (Deinhardt et al., 2006). These results indicate either a dynamic maturation of early stationary Rab5-endosomes to late Rab7-endosomes undergoing retrograde traffic, or a coexistence in parallel (Scott-Solomon and Kuruvilla, 2018). A very early study using Iodine-125 labelled NGF in sympathetic neurons predominantly places NGF in MVBs in the soma (Claude et al., 1982). Also, gold labeled NGF and phosphorylated TrkA has been associated with axonal MVBs *in vivo* (Bhattacharyya 2002, Sandow 2000). More recently, Ye et al. used a *flag-TrkA* mouse line and revealed that 70% of intracellular TrkA in the axon are located in MVBs positive for Rab7 (Ye et al., 2018). In hippocampal and cortical neurons, Rab7-positive autophagosomes are reported to carry TrkB retrogradely to the soma with a microtubule-associated protein light chain 3 (LC3), adaptor protein complex 2 (AP2) and p150^{Glued} of dynactin complex (Kononenko et al., 2017). However, autophagosomes are mostly generated in distal axons and transported in retrograde direction, maturing on the way to the cell body (Maday et al., 2012), they are generated from the endoplasmic reticulum (ER) in the axon and not the plasma membrane. This leaves the question of how TrkB would get into the autophagosome (Scott-Solomon and Kuruvilla, 2018). The hypothesis that Trks are transported in MVBs that are distinct from lysosome-fusing degradative MVBs, as often described for epidermal growth factor receptor (EGFR) degradation, has been postulated by Weible and Hendry in 2004, terming these MVBs “retrosomes” (Weible and Hendry, 2004). What they fail to discuss is how these MVBs, described as organelles engulfing signalling competent endosomes, build up and how these signalling competent endosomes are again released upon arrival at the soma. Ye et al. propose a maturation of single membrane vesicles that is signalling competent at the soma, though a mechanism how these vesicles evolve remained unanswered (Ye et al., 2018).

1.8 RECEPTOR SIGNALLING DEPENDS ON ITS LOCATION

Even though the exact nature of the signalling endosome remains to be determined, the importance of this question has already been established as downstream signalling depends greatly on the receptor's location.

As discussed above, bead-coupled NGF that was not able to be internalized applied to the nerve terminals could not induce downstream signalling cascades. However, when applied to the soma, bead-coupled NGF was able to elicit a response, indicating two different signalling pathways for NGF, depending on where it is applied (Riccio et al., 1997). Indeed, treatment of sympathetic axons leads to axonal growth, whereas the application of NGF to the soma did not initiate axonal growth but only induced survival-signalling (Campenot, 1982). Further, CREB signalling was shown to be different depending on neurotrophin application to the soma or axon terminals (Riccio et al., 1997; Watson et al., 1999). In PC12 cells, TrkA regulates survival when signalling from the plasma

membrane but regulates differentiation when endocytosed. This is facilitated via differences in PI3K/Akt peak activity as well as signal duration (Zhang et al., 2000).

The difference in downstream signalling based on the subcellular location is a crucial factor for the signal diversification needed by neurons to respond to a limited number of guidance cues while generating trillions of synaptic connections. One of the reasons why subcellular location is so important for correct signalling is the proximity to downstream interacting proteins.

This has been studied in another guidance receptor called PlexinD1, the receptor for semaphorin 3E. As neurotrophic receptors, PlexinD1 is internalized upon stimulation and sorted by a sorting sequence (an SEA-domain) on its C-terminal into recycling endosomes. This sorting relies on an interaction of the SEA domain with a PDZ domain-containing protein called GIPC1 and is essential for PlexinD1's downstream signalling cascade. Located on recycling endosomes PlexinD1 is in close proximity to its downstream interactor R-Ras, facilitating the inactivation of R-Ras by PlexinD1. This leads to the subsequent deactivation of the PI3K/Akt pathway. Deletion of the SEA domain or knock-out of GIPC1 results in mis-sorting of PlexinD1 into late endosomes. These endosomes have very limited numbers of R-Ras attached to their limiting membrane, which therefore prevents interaction of PlexinD1. Consequently, downstream signalling is disrupted, leading to an increased activity of the PI3K/Akt pathway and therefore inhibition of the repulsive response to semaphorin 3E (Burk et al., 2017c). This example highlights the importance of proper receptor/endosomal location for interaction with target proteins and offers the opportunity for differential signalling from different cellular compartments.

The effect of proper signalling due to intracellular transport has shifted focus on how possible defects in the trafficking machinery could lead to neurodegenerative disorders (Burk and Pasterkamp, 2019; Kruttgen et al., 2003; Prior et al., 2017). One of these disorders is Charcot-Marie-Tooth.

1.9 HELD UP IN TRAFFIC - DEFECTS IN THE TRAFFICKING MACHINERY IN CHARCOT-MARIE-TOOTH DISEASE

REVIEW - ACCEPTED

AUTHORS:

Ronja Markworth^{1,2}, Mathias Bähr¹ and Katja Burk^{1,2}

¹ University Medical Center Göttingen, Department of Neurology, Robert Koch Straße 40, 37075 Göttingen, Germany

² Center for Biostructural Imaging of Neurodegeneration, 37075 Göttingen, Germany

Personal contribution: I wrote the manuscript and generated the figures and the table.

This manuscript was submitted to Frontiers in Molecular Neuroscience on the 14th of April 2021 upon invitation. It has been revised and accepted in its current form on July 23rd, 2021:

Markworth, R., Bähr, M., and Burk, K. (2021). Held Up in Traffic—Defects in the Trafficking Machinery in Charcot-Marie-Tooth Disease. *Front. Mol. Neurosci.* 14, 167. Available at: <https://www.frontiersin.org/article/10.3389/fnmol.2021.695294>.

ABSTRACT

Charcot-Marie-Tooth disease (CMT), also known as motor and sensory neuropathy, describes a clinically and genetically heterogeneous group of disorders affecting the peripheral nervous system. CMT typically arises in early adulthood and is manifested by progressive loss of motor and sensory functions; however, the mechanisms leading to the pathogenesis are not fully understood. In this review, we discuss disrupted intracellular transport as a common denominator in the pathogenesis of different CMT subtypes. Intracellular transport via the endosomal system is essential for the delivery of lipids, proteins and organelles bidirectionally to synapses and the soma. As neurons of the peripheral nervous system are amongst the longest neurons in the human body, they are particularly susceptible to damage of the intracellular transport system, leading to a loss in axonal integrity and neuronal death.

Interestingly, defects in intracellular transport, both in neurons and Schwann cells, have been found to provoke disease. This review explains the mechanisms of trafficking and subsequently summarizes and discusses the latest findings on how defects in trafficking lead to CMT. A deeper understanding of intracellular trafficking defects in CMT will expand our understanding of CMT pathogenesis and will provide novel approaches for therapeutic treatments.

INTRODUCTION

Charcot-Marie-Tooth disorder (CMT) is a group of hereditary peripheral neuropathies leading to loss of sensation and fine motor control in the extremities with a prevalence of over 1:2500. Over 100 genes are identified to cause CMT (Timmerman et al. 2014; Rudnik-Schöneborn et al. 2020). CMT is diagnosed and categorized into several subtypes based on clinical presentation including a loss of sensation and fine motor control in the extremities, nerve conduction velocity, neuropathological findings, as well as mode of inheritance and genes involved (Bird 2020). Classically, CMT1 is a demyelinating neuropathy, CMT2 is an axonal neuropathy, and dominant-intermediate CMT (DI-CMT) is an intermediate type showing both demyelinating and axonal pathologies. Since many more genes causing CMT were discovered showing overlaps of the phenotypes, a gene-based classification of inherited neuropathies has been proposed. Since so far this classification is not established, we stick to the classification by genes with the corresponding alphanumeric classification according to OMIM (Magy et al. 2018).

The observation that so many different mutations lead to a very similar phenotype has stirred the idea for a common pathomechanism and led to a search of a molecular pathway that covers many of the proteins recorded in CMT. Another interesting aspect of CMT is the peripheral nerve specificity, regardless of the ubiquitous expression of many of the proteins associated with CMT. Peripheral neurons stand out due to their length and polarity. Both sensory and motor neurons of the peripheral nervous system (PNS) can be up to over a meter in length and symptoms often arise earliest in the extremities. This, in combination with the post mitotic state of the neurons, makes these cells particularly susceptible to changes in the intracellular transport machinery.

The intracellular transport machinery ranging from endocytosis to protein degradation is a tightly regulated, yet extremely dynamic system that is crucial for energy metabolism, signaling and protein homeostasis. Even though many studies look at trafficking aspects in the different types of CMT, we are lacking studies that look at multiple CMT types at once to benefit from directly comparable results. Here we will give an overview of the different aspects involved in intracellular trafficking (the irony of trying to divide such a dynamic system into clearly defined sections is not lost on us). We briefly mention which CMT-mutations show defects in the respective sections but discuss several CMT disorders, their trafficking defects and similarities between them after presenting the cell biological mechanisms. Our main approach is to link the different pathological mechanisms seen in CMT to find common denominators. An overall summary of how genes causing CMT affect trafficking can be found in figure 1 (axonal) and figure 2 (Schwann cell).

ENDOCYTOSIS

Arguably, the first step for intracellular transport is endocytosis. The most common and well-studied pathway for the uptake of nutrients, signaling receptors but also ion channels, transporters or pathogens, as well as vesicles is clathrin mediated endocytosis. Upon initiation signal (for many signaling receptors this involves kinase activity and mono-ubiquitination of the intracellular domain (Haglund et al. 2003)) Phosphatidylinositol (PI) 4,5-bisphosphate ($PI_{4,5}P_2$) is generated at the plasma membrane, which recruits AP2, an adaptor protein complex. AP2 then recruits clathrin triskella that- with the involvement of several other proteins such as F-BAR domain-containing Fer/Cip4 homology domain-only proteins and Epsins- induce and stabilize membrane curvature and form a

clathrin-coated pit, in which cargo gathers. Subsequently, Dynamin is recruited to the neck of the pit and self-polymerizes to induce membrane scission by GTP hydrolysis. The clathrin-coated vesicle pinches off subsequently (reviewed in (McMahon and Boucrot 2011)). Upon removal of the clathrin coat, the vesicle is ready to fuse with early endosomes and begins its journey along the intracellular trafficking pathways.

Several genes known to cause CMT have been associated with dysfunctional endocytic processes, namely *MTMR2*, *13*, *5*, *SH3TC2*, *FGD4*, *DNM2* (relating to the subtypes CMT4B, CMT4C, CMT4H and DI-CMTB respectively), which will be discussed below. Defects in endocytosis have brought consequences on neuronal health for example lack of endocytosis of neurotrophic receptors would eventually affect gene expression of pro survival genes (Scott-Solomon and Kuruville 2018).

From the early endosome, cargo continues its intracellular journey. The early endosome is characterized by the binding of the Rab5 GTPase, a small Rab GTPase that is cytosolic in its inactive GDP bound state. Upon activation by a Guanine nucleotide exchange factor (GEF) Rab5 is membrane tethered and activates several effector proteins, such as early endosome antigen 1 (EEA1) (Gorvel et al. 1991; Bucci et al. 1992; Simonsen et al. 1998). The early endosome has a slightly acidic milieu with a pH of 6, which is generated by the vacuolar H-ATPase (Johnson et al. 1993). The membrane contains a high content of PI₃P and its shape is characterized by tubular extensions from its sorting activity (Jovic et al. 2010). The early endosome is also often referred to as the sorting platform. From there, cargo is sorted into one of three possible pathways. The recycling pathway, which is considered the default pathway, the retrograde pathway back to the trans golgi network (TGN) or to the soma, and lastly the degradative pathway (Schreij et al. 2016).

RECYCLING

After the clathrin coat is shed, the early endosome acts as a sorting station where bulk recycling is the default pathway due to probability: The endosome extends tubular domains increasing the amount of membrane in this section. Therefore, more receptors per volume will end up on that tubular domain, which is pinched off and recycled back to the plasma membrane (Frederick R. Maxfield and McGraw 2004). Due to the acidic lumen of the endosome, many ligands dissociate from their receptors. Consequently, only the receptor is shuttled back to the plasma membrane for another round of signaling. Ligands, however, remain in the endosome for maturation and subsequent degradation. A prime example for this pathway is Transferrin and its receptor (Hopkins and Trowbridge 1983). Receptors can also be recycled specifically via the so-called retromer complex together with the WASH complex and dynamin 2 (Derivery et al. 2009; Seaman et al. 2013). For example, the β -adrenergic receptor is recycled via a guided retromer sorting nexin (SNx) 27 complex. Where SNx27 recognizes a recycling sequence at the C-terminal of β -adrenergic receptor (Seaman 2012; Temkin et al. 2011; Lauffer et al. 2010). This recycling mechanism has also been reported for other receptors, using different retromer/SNx combinations (Weeratunga et al. 2020). It is to be expected that many more receptors have specific sorting sequences interacting with different adaptors leading to a highly selective sorting mechanism. Rab4 and Rab11 decorate recycling endosomes undergoing fast and slow recycling, respectively (Jovic et al. 2010). Defects in recycling can either affect re-activation due to decreased surface levels of the receptor or affect downstream signalling from endosomes causing for example growth defects (Pasterkamp and Burk 2020).

Defects in recycling have been reported for mutations in *DNM2*, *MTMR2*, *13*, *5* *SH3TC2* and *NDRG1*, causing DI-CMT, CMT4B, C and 4D respectively.

ENDOSOMAL MATURATION

As mentioned above, the early endosome undergoes a maturation process, from so-called early endosomes to late endosomes. This maturation is manifested in a Rab switch, where Rab5 activates effectors that are Rab7 GEFs, which, in turn, activate Rab7 (Rink et al. 2005). The luminal content of the endosome further acidifies (pH between 4.5-6) and a shift in PI composition (PI₃P to PI_{3,5}P₂) by 1-phosphatidylinositol 3-phosphate 5-kinase (PIKfyve) is reported (Wallroth and Haucke 2018; F. R. Maxfield and Yamashiro 1987). Maturation is further manifested by the formation of intraluminal vesicles (ILVs) by inward budding of the maturing endosomal membrane. These ILVs contain cargos marked for degradation by ubiquitination. At this point, late endosomes are often referred to as multi vesicular bodies (MVBs). Late endosomes/MVBs have also been reported to be involved in retrograde trafficking. The following sections describe the three different pathways that all fall under the category of retrograde transport, namely, retrograde transport for signaling, retrograde transport to the TGN, and retrograde transport for degradation.

RETROGRADE TRANSPORT FOR SIGNALING

While many receptors signal from the plasma membrane, others rely on internalization in signaling endosomes to propagate their signaling cascade. Neurotrophins as well as neurocytokines are retrogradely trafficked, mostly during development. Even though tropomyosin-related kinase A (TrkA) and B (TrkB), the receptors for neurotrophins nerve growth factor (NGF) and brain-derived neurotrophic factor (BDNF), respectively, are mostly studied for their role in neurodevelopment, TrkB has been shown to be important for the maintenance of neurons in the adult neocortex (B. Xu et al. 2000). In addition, peripheral sympathetic neurons that were treated with an anti-NGF antibody slowly degenerated, indicating that not only TrkB but also TrkA has a role in maintenance of the nervous system (Ruit et al. 1990).

Neurotrophic receptors that were endocytosed after monoubiquitination, have been shown to be transported in early or late endosomes in different model systems (Delcroix et al. 2003; Deinhardt et al. 2006). Recently a study showed that TrkA is transported along the axon of sympathetic neurons in MVBs but signals from small vesicles at the soma (Ye et al. 2018). However, endosomal maturation is a fluent process (e.g. as described during the Rab-switch), making it hard to pinpoint the exact maturation state of endosomes. In addition, static studies without any live-cell imaging, only give very limited insight.

Disruption in retrograde traffic for signaling have been observed in mutations in *RAB7* (CMT2B), *GARS1* (CMT2D), *HSPB1* (CMT2F). Neurotrophic signalling regulating neuronal survival depends on retrograde trafficking (Scott-Solomon and Kuruvilla 2018).

RETROGRADE TRANSPORT TO THE TGN

When retrograde transport is mentioned in non-neuronal cells, it is referring to the transport of cargo from endosomes to the TGN. In this context, the most studied cargo being the cation-independent mannose 6 phosphate receptor (CIMPR) that delivers hydrolases to late endosomes/lysosomes. The retromer complex, a key player in the endosomal sorting machinery, regulates this process. Composed of a vacuolar protein sorting-associated protein (VPS) trimer (VPS26,29,35), termed cargo recognition complex, and a SNx dimer (SNx1, 2 with SNx5 or 6), this protein complex returns the receptor back to the TGN, where it can pick up a fresh round of

hydrolases (Seaman 2012; 2004). SNxs are BAR-domain containing proteins, which drive membrane binding and curvature via their PI₃P membrane binding domain. The VPS trimer recruits CIMPR into a tubulus, which is stabilized by another protein complex termed WASH complex (Wiskott–Aldrich syndrome protein and SCAR homolog complex). Thoroughly studied in yeast, the exact roles of the VPS trimer and SNxs are still being debated in human cells (Simonetti et al. 2017; Kvainickas et al. 2017). When retrograde vesicles containing CIMPR reach the TGN, they need to dock and fuse for further hydrolase uptake by the receptor. This docking and fusion is orchestrated by Golgi-associated retrograde protein complex (GARP) and Rab29 (Bonifacino and Hierro 2011; Wang et al. 2014). If this pathway is disrupted no more hydrolases are delivered to lysosomes, leading to a lack in degradation, therefore to an accumulation of neurotoxic waste, a lack of nutrients and triggered apoptosis.

Disruptions of retrograde traffic and accumulations in the TGN were observed for mutations in *GIB1* causing, CMT1X.

RETROGRADE TRANSPORT FOR DEGRADATION

As just discussed, retrograde transport of CIMPR is very important for proper lysosomal function, a process essential for protein degradation. Internalization and subsequent degradation of signaling receptors is an important step in signal termination. Polyubiquitinated proteins at the cell surface that are marked for degradation remain in the early endosome (aka no recycling) while this endosome matures into a late endosome. The ubiquitinated cargo is recognized by hepatocyte growth factor-regulated tyrosine kinase substrate (Hrs) of the endosomal sorting complexes required for transport (ESCRT)-0 complex (Raiborg et al. 2002). Interacting with PI₃P ESCRT-0 recruits ESCRT-I and II, ubiquitinated cargo is concentrated in clathrin coated microdomains (Katzmann et al. 2001; Bache et al. 2003). ESCRT-III recruits membrane curving proteins to generate ILVs (Adell et al. 2014). Once a late endosome contains such ILVs, it is classified as a MVB. The definition of a MVB throughout the literature is quite vague when it comes to marker proteins- MVBs are only definitely characterized structurally in electron microscopy images. Upon ILV generation, the MVB fuses with lysosomes, degrading its content (Futter et al. 1996). The degradative pathway is not only used by signaling receptors to terminate signaling but also for the degradation of lipids. For example, Rab8 is involved in the regulation of cholesterol efflux via this pathway, an important step for myelination (Linder et al. 2009; Zhou et al. 2019).

Interestingly, the ErbB pathway, a crucial pathway for Schwann cell myelination, relies heavily on proper degradation and recycling. Neuregulin1 signaling through ErbB leads to Schwann cell myelination, both ErbB2 and ErbB3 are expressed in Schwann cells (Michailov et al. 2004; Taveggia et al. 2005). However, both receptors follow different pathways in this process- ErbB2 is recycled, whereas ErbB3 is degraded via the ESCRT pathway. Ubiquitinated ErbB recognizes ESCRT-0, recruits ESCRT-I-III and is subsequently incorporated into the invaginations- which bud off ILVs within MVBs (for a good review please see (Lee et al. 2017)). This process attenuates signal transduction and ends in receptor degradation. Abnormalities in this pathway again lead to increased neurotoxic waste and apoptosis.

Abnormalities in lysosomal degradation have been reported for mutations in *PMP22*, *LITAF*, *RAB7*, *DYNC1H1*, *LRSAM1*, *MTMR2,13,5*, *NDRG1* and *FIG4* causing CMT1A, 1C, 2B, 2O, 2P, 4B, 4D and 4J respectively.

AUTOPHAGY

Another degradative pathway is the one of autophagy. A pathway mostly used for the degradation of aggregated and misfolded proteins but also whole organelles (like mitochondria, termed mitophagy), induced by cellular stress. For this, a double membrane structure called phagophore forms, expands and closes upon itself to generate an autophagosome engulfing protein aggregate. The autophagosome then fuses with a lysosome leading to the degradation of its content and a subsequent nutrient release into the cytosol (also referred to as macroautophagy). Rab1, 4 and 11 are involved in the membrane delivery for the formation of the phagophore, whereas autophagy receptor p62 binds ubiquitinated cargo and Microtubule-associated protein 1A/1B-light chain 3 (LC3) on autophagosomes (Komatsu et al. 2007; Kiral et al. 2018). The class 3 phosphoinositide 3-kinase (PI3K) complex, recruited by Rab5, produces PI₃P for the nucleation of the phagophore, whereas Rab33 is involved in the elongation. Autophagosomes fuse with late endosomes to so called amphisomes that traffic retrogradely- possibly by the same Rab7/Rab-interacting lysosomal protein (RILP)/dynactin complex that regulates the transport of late endosomes (Cheng et al. 2015; Jordens et al. 2001). Rab7 and Rab24 then mediate the fusion with lysosomes (Kiral et al. 2018). The autophagic flux depends on the autophagosomal transport, and fusion with lysosomes. In healthy neurons, few autophagosomes are observed indicating a low level of autophagy or a very quick turnover (Boland et al. 2008; Mizushima et al. 2004).

Autophagy related proteins have also been shown in Schwann cells, where autophagy plays an important role for cell plasticity, myelin maturation and compaction. Excess cytoplasm is removed by autophagy leading to more compact myelin. Furthermore, Schwann cells rely on autophagy after nerve injury for the phagocytosis of myelin debris (Belgrad et al. 2020).

Alterations in autophagy were seen with mutations in *PMP22*, *RAB7*, *HSPB1* and *FIG4* causing CMT1A, 2B, 2F and 4J respectively.

MITOCHONDRIA TRANSPORT

Neuronal cells have a relatively large energy consumption, which is why they rely heavily on a functioning mitochondria system. Trafficking is an important process for mitochondrial maintenance. Mitochondria need to be transported to regions of high energy demand. If mitochondria transport is disturbed this would lead to a local energy crisis and to degradation of the long neurons of the PNS. Transport is regulated by a Miro/Milton complex (Fransson et al. 2006; Stowers et al. 2002; Glater et al. 2006). Miro binds the outer mitochondrial membrane via its carboxyterminal, whereas Milton is the adaptor protein of Miro and the motor proteins. Accumulated damaged mitochondria are degraded by mitophagy as described above. Disruptions in mitochondria transport and location have been described in many sub-types of CMT including mutations in *MFN2* (CMT2A2), *RAB7* (CMT2B), *GARS1* (CMT2D), *NEFL* (CMT2E), *HSPB1* (CMT2F) and *DYNC1H1* (CMT2O). For a recent review on mitochondria transport in a disease context refer to (Schiavon et al. 2021).

CYTOSKELETAL BASIS FOR TRANSPORT

The basic structure or architecture of neurons is provided by its cytoskeleton, which also serves as the tracks for intracellular trafficking. The cytoskeleton is comprised of three building blocks, microfilaments, intermediate filaments and microtubules. Microfilaments are made by actin and

are mostly found in mobile/changing structures like the growth cone or newly formed synapses. Intermediate filaments are made from 3 different neurofilaments (light, medium, and heavy polypeptide) and peripherin in the PNS. The filaments share a structural organization of a central α -helical rod that drives assembly of dimers, protofilaments and filaments of 10nm diameter (Laser-Azogui et al. 2015). Neurofilaments are the most abundant cytoskeletal component in myelinated axons. They have the intrinsic role to form and maintain the axonal architecture, its diameter and the intracellular transport of cargo in dendrites. Posttranslational modifications influence neurofilament assembly, hence the axonal size of large myelinated axons.

Lastly, microtubules are composed of α and β tubulin forming protofilaments, where 13 protofilaments make 1 microtubule with a diameter of about 25nm (Prior et al. 2017). Microtubules, also referred to as molecular tracks, are modified by acetylation and detyrosination, which influences trafficking. Acetylation increases the binding of motor proteins thus enhancing transport and is highest in stable and long-lived microtubules, like axons (Reed et al. 2006). Acetylation of α -tubulin improves the binding capacities of kinesins to the microtubules thus enhancing transport (Reed et al. 2006) but has also shown to increase dynein recruitment to microtubules (Dompierre et al. 2007). Whereas, detyrosination guides kinesin-1 to the axon (Konishi and Setou 2009) and regulates dynein based transport (Nirschl et al. 2016).

Kinesins are the motor proteins involved in the plus-end directed (anterograde) transport. Dyneins are involved in minus-end directed or retrograde transport. Dynein interacts with cargo via a dynein/dynactin complex involving p150^{Glued}. Deregulation in microtubule assembly and disassembly has been shown to affect axonal growth (Markworth et al. 2019). Importantly, neurotrophic signalling can affect microtubule stability (Goold and Gordon-Weeks 2003).

Many types of CMT have shown to have cytoskeletal abnormalities (Brownlees et al. 2002), including mutations in *PMP22* (CMT1A), *MFN2* (CMT2A2), *RAB7* (CMT2B), *GARS1* (CMT2D), *NEFL* (CMT2E), *HSPB1* (CMT2F), *FIG4* (CMT4J), *FGD4* (CMT4H), *DNM2* (DI-CMT) and *GJB1* (CMT1X). Whether these are causative or secondary remains to be shown in many cases.

PHOSPHOLIPIDS

Finally yet importantly, while the phospholipid system is involved in every step of intracellular trafficking, it is worthy of its own section. As already mentioned, the endosomal trafficking journey begins with the synthesis of $PI_{4,5}P_2$ at the site of endocytosis and changes over the course of endosomal maturation, making phospholipids not only a marker for endosomal maturation but an important regulator of the endosomal system (Wallroth and Haucke 2018). Early endosomes are mostly comprised of PI_3P , generated by class III phosphoinositide VPS34, which, in turn, is recruited by Rab5. PI_3P is then recognized by the FYVE domain of ESCRT-0 subunit Hrs, which is recruited to the endosomes to promote ESCRT sorting and MVB formation. During endosomal maturation PI_3P is phosphorylated by PIKFYVE complex/PI5K to $PI_{3,5}P_2$. PI regulating enzymes can affect endosome to lysosome trafficking and therefore inhibit the degradation of cell surface proteins (Berger et al. 2011).

Interestingly, as a component of the plasma membrane, phospholipids have been shown to play an important role in Schwann cells too. More precisely, phospholipids on Schwann cells have shown to be regulators of compact myelination. As PI3K generates $PI_{3,4,5}P_3$ at the plasma membrane, which then activates the Akt pathway, a promyelinating signaling cascade in the PNS, that is tightly regulated by phosphatase and tensin homolog (PTEN), downregulating $PI_{3,4,5}P_3$ (S. M. Lee et al. 2017). This again shows that phosphoinositides do not only function as membrane markers for

different organelles, but also hold a signaling and regulating function in the PNS. This makes them interesting candidates to investigate in axonal and demyelinating CMT as a deregulation would affect the whole intracellular trafficking pathway spanning from endocytosis to degradation. Specifically mutations in *MTMR2,13,5* and *FIG4* causing CMT4B and CMT4J, respectively, have shown to disrupt the phospholipid system.

CMT SUBTYPES SHOWING IMPAIRED INTRACELLULAR TRAFFICKING

While genetic mutations leading to CMT also affect other cellular processes (e.g. genes coding for human aminoacyl tRNA synthetases such as **GARS1** (glycyl-tRNA synthetase (GlyRS)), which catalyzes the first step of protein synthesis), eventually many processes meet at the platform of intracellular trafficking. For example, CMT2D-associated mutants of GlyRS stimulate deacetylase activity on α -tubulin (Mo et al. 2018). Further, even protein synthesis is linked to intracellular trafficking: mRNAs made in the nucleus associate with so-called RNA-binding proteins (RBPs). These RBPs are transported as ribonucleoprotein particles (RNPs) to distal subcellular locations for local translation. To perform local translation, RNPs associate with late endosomes/lysosomes, which are transported along the axons. Finally, These RNP-associated late endosomes have been found to dock at mitochondria sustaining mitochondrial health (Cioni et al. 2019). Intriguingly, this process is disrupted in CMT2B, caused by mutations in the late-endosomal Rab7-GTPase (Cioni et al. 2019). Therefore, rather than listing CMT-causing mutations based on their functions, we deciphered where and how, to today's knowledge, CMT mutations affect intracellular trafficking and how this then could explain the observed phenotypes.

The length, polarity and post-mitotic state make peripheral sensory and motor neurons extremely dependent on intracellular axonal transport for proper function and maintenance. It is therefore understandable that even mutations in ubiquitously expressed proteins cause a cell type specific phenotype in these neurons. Importantly, also subtypes that show both, axonal and demyelinating phenotypes show many mutations involved in intracellular transport in neurons but also in Schwann cells, hindering proper myelination.

Schwann cells have a highly polar structure and rely heavily on membrane transport for myelination. This can be seen in the involvement of the intracellular transport machinery in the pathology of demyelinating CMT1 as described below. Although many other factors are involved in the pathology, the involvement of intracellular traffic in CMT is intriguing as it highlights the importance of the intracellular transport machinery for many aspects of proper cellular function. Further, it sheds light on the importance of considering intracellular dynamics when looking for potential disease mechanisms. The fluidity yet tight regulation of this system is its toughest aspect to study. However, the following examples highlight the importance of considering this system as highly dynamic when interpreting static results. The CMT subtypes discussed in this review and their corresponding trafficking phenotypes are summarized in table 1.

AXONAL CMT2

CMT2A1-KIF1B β

In CMT2, several defects in intracellular trafficking have been reported (Fig. 1).

CMT2A1 is caused by mutant KIF1B β , a kinesin family member that plays a role in neuronal survival and function due to its role in anterograde transport (C. Zhao et al. 2001). KIF1B β directly binds to insulin like growth factor (IGF) receptor (IGFR) 1 β , a receptor tyrosine kinase that signals for axonal outgrowth via IGF-I signaling and activation of the PI3K-Akt pathway (Laurino et al. 2005; Scolnick et al. 2008). In one of the studied CMT2A1 mutations (Y1087C) binding of KIF1B β to IGFR is significantly reduced, leading to less IGF1R transport, reduced surface expression and reduced axonal outgrowth in mouse hippocampal neurons (F. Xu et al. 2018). Further, KIF1B β is involved in the development of myelinated axons, both in the CNS and PNS (Lyons et al 2009 in Xu). Other mutations have been reported in the conserved ATP binding site of the kinesin motor (Q98L), leading to a perinuclear accumulation of the protein and defects in cargo transport. This defect in transport was visible by decreased levels of synaptic vesicle proteins including synaptotagmin and synaptic vesicle protein 2 (SV2) in western blots of proximal and distal nerve sections after sciatic nerve ligation of heterozygous *kif1B*^{+/-} mice in comparison to *kif1B*^{+/+} mice (Zhao 2001). This study concluded a trafficking defect due to decreased protein levels on western blots of lysed nerve sections comparing distal and proximal parts. Levels of synaptotagmin and SV2 were reduced in both, distal and proximal section of the heterozygous mice compared to control. While the authors concluded a Kif1B- dependent trafficking defect, decreased levels could also occur from downregulation of these proteins or altered degradation instead of altered trafficking. Therefore, to specifically pinpoint trafficking defects, live-imaging using trafficking markers would help to decipher this question. In addition, KIF1B β is able to bind to other cargo. Therefore, it would be interesting to see if other intracellular transport systems are also affected, including the transport and signalling of epidermal growth factor receptor (EGFR), mitochondrial transport and autophagic turnover as presented for other CMT types (see below). Lastly, the effect on IGF1R trafficking and signalling in other CMT types would be intriguing to unwrap, to see if it is a common denominator or if commonalities can be found in the effect on the downstream signalling cascade.

CMT2A2

The most common type of CMT2 is CMT2A2, caused by dominantly inherited point mutations in *Mitofusin 2* (*MFN2*) (Züchner et al. 2004). MFN2 is a dynamin family GTPase located on the outer mitochondrial membrane protein and part of the Miro/Milton tethering complex, tethering mitochondria to kinesin. MFN2 is further involved in mitochondria morphology, fusion and motility, endoplasmic reticulum tethering and synapse formation (Chen et al. 2003; De Brito and Scorrano 2008; Misko et al. 2010). CMT2A2 mutations cause a decrease between mitochondria and endoplasmic reticulum tethering and a reduction in neurite length of primary motor neurons. Live cell imaging also revealed fewer mitochondria in the sciatic nerve axons with a higher proportion of very slow-moving mitochondria compared to control (Bernard-Marissal et al. 2019). This is in line with data from primary sensory neurons, where overexpressed mutant MFN2 led to a loss of mitochondria in distal and an aggregation in the proximal axonal segments with fewer mobile mitochondria (Baloh et al. 2007). The phenotype of slower mitochondrial movement was also observed in spinal motor neurons derived from patient induced pluripotent stem cells, but to lesser

extent (Saporta et al. 2015). In a CMT2A2 mouse model, loss of mitochondria was observed in the distal part of sciatic nerve axons as well as a loss of tubulin acetylation that worsened with age (Picci et al. 2020). However, since these mice display a neuropathic phenotype before the decrease of acetylation is detected, another pathomechanism has to be in play. Yet treatment with an histone deacetylase 6 (HDAC6) inhibitor ameliorated some of the motor and sensory phenotypes in these mouse models (Picci et al. 2020). It would be very interesting to see if and how the treatment affected mitochondrial transport and how it acted on a molecular level by applying it *in vitro*. This, in turn, would help to put this finding in context with previous studies focusing on the molecular pathomechanisms (like they did for CMT2D causing GlyRS (Benoy et al. 2018)). Still, the questions that remain are: is the deacetylation of tubulin a cause of the decreased mitochondrial transport? Would the deacetylation then, in turn, amplify the trafficking defect by decreased motor protein association, or do the pathomechanisms work in parallel? If mitochondria can no longer be transported to sites of high energy demand, like synapses or nodes of Ranvier, this would lead to a local energy crisis and explain neuronal malfunction in the longest and most distal parts as seen in CMT2A. Therefore, future studies on mitochondrial transport, or how to overcome disruptions in kinesin tethering would be an interesting point of investigation.

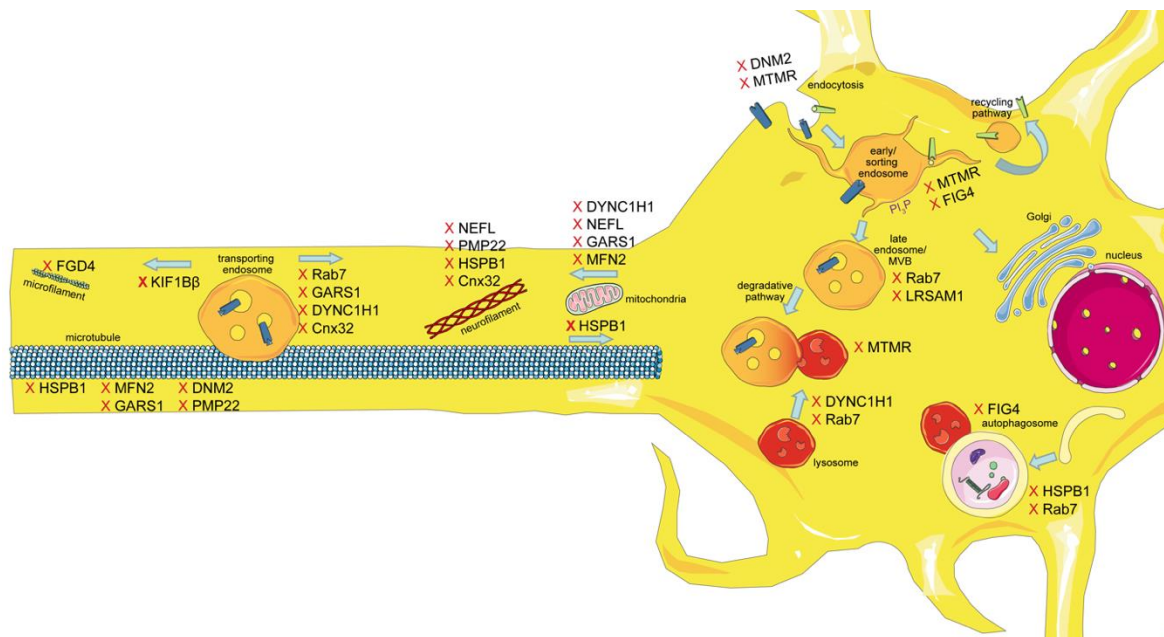


Figure 1: Schematic overview of the intracellular trafficking processes in a neuron of the PNS. Highlighting all the steps where proteins involved in CMT can cause dysregulation. This figure was created using Servier Medical Art templates, which are licensed under a Creative Commons Attribution 3.0 Unported License; <https://smart.servier.com>.

CMT2B

Autosomal dominant CMT2B, marked by primarily axonal degeneration, is caused by mutations in the late Rab7 GTPase. As of today 6 mutations are known to cause CMT2B, with all mutations being located close to the GTP binding pocket altering the binding kinetics (McCray et al. 2010; Spinosa et al. 2008; Saveri et al. 2020). Rab7 has been shown to transport ligand bound neurotrophic receptors TrkA and TrkB retrogradely to the soma (Deinhardt et al. 2006). Even though the CMT2B-causing Rab7 mutations are no loss of function mutations, alterations in retrograde traffic were

observed in a drosophila model and in cultured mouse dorsal root ganglia overexpressing the mutant Rab7 proteins (Janssens et al. 2014; Zhang et al. 2013). The binding of Rab7 and TrkA was not changed by the mutations. However, signaling of TrkA and EGFR was altered in cells expressing CMT2B mutant Rab7, possibly as a result of defective signaling from endosomes (Rink et al. 2005; F. R. Maxfield and Yamashiro 1987; Marat and Haucke 2016; Bakker et al. 2017)- since signaling from the plasma membrane was still intact (Basuray et al. 2010; BasuRay et al. 2013). In addition, the different mutants showed decreased expression of RILP, a Rab7 effector important for lysosomal transport by recruiting dynein-dynactin motors, as well as an increased interaction with peripherin, an intermediate filament of the PNS (Spinosa et al. 2008; Cogli et al. 2013). Further, one of the mutants showed disturbed binding to the protein sorting complex retromer by co-immunoprecipitation, suggesting a pathomechanism that involves mis-sorting of receptors on their trafficking route (Seaman et al. 2009). A study from 2018 also reported alterations in autophagy in CMT2B. All tested mutants displayed reduced localization on autophagic compartments and reduced autophagic flux in HeLa cells, similarly to a dominant negative mutant of Rab7. Further, basal and induced autophagy were decreased in skin fibroblasts from a CMT2B patient (Colecchia et al. 2018; Romano et al. 2020). As mentioned, local translation by ribonucleoprotein particles localizing to late-Rab7 endosomes and mitochondria is disrupted in CMT2B (Cioni et al. 2019). The diverse phenotypes of CMT2B-causing mutations in Rab7 is explainable by the involvement of Rab7 in many aspects of this highly dynamic system (e.g. transport, signaling of receptors, degradation, local translation), which makes pinpointing the causal effect of mutant Rab7 extremely difficult. It would therefore be very interesting to study if within these mechanisms some common modalities are present- e.g. do CMT2B-causing mutations have difficulties binding to dynein which would disrupt trafficking, signaling, maturation and degradation.

CMT2D

Mutant glycyl-tRNA synthetase (GlyRS) encoded by *GARS1* causes autosomal dominant CMT2D and distal hereditary motor neuronopathy (Antonellis et al. 2003). A mutant mouse model shows reduced acetylated α -tubulin levels and disrupted mitochondrial transport (Benoy et al. 2018; Mo et al. 2018). How the molecular mechanism of tRNA generation influences intracellular trafficking is not yet understood. To date, GlyRS mutants have been found to show novel and increased binding properties to cytoskeletal proteins and receptors (He et al. 2015). Mutant but not wild type GlyRS co-immunoprecipitates with HDAC6. HDAC6 deacetylates tubulin leading to unstable tubulin. Therefore, binding of mutant GlyRS to HDAC6 is believed to increase the deacetylase activity. A HDAC6 specific inhibitor has been found to improve mitochondrial axonal transport and relieve both, motor and sensory systems in mice (Benoy et al. 2018; Mo et al. 2018). The similarity to MFN2 causing CMT2A2 is striking, yet needs to be confirmed by producing more comparable studies and results. Both mutant MFN2 and GlyRS show reduced acetylated tubulin levels and decreased mitochondrial transport (Benoy et al. 2018; Mo et al. 2018; Baloh et al. 2007; Picci et al. 2020). Further, mouse models of each show an improvement of motor and sensory phenotypes upon treatment with HDAC6 inhibitors. How mutations in MFN2 lead to decreased acetylated tubulin, which in turn could lead to decreased binding of motor proteins to it and therefore to decreased transport of cargo/mitochondria, is still open. It is possible that MFN2 has a direct impact on the acetylation levels or that it is a secondary effect to the disrupted mitochondrial transport. It would therefore, be of interest if mitochondrial transport was improved upon HDAC6 inhibitor treatment

in models of CMT2A2 (MFN2) or if deliberately disrupting mitochondrial transport leads to a decrease in tubulin acetylation.

GlyRS also shows increased interactions with receptors. GlyRS binds neuropilin-1, a co-receptor of the vascular endothelial growth factor receptor (VEGFR). This interaction is enhanced by the GlyRS-CMT2D causing mutations. The increased binding of mutant GlyRS to neuropilin-1 disrupts its interaction with VEGFR. While genetic depletion of neuropilin-1 worsens the CMT phenotype, overexpression of VEGF improves motor problems (He et al. 2015), indicating that this pathway is also involved in the pathogenesis. Interestingly, VEGF signaling has been shown to be regulated by intracellular trafficking (Horowitz and Seerapu 2012). Whether the altered VEGF pathway contributes to the pathology in parallel or in stream with the altered tubulin acetylation remains unknown. To pinpoint the effects of VEGFR signaling in CMT2D, trafficking and downstream signaling could be followed. For example, does VEGFR change its downstream targets since neuropilin-1 has been found to act as a “gating” protein switching downstream signaling of PlexinD1 to VEGFR2 (Chauvet et al. 2007)?

Lastly, mutant GlyRS but not wild type GlyRS binds to TrkA. There is a correlation between binding intensity and disease severity. Even though the molecular effect on Trk binding is not clear, an increased Trk activation by increased ERK1/2 phosphorylation is indicated (Sleigh et al. 2017). Whether the disrupted transport of NGF (Mo et al. 2018) is a consequence of altered tubulin acetylation and transport defects in general or due to GlyRS' increased binding to NGF-receptor TrkA remains to be answered. The causal relationship of growth factor trafficking and tubulin acetylation needs to be determined. It is known that neurotrophic factor signaling affect microtubule dynamics (Goold and Gordon-Weeks 2003). Other options are changes in downstream signaling due to increased TrkA/GlyRS binding.

CMT2E

Mutations in NEFL are quite intriguing as they cause mostly axonal CMT2E but can also be classified as CMT1F because severely reduced nerve conduction velocity is a reported phenotype. However, the decreased conduction velocity that usually stems from demyelination is proposed to be caused by a decrease in axonal diameters in CMT2E, making it ultimately axonal (Lancaster et al. 2018). The mutations associated with CMT2E/1F are most commonly missense mutations in the head domain or in the central rod domain of neurofilament light polypeptide (NEFL) (Mersiyanova et al. 2000; De Jonghe et al. 2001; Lerat et al. 2019). Mutations disturb axonal transport of NEFL that is generated in the soma and transported along the axon, shown by lack of NEFL in the distal part of axons and accumulation in the proximal part and soma (Brownlees et al. 2002). However, live cell imaging of fluorescently tagged mutant NEFL in primary rat neurons did not show any alteration of NEFL movement compared to WT indicating that NEFL traffic greatly depends on the model being used (Stone et al. 2019). In contrast, transport of mitochondria is disrupted- seen in an accumulation of mitochondria in the cell body region and loss in the distal axon of sympathetic neurons (Brownlees et al. 2002; Pérez-Ollé et al. 2005). In patient derived iPSCs differentiated into spinal motor neurons, mitochondria movement was reported to be slower and shorter distanced (Saporta et al. 2015). Aggregates of mutated NEFL were observed in transfected rat cortical neurons and mouse models, as seen for other neuropathies. However, patient nerve biopsies and patient derived motor neurons only showed disorganized NEFL polymer accumulation not aggregation (Brownlees et al. 2002; Jian Zhao et al. 2017; Fabrizi et al. 2007; Adebola et al. 2015; Saporta et al.

2015). Overall, above studies should be carefully interpreted since data arose from different model systems- as phenotype depends greatly on the accompanying neurofilament proteins available for co-assembly (Stone et al. 2019).

CMT2F

Similar effects as described for CMT2D (mutant GlyRS) on α -tubulin acetylation and axonal transport have also been reported for CMT2F, which is caused by a mutation in heat shock protein family B (small) member 1 (*HSPB1*). CMT2- causing *HSPB1* has been found to cause intracellular aggregates of components including neurofilament medium polypeptide (NEFM) and p150 dynactin (Ackerley et al. 2006). In sensory and motor neurons, expression of mutant *HSPB1* lead to disturbed retrograde mitochondrial transport, whereas axonal transport of neurotrophic factor p75 was only minimally affected, indicating a cargo specific defect (D'Ydewalle et al. 2011; Kalmar et al. 2017; J. Y. Kim et al. 2016). This mitochondrial transport defect was partially rescued by an HDAC6 inhibitor. Almeida-Souza et al. have shown that mutant *HSPB1* reveals an enhanced binding efficiency to α -tubulin leading to stabilization of microtubules without changing the acetylation pattern of tubulin (Almeida-Souza et al. 2011). This seems counterintuitive to the beneficial effect of HDAC6 inhibitors and shows that more studies are needed to figure out the molecular pathway of *HSPB1* and HDAC6 inhibitors in the cytoskeleton. Interestingly, the commonalities of phenotypes between CMT2D (*GARS1*), CMT2E (*NEFL*) and CMT2F (*HSPB1*) all share a common defect: disruption in α -tubulin acetylation. A comparison on tubulin dynamics and structure could reveal additional shared phenotypes and increase the understanding of how these common phenotypes occur despite different genes affected. Furthermore, starvation induced autophagic flux was reduced in patient derived motor neurons. The exact molecular pathway of how *HSPB1* is involved in autophagy remains to be answered but it has been shown that *HSPB1* binds to the autophagy inducing receptor SQSTM1 and that this binding is increased by some mutants of *HSPB1*. Those mutants failed to induce autophagic pores upon starvation (Haidar et al. 2019).

CMT2O

CMT2O is an autosomal dominant type of CMT, caused by a His306Arg mutation of dynein cytoplasmic 1 heavy chain 1 (*DYNC1H1*). The His306Arg mutation resides in the highly conserved residue of the homodimerization domain of *DYNC1H1* (Weedon et al. 2011). As dynein is the main motor protein responsible for minus-end/retrograde transport, a pathomechanism involving defective axonal transport is expected. Indeed, tagged dynein from the Loa mice line, which carries a mutation in the binding domain of *DYNC1H1*, show decreased run length of retrograde transport of lysosomes (Ori-McKenney et al. 2010; Hafezparast et al. 2003) as well as decreased transport of trophic factors in a sciatic nerve ligation assay (Perlson et al. 2009). In mouse models with a 9bp deletion mutation in the stem domain of *DYNC1H1* (responsible for cargo binding and homodimerization), retrograde axonal transport of NGF was reduced, which caused increased apoptosis upon NGF stimulation at the peripheral axon (Jing Zhao et al. 2016). Whether the downstream signaling cascade of TrkA, the receptor for NGF, was altered as reported for mutated Rab7 and GlyRS has not been investigated yet. Further, mitochondrial transport is reduced in these mice as also reported for mutated MFN2, GlyRS and NEFL. The model shows that *DYNC1H1* has a crucial role in the transport of both neurotrophic factors and mitochondria a defect shared among several CMT subtypes.

CMT2P

Recessive and dominant axonal CMT2P are caused by mutations in *LRSAM1* (leucine rich and sterile alpha motif containing) encoding a universally expressed RING-type E3 ubiquitin ligase (Guemsey et al. 2010). Thus far, its only known target is TSG101, a member of ESCRT I, involved in the degradation pathway of EGFR (Palaima et al. 2021). Though only known since the last decade, first results already show the involvement of LRSAM1 in the intracellular trafficking pathway and more results regarding its exact involvement in the molecular processes of EGFR degradation and possible other trafficking phenotypes are to be expected in the future.

In summary, the most prominent shared defects in axonal CMT include abnormalities in mitochondrial transport, transport of neurotrophic factors, tubulin acetylation and altered autophagy. These mechanisms, in turn, could affect downstream signaling from endosomes as well as microtubule dynamics via trophic signaling (Goold and Gordon-Weeks 2003). One downside of interpretation is that experiments conducted vary between model systems used. Further, the level of detail in how the transport mechanisms are studied also shows variability. Therefore, comparative studies focusing on the effect of the different CMT mutated proteins would be ideal to identify common pathologies. Further, checking for phenotypes reported in one subtype (like altered IGFR transported as reported for CMT2A1) in other subtypes will complete the picture of possible shared mechanisms. The same holds true for CMT subtypes not mentioned in this review because not enough data to altered trafficking mechanism were reported as of yet.

CMT SUBTYPES WITH DEMYELINATING AND AXONAL PHENOTYPES

Importantly, not only predominantly axonal types of CMT show intracellular transport defects. In fact, several of the demyelinating subtypes have shown abnormal trafficking including CMT1, the most common type of CMT, as well as CMT1X, CMT4 and DI-CMT (Fig. 1 and Fig. 2). This indicates that trafficking is also a crucial step in Schwann cells. Of note is that the majority of trafficking defects in CMT subtypes with more demyelinating phenotypes is seen in the endocytic and recycling pathway indicating these two steps critical in Schwann cell myelination. DI-CMT, CMT4B, 4C, 4D and 4H all show endocytic alterations, recycling defects or both. On the other hand, CMT4B and CMT4J affect phosphoinositide compositions altering endocytic processes, recycling, maturation and degradation pathways. This shows that the PI regulation is essential for the complete dynamic process of intracellular trafficking and cannot be pinpointed to a single subsection.

DI-CMTB

Mutations in dynamin 2 cause dominant intermediate CMT (DI-CMTB) displaying both axonal and demyelinating phenotypes, sometimes also classified as axonal CMT2M (Züchner et al. 2005). Dynamin 2 is a ubiquitously expressed fission protein, responsible for the fission of intracellular vesicles after endocytosis and for the fission from endosomes. The mutations causing Di-CMTB are located in the Pleckstrin homology domain of dynamin 2, which binds to $PI_{4,5}P_2$ required for membrane localization. One of the DI-CMTB causing mutants (K558E) blocks dynamin-dependent endocytosis in a dominant negative fashion, whereas another (551 Δ 3) showed defects in microtubule stability, indicating two different pathogenic mechanisms (Tanabe and Takei 2009). Of note, dynamin 2 also plays a role in receptor trafficking as it is involved in targeting receptors into

the recycling pathway from early endosomes (Jovic et al. 2010). Therefore, defects in dynamin 2 could affect receptor signaling by blocking receptor endocytosis as well as re-activation if receptor re-insertion to the plasma membrane is disrupted. Although live cell imaging experiments are sparse for DI-CMTB, the disturbances in three of the main fundamentals for intracellular transport-endocytosis, recycling and microtubules, could lead to trafficking defects and would be ideal candidates to receive further investigation. Interestingly, dynamin 2 is essential for Schwann cell myelination of the peripheral nerves. An induced dynamin 2 deletion in adult Schwann cells leads to a demyelinating neuropathy (Gerber et al. 2019). However, it is unclear if this defect is caused by disrupted endocytosis as seen by a Transferrin uptake assay, or caused by altered levels of ErbB2 receptors on the plasma membrane (Sidiropoulos et al. 2012). The involvement of dynamin 2 in Schwann cell myelin maintenance provides a basis for the intermediate pathogenesis seen in DI-CMTB.

CMT4B

CMT4 is a rather rare subtype of the disease mostly inherited in an autosomal recessive pattern characterized by myelin deformities and a relatively early onset.

CMT4B is caused by autosomal recessive mutations in three of the myotubularin-related protein (MTMR) family of phosphoinositide 3-phosphatases with a mostly demyelinating phenotype with focal hypermyelination. CMT4B1 is caused by loss-of-function mutations in the catalytically active MTMR2, whereas CMT4B2 and CMT4B3 are caused by mutations in catalytically inactive MTMR13 and MTMR5, respectively (Berger et al. 2002; Robinson and Dixon 2005; Bolino et al. 2000). MTMR2 dephosphorylates PI_3P (mainly present on early endosomes) to PI , and $PI_{3,5}P_2$ (mainly present on late endosomes) to PI_5P . MTMR5 and MTMR13 directly interact with active MTMR2 and increase its catalytic activity as well as recruit MTMR2 to membrane compartments (S. A. Kim et al. 2003; Robinson and Dixon 2005). Due to faulty phosphatase activity, PI_3P and $PI_{3,5}P_2$ are predicted to accumulate on endosomes in CMT4B.

As discussed above, phosphoinositides are an important regulator of many steps along the intracellular trafficking pathway, as well as of myelination. Therefore, it is of no surprise that several studies have found effects of CMT4B mutations in many different aspects of the intracellular pathways. Even though expression of MTMR in Schwann cells is very low (Berger et al. 2002), mutations in Schwann cells is sufficient to induce CMT4B-like pathology (Bolis et al. 2005).

A study in cortical neurons has located MTMR2 to synapses by interaction with PSD95. Here, MTMR2 seems to function as a negative regulator of endocytosis, as the uptake of AMPAR subunit GluR2 increases upon loss of functional protein (H. W. Lee et al. 2010). As MTMR2 has been shown to interact with SAP97/Dlg1 a part of the PSD family in Schwann cells, it is plausible for MTMR to play a regulatory role of endocytosis in Schwann cells (Bolino et al. 2004). Whether this process contributes to the pathology remains to be answered.

Further, loss of MTMR2 promotes the sorting of internalized AMPA receptors to lysosomes, indicating that active MTMR2 plays a role in preventing AMPA degradation, possibly by initiating a recycling pathway (H. W. Lee et al. 2010). However, in epithelial cells, knockdown or overexpression of MTMR2 leads to a blockage of EGFR degradation *in vitro* in two different studies, implicating MTMR directly in the degradative pathway (Cao et al. 2008; Berger et al. 2011). Further, MTMR2 shows binding to PI3K adaptor hVPS34/hVPS15 complex that also interacts with Rab7, indicating a possible link in pathology of CMT4B and CMT2B. Although the direct effect of CMT4B mutations on the degradative pathway are not shown, the general involvement of MTMR in the degradative

pathway offers many possible pathomechanisms. Normally, MTMR2 recruits RME8 via PI₃P, which, in turn, regulates EGFR traffic from endosomes to lysosomes- a pathway that could be disrupted in CMT4B (Xhabija et al. 2011). Overall, CMT4B shows that misregulation of phospholipid composition can lead to disruptions in endocytosis, recycling and degradation. Since CMT4B shows predominantly demyelinating phenotypes, it will now be interesting to see how CMT4B mutations affect ErbB endocytosis, recycling and degradation in Schwann cells, considering that this is a major signaling pathway for myelination, as well as its downstream promyelinating PI3K/Akt signaling cascade. Interestingly, Akt levels were altered in sciatic nerve sections from MTMR2,13 knockout mice (Berger et al. 2011). The direct effect on phosphoinositide composition could alter the promyelinating signaling cascade and link the mutation to the demyelinating phenotype. (For a good review on ErbB signaling and trafficking in CMT we refer the reader to (S. M. Lee et al. 2017)) Lastly, MTMR2 has been shown to interact with NEFL, indicating a common pathway could underlie the pathology causing CMT4B and CMT2E explaining the similar phenotypes observed (Previtali et al. 2003).

CMT4C

CMT4C, also an autosomal recessive disorder with an early onset, is characterized by hypomyelination. This hypomyelination is caused by both, nonsense and missense mutations in the *SH3TC2* gene leading to a loss of function (Senderek et al. 2003). Over 20 different mutations have been reported to date. *SH3TC2* is expressed in Schwann cells but not neurons of the PNS (Vijay et al. 2016). Although its exact molecular mechanism has not been identified, *SH3TC2* has been implicated in the ErbB-neuregulin1 signaling axis, a crucial pathway for PNS myelination. Neuregulin1 binds ErbB3, which activates ErbB2. This receptor complex is internalized for downstream promyelin-signaling (Di Guglielmo et al. 1994; Zastrow and Sorkin 2007; Birchmeier and Bennett 2016). It has been proposed that *SH3TC2* plays a role in endocytosis, as ErbB2 internalization is reduced in *SH3TC2* knockout Schwann cells. Moreover, overexpression of *SH3TC2* increased internalization of ErbB2, co-immunoprecipitated with ErbB2 and is co-internalized with it upon stimulation (Gouttenoire et al. 2013). To date, the molecular role of *SH3TC2* in endocytosis remains undetermined. CMT4C mutations of *SH3TC2* impair the localization of *SH3TC2* to the plasma membrane (Lupo et al. 2009) and impair ErbB2 uptake in Schwann cells (Gouttenoire et al. 2013). These findings indicate a role for *SH3TC2* in receptor uptake and that endocytic dysfunctions in CMT mutants contribute to the pathology. However, many more roles of *SH3TC2* at different stages of the endolysosomal pathway have arisen that may contribute to the pathology seen in CMT4C.

Besides localizing to the plasma membrane, *SH3TC2* is found on recycling endosomes (the perinuclear recycling compartment in Schwann cells) that bind to active Rab11 (Stendel et al. 2010; Roberts et al. 2010; Arnaud et al. 2009). Interestingly, CMT4C mutants of *SH3TC2* showed no interaction with Rab11 and no localization to recycling endosomes. In HeLa cells, mutant *SH3TC2* has been shown to promote the recycling of the transferrin receptor (TfR) back to the plasma membrane, whereas transient expression of WT *SH3TC2* decreased TfR recycling (Roberts et al. 2010). This suggests that *SH3TC2* either acts as a competitor to TfR recycling or negatively regulates the recycling of TfR directly and that this is disrupted by the CMT4C mutations. Lastly, the *SH3TC2* mutants show decreased myelin protein synthesis in Schwann cells and dominant negative Rab11 has been shown to lead to myelin defects *in vitro*, whereas constitutively active Rab11 increased myelination (Stendel et al. 2010). This indicates a direct role of Rab11 in the myelination process

and therefore a likely role for its effector SH3TC2. Vijay et al have identified Integrin $\alpha 6$ as a SH3TC2 associated protein in retinal pigment epithelial cells. Integrin $\alpha 6$ is a laminin receptor known to recycle via Rab11 endosomes involved in maintaining structural integrity of the myelin sheath (Vijay et al. 2016). It would be interesting to see if the recycling of ErbB and Integrin $\alpha 6$ is also disrupted by the CMT4C mutations, as ErbB2 depends on rapid recycling for proper signaling. Further, it remains to be dissected, whether the effects described for SH3TC2 affecting endocytosis and recycling are shared effects of the same pathway or separate pathways.

CMT4D

CMT4D is a demyelinating, autosomal recessive type of the disorder caused by a mutation in N-myc downstream regulated 1 (NDRG1) (Kalaydjieva et al. 2000). The most common truncation mutation (R148X) leads to a loss of function showing similar phenotypes as complete deletion of the protein (King et al. 2011). Its high and exclusive expression in Schwann cells in the PNS suggest a Schwann cell specific role, although the precise role remains to be determined (Okuda et al. 2004). In prostate cancer cell lines, NDRG1 was identified as a Rab4 effector protein. NDRG1 was shown to be involved in the fast recycling of TfR, as recycling was slowed down when NDRG1 was knocked down. Further, NDRG1 binds PI_4P but is recruited to endosomes independently of its effector Rab4 (Kachhap et al. 2007). Yet overexpression of mutant NDRG1 with Rab4 in HeLa cells resulted in enlarged Rab4 endosomes compared to WT NDRG1 (L. X. Li et al. 2017). In cancer cell lines, NDRG1 is involved in recycling of e-cadherin (Kachhap et al. 2007). This leads to speculate that other recycling pathways specific to Schwann cell myelination and Schwann cell/axonal communication might be disrupted by loss of NDRG1 function. Recycling of both, ErbB and the low density lipoprotein (LDL) receptor are significantly reduced in CMT4D (Pietiäinen et al. 2013). Investigating this abnormality in LDL receptor recycling showed that NDRG1 has a role as a negative regulator of receptor degradation. The observation of decreased LDL receptor recycling led to the hypothesis that NDRG1 normally prevents ubiquitination of LDL receptor, leading to its recycling back to the plasma membrane. When NDRG1 is dysfunctional, LDL receptor is marked for degradation, therefore the receptor is not recycled back to the plasma membrane. This leads to a shortage of receptors available for endocytosis and thus a shortage of LDL (Pietiäinen et al. 2013). In addition, this experimental set up also showed a second effect of NDRG1 depletion: abnormal endosomal maturation. LDL receptors were found to be trapped in MVBs. These MVBs showed an increased number of ILVs (despite a downregulation of ESCRT proteins), yet were still positive for early endosomal marker EEA1, indicating disturbed endosomal maturation. This phenotype in combination with the observed slowed degradation of LDL receptor indicates a delayed fusion of MVBs with lysosomes. Prenylated Rab Acceptor 1 protein (PRA1) was identified as a NDRG1 interactor (King et al. 2011) and overexpression of PRA1 was able to partially rescue LDL receptor phenotype of NDRG1 depletion (Pietiäinen et al. 2013). PRA1 regulates several Rab GTPases including Rab4, Rab5, Rab7 and Rab9 (Bucci et al. 1999). Since Rabs are key players in intracellular trafficking, it is likely that dysregulation of PRA1 contributes to the pathomechanism of delayed lysosomal fusion. However, how PRA1 function is altered by the loss of function in *NDRG1* remains to be investigated.

Interestingly, NDRG1 showed interaction with ApoA1 and A2, both are proposed to be involved in Schwann cell lipid trafficking (Hunter et al. 2005). Whether a parallel recycling effect based on NDRG1s interaction with Rab4 is involved, how NDRG1 functions as a ubiquitin inhibitor and what mechanisms are altered by PRA1 activity in CMT4D are all questions that remain to be answered.

CMT4H

Another autosomal recessive, early onset disorder is CMT4H caused by mutations in the *FGD4* gene encoding FYVE, RhoGEF and PH domain containing protein 4 (FGD4) (Delague et al. 2007). Over 20 mutations have been reported so far, many of which result in a truncated and loss of function mutation or missense mutations in the PI-recognition domains (two PH domains recognize $PI_{3,4,5}P_3$, $PI_{4,5}P_2$ and $PI_{3,4}P_2$, FYVE domain binds PI_3P) (Argente-Escrig et al. 2019). FGD4 is a GEF for the Rho GTPase Cdc42 and Rac1 (Obaishi et al. 1998; Umikawa et al. 1999). As deletion of Cdc42 in adult Schwann cells of mice shows a similar phenotype to adult deletion of FGD4 and levels of active Cdc42 are reduced in sciatic nerves of adult FGD4 knockouts as well as in cultured Schwann cells (Horn et al. 2012), the Cdc42 pathway is probably disrupted in CMT4H. Even though CMT4H is an early onset disorder and FGD4 expression in Schwann cells is required for proper myelin development it is also important for myelin maintenance as an induced knockout in adult Schwann cells leads to myelin defects. Interestingly and tying FGD4 to the endocytic section of this review: depletion of endogenous FGD4 inhibits the internalization of TfR in rat Schwann cells (Horn et al. 2012). Unfortunately, the molecular mechanism of FGD4's involvement in endocytosis is still unknown. However, Cdc42 has a proposed role in endocytosis, by enabling clathrin mediated endocytosis via actin polymerization (Bu et al. 2010; Yang et al. 2001). This observation opens up the possibility that other internalization processes i.e. ErbB are disrupted leading to the pathology.

When overexpressed in rat motoneurons or rat RT4 schwannoma cells, wild type FGD4 co-localized with f-actin in the growth cone and tips of neurites and increased the number of filopodia-like microspikes. Overexpression of truncated FGD4, still revealed colocalization with f-actin, but showed a reduced number of microspikes with altered curly morphology (Delague et al. 2007). This observation indicates that FGD4 plays a role in the structural organization of microfilaments during cellular growth, which is possibly disrupted by the loss of function mutations in CMT4H. Further, Cdc42 has been implicated in the reorganization of the cytoskeleton (Daub et al. 2001; Nakanishi and Takai 2008; A. Li et al. 2021). However, no abnormalities in the organization of microfilaments or microtubules were observed in patient fibroblasts (Delague et al. 2007). It is possible that changes unnoticed in fibroblasts are detrimental for neurons or Schwann cells, considering their long and polarized structure.

CMT4J

CMT4J is caused by a partial loss-of-function mutation on fat induced gene4 (FIG4), a ubiquitously expressed phosphoinositide 5 phosphatase, dephosphorylating $PI_{3,5}P_2$ to PI_3P . CMT4J is a neuropathy with myelin defects and axonal loss in the periphery caused by a compound heterozygotic combination of a missense allele with a null allele. A loss of FIG4 function, counterintuitively, decreases the levels of $PI_{3,5}P_2$ (Chow et al. 2007), as FIG4 also activates PIKFYVE, a PI5K on endosomes (Rudge et al. 2004). The CMT mutant of FIG4 is not stabilized, leading to protein instability and reduced levels of FIG4 (Lenk et al. 2011). In FIG4 deficient cells, lysosomes and endosomes are enlarged, showing that a tight PI regulation is important for proper endosome maturation and following fusion with lysosomes. Interestingly, this phenotype can be rescued in drosophila by overexpression of an enzymatically inactive FIG4, indicating that its loss of function goes beyond its phosphatase activity (Bharadwaj et al. 2016). FIG4 also interacts with MTMR2 in neurons and Schwann cells, indicating a shared pathomechanism in CMT4B and CMT4J. As they

both have an effect on $PI_{3,5}P_2$, in Schwann cells the loss of FIG4 function in MTMR2 null mice rescues the myelin outfolding phenotype. As the loss of MTMR2 leads to more $PI_{3,5}P_2$, the reduction of FIG4 and therefore the decrease in PIKFYVE reduces levels of $PI_{3,5}P_2$ (Vaccari et al. 2011). The overlap of these two CMT subtypes working on a shared pathway are a great opportunity to figure out the downstream changes of altered $PI_{3,5}P_2$ levels leading to the pathology and should be investigated in more detail. *In vivo*, conditional inactivation of FIG4 lead to axonal degeneration and Schwann cell demyelination, possibly by a defective transport of cholesterol (Vaccari et al. 2015). Further, altered levels of autophagic markers were observed in neurons and astrocytes of mice models of CMT4J. These altered levels indicate a decrease in autophagic flux, proposed to be due to defective fusion with lysosomes (Vaccari et al. 2015; Ferguson et al. 2009).

CMT1X

CMT1X is caused by mutations in the *GJB1* gene located on the X chromosome encoding Gap junction protein beta 1 (GJB1) also known as Connexin32 (Bergoffen et al. 1993). Over 400 mutations have been reported to cause CMT1X, with many of them being loss of function mutations, where WT GJB1 normally forms gap junctions in the peripheral nerve ensuring intercellular communication (Kleopas A. Kleopa et al. 2012). Abnormal trafficking has been reported for CMT1X in two ways. First, mutant GJB1 is not properly trafficked anterogradely to the plasma membrane. Instead, mutant GJB1 accumulates in the endoplasmic reticulum or Golgi leading to a lack of intercellular gap junctions (Abrams et al. 2003; Deschênes et al. 1997; K. A. Kleopa et al. 2006; Yum et al. 2002). However, some mutant forms of GJB1 form functional gap junctions indicating a second, parallel pathogenic mechanisms (Castro et al. 1999). Valvitou et al. have shown that lack of GJB1 can cause defects in axonal retrograde transport and neurofilament abnormalities before onset of demyelination in mice. Neurofilaments were more densely packed and dephosphorylated in the absence of GJB1, probably leading to deficient axonal transport as indicated by the accumulation of dynein and other markers usually transported along the axon (Vavlitou et al. 2010). Although direct evidence for trafficking defects is missing this indicates a pathomechanism beyond the lack of gap junctions that requires further investigation as to how GJB1 affects neurofilaments and thus trafficking, especially if the trafficking of receptor tyrosine kinases is altered by the neurofilament abnormalities observed. A potentially common pathway could be the altered MEK-ERK signaling observed in GJB1 deficient Schwann cells leading to altered expression profiles of MEK-ERK regulated proteins (Groh et al. 2010).

With all studies targeting the experimental questions using specific approaches (e.g. looking at one receptor or one specific downstream protein related to the affected GEFs), it would be interesting to set up comparative studies between the CMT subtypes targeting potential shared proteins. This would help to reveal if there are common denominators affected.

DEMYELINATING CMT

CMT1A

Also prominently demyelinating subtypes of CMT have shown several transport deficits (Fig. 2). CMT1A is the most common cause of CMT, an autosomal dominant type caused by a duplication of the gene encoding peripheral myelin protein 22 (PMP22), leading to overexpression and aggregation. Even though not the focus of many studies, intracellular transport is heavily involved in the processing of PMP22 in several aspects. For example, a prominent pathway in the

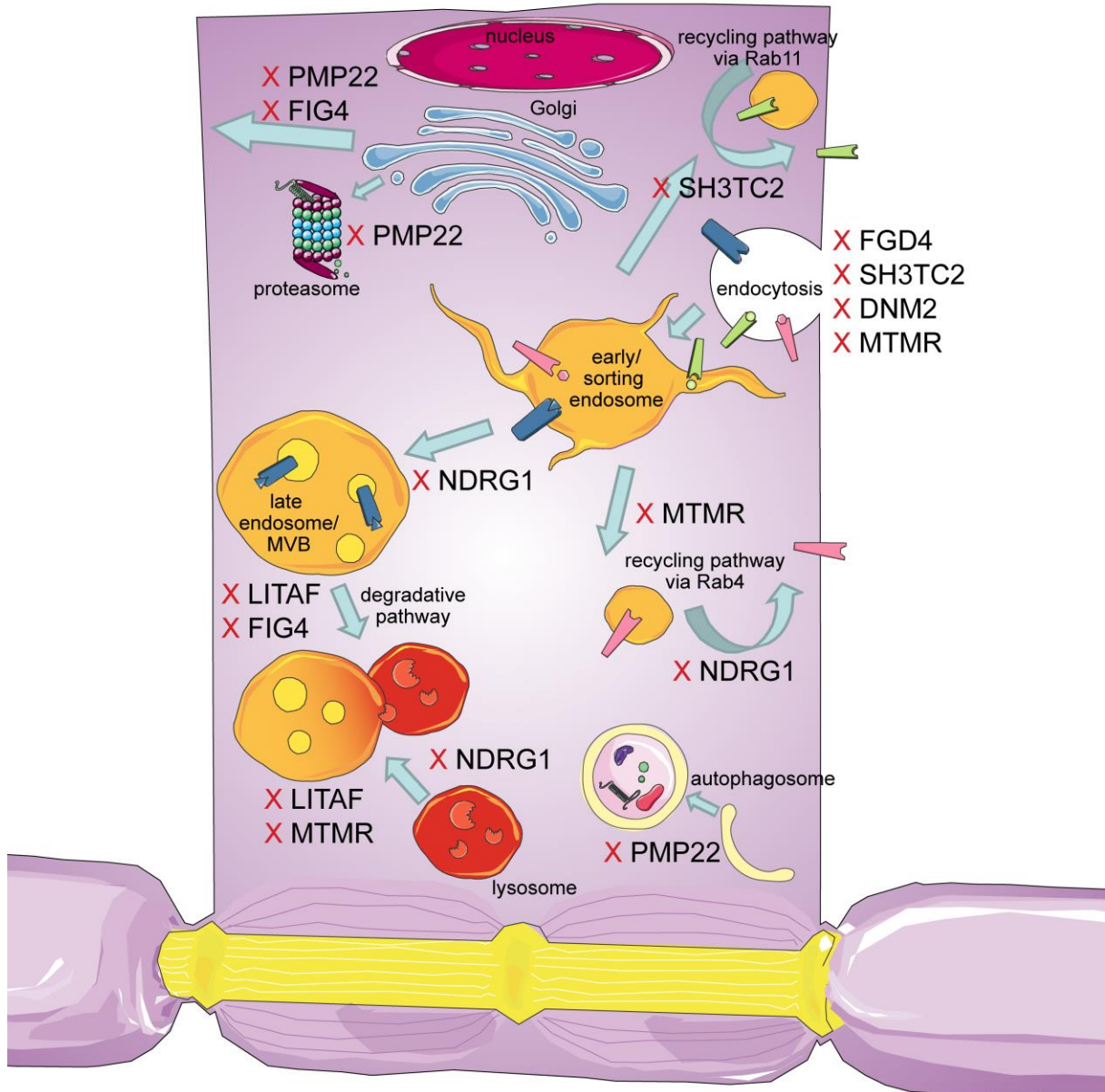


Figure 2: Schematic overview of the intracellular trafficking processes in a myelinating Schwann cell. Highlighting all the steps where proteins involved in CMT can cause dysregulation.

This figure was created using Servier Medical Art templates, which are licensed under a Creative Commons Attribution 3.0 Unported License; <https://smart.servier.com>.

degradation of misfolded proteins and aggregates is autophagy. With the observation of an increase in misfolded PMP22 and its aggregates, it is reasonable to speculate that autophagy plays an important role in protein clearance of CMT1A. Patient derived fibroblasts show increased levels of autophagic markers (S. Lee et al. 2018). Indeed, autophagy activation by rapamycin was shown to improve myelination in demyelinating CMT mouse DRG cultures (Rangaraju et al. 2010) and in mice (Nicks et al. 2014). Further, a recent study by Marinko et al. shows that the expression of PMP22 is negatively correlated to the trafficking of newly synthesized PMP22 to the plasma membrane. When too much PMP22 is expressed, the proteasomes of the ER's membrane protein quality control become saturated as most of PMP22 is very unstable and needs to be degraded. Upon saturation of the proteasomes, misfolded PMP22 is accumulating and aggregating, leading to a decrease of functional PMP22 being trafficked to the plasma membrane, ultimately leading to demyelination (Marinko et al. 2020; D'Urso et al. 1998). Increasing autophagy can lessen the burden of proteasomes and thus increase PMP22 transport to the plasma membrane, showing how trafficking defects in Schwann cells as secondary mechanisms can lead to demyelination (Fortun et al. 2007; Rangaraju et al. 2010). Further, in patient nerves increased levels of ErbB2/3 were found in Schwann cells, this could potentially mean a defective degradation pathway (Massa et al. 2006). Whether the possible defect in degradation is a secondary effect due to a saturated autophagic system or a parallel defect remains to be investigated. Interestingly, early studies report axonal transport defects in mice with mutated PMP22 showing slowed axonal transport of neurofilaments, decreased microtubule stability and abnormal neurofilament phosphorylation opening up the possibility of secondary trafficking defects in demyelinated neurons (S. M. de Waegh et al. 1992; S. De Waegh and Brady 1990).

CMT1C

In autosomal dominant CMT1C point mutations in *LITAF*, also known as *SIMPLE*, are identified to cause the disease (Street et al. 2003). *LITAF* encodes a 161 amino acid protein (Lipopolysaccharide-induced tumor necrosis factor- α factor) with one transmembrane domain that is inserted to the membrane post-translationally, all mutations occur in this domain. Therefore, mutated *LITAF* no longer localizes to endosomes but is cytosolic (S. M. Lee et al. 2011). *LITAF* interacts with *STAM1*, *Hrs* and *TSG101*, ESCRT proteins of the degradative pathway (S. M. Lee et al. 2012). The cytosolic mutant competes with endosomally located *LITAF* for *Hrs*, leading to deficient *Hrs* recruitment to endosomes and a lack of ESCRT recruitment. This lack of recruitment has been shown to decrease EGFR degradation leading to prolonged ERK1/2 signaling. Late endosomes/lysosomes are enlarged in patients' fibroblasts, similarly to the phenotype reported for mutant *FIG4* in CMT4J showing a defect in the degradative pathway (Edgar et al. 2020). By activating cation channel *TRPML1*, a homeostasis regulator of lysosomes in mammalian cells, the authors were able to rescue the vacuolar phenotype of both *LITAF* or *FIG4* knockout cells demonstrating a common pathway. It will be essential to unravel how the enlarged endolysosomes in both CMT types lead to the pathology. A possibility offers deficient ErbB3 degradation that has been shown in CMT mutants also leading to prolonged ERK1/2 signaling and demyelination (S. M. Lee et al. 2012). An overall summary of how genes causing CMT affect trafficking in Schwann cells is shown in figure 2.

TREATMENTS

Currently there is no cure for CMT, nor is there a treatment that addresses the specific phenotypes of CMT. Patients can only battle the disorder with physical and occupational therapies, as well as with pain-relief medication or surgeries to cope with the symptoms. Pinpointing the specific disruption in intracellular transport can help to identify new therapeutic targets, for current therapeutic prospects in CMT, we refer to two excellent recent reviews (Beijer et al. 2019; Morena et al. 2019). However, since axonal transport is disrupted in many subtypes of CMT, we briefly want to discuss the potential of HDAC6 inhibitors as a treatment for CMT.

HDAC6 inhibitor treatment alleviates many of the trafficking phenotypes in several models of different CMT types. HDAC6 deacetylates tubulin, making it unstable. By inhibiting HDAC6, tubulin remains more stable, which improves the basis for intracellular transport. Other targets of HDAC6's deacetylation function include heat shock protein 90, cortactin and Miro1, linking it to the elimination process of misfolded proteins and mitochondrial transport. HDAC6 is also proposed to play a role in response to eliminate misfolded proteins independent of its deacetylation function. It shows a high binding affinity for ubiquitinated proteins and can interact with dynein motor proteins directly. Especially in different CMT2 types HDAC6 inhibitors have been shown to be beneficial (for a review please see (Rossaert and Van Den Bosch 2020)). For example, treatment with HDAC6 inhibitor partially rescued phenotypes displayed by mice with mutant HSPB1, models for CMT2F (D'Ydewalle et al. 2011). But also in mice modelling CMT2D (caused by mutated GlyRS) the treatment with HDAC6 inhibitor has been shown to restore function (Benoy et al. 2018; Mo et al. 2018). Due to its direct interaction with Miro1 HDAC6 inhibitor was also tested as a treatment for CMT2A in a mouse model, where it even rescued motor dysfunction when given after symptom onset, giving it great therapeutic potential (Picci et al. 2020). Its role in misfolded protein clearance has shown a promising treatment strategy for CMT1A, where an HDAC6 inhibitor leads to improved nerve integrity as well as improved motor behaviour in C22 mice (Ha et al. 2020). Overall, HDAC6's inhibitors are shown to be promising therapeutic targets for several CMT subtypes that are currently being developed (Shen and Kozikowski 2020). The beneficial effect of HDAC6 inhibitors on different CMT subtypes also shifts HDAC6's involvement in the pathogenesis into focus of future research, also in the subtypes not yet explored. To develop new therapeutic strategies and model systems we refer to an excellent review by the Timmerman lab, highlighting recent advances in modelling CMT (Juneja et al. 2019).

CONCLUDING REMARKS

Overall, it is fascinating to see that mutations in very diverse proteins can all lead to similar defects in intracellular transport. Whether the mutations cause a direct defect in traffic by affecting the stability of the cytoskeleton, or whether the trafficking defects are secondary due to disrupted signaling (which ultimately also affects the stability of the cytoskeleton) remains to be elucidated for many CMT subtypes. Here we tried to give enough detailed insights into the different trafficking defects observed to encourage more studies that investigate similar defects in multiple CMT disorders for better comparability in the search for a common denominator and to look at the system of intracellular transport as a highly fluid and dynamic system. The sheer number of results indicating trafficking defects in all the different CMT subtypes is a solid basis to suspect abnormal trafficking as the underlying pathomechanism. However, many studies that claim trafficking defects only look at static data and lack comparability with each other. More experiments generally looking

at cytoskeletal integrity, mitochondrial transport, retrograde transport of receptors, recycling and degradation for each subtype are needed for a holistic approach to CMT pathology as well as, checking phenotypes reported for one subtype in the others. This also applies for CMT subtypes not mentioned in this review that have, as of yet, no or less reported trafficking phenotypes.

CONFLICT OF INTEREST

The authors declare that the research was conducted in the absence of any commercial or financial relationships that could be construed as a potential conflict of interest.

FUNDING

This work was funded by the Deutsche Forschungsgemeinschaft (DFG) Grant No. 427899738, and the Forschungsförderung of the University Medical Center Göttingen to KB.

Table1: An overview of the CMT mutations involved in intracellular trafficking discussed in this review, including their relevant phenotypes.

Type	Gene symbol	Gene name	Trafficking phenotype	References
CMT1A	<i>PMP22</i>	Peripheral myelin protein 22	autophagy/saturation of proteasome, disrupted PMP22 transport, elevated ErbB levels, reduction in slow axonal transport, altered cytoskeletal organization and NF phosphorylation	(Marinko et al. 2020; Fortun et al. 2007; Rangaraju et al. 2010; Massa et al. 2006; S. M. de Waegh et al. 1992; S. De Waegh and Brady 1990)
CMT1C	<i>LITAF</i>	Lipopolysaccharide induced TNF factor	mislocalization from early endosomes to cytosol, reduced ESCRT recruitment, decreased EGFR degradation, enlarged endosomes/lysosomes	(S. M. Lee et al. 2011; 2012; Edgar et al. 2020)
CMTX	<i>GJB1</i>	Gap junction protein beta 1	dysfunctional anterograde trafficking of GJB1, defects in retrograde axonal transport and neurofilament phosphorylation	(Vavlitou et al. 2010; Abrams et al. 2003; Deschênes et al. 1997; K. A. Kleopa et al. 2006; Yum et al. 2002)
CMT2A1	<i>KIF1B</i>	Kinesin family member 1B	defects in IGFR1 transport, perinuclear accumulation and defects in anterograde cargo transport	(F. Xu et al. 2018; C. Zhao et al. 2001)
CMT2A2	<i>MFN2</i>	Mitofusin 2	disturbed mitochondrial transport, mitochondria aggregation in proximal segment, loss of tubulin acetylation	(Bernard-Marissal et al. 2019; Baloh et al. 2007; Saporta et al. 2015; Picci et al. 2020)

Type	Gene symbol	Gene name	Trafficking phenotype	References
CMT2B	<i>RAB7A</i>	Rab7A, Member RAS oncogene family	altered retrograde traffic, altered TrkA/EGFR signaling, decreased RILP levels, increased peripherin interaction, disturbed retromer binding, reduced autophagic flux	(Janssens et al. 2014; Zhang et al. 2013; BasuRay et al. 2013; Basuray et al. 2010; Seaman et al. 2009; Cogli et al. 2013; Spinosa et al. 2008; Colecchia et al. 2018)
CMT2D	<i>GARS1</i>	Glycyl-tRNA synthetase 1	reduced acetylated tubulin levels, disrupted mitochondria transport, novel binding to HDAC6 and TrkA, disrupted NGF transport, increased interaction with neuropilin-1 → disrupted interaction with VEGFR	(He et al. 2015; Benoy et al. 2018; Mo et al. 2018; J. Y. Kim et al. 2016; Sleight et al. 2017)
CMT2E/ CMT1F	<i>NEFL</i>	Neurofilament light	disrupted anterograde traffic of NF-L (aggregation/accumulation) and mitochondria	(Brownlees et al. 2002; Pérez-Ollé et al. 2005; Saporta et al. 2015)
CMT2F	<i>HSPB1</i>	Heat shock protein family B (small) member 1	intracellular aggregates NF-M, disturbed retrograde mitochondrial transport, increased binding to α -tubulin, reduced autophagic flux	(Ackerley et al. 2006; D'Ydewalle et al. 2011; Kalmar et al. 2017; J. Y. Kim et al. 2016; Almeida-Souza et al. 2011; Haidar et al. 2019)
CMT2O	<i>DYNC1H1</i>	Dynein cytoplasmic 1, heavy chain 1	decreased retrograde transport of lysosomes and trophic factors, reduced mitochondrial transport	(Hafezparast et al. 2003; Ori-McKenney et al. 2010; Perlson et al. 2009; Jing Zhao et al. 2016)
CMT2P/ CMT2G	<i>LRSAM1</i>	Leucine-rich repeat- and sterile alpha motif-containing 1	Altered interaction with ESCRT protein TSG101 and altered EGFR degradation	(Guernsey et al. 2010; Palaima et al. 2021)
DI- CMTB	<i>DNM2</i>	Dynamin 2	blocks dynamin-dependent endocytosis, defects in microtubule stability	(Tanabe and Takei 2009; Sidiropoulos et al. 2012)
CMT4B1	<i>MTMR2</i>	Myotubularin related protein 2	GluR2 uptake increases upon loss of functional protein, also lack of recycling	(H. W. Lee et al. 2010; Bolino et al. 2004; Berger et al.

Type	Gene symbol	Gene name	Trafficking phenotype	References
CMT4B2	<i>MTMR13</i>	Myotubularin related protein 13	initiation/missorting into lysosomes, altered EGFR degradation	2011; Cao et al. 2008)
CMT4B3	<i>MTMR5</i>	Myotubularin related protein 5		
CMT4C	<i>SH3TC2</i>	SH3 domain and teratricopeptide repeats 2	decreased ErbB2 internalization, decreased interaction with Rab11, increased recycling of TF	(Gouttenoire et al. 2013; Roberts et al. 2010; Arnaud et al. 2009)
CMT4D	<i>NDRG1</i>	N-myc downstream regulated 1	disturbed Rab4 endosomes, disturbed TFR, e-cadherin, ErbB and LDL recycling, abnormal endosomal maturation, delayed fusion of MVBs with lysosomes	(L. X. Li et al. 2017; Kachhap et al. 2007; Pietiäinen et al. 2013)
CMT4H	<i>FGD4</i>	FYVE, RhoGEF and PH domain containing 4	defective TF internalization, alterations in microfilament structure	(Horn et al. 2012; Delague et al. 2007)
CMT4J	<i>FIG4</i>	Fig4 phosphoinositide 5-phosphatase	decreased levels of PI3,5P2 on endosomes, enlarged endosomes and lysosomes, decreased autophagic flux, defective cholesterol transport	(Bharadwaj et al. 2016; Ferguson et al. 2009; Vaccari et al. 2015)

REFERENCES

- Abrams, Charles K., Mona Freidin, Feliksas Bukauskas, Kostantin Dobrenis, Thaddeus A. Bargiello, Vytas K. Verselis, Michael V.L. Bennett, Lei Chen, and Zarife Sahenk. 2003. "Pathogenesis of X-Linked Charcot-Marie-Tooth Disease: Differential Effects of Two Mutations in Connexin 32." *Journal of Neuroscience* 23 (33): 10548–58. <https://doi.org/10.1523/jneurosci.23-33-10548.2003>.
- Ackerley, Steven, Paul A. James, Arran Kalli, Sarah French, Kay E. Davies, and Kevin Talbot. 2006. "A Mutation in the Small Heat-Shock Protein HSPB1 Leading to Distal Hereditary Motor Neuronopathy Disrupts Neurofilament Assembly and the Axonal Transport of Specific Cellular Cargoes." *Human Molecular Genetics* 15 (2): 347–54. <https://doi.org/10.1093/hmg/ddi452>.
- Adebola, Adijat A., Theo Di Castri, Chui Zhen He, Laura A. Salvatierra, Jian Zhao, Kristy Brown, Chyuan Sheng Lin, Howard J. Worman, and Ronald K.H. Liem. 2015. "Neurofilament Light Polypeptide Gene N98S Mutation in Mice Leads to Neurofilament Network Abnormalities and a Charcot-Marie-Tooth Type 2E Phenotype." *Human Molecular Genetics* 24 (8): 2163–74. <https://doi.org/10.1093/hmg/ddu736>.
- Adell, Manuel Alonso Y., Georg F. Vogel, Mehrshad Pakdel, Martin Müller, Herbert Lindner, Michael W. Hess, and David Teis. 2014. "Coordinated Binding of Vps4 to ESCRT-III Drives Membrane Neck Constriction during MVB Vesicle Formation." *Journal of Cell Biology* 205 (1): 33–49. <https://doi.org/10.1083/jcb.201310114>.
- Almeida-Souza, Leonardo, Bob Asselbergh, Constantin d'Ydewalle, Kristof Moonens, Sofie Goethals, Vicky de Winter, Abdelkrim Azmi, et al. 2011. "Small Heat-Shock Protein HSPB1 Mutants Stabilize Microtubules in Charcot-Marie-Tooth Neuropathy." *Journal of Neuroscience* 31 (43): 15320–28. <https://doi.org/10.1523/JNEUROSCI.3266-11.2011>.
- Antonellis, Anthony, Rachel E. Ellsworth, Nyamkhisig Sambughin, Imke Puls, Annette Abel, Shih Queen Lee-Lin, Alben Jordanova, et al. 2003. "Glycyl TRNA Synthetase Mutations in Charcot-Marie-Tooth Disease Type 2D and Distal Spinal Muscular Atrophy Type V." *American Journal of Human Genetics* 72 (5): 1293–

99. <https://doi.org/10.1086/375039>.
- Argente-Escrig, Herminia, Ana Sánchez-Monteaudo, Marina Frascuet, Elvira Millet-Sancho, Maria Dolores Martínez-Rubio, Inmaculada Pitarch, Miguel Tomás, Carmen Espinós, Vincenzo Lupo, and Teresa Sevilla. 2019. "A Very Mild Phenotype of Charcot-Marie-Tooth Disease Type 4H Caused by Two Novel Mutations in FGD4." *Journal of the Neurological Sciences* 402 (May): 156–61. <https://doi.org/10.1016/j.jns.2019.05.015>.
- Arnaud, Estelle, Jennifer Zenker, A.-S. de Preux Charles, Claudia Stendel, Andreas Roos, Jean Jacques Médard, Nicolas Tricaud, et al. 2009. "SH3TC2/KIAA1985 Protein Is Required for Proper Myelination and the Integrity of the Node of Ranvier in the Peripheral Nervous System." *Proceedings of the National Academy of Sciences of the United States of America* 106 (41): 17528–33. <https://doi.org/10.1073/pnas.1011320107>.
- Bache, Kristi G., Andreas Brech, Anja Mehlum, and Harald Stenmark. 2003. "Hrs Regulates Multivesicular Body Formation via ESCRT Recruitment to Endosomes." *Journal of Cell Biology* 162 (3): 435–42. <https://doi.org/10.1083/jcb.200302131>.
- Bakker, Jeroen, Menno Spits, Jacques Neefjes, and Ilana Berlin. 2017. "The EGFR Odyssey - from Activation to Destruction in Space and Time." *Journal of Cell Science* 130 (24): 4087–96. <https://doi.org/10.1242/jcs.209197>.
- Baloh, Robert H., Robert E. Schmidt, Alan Pestronk, and Jeffrey Milbrandt. 2007. "Altered Axonal Mitochondrial Transport in the Pathogenesis of Charcot-Marie-Tooth Disease from Mitofusin 2 Mutations." *Journal of Neuroscience* 27 (2): 422–30. <https://doi.org/10.1523/JNEUROSCI.4798-06.2007>.
- BasuRay, Soumik, Sanchita Mukherjee, Elsa G Romero, Matthew N J Seaman, and Angela Wandinger-Ness. 2013. "Rab7 Mutants Associated with Charcot-Marie-Tooth Disease Cause Delayed Growth Factor Receptor Transport and Altered Endosomal and Nuclear Signaling." *The Journal of Biological Chemistry* 288 (2): 1135–49. <https://doi.org/10.1074/jbc.M112.417766>.
- Basuray, Soumik, Sanchita Mukherjee, Elsa Romero, Michael C. Wilson, and Angela Wandinger-ness. 2010. "Rab7 Mutants Associated with Charcot-Marie-Tooth Disease Exhibit Enhanced NGF-Stimulated Signaling." *PLoS ONE* 5 (12). <https://doi.org/10.1371/journal.pone.0015351>.
- Beijer, Danique, Angela Sisto, Jonas Van Lent, Jonathan Baets, and Vincent Timmerman. 2019. "Defects in Axonal Transport in Inherited Neuropathies." *Journal of Neuromuscular Diseases* 6 (4): 401–19. <https://doi.org/10.3233/JND-190427>.
- Belgrad, Jillian, Raffaella de Pace, and R. Douglas Fields. 2020. "Autophagy in Myelinating Glia." *Journal of Neuroscience* 40 (2): 256–66. <https://doi.org/10.1523/JNEUROSCI.1066-19.2019>.
- Benoy, Veronick, Lawrence Van Helleputte, Robert Prior, Constantin D'Ydewalle, Wanda Haeck, Natasja Geens, Wendy Scheveneels, et al. 2018. "HDAC6 Is a Therapeutic Target in Mutant GARS-Induced Charcot-Marie-Tooth Disease." *Brain* 141 (3): 673–87. <https://doi.org/10.1093/brain/awx375>.
- Berger, Philipp, Sonja Bonneick, Susan Willi, Matthias Wymann, and Ueli Suter. 2002. "Loss of Phosphatase Activity in Myotubularin-Related Protein 2 Is Associated with Charcot-Marie-Tooth Disease Type 4B1." *Human Molecular Genetics* 11 (13): 1569–79. <https://doi.org/10.1093/hmg/11.13.1569>.
- Berger, Philipp, Kristian Tersar, Kurt Ballmer-Hofer, and Ueli Suter. 2011. "The CMT4B Disease-Causing Proteins MTMR2 and MTMR13/SBF2 Regulate AKT Signalling." *Journal of Cellular and Molecular Medicine* 15 (2): 307–15. <https://doi.org/10.1111/j.1582-4934.2009.00967.x>.
- Bergoffen, J., S. S. Scherer, S. Wang, M. Oronzi Scott, L. J. Bone, D. L. Paul, K. Chen, M. W. Lensch, P. F. Chance, and K. H. Fischbeck. 1993. "Connexin Mutations in X-Linked Charcot-Marie-Tooth Disease." *Science* 262 (5142): 2039–42. <https://doi.org/10.1126/science.8266101>.
- Bernard-Marissal, Nathalie, Gerben Van Hameren, Manisha Juneja, Christophe Pellegrino, Lauri Louhivuori, Luca Bartesaghi, Cylia Rochat, et al. 2019. "Altered Interplay between Endoplasmic Reticulum and Mitochondria in Charcot-Marie-Tooth Type 2A Neuropathy." *Proceedings of the National Academy of Sciences of the United States of America* 116 (6): 2328–37. <https://doi.org/10.1073/pnas.1810932116>.
- Bharadwaj, Rajnish, Kathleen M. Cunningham, Ke Zhang, and Thomas E. Lloyd. 2016. "FIG4 Regulates Lysosome Membrane Homeostasis Independent of Phosphatase Function." *Human Molecular Genetics* 25 (4): 681–92. <https://doi.org/10.1093/HMG/DDV505>.
- Birchmeier, Carmen, and David L.H. Bennett. 2016. *Neuregulin/ErbB Signaling in Developmental Myelin Formation and Nerve Repair. Current Topics in Developmental Biology*. 1st ed. Vol. 116. Elsevier Inc. <https://doi.org/10.1016/bs.ctdb.2015.11.009>.
- Bird, Thomas D. 2020. "Charcot-Marie-Tooth (CMT) Hereditary Neuropathy Overview 1 . Clinical Characteristics of Charcot-Marie-Tooth (CMT) Hereditary Neuropathy." *GeneReviews*, 1–22. <https://www.ncbi.nlm.nih.gov/books/NBK1358/>.

- Boland, Barry, Asok Kumar, Sooyeon Lee, Frances M. Platt, Jerzy Wegiel, W. Haung Yu, and Ralph A. Nixon. 2008. "Autophagy Induction and Autophagosome Clearance in Neurons: Relationship to Autophagic Pathology in Alzheimer's Disease." *Journal of Neuroscience* 28 (27): 6926–37. <https://doi.org/10.1523/JNEUROSCI.0800-08.2008>.
- Bolino, Alessandra, Annalisa Bolis, Stefano Carlo Previtali, Giorgia Dina, Simona Bussini, Gabriele Dati, Stefano Amadio, et al. 2004. "Disruption of Mtmr2 CMT4B1-like Neuropathy with Myelin Outfolding and Impaired Spermatogenesis." *Journal of Cell Biology* 167 (4): 711–21. <https://doi.org/10.1083/jcb.200407010>.
- Bolino, Alessandra, Maria Muglia, Francesca Luisa Conforti, Eric LeGuern, Mustafa A.M. Salih, Domna Maria Georgiou, Kyproula Christodoulou, et al. 2000. "Charcot-Marie-Tooth Type 4B Is Caused by Mutations in the Gene Encoding Myotubularin-Related Protein-2." *Nature Genetics* 25 (1): 17–19. <https://doi.org/10.1038/75542>.
- Bolis, Annalisa, Silvia Coviello, Simona Bussini, Giorgia Dina, Celia Pardini, Stefano Carlo Previtali, Mariachiara Malaguti, et al. 2005. "Loss of Mtmr2 Phosphatase in Schwann Cells but Not in Motor Neurons Causes Charcot-Marie-Tooth Type 4B1 Neuropathy with Myelin Outfoldings." *Journal of Neuroscience* 25 (37): 8567–77. <https://doi.org/10.1523/JNEUROSCI.2493-05.2005>.
- Bonifacino, Juan S., and Aitor Hierro. 2011. "Transport According to GARP: Receiving Retrograde Cargo at the Trans-Golgi Network." *Trends in Cell Biology* 21 (3): 159–67. <https://doi.org/10.1016/j.tcb.2010.11.003>.
- Brito, Olga Martins De, and Luca Scorrano. 2008. "Mitofusin 2 Tethers Endoplasmic Reticulum to Mitochondria." *Nature* 456 (7222): 605–10. <https://doi.org/10.1038/nature07534>.
- Brownlees, Janet, Steven Ackerley, Andrew J. Grierson, Nick J.O. Jacobsen, Kerry Shea, Brian H. Anderton, P. Nigel Leigh, Christopher E. Shaw, and Christopher C.J. Miller. 2002. "Charcot-Marie-Tooth Disease Neurofilament Mutations Disrupt Neurofilament Assembly and Axonal Transport." *Human Molecular Genetics* 11 (23): 2837–44. <https://doi.org/10.1093/hmg/11.23.2837>.
- Bu, Wenyu, Kim Buay Lim, Yuan Hong Yu, Ai Mei Chou, Thankiah Sudhaharan, and Sohail Ahmed. 2010. "Cdc42 Interaction with N-WASP and Toca-1 Regulates Membrane Tubulation, Vesicle Formation and Vesicle Motility: Implications for Endocytosis." *PLoS ONE* 5 (8). <https://doi.org/10.1371/journal.pone.0012153>.
- Bucci, Cecilia, Mario Chiariello, Daniela Lattero, Monica Maiorano, and Carmelo B. Bruni. 1999. "Interaction Cloning and Characterization of the cDNA Encoding the Human Prenylated Rab Acceptor (PRA1)." *Biochemical and Biophysical Research Communications* 258 (3): 657–62. <https://doi.org/10.1006/bbrc.1999.0651>.
- Bucci, Cecilia, Robert G. Parton, Ian H. Mather, Henk Stunnenberg, Kai Simons, Bernard Hoflack, and Marino Zerial. 1992. "The Small GTPase Rab5 Functions as a Regulatory Factor in the Early Endocytic Pathway." *Cell* 70 (5): 715–28. [https://doi.org/10.1016/0092-8674\(92\)90306-W](https://doi.org/10.1016/0092-8674(92)90306-W).
- Cao, Canhong, Jonathan M Backer, Jocelyn Laporte, Edward J Bedrick, and Angela Wandinger-Ness. 2008. "Sequential Actions of Myotubularin Lipid Phosphatases Regulate Endosomal PI(3)P and Growth Factor Receptor Trafficking." *Molecular Biology of the Cell* 19 (August): 3334–46. <https://doi.org/10.1091/mbc.E08>.
- Castro, Carmen, Juan M. Gómez-Hernandez, Kaisa Silander, and Luis C. Barrio. 1999. "Altered Formation of Hemichannels and Gap Junction Channels Caused by C-Terminal Connexin-32 Mutations." *Journal of Neuroscience* 19 (10): 3752–60. <https://doi.org/10.1523/jneurosci.19-10-03752.1999>.
- Chauvet, Sophie, Samia Cohen, Yutaka Yoshida, Lylia Fekrane, Jean Livet, Odile Gayet, Louis Segu, et al. 2007. "Gating of Sema3E/PlexinD1 Signaling by Neuropilin-1 Switches Axonal Repulsion to Attraction during Brain Development." *Neuron* 56 (5): 807–22. <https://doi.org/10.1016/j.neuron.2007.10.019>.
- Chen, Hsiuchen, Scott A. Detmer, Andrew J. Ewald, Erik E. Griffin, Scott E. Fraser, and David C. Chan. 2003. "Mitofusins Mfn1 and Mfn2 Coordinately Regulate Mitochondrial Fusion and Are Essential for Embryonic Development." *Journal of Cell Biology* 160 (2): 189–200. <https://doi.org/10.1083/jcb.200211046>.
- Cheng, Xiu Tang, Bing Zhou, Mei Yao Lin, Qian Cai, and Zu Hang Sheng. 2015. "Axonal Autophagosomes Recruit Dynein for Retrograde Transport through Fusion with Late Endosomes." *Journal of Cell Biology* 209 (3): 377–86. <https://doi.org/10.1083/jcb.201412046>.
- Chow, Clement Y, Yanling Zhang, James J Dowling, Natsuko Jin, Maja Adamska, Kensuke Shiga, Kinga Szigeti, et al. 2007. "Mutation of FIG4 Causes Neurodegeneration in the Pale Tremor Mouse and Patients with CMT4J." *Nature* 448 (7149): 68–72.
- Cioni, Jean Michel, Julie Qiaojin Lin, Anne V. Holtermann, Max Koppers, Maximilian A.H. Jakobs, Afnan Azizi, Benita Turner-Bridger, et al. 2019. "Late Endosomes Act as mRNA Translation Platforms and Sustain Mitochondria in Axons." *Cell* 176 (1–2): 56–72.e15. <https://doi.org/10.1016/j.cell.2018.11.030>.

- Cogli, Laura, Cinzia Progida, Claire L. Thomas, Bradley Spencer-Dene, Claudia Donno, Giampietro Schiavo, and Cecilia Bucci. 2013. "Charcot-Marie-Tooth Type 2B Disease-Causing RAB7A Mutant Proteins Show Altered Interaction with the Neuronal Intermediate Filament Peripherin." *Acta Neuropathologica* 125 (2): 257–72. <https://doi.org/10.1007/s00401-012-1063-8>.
- Colecchia, David, Mariangela Stasi, Margherita Leonardi, Fiore Manganelli, Maria Nolano, Bianca Maria Veneziani, Lucio Santoro, Eeva Liisa Eskelinen, Mario Chiariello, and Cecilia Bucci. 2018. "Alterations of Autophagy in the Peripheral Neuropathy Charcot-Marie-Tooth Type 2B." *Autophagy* 14 (6): 930–41. <https://doi.org/10.1080/15548627.2017.1388475>.
- D'Urso, Donatella, Reinhard Prior, Regine Greiner-Petter, Anneke A.W.M. Gabreëls-Festen, and Hans Werner Müller. 1998. "Overloaded Endoplasmic Reticulum-Golgi Compartments, a Possible Pathomechanism of Peripheral Neuropathies Caused by Mutations of the Peripheral Myelin Protein PMP22." *Journal of Neuroscience* 18 (2): 731–40. <https://doi.org/10.1523/jneurosci.18-02-00731.1998>.
- D'Ydewalle, Constantin, Jyothsna Krishnan, Driss M. Chiheb, Philip Van Damme, Joy Irobi, Alan P. Kozikowski, Pieter Vanden Berghe, Vincent Timmerman, Wim Robberecht, and Ludo Van Den Bosch. 2011. "HDAC6 Inhibitors Reverse Axonal Loss in a Mouse Model of Mutant HSPB1-Induced Charcot-Marie-Tooth Disease." *Nature Medicine* 17 (8): 968–74. <https://doi.org/10.1038/nm.2396>.
- Daub, Henrik, Kris Gevaert, Joel Vandekerckhove, André Sobel, and Alan Hall. 2001. "Rac/Cdc42 and P65PAK Regulate the Microtubule-Destabilizing Protein Stathmin through Phosphorylation at Serine 16." *Journal of Biological Chemistry* 276 (3): 1677–80. <https://doi.org/10.1074/jbc.C000635200>.
- Deinhardt, Katrin, Sara Salinas, Carole Verastegui, Rose Watson, Daniel Worth, Sarah Hanrahan, Cecilia Bucci, and Giampietro Schiavo. 2006. "Rab5 and Rab7 Control Endocytic Sorting along the Axonal Retrograde Transport Pathway." *Neuron* 52 (2): 293–305. <https://doi.org/10.1016/j.neuron.2006.08.018>.
- Delague, Valérie, Arnaud Jacquier, Tarik Hamadouche, Yannick Poitelon, Cécile Baudot, Irène Boccaccio, Eliane Chouery, et al. 2007. "Mutations in FGD4 Encoding the Rho GDP/GTP Exchange Factor FRABIN Cause Autosomal Recessive Charcot-Marie-Tooth Type 4H." *American Journal of Human Genetics* 81 (1): 1–16. <https://doi.org/10.1086/518428>.
- Delcroix, Jean Dominique, Janice S. Valletta, Chengbiao Wu, Stephen J. Hunt, Anthony S. Kowal, and William C. Mobley. 2003. "NGF Signaling in Sensory Neurons: Evidence That Early Endosomes Carry NGF Retrograde Signals." *Neuron* 39 (1): 69–84. [https://doi.org/10.1016/S0896-6273\(03\)00397-0](https://doi.org/10.1016/S0896-6273(03)00397-0).
- Derivery, Emmanuel, Carla Sousa, Jérémie J. Gautier, Bérangère Lombard, Damarys Loew, and Alexis Gautreau. 2009. "The Arp2/3 Activator WASH Controls the Fission of Endosomes through a Large Multiprotein Complex." *Developmental Cell* 17 (5): 712–23. <https://doi.org/10.1016/j.devcel.2009.09.010>.
- Deschênes, Suzanne M., Jessica L. Walcott, Tamara L. Wexler, Steven S. Scherer, and Kenneth H. Fischbeck. 1997. "Altered Trafficking of Mutant Connexin32." *Journal of Neuroscience* 17 (23): 9077–84. <https://doi.org/10.1523/jneurosci.17-23-09077.1997>.
- Dompierre, Jim P., Juliette D. Godin, Bénédicte C. Charrin, Fabrice P. Cordelières, Stephen J. King, Sandrine Humbert, and Frédéric Saudou. 2007. "Histone Deacetylase 6 Inhibition Compensates for the Transport Deficit in Huntington's Disease by Increasing Tubulin Acetylation." *Journal of Neuroscience* 27 (13): 3571–83. <https://doi.org/10.1523/JNEUROSCI.0037-07.2007>.
- Edgar, James R., Anita K. Ho, Matilde Laurá, Rita Horvath, Mary M. Reilly, J. Paul Luzio, and Rhys C. Roberts. 2020. "A Dysfunctional Endolysosomal Pathway Common to Two Sub-Types of Demyelinating Charcot-Marie-Tooth Disease." *Acta Neuropathologica Communications* 8 (1): 1–16. <https://doi.org/10.1186/s40478-020-01043-z>.
- Fabrizi, Gian Maria, Tiziana Cavallaro, Chiara Angiari, Ilaria Cabrini, Federica Taioli, Giovanni Malerba, Laura Bertolasi, and Nicolo Rizzuto. 2007. "Charcot-Marie-Tooth Disease Type 2E, a Disorder of the Cytoskeleton." *Brain* 130 (2): 394–403. <https://doi.org/10.1093/brain/awl284>.
- Ferguson, Cole J., Guy M. Lenk, and Miriam H. Meisler. 2009. "Defective Autophagy in Neurons and Astrocytes from Mice Deficient in PI(3,5)P2." *Human Molecular Genetics* 18 (24): 4868–78. <https://doi.org/10.1093/hmg/ddp460>.
- Fortun, Jenny, Jonathan D. Verrier, Jocelyn C. Go, Irina Madorsky, William A. Jr. Dunn, and Lucia Notterpek. 2007. "The Formation of Peripheral Myelin Protein 22 Aggregates Is Hindered by the Enhancement of Autophagy and Expression of Cytoplasmic Chaperones." *Neurobiology of Disease* 25 (2): 252–65. <https://www.ncbi.nlm.nih.gov/pmc/articles/PMC3624763/pdf/nihms412728.pdf>.
- Fransson, Åsa, Aino Ruusala, and Pontus Aspenström. 2006. "The Atypical Rho GTPases Miro-1 and Miro-2 Have Essential Roles in Mitochondrial Trafficking." *Biochemical and Biophysical Research Communications* 344 (2): 500–510. <https://doi.org/10.1016/j.bbrc.2006.03.163>.
- Futter, Clare E., Adele Pearse, Lindsay J. Hewlett, and Colin R. Hopkins. 1996. "Multivesicular Endosomes

- Containing Internalized EGF-EGF Receptor Complexes Mature and Then Fuse Directly with Lysosomes." *Journal of Cell Biology* 132 (6): 1011–23. <https://doi.org/10.1083/jcb.132.6.1011>.
- Gerber, Daniel, Monica Ghidinelli, Elisa Tinelli, Christian Somandin, Joanne Gerber, Jorge A. Pereira, Andrea Ommer, et al. 2019. "Schwann Cells, but Not Oligodendrocytes, Depend Strictly on Dynamin 2 Function." *eLife* 8: 1–26. <https://doi.org/10.7554/eLife.42404>.
- Glater, Elizabeth E., Laura J. Megeath, R. Steven Stowers, and Thomas L. Schwarz. 2006. "Axonal Transport of Mitochondria Requires Milton to Recruit Kinesin Heavy Chain and Is Light Chain Independent." *Journal of Cell Biology* 173 (4): 545–57. <https://doi.org/10.1083/jcb.200601067>.
- Goold, Robert G., and Phillip R. Gordon-Weeks. 2003. "NGF Activates the Phosphorylation of MAP1B by GSK3 β through the TrkA Receptor and Not the P75NTR Receptor." *Journal of Neurochemistry* 87 (4): 935–46. <https://doi.org/10.1046/j.1471-4159.2003.02062.x>.
- Gorvel, Jean-Pierre, Philippe Chavrier, Marino Zerial, and Jean Gruenberg. 1991. "Rab5 Controls Early Endosome." *Cell* 64: 915–25.
- Gouttenoire, Estelle Arnaud, Vincenzo Lupo, Eduardo Calpena, Luca Bartesaghi, Fanny Schüpfer, Jean Jacques Médard, Fabienne Maurer, et al. 2013. "Sh3tc2 Deficiency Affects Neuregulin-1/ErbB Signaling." *Glia* 61 (7): 1041–51. <https://doi.org/10.1002/glia.22493>.
- Groh, Janos, Kristina Heintz, Bianca Kohl, Carsten Wessig, Juliane Greeske, Stefan Fischer, and Rudolf Martini. 2010. "Attenuation of MCP-1/CCL2 Expression Ameliorates Neuropathy in a Mouse Model for Charcot-Marie-Tooth 1X." *Human Molecular Genetics* 19 (18): 3530–43. <https://doi.org/10.1093/hmg/ddq269>.
- Guernsey, Duane L., Haiyan Jiang, Karen Bedard, Susan C. Evans, Meghan Ferguson, Makoto Matsuoka, Christine Macgillivray, et al. 2010. "Mutation in the Gene Encoding Ubiquitin Ligase LRSAM1 in Patients with Charcot-Marie-Tooth Disease." *PLoS Genetics* 6 (8). <https://doi.org/10.1371/journal.pgen.1001081>.
- Guglielmo, Gianni M. Di, Patricia C. Baass, Wei Jia Ou, Barry I. Posner, and John J.M. Bergeron. 1994. "Compartmentalization of SHC, GRB2 and MSOS, and Hyperphosphorylation of Raf-1 by EGF but Not Insulin in Liver Parenchyma." *EMBO Journal* 13 (18): 4269–77. <https://doi.org/10.1002/j.1460-2075.1994.tb06747.x>.
- Ha, Nina, Young Il Choi, Namhee Jung, Ju Young Song, Dae Kwon Bae, Min Cheol Kim, Yong Jae Lee, et al. 2020. "A Novel Histone Deacetylase 6 Inhibitor Improves Myelination of Schwann Cells in a Model of Charcot-Marie-Tooth Disease Type 1A." *British Journal of Pharmacology* 177 (22): 5096–5113. <https://doi.org/10.1111/bph.15231>.
- Hafezparast, Majid, Rainer Klocke, Christiana Ruhrberg, Andreas Marquardt, Azlina Ahmad-Annur, Samantha Bowen, Giovanna Lalli, et al. 2003. "Mutations in Dynein Link Motor Neuron Degeneration to Defects in Retrograde Transport." *Science* 300 (5620): 808–12. <https://doi.org/10.1126/science.1083129>.
- Haglund, Kaisa, Sara Sigismund, Simona Polo, Iwona Szymkiewicz, Pier Paolo Di Fiore, and Ivan Dikic. 2003. "Multiple Monoubiquitination of RTKs Is Sufficient for Their Endocytosis and Degradation." *Nature Cell Biology* 5 (5): 461–66. <https://doi.org/10.1038/ncb983>.
- Haidar, Mansour, Bob Asselbergh, Elias Adriaenssens, Vicky De Winter, Jean Pierre Timmermans, Michaela Auer-Grumbach, Manisha Juneja, and Vincent Timmerman. 2019. "Neuropathy-Causing Mutations in HSPB1 Impair Autophagy by Disturbing the Formation of SQSTM1/P62 Bodies." *Autophagy* 15 (6): 1051–68. <https://doi.org/10.1080/15548627.2019.1569930>.
- He, Weiwei, Ge Bai, Huihao Zhou, Na Wei, Nicholas M White, Janelle Lauer, Huaqing Liu, et al. 2015. "CMT2D Neuropathy Is Linked to the Neomorphic Binding Activity of Glycyl-TRNA Synthetase." *Nature* 526 (7575): 710–14. <https://doi.org/10.1038/nature15510.CMT2D>.
- Hopkins, C. R., and I. S. Trowbridge. 1983. "Internalization and Processing of Transferrin and the Transferrin Receptor in Human Carcinoma A431 Cells." *Journal of Cell Biology* 97 (2): 508–21. <https://doi.org/10.1083/jcb.97.2.508>.
- Horn, Michael, Reto Baumann, Jorge A. Pereira, Páris N.M. Sidiropoulos, Christian Somandin, Hans Welzl, Claudia Stendel, et al. 2012. "Myelin Is Dependent on the Charcot-Marie-Tooth Type 4H Disease Culprit Protein FRABIN/FGD4 in Schwann Cells." *Brain* 135 (12): 3567–83. <https://doi.org/10.1093/brain/aws275>.
- Horowitz, Arie, and Himabindu Reddy Seerapu. 2012. "Regulation of VEGF Signaling by Membrane Traffic." *Cell Signal* 24 (9): 1810–20. <https://doi.org/10.1016/j.cellsig.2012.05.007>.
- Hunter, Michael, Dora Angelicheva, Ivailo Tournev, Evan Ingley, Dick C. Chan, Gerald F. Watts, Ivo Kremensky, and Luba Kalaydjieva. 2005. "NDRG1 Interacts with APO A-I and A-II and Is a Functional Candidate for the HDL-C QTL on 8q24." *Biochemical and Biophysical Research Communications* 332 (4): 982–92. <https://doi.org/10.1016/j.bbrc.2005.05.050>.

- Janssens, Katrien, Sofie Goethals, Derek Atkinson, Biljana Ermanoska, Erik Fransen, Albena Jordanova, Michaela Auer-Grumbach, Bob Asselbergh, and Vincent Timmerman. 2014. "Human Rab7 Mutation Mimics Features of Charcot-Marie-Tooth Neuropathy Type 2B in Drosophila." *Neurobiology of Disease* 65: 211–19. <https://doi.org/10.1016/j.nbd.2014.01.021>.
- Johnson, L. S., K. W. Dunn, B. Pytowski, and T. E. McGraw. 1993. "Endosome Acidification and Receptor Trafficking: Bafilomycin A1 Slows Receptor Externalization by a Mechanism Involving the Receptor's Internalization Motif." *Molecular Biology of the Cell* 4 (12): 1251–66. <https://doi.org/10.1091/mbc.4.12.1251>.
- Jonghe, Peter De, Irina Mersivanova, Eva Nelis, Jurgen Del Favero, Jean Jacques Martin, Christine Van Broeckhoven, Oleg Evgrafov, and Vincent Timmerman. 2001. "Further Evidence That Neurofilament Light Chain Gene Mutations Can Cause Charcot-Marie-Tooth Disease Type 2E." *Annals of Neurology* 49 (2): 245–49. [https://doi.org/10.1002/1531-8249\(20010201\)49:2<245::AID-ANA45>3.0.CO;2-A](https://doi.org/10.1002/1531-8249(20010201)49:2<245::AID-ANA45>3.0.CO;2-A).
- Jordens, Ingrid, Mar Fernandez-Borja, Marije Marsman, Simone Dusseljee, Lennert Janssen, Jero Calafat, Hans Janssen, Richard Wubbolts, and Jacques Neefjes. 2001. "The Rab7 Effector Protein RILP Controls Lysosomal Transport by Inducing the Recruitment of Dynein-Dynactin Motors." *Current Biology* 11 (21): 1680–85. [https://doi.org/10.1016/S0960-9822\(01\)00531-0](https://doi.org/10.1016/S0960-9822(01)00531-0).
- Jovic, M, M Sharma, J Rahajeng, and S Caplan. 2010. "The Early Endosome: A Busy Sorting Station for Proteins at the Crossroads." *Histol Histopathol* 25 (1): 99–112. <https://doi.org/10.1007/s12020-009-9266-z.A>.
- Juneja, Manisha, Joshua Burns, Mario A. Saporta, and Vincent Timmerman. 2019. "Challenges in Modelling the Charcot-Marie-Tooth Neuropathies for Therapy Development." *Journal of Neurology, Neurosurgery and Psychiatry* 90 (1): 58–67. <https://doi.org/10.1136/jnnp-2018-318834>.
- Kachhap, Sushant K., Dennis Faith, David Z. Qian, Shabana Shabbeer, Nathan L. Galloway, Roberto Pili, Samuel R. Denmeade, Angelo M. DeMarzo, and Michael A. Carducci. 2007. "The N-Myc down Regulated Gene1 (NDRG1) Is a Rab4a Effector Involved in Vesicular Recycling of E-Cadherin." *PLoS ONE* 2 (9). <https://doi.org/10.1371/journal.pone.0000844>.
- Kalaydjieva, Luba, David Gresham, Rebecca Gooding, Lisa Heather, Frank Baas, Rosalein De Jonge, Karin Blechschmidt, et al. 2000. "N-Myc Downstream-Regulated Gene 1 Is Mutated in Hereditary Motor and Sensory Neuropathy-Lom." *American Journal of Human Genetics* 67 (1): 47–58. <https://doi.org/10.1086/302978>.
- Kalmar, Bernadett, Amy Innes, Klaus Wanisch, Alicia Koyen Kolaszynska, Amelie Pandraud, Gavin Kelly, Andrey Y. Abramov, Mary M. Reilly, Giampietro Schiavo, and Linda Greensmith. 2017. "Mitochondrial Deficits and Abnormal Mitochondrial Retrograde Axonal Transport Play a Role in the Pathogenesis of Mutant Hsp27-Induced Charcot Marie Tooth Disease." *Human Molecular Genetics* 26 (17): 3313–26. <https://doi.org/10.1093/hmg/ddx216>.
- Katzmann, David J., Markus Babst, and Scott D. Emr. 2001. "Ubiquitin-Dependent Sorting into the Multivesicular Body Pathway Requires the Function of a Conserved Endosomal Protein Sorting Complex, ESCRT-I." *Cell* 106 (2): 145–55. [https://doi.org/10.1016/S0092-8674\(01\)00434-2](https://doi.org/10.1016/S0092-8674(01)00434-2).
- Kim, Ji Yon, So Youn Woo, Young Bin Hong, Heesun Choi, Jisoo Kim, Hyunjung Choi, Inhee Mook-Jung, et al. 2016. "HDAC6 Inhibitors Rescued the Defective Axonal Mitochondrial Movement in Motor Neurons Derived from the Induced Pluripotent Stem Cells of Peripheral Neuropathy Patients with HSPB1 Mutation." *Stem Cells International* 2016. <https://doi.org/10.1155/2016/9475981>.
- Kim, Soo A., Panayiotis O. Vacratsis, Ron Firesteint, Michael L. Clearyt, and Jack E. Dixon. 2003. "Regulation of Myotubularin-Related (MTMR)2 Phosphatidylinositol Phosphatase by MTMR5, a Catalytically Inactive Phosphatase." *Proceedings of the National Academy of Sciences of the United States of America* 100 (8): 4492–97. <https://doi.org/10.1073/pnas.0431052100>.
- King, Rosalind H.M., David Chandler, Sash Lopaticki, Dexing Huang, Julian Blake, John R. Muddle, Trevor Kilpatrick, et al. 2011. "Ndr1 in Development and Maintenance of the Myelin Sheath." *Neurobiology of Disease* 42 (3): 368–80. <https://doi.org/10.1016/j.nbd.2011.01.030>.
- Kiral, Ferdi Ridvan, Friederike Elisabeth Kohrs, Eugene Jennifer Jin, and Peter Robin Hiesinger. 2018. "Rab GTPases and Membrane Trafficking in Neurodegeneration." *Current Biology* 28 (8): R471–86. <https://doi.org/10.1016/j.cub.2018.02.010>.
- Kleopa, K. A., E. Zamba-Papanicolaou, X. Alevra, P. Nicolaou, D. M. Georgiou, A. Hadjisavvas, T. Kyriakides, and K. Christodoulou. 2006. "Phenotypic and Cellular Expression of Two Novel Connexin32 Mutations Causing CMT1X." *Neurology* 66 (3): 396–402. <https://doi.org/10.1212/01.wnl.0000196479.93722.59>.
- Kleopa, Kleopas A., Charles K. Abrams, and Steven S. Scherer. 2012. "How Do Mutations in GJB1 Cause X-Linked Charcot-Marie-Tooth Disease?" *Brain Research* 1487: 198–205. <https://doi.org/10.1016/j.brainres.2012.03.068>.
- Komatsu, Masaaki, Satoshi Waguri, Masato Koike, Yu shin Sou, Takashi Ueno, Taiichi Hara, Noboru Mizushima,

- et al. 2007. "Homeostatic Levels of P62 Control Cytoplasmic Inclusion Body Formation in Autophagy-Deficient Mice." *Cell* 131 (6): 1149–63. <https://doi.org/10.1016/j.cell.2007.10.035>.
- Konishi, Yoshiyuki, and Mitsutoshi Setou. 2009. "Tubulin Tyrosination Navigates the Kinesin-1 Motor Domain to Axons." *Nature Neuroscience* 12 (5): 559–67. <https://doi.org/10.1038/nn.2314>.
- Kvainickas, Arunas, Ana Jimenez-Orgaz, Heike Nägele, Zehan Hu, Jörn Dengjel, and Florian Steinberg. 2017. "Cargo-Selective SNX-BAR Proteins Mediate Retromer Trimer Independent Retrograde Transport." *Journal of Cell Biology* 216 (11): 3677–93. <https://doi.org/10.1083/jcb.201702137>.
- Lancaster, Eunjoo, Jian Li, Taleen Hanania, Ronald Liem, Mark A. Scheideler, and Steven S. Scherer. 2018. "Myelinated Axons Fail to Develop Properly in a Genetically Authentic Mouse Model of Charcot-Marie-Tooth Disease Type 2E." *Experimental Neurology* 308 (June): 13–25. <https://doi.org/10.1016/j.expneurol.2018.06.010>.
- Laser-Azogui, Adi, Micha Kornreich, Eti Malka-Gibor, and Roy Beck. 2015. "Neurofilament Assembly and Function during Neuronal Development." *Current Opinion in Cell Biology* 32: 92–101. <https://doi.org/10.1016/j.ceb.2015.01.003>.
- Lauffer, Benjamin E.L., Cristina Melero, Paul Temkin, Cai Lei, Wanjin Hong, Tanja Kortemme, and Mark Von Zastrow. 2010. "SNX27 Mediates PDZ-Directed Sorting from Endosomes to the Plasma Membrane." *Journal of Cell Biology* 190 (4): 565–74. <https://doi.org/10.1083/jcb.201004060>.
- Laurino, Lisandro, Xiaoxin X. Wang, Becky A. de la Houssaye, Lucas Sosa, Sebastian Dupraz, Alfredo Cáceres, Karl H. Pfenniger, and Santiago Quiroga. 2005. "PI3K Activation by IGF-1 Is Essential for the Regulation of Membrane Expansion at the Nerve Growth Cone." *Journal of Cell Science* 118 (16): 3653–63. <https://doi.org/10.1242/jcs.02490>.
- Lee, Hyun Woo, Youngrim Kim, Kihoon Han, Hyun Kim, and Eunjoon Kim. 2010. "The Phosphoinositide 3-Phosphatase MTMR2 Interacts with PSD-95 and Maintains Excitatory Synapses by Modulating Endosomal Traffic." *Journal of Neuroscience* 30 (16): 5508–18. <https://doi.org/10.1523/JNEUROSCI.4283-09.2010>.
- Lee, Samuel M., Lih-Shen Chin, and Lian Li. 2012. "Charcot-Marie-Tooth Disease-Linked Protein SIMPLE Functions with the ESCRT Machinery in Endosomal Trafficking." *The Journal of Cell Biology* 199 (5): 799–816. <https://doi.org/10.1083/jcb.201204137>.
- Lee, Samuel M., James A. Olzmann, Lih Shen Chin, and Lian Li. 2011. "Mutations Associated with Charcot-Marie-Tooth Disease Cause SIMPLE Protein Mislocalization and Degradation by the Proteasome and Aggresome-Autophagy Pathways." *Journal of Cell Science* 124 (19): 3319–31. <https://doi.org/10.1242/jcs.087114>.
- Lee, Samuel M., Lih-Shen Chin, and Lian Li. 2017. "Dysregulation of ErbB Receptor Trafficking and Signaling in Demyelinating Charcot-Marie-Tooth Disease." *Molecular Neurobiology* 54 (1): 87–100. <https://doi.org/10.1007/s12035-015-9668-2>. Dysregulation.
- Lee, Sooyeon, Hannah Bazick, Vinita Chittoor-Vinod, Mohammed Omar Al Salihi, Guangbin Xia, and Lucia Notterpek. 2018. "Elevated Peripheral Myelin Protein 22, Reduced Mitotic Potential, and Proteasome Impairment in Dermal Fibroblasts from Charcot-Marie-Tooth Disease Type 1A Patients." *American Journal of Pathology* 188 (3): 728–38. <https://doi.org/10.1016/j.ajpath.2017.10.021>.
- Lenk, Guy M., Cole J. Ferguson, Clement Y. Chow, Natsuko Jin, Julie M. Jones, Adrienne E. Grant, Sergey N. Zolov, et al. 2011. "Pathogenic Mechanism of the FIG4 Mutation Responsible for Charcot-Marie-Tooth Disease CMT4J." *PLoS Genetics* 7 (6). <https://doi.org/10.1371/journal.pgen.1002104>.
- Lerat, Justine, Corinne Magdelaine, H el ene Beauvais-Dzugan, Caroline Espil, Karima Ghorab, Philippe Latour, Paco Derouault, Franck Sturtz, and Anne Sophie Lia. 2019. "A Novel Pathogenic Variant of NEFL Responsible for Deafness Associated with Peripheral Neuropathy Discovered through Next-Generation Sequencing and Review of the Literature." *Journal of the Peripheral Nervous System* 24 (1): 139–44. <https://doi.org/10.1111/jns.12310>.
- Li, Ang, Hui-Ming Zhu, Yu Chen, Fang Yan, Zhong-Ying Liu, Zhen-Lin Li, Wei-Ren Dong, Lin Zhang, and Hai-Hong Wang. 2021. "Cdc42 Facilitates Axonogenesis by Enhancing Microtubule Stabilization in Primary Hippocampal Neurons." *Cellular and Molecular Neurobiology*. <https://doi.org/10.1007/s10571-021-01051-0>.
- Li, Li Xi, Gong Lu Liu, Zhi Jun Liu, Cong Lu, and Zhi Ying Wu. 2017. "Identification and Functional Characterization of Two Missense Mutations in NDRG1 Associated with Charcot-Marie-Tooth Disease Type 4D." *Human Mutation* 38 (11): 1569–78. <https://doi.org/10.1002/humu.23309>.
- Linder, Matts D., Mikko I. M ayr anp  a, Johan Per anen, Taija E. Pietil a, Vilja M. Pieti inen, Riikka Liisa Uronen, Vesa M. Olkkonen, Petri T. Kovanen, and Elina Ikonen. 2009. "Rab8 Regulates ABCA1 Cell Surface Expression and Facilitates Cholesterol Efflux in Primary Human Macrophages." *Arteriosclerosis, Thrombosis, and Vascular Biology* 29 (6): 883–88. <https://doi.org/10.1161/ATVBAHA.108.179481>.

- Lupo, Vincenzo, Máximo I. Galindo, Dolores Martínez-Rubio, Teresa Sevilla, Juan J. Vílchez, Francesc Palau, and Carmen Espinós. 2009. "Missense Mutations in the SH3TC2 Protein Causing Charcot-Marie-Tooth Disease Type 4C Affect Its Localization in the Plasma Membrane and Endocytic Pathway." *Human Molecular Genetics* 18 (23): 4603–14. <https://doi.org/10.1093/hmg/ddp427>.
- Magy, Laurent, Stéphane Mathis, Gwendal Le Masson, Cyril Goizet, Meriem Tazir, and Jean-Michel Vallat. 2018. "Updating the Classification of Inherited Neuropathies." *Neurology* 90 (10): e870–76. <https://doi.org/10.1212/wnl.0000000000005074>.
- Marat, Andrea L, and Volker Haucke. 2016. "Phosphatidylinositol 3-phosphates—at the Interface between Cell Signalling and Membrane Traffic." *The EMBO Journal* 35 (6): 561–79. <https://doi.org/10.15252/embj.201593564>.
- Marinko, Justin T., Bruce D. Carter, and Charles R. Sanders. 2020. "Direct Relationship between Increased Expression and Mistrafficking of the Charcot-Marie-Tooth-Associated Protein PMP22." *Journal of Biological Chemistry* 295 (34): 11963–70. <https://doi.org/10.1074/jbc.AC120.014940>.
- Markworth, Ronja, Youri Adolfs, Vivian Dambeck, Lars M. Steinbeck, Muriel Lizé, R. Jeroen Pasterkamp, Mathias Bähr, Camin Dean, and Katja Burk. 2019. "Sensory Axon Growth Requires Spatiotemporal Integration of CaSR and TrkB Signaling." *Journal of Neuroscience* 39 (30): 5842–60. <https://doi.org/10.1523/JNEUROSCI.0027-19.2019>.
- Massa, Roberto, Camilla Palumbo, Tiziana Cavallaro, Maria Beatrice Panico, Roberto Bei, Chiara Terracciano, Nicolò Rizzuto, Giorgio Bernardi, and Andrea Modesti. 2006. "Overexpression of ErbB2 and ErbB3 Receptors in Schwann Cells of Patients with Charcot-Marie-Tooth Disease Type 1A." *Muscle and Nerve* 33 (3): 342–49. <https://doi.org/10.1002/mus.20460>.
- Maxfield, F. R., and D. J. Yamashiro. 1987. "Endosome Acidification and the Pathways of Receptor-Mediated Endocytosis." *Advances in Experimental Medicine and Biology* 225: 189–98. https://doi.org/10.1007/978-1-4684-5442-0_16.
- Maxfield, Frederick R., and Timothy E. McGraw. 2004. "Endocytic Recycling." *Nature Reviews Molecular Cell Biology* 5 (2): 121–32. <https://doi.org/10.1038/nrm1315>.
- McCray, Brett A., Emmanuel Skordalakes, and J. Paul Taylor. 2010. "Disease Mutations in Rab7 Result in Unregulated Nucleotide Exchange and Inappropriate Activation." *Human Molecular Genetics* 19 (6): 1033–47. <https://doi.org/10.1093/hmg/ddp567>.
- McMahon, Harvey T., and Emmanuel Boucrot. 2011. "Molecular Mechanism and Physiological Functions of Clathrin-Mediated Endocytosis." *Nature Reviews Molecular Cell Biology* 12 (8): 517–33. <https://doi.org/10.1038/nrm3151>.
- Mersianova, Irina V., Alexander V. Perepelov, Alexander V. Polyakov, Vladimir F. Sitnikov, Elena L. Dadali, Roman B. Oparin, Alexander N. Petrin, and Oleg V. Evgrafov. 2000. "A New Variant of Charcot-Marie-Tooth Disease Type 2 Is Probably the Result of a Mutation in the Neurofilament-Light Gene." *American Journal of Human Genetics* 67 (1): 37–46. <https://doi.org/10.1086/302962>.
- Michailov, Galin V., Michael W. Sereda, Bastian G. Brinkmann, Tobias H. Fischer, Bernhard Haug, Carmen Birchmeier, Lorna Role, Cary Lai, Markus H. Schwab, and Klaus Armin Nave. 2004. "Axonal Neuregulin-1 Regulates Myelin Sheath Thickness." *Science* 304 (5671): 700–703. <https://doi.org/10.1126/science.1095862>.
- Misko, Albert, Sirui Jiang, Iga Wegorzewska, Jeffrey Milbrandt, and Robert H. Baloh. 2010. "Mitofusin 2 Is Necessary for Transport of Axonal Mitochondria and Interacts with the Miro/Milton Complex." *Journal of Neuroscience* 30 (12): 4232–40. <https://doi.org/10.1523/JNEUROSCI.6248-09.2010>.
- Mizushima, Noboru, Akitsugu Yamamoto, Makoto Matsui, Tamotsu Yoshimori, and Yoshinori Ohsumi. 2004. "In Vivo Analysis of Autophagy in Response to Nutrient Starvation Using Transgenic Mice Expressing a Fluorescent Autophagosomal Marker." *Molecular Biology of the Cell* 15: 1101–11. <https://doi.org/10.1091/mbc.E03>.
- Mo, Zhongying, Xiaobei Zhao, Huaqing Liu, Qinghua Hu, Xu Qiao Chen, Jessica Pham, Na Wei, et al. 2018. "Aberrant GlyRS-HDAC6 Interaction Linked to Axonal Transport Deficits in Charcot-Marie-Tooth Neuropathy." *Nature Communications* 9 (1): 1–11. <https://doi.org/10.1038/s41467-018-03461-z>.
- Morena, Jonathan, Anirudh Gupta, and J. Chad Hoyle. 2019. "Charcot-Marie-Tooth: From Molecules to Therapy." *International Journal of Molecular Sciences* 20 (14): 1–15. <https://doi.org/10.3390/ijms20143419>.
- Nakanishi, Hiroyuki, and Yoshimi Takai. 2008. "Frabin and Other Related Cdc42-Specific Guanine Nucleotide Exchange Factors Couple the Actin Cytoskeleton with the Plasma Membrane." *Journal of Cellular and Molecular Medicine* 12 (4): 1169–76. <https://doi.org/10.1111/j.1582-4934.2008.00345.x>.
- Nicks, Jessica, Sooyeon Lee, Andrew Harris, Darin J. Falk, Adrian G. Todd, Karla Arredondo, William A. Dunn, and Lucia Notterpek. 2014. "Rapamycin Improves Peripheral Nerve Myelination While It Fails to Benefit

- Neuromuscular Performance in Neuropathic Mice." *Neurobiology of Disease* 70: 224–36. <https://doi.org/10.1016/j.nbd.2014.06.023>.
- Nirschl, Jeffrey J., Maria M. Magiera, Jacob E. Lazarus, Carsten Janke, and Erika L.F. Holzbaur. 2016. "α-Tubulin Tyrosination and CLIP-170 Phosphorylation Regulate the Initiation of Dynein-Driven Transport in Neurons." *Cell Reports* 14 (11): 2637–52. <https://doi.org/10.1016/j.celrep.2016.02.046>.
- Obaishi, Hiroshi, Hiroyuki Nakanishi, Kenji Mandai, Keiko Satoh, Ayako Satoh, Kenichi Takahashi, Masako Miyahara, Hideo Nishioka, Kenji Takaishi, and Yoshimi Takai. 1998. "Frabin, a Novel FGD1-Related Actin Filament-Binding Protein Capable of Changing Cell Shape and Activating c-Jun N-Terminal Kinase." *Journal of Biological Chemistry* 273 (30): 18697–700. <https://doi.org/10.1074/jbc.273.30.18697>.
- Okuda, Tomohiko, Yujiro Higashi, Koichi Kokame, Chihiro Tanaka, Hisato Kondoh, and Toshiyuki Miyata. 2004. "Ndr1-Deficient Mice Exhibit a Progressive Demyelinating Disorder of Peripheral Nerves." *Molecular and Cellular Biology* 24 (9): 3949–56. <https://doi.org/10.1128/mcb.24.9.3949-3956.2004>.
- Ori-McKenney, Cassandra M, Jing Xu, Steven P Gross, and Richard B Vallee. 2010. "A Cytoplasmic Dynein Tail Mutation Impairs Motor Processivity." *Nature Cell Biology* 12 (12): 1228–34. <https://doi.org/10.1038/ncb2127>.
- Palaima, Paulius, José Berciano, Kristien Peeters, and Albena Jordanova. 2021. "LRSAM1 and the RING Domain: Charcot-Marie-Tooth Disease and Beyond." *Orphanet Journal of Rare Diseases* 16 (1): 1–12. <https://doi.org/10.1186/s13023-020-01654-8>.
- Pasterkamp, R. J., and K. Burk. 2020. "Axon Guidance Receptors: Endocytosis, Trafficking and Downstream Signaling from Endosomes." *Progress in Neurobiology*, no. September: 101916. <https://doi.org/10.1016/j.pneurobio.2020.101916>.
- Pérez-Ollé, Raül, Miguel A. López-Toledano, Dmitry Goryunov, Noemi Cabrera-Poch, Leonidas Stefanis, Kristy Brown, and Ronald K.H. Liem. 2005. "Mutations in the Neurofilament Light Gene Linked to Charcot-Marie-Tooth Disease Cause Defects in Transport." *Journal of Neurochemistry* 93 (4): 861–74. <https://doi.org/10.1111/j.1471-4159.2005.03095.x>.
- Perlson, Eran, Goo Bo Jeong, Jenny L. Ross, Ram Dixit, Karen E. Wallace, Robert G. Kalb, and Erika L.F. Holzbaur. 2009. "A Switch in Retrograde Signaling from Survival to Stress in Rapid-Onset Neurodegeneration." *Journal of Neuroscience* 29 (31): 9903–17. <https://doi.org/10.1523/JNEUROSCI.0813-09.2009>.
- Picci, Cristina, Victor S.C. Wong, Christopher J. Costa, Marion C. McKinnon, David C. Goldberg, Michelle Swift, Nazia M. Alam, et al. 2020. "HDAC6 Inhibition Promotes α-Tubulin Acetylation and Ameliorates CMT2A Peripheral Neuropathy in Mice." *Experimental Neurology* 328: 113281. <https://doi.org/10.1016/j.expneurol.2020.113281>.
- Pietiäinen, Vilja, Boris Vassilev, Tomas Blom, Wei Wang, Jessica Nelson, Robert Bittman, Nils Bäck, Noam Zelcer, and Elina Ikonen. 2013. "NDRG1 Functions in LDL Receptor Trafficking by Regulating Endosomal Recycling and Degradation." *Journal of Cell Science* 126 (17): 3961–71. <https://doi.org/10.1242/jcs.128132>.
- Prevaliti, Stefano C., Barbara Zerega, Diane L. Sherman, Peter J. Brophy, Giordina Dina, Rosalind H.M. King, Mustafa M. Salih, et al. 2003. "Myotubularin-Related 2 Protein Phosphatase and Neurofilament Light Chain Protein, Both Mutated in CMT Neuropathies, Interact in Peripheral Nerve." *Human Molecular Genetics* 12 (14): 1713–23. <https://doi.org/10.1093/hmg/ddg179>.
- Prior, Robert, Lawrence Van Helleputte, Veronick Benoy, and Ludo Van Den Bosch. 2017. "Defective Axonal Transport: A Common Pathological Mechanism in Inherited and Acquired Peripheral Neuropathies." *Neurobiology of Disease* 105: 300–320. <https://doi.org/10.1016/j.nbd.2017.02.009>.
- Raiborg, Camilla, Kristi G. Bache, David J. Gillooly, Inger Helene Madshus, Espen Stang, and Harald Stenmark. 2002. "Hrs Sorts Ubiquitinated Proteins into Clathrin-Coated Microdomains of Early Endosomes." *Nature Cell Biology* 4 (5): 394–98. <https://doi.org/10.1038/ncb791>.
- Rangaraju, Sunitha, Jonathan D. Verrier, Irina Madorsky, Jessica Nicks, William A. Dunn, and Lucia Notterpek. 2010. "Rapamycin Activates Autophagy and Improves Myelination in Explant Cultures from Neuropathic Mice." *Journal of Neuroscience* 30 (34): 11388–97. <https://doi.org/10.1523/JNEUROSCI.1356-10.2010>.
- Reed, Nathan A., Dawen Cai, T. Lynne Blasius, Gloria T. Jih, Edgar Meyhofer, Jacek Gaertig, and Kristen J. Verhey. 2006. "Microtubule Acetylation Promotes Kinesin-1 Binding and Transport." *Current Biology* 16 (21): 2166–72. <https://doi.org/10.1016/j.cub.2006.09.014>.
- Rink, Jochen, Eric Ghigo, Yannis Kalaidzidis, and Marino Zerial. 2005. "Rab Conversion as a Mechanism of Progression from Early to Late Endosomes." *Cell* 122 (5): 735–49. <https://doi.org/10.1016/j.cell.2005.06.043>.
- Roberts, Rhys C., Andrew A. Peden, Folma Buss, Nicholas A. Bright, Morwena Latouche, Mary M. Reilly, John

- Kendrick-Jones, and J. Paul Luzio. 2010. "Mistargeting of SH3TC2 Away from the Recycling Endosome Causes Charcot-Marie-Tooth Disease Type 4C." *Human Molecular Genetics* 19 (6): 1009–18. <https://doi.org/10.1093/hmg/ddp565>.
- Robinson, Fred L., and Jack E. Dixon. 2005. "The Phosphoinositide-3-Phosphatase MTMR2 Associates with MTMR13, a Membrane-Associated Pseudophosphatase Also Mutated in Type 4B Charcot-Marie-Tooth Disease." *Journal of Biological Chemistry* 280 (36): 31699–707. <https://doi.org/10.1074/jbc.M505159200>.
- Romano, Roberta, Cristina Rivellini, Maria De Luca, Rossana Tonlorenzi, Raffaella Belì, Fiore Manganelli, Maria Nolano, et al. 2020. "Alteration of the Late Endocytic Pathway in Charcot-Marie-Tooth Type 2B Disease." *Cellular and Molecular Life Sciences* 78 (1): 351–72. <https://doi.org/10.1007/s00018-020-03510-1>.
- Rossaert, Elisabeth, and Ludo Van Den Bosch. 2020. "HDAC6 Inhibitors: Translating Genetic and Molecular Insights into a Therapy for Axonal CMT." *Brain Research* 1733 (September 2019): 146692. <https://doi.org/10.1016/j.brainres.2020.146692>.
- Rudge, Simon A, Deborah M Anderson, and Scott D. Emr. 2004. "Vacuole Size Control: Regulation of PtdIns(3,5)P2 Levels by the Vacuole-Associated Vac14-Fig4 Complex, a PtdIns(3,5)P2-Specific Phosphatase." *Molecular Biology of the Cell* 15 (January): 24–36. <https://doi.org/10.1091/mbc.E03>.
- Rudnik-Schöneborn, Sabine, Michaela Auer-Grumbach, and Jan Senderek. 2020. "Charcot-Marie-Tooth Disease and Hereditary Motor Neuropathies - Update 2020." *Medizinische Genetik* 32 (3): 207–19. <https://doi.org/10.1515/medgen-2020-2038>.
- Ruit, Kenneth G., Patricia A. Osborne, Robert E. Schmidt, Eugene M. Johnson, and William D. Snider. 1990. "Nerve Growth Factor Regulates Sympathetic Ganglion Cell Morphology and Survival in the Adult Mouse." *Journal of Neuroscience* 10 (7): 2412–19. <https://doi.org/10.1523/jneurosci.10-07-02412.1990>.
- Saporta, Mario A., Vu Dang, Dmitri Volfson, Bende Zou, Xinmin Simon Xie, Adijat Adebola, Ronald K. Liem, Michael Shy, and John T. Dimos. 2015. "Axonal Charcot-Marie-Tooth Disease Patient-Derived Motor Neurons Demonstrate Disease-Specific Phenotypes Including Abnormal Electrophysiological Properties." *Experimental Neurology* 263:190–99. <https://doi.org/10.1016/j.expneurol.2014.10.005>.
- Saveri, Paola, Maria De Luca, Veronica Nisi, Chiara Pisciotta, Roberta Romano, Giuseppe Piscoquito, Mary M. Reilly, et al. 2020. "Charcot-Marie-Tooth Type 2B: A New Phenotype Associated with a Novel RAB7A Mutation and Inhibited EGFR Degradation." *Cells* 9 (4). <https://doi.org/10.3390/cells9041028>.
- Schiavon, Cara R., Gerald S. Shadel, and Uri Manor. 2021. "Impaired Mitochondrial Mobility in Charcot-Marie-Tooth Disease." *Frontiers in Cell and Developmental Biology* 9 (February): 1–15. <https://doi.org/10.3389/fcell.2021.624823>.
- Schreij, Andrea M.A., Edward A. Fon, and Peter S. McPherson. 2016. "Endocytic Membrane Trafficking and Neurodegenerative Disease." *Cellular and Molecular Life Sciences* 73 (8): 1529–45. <https://doi.org/10.1007/s00018-015-2105-x>.
- Scolnick, Jonathan A., Kai Cui, Cynthia D. Duggan, Shouhong Xuan, Xiao bing Yuan, Argiris Efstratiadis, and John Ngai. 2008. "Role of IGF Signaling in Olfactory Sensory Map Formation and Axon Guidance." *Neuron* 57 (6): 847–57. <https://doi.org/10.1016/j.neuron.2008.01.027>.
- Scott-Solomon, Emily, and Reiji Kuruville. 2018. "Mechanisms of Neurotrophin Trafficking via Trk Receptors." *Molecular and Cellular Neuroscience* 91 (January): 25–33. <https://doi.org/10.1016/j.mcn.2018.03.013>.
- Seaman, Matthew N.J. 2012. "The Retromer Complex-Endosomal Protein Recycling and Beyond." *Journal of Cell Science* 125 (20): 4693–4702. <https://doi.org/10.1242/jcs.103440>.
- Seaman, Matthew N J. 2004. "Cargo-Selective Endosomal Sorting for Retrieval to the Golgi Requires Retromer." *Journal of Cell Biology* 165 (1): 111–22. <https://doi.org/10.1083/jcb.200312034>.
- Seaman, Matthew N J, Alexis Gautreau, and Daniel D. Billadeau. 2013. "Retromer-Mediated Endosomal Protein Sorting: All WASHed Up!" *Trends in Cell Biology* 23 (11): 522–28. <https://doi.org/10.1016/j.tcb.2013.04.010>.
- Seaman, Matthew N J, Michael E. Harbour, Daniel Tattersall, Eliot Read, and Nicholas Bright. 2009. "Membrane Recruitment of the Cargo-Selective Retromer Subcomplex Is Catalysed by the Small GTPase Rab7 and Inhibited by the Rab-GAP TBC1D5." *Journal of Cell Science* 122 (14): 2371–82. <https://doi.org/10.1242/jcs.048686>.
- Senderek, Jan, Carsten Bergmann, Claudia Stendel, Jutta Kirfel, Nathalie Verpoorten, Peter De Jonghe, Vincent Timmerman, et al. 2003. "Mutations in a Gene Encoding a Novel SH3/TPR Domain Protein Cause Autosomal Recessive Charcot-Marie-Tooth Type 4C Neuropathy." *American Journal of Human Genetics* 73 (5): 1106–19. <https://doi.org/10.1086/379525>.
- Shen, Sida, and Alan P. Kozikowski. 2020. "A Patent Review of Histone Deacetylase 6 Inhibitors in

- Neurodegenerative Diseases (2014-2019).” *Expert Opinion on Therapeutic Patents* 30 (2): 121–36. <https://doi.org/10.1080/13543776.2019.1708901>.
- Sidiropoulos, Páris N.M., Michaela Mieke, Thomas Bock, Elisa Tinelli, Carole I. Oertli, Rohini Kuner, Dies Meijer, Bernd Wollscheid, Axel Niemann, and Ueli Suter. 2012. “Dynamin 2 Mutations in Charcot-Marie-Tooth Neuropathy Highlight the Importance of Clathrin-Mediated Endocytosis in Myelination.” *Brain* 135 (5): 1395–1411. <https://doi.org/10.1093/brain/aws061>.
- Simonetti, Boris, Chris M. Danson, Kate J. Heesom, and Peter J. Cullen. 2017. “Sequence-Dependent Cargo Recognition by SNX-BARs Mediates Retromer-Independent Transport of CI-MPR.” *Journal of Cell Biology* 216 (11): 3695–3712. <https://doi.org/10.1083/jcb.201703015>.
- Simonsen, Anne, Roger Lippé, Savvas Christoforidis, Jean Michel Gaullier, Andreas Brech, Judy Callaghan, Ban Hock Toh, Carol Murphy, Marino Zerial, and Harald Stenmark. 1998. “EEA1 Links PI(3)K Function to Rab5 Regulation of Endosome Fusion.” *Nature* 394 (6692): 494–98. <https://doi.org/10.1038/28879>.
- Sleigh, James N., John M. Dawes, Steven J. West, Na Wei, Emily L. Spaulding, Adriana Gómez-Martín, Qian Zhang, et al. 2017. “Trk Receptor Signaling and Sensory Neuron Fate Are Perturbed in Human Neuropathy Caused by Gars Mutations.” *Proceedings of the National Academy of Sciences of the United States of America* 114 (16): E3324–33. <https://doi.org/10.1073/pnas.1614557114>.
- Spinosa, Maria Rita, Cinzia Progida, Azzurra De Luca, Anna Maria Rosaria Colucci, Pietro Alifano, and Cecilia Bucci. 2008. “Functional Characterization of Rab7 Mutant Proteins Associated with Charcot-Marie-Tooth Type 2B Disease.” *Journal of Neuroscience* 28 (7): 1640–48. <https://doi.org/10.1523/JNEUROSCI.3677-07.2008>.
- Stendel, Claudia, Andreas Roos, Henning Kleine, Estelle Arnaud, Murat Özçelik, Páris N.M. Sidiropoulos, Jennifer Zenker, et al. 2010. “SH3TC2, a Protein Mutant in Charcot-Marie-Tooth Neuropathy, Links Peripheral Nerve Myelination to Endosomal Recycling.” *Brain* 133 (8): 2462–74. <https://doi.org/10.1093/brain/awq168>.
- Stone, Elizabeth J, Atsuko Uchida, and Anthony Brown. 2019. “Charcot-Marie-Tooth Disease Type 2E/1F Mutant Neurofilament Proteins Assemble into Neurofilaments.” *Cytoskeleton (Hoboken)* 76 (7–8): 423–39. <https://doi.org/10.1002/cm.21566>.
- Stowers, R. Steven, Laura J. Megeath, Jolanta Górka-Andrzejak, Ian A. Meinertzhagen, and Thomas L. Schwarz. 2002. “Axonal Transport of Mitochondria to Synapses Depends on Milton, a Novel Drosophila Protein.” *Neuron* 36 (6): 1063–77. [https://doi.org/10.1016/S0896-6273\(02\)01094-2](https://doi.org/10.1016/S0896-6273(02)01094-2).
- Street, V. A., C. L. Bennett, J. D. Goldy, A. J. Shirk, K. A. Kleopa, B. L. Tempel, H. P. Lipe, S. S. Scherer, T. D. Bird, and P. F. Chance. 2003. “Mutation of a Putative Protein Degradation Gene LITAF/SIMPLE in Charcot-Marie-Tooth Disease 1C.” *Neurology* 60 (1): 22–26. <https://doi.org/10.1212/WNL.60.1.22>.
- Tanabe, Kenji, and Kohji Takei. 2009. “Dynamic Instability of Microtubules Requires Dynamin 2 and Is Impaired in a Charcot-Marie-Tooth Mutant.” *Journal of Cell Biology* 185 (6): 939–48. <https://doi.org/10.1083/jcb.200803153>.
- Taveggia, Carla, George Zanazzi, Ashley Petrylak, Hiroko Yano, Jack Rosenbluth, Steven Einheber, Xiaorong Xu, et al. 2005. “Neuregulin-1 Type III Determines the Ensheathment Fate of Axons.” *Neuron* 47 (5): 681–94. <https://doi.org/10.1016/j.neuron.2005.08.017>.
- Temkin, Paul, Benjamin Lauffer, Stefanie Jager, Peter Cimermacic, Nevan J Krogan, and Mark Von Zastrow. 2011. “SNX27 Mediates Retromer Tubule Entry and Endosome-to-Plasma Membrane Trafficking of Signaling Receptors.” *Nature Cell Biology* 13 (6): 715–21. <https://doi.org/10.1038/ncb2252.SNX27>.
- Timmerman, Vincent, Alleene V. Strickland, and Stephan Züchner. 2014. “Genetics of Charcot-Marie-Tooth (CMT) Disease within the Frame of the Human Genome Project Success.” *Genes* 5 (1): 13–32. <https://doi.org/10.3390/genes5010013>.
- Umikawa, Masato, Hiroshi Obaishi, Hiroyuki Nakanishi, Keiko Satoh-Horikawa, Kenichi Takahashi, Ikuko Hotta, Yoshiharu Matsuura, and Yoshimi Takai. 1999. “Association of Frabin with the Actin Cytoskeleton Is Essential for Microspike Formation through Activation of Cdc42 Small G Protein.” *Journal of Biological Chemistry* 274 (36): 25197–200. <https://doi.org/10.1074/jbc.274.36.25197>.
- Vaccari, Iliaria, Antonietta Carbone, Stefano Carlo Previtali, Yevgeniya A. Mironova, Valeria Alberizzi, Roberta Nosedà, Cristina Rivellini, et al. 2015. “Loss of Fig4 in Both Schwann Cells and Motor Neurons Contributes to CMT4J Neuropathy.” *Human Molecular Genetics* 24 (2): 383–96. <https://doi.org/10.1093/hmg/ddu451>.
- Vaccari, Iliaria, Giorgia Dina, Hélène Tronchère, Emily Kaufman, Gaëtan Chicanne, Federica Cerri, Lawrence Wrabetz, et al. 2011. “Genetic Interaction between MTMR2 and FIG4 Phospholipid Phosphatases Involved in Charcot-Marie-Tooth Neuropathies.” *PLoS Genetics* 7 (10). <https://doi.org/10.1371/journal.pgen.1002319>.
- Vavlitou, Natalie, Irene Sargiannidou, Kyriaki Markoullis, Kyriacos Kyriacou, Steven S. Scherer, and Kleopas A.

- Kleopa. 2010. "Axonal Pathology Precedes Demyelination in a Mouse Model of X-Linked Demyelinating/Type I Charcot-Marie-Tooth Neuropathy." *Journal of Neuropathology and Experimental Neurology* 69 (9): 945–58. <https://doi.org/10.1097/NEN.0b013e3181efa658>.
- Vijay, Sauparnika, Meagan Chiu, Joel B. Dacks, and Rhys C. Roberts. 2016. "Exclusive Expression of the Rab11 Effector SH3TC2 in Schwann Cells Links Integrin- α 6 and Myelin Maintenance to Charcot-Marie-Tooth Disease Type 4C." *Biochimica et Biophysica Acta - Molecular Basis of Disease* 1862 (7): 1279–90. <https://doi.org/10.1016/j.bbadis.2016.04.003>.
- Waegh, Sylvie De, and Scott T. Brady. 1990. "Altered Slow Axonal Transport and Regeneration in a Myelin-Deficient Mutant Mouse: The Trembler as an in Vivo Model for Schwann Cell-Axon Interactions." *Journal of Neuroscience* 10 (6): 1855–65. <https://doi.org/10.1523/jneurosci.10-06-01855.1990>.
- Waegh, Sylvie M. de, Virginia M.Y. Lee, and Scott T. Brady. 1992. "Local Modulation of Neurofilament Phosphorylation, Axonal Caliber, and Slow Axonal Transport by Myelinating Schwann Cells." *Cell* 68 (3): 451–63. [https://doi.org/10.1016/0092-8674\(92\)90183-D](https://doi.org/10.1016/0092-8674(92)90183-D).
- Wallroth, Alexander, and Volker Haucke. 2018. "Phosphoinositide Conversion in Endocytosis and the Endolysosomal System." *Journal of Biological Chemistry* 293 (5): 1526–35. <https://doi.org/10.1074/jbc.R117.000629>.
- Wang, Shicong, Zexu Ma, Xiaohui Xu, Zhen Wang, Lixiang Sun, Yunhe Zhou, Xiaosi Lin, Wanjin Hong, and Tuanlao Wang. 2014. "A Role of Rab29 in the Integrity of the Trans-Golgi Network and Retrograde Trafficking of Mannose-6-Phosphate Receptor." *PLoS ONE* 9 (5): 1–12. <https://doi.org/10.1371/journal.pone.0096242>.
- Weedon, Michael N., Robert Hastings, Richard Caswell, Weijia Xie, Konrad Paszkiewicz, Thalia Antoniadis, Maggie Williams, et al. 2011. "Exome Sequencing Identifies a DYNC1H1 Mutation in a Large Pedigree with Dominant Axonal Charcot-Marie-Tooth Disease." *American Journal of Human Genetics* 89 (2): 308–12. <https://doi.org/10.1016/j.ajhg.2011.07.002>.
- Weeratunga, Saroja, Blessy Paul, and Brett M. Collins. 2020. "Recognising the Signals for Endosomal Trafficking." *Current Opinion in Cell Biology* 65: 17–27. <https://doi.org/10.1016/j.cceb.2020.02.005>.
- Xhabija, Besa, Gregory S Taylor, Akemi Fujibayashi, Kiyotoshi Sekiguchi, and Panayiotis O Vacratis. 2011. "Receptor Mediated Endocytosis of PI(3)P Binding Protein Regulated by Myotubularin-Related 2." *FEBS Letters* 585 (12): 1722–28. <https://doi.org/10.1016/j.febslet.2011.04.016>.
- Xu, Baoji, Keling Zang, Naomi L Ruff, Y. Alex Zhang, Susan K McConnell, Michael P Stryker, and Louis F Reichardt. 2000. "Cortical Degeneration in the Absence of Neurotrophin Signaling." *Neuron* 26 (1): 233–45. [https://doi.org/10.1016/S0896-6273\(00\)81153-8](https://doi.org/10.1016/S0896-6273(00)81153-8).
- Xu, Fang, Hironori Takahashi, Yosuke Tanaka, Sotaro Ichinose, Shinsuke Niwa, Matthew P. Wicklund, and Nobutaka Hirokawa. 2018. "KIF1B Mutations Detected in Hereditary Neuropathy Impair IGF1R Transport and Axon Growth." *Journal of Cell Biology* 217 (10): 3480–96. <https://doi.org/10.1083/JCB.201801085>.
- Yang, Wannian, Charles G. Lo, Tom Dispenza, and Richard A. Cerione. 2001. "The Cdc42 Target ACK2 Directly Interacts with Clathrin and Influences Clathrin Assembly." *Journal of Biological Chemistry* 276 (20): 17468–73. <https://doi.org/10.1074/jbc.M010893200>.
- Ye, Mengchen, Kathryn M. Lehigh, and David D. Ginty. 2018. "Multivesicular Bodies Mediate Long-Range Retrograde NGF-TrkA Signaling." *ELife* 7: 1–29. <https://doi.org/10.7554/eLife.33012>.
- Yum, Sabrina W., Kleopas A. Kleopa, Susan Shumas, and Steven S. Scherer. 2002. "Diverse Trafficking Abnormalities of Connexin32 Mutants Causing CMTX." *Neurobiology of Disease* 11 (1): 43–52. <https://doi.org/10.1006/nbdi.2002.0545>.
- Zastrow, Mark Von, and Alexander Sorkin. 2007. "Signaling on the Endocytic Pathway." *Current Opinion in Cell Biology* 19: 436–45. <https://doi.org/10.1016/j.cceb.2007.04.021>.
- Zhang, Kai, R. Fishel Ben Kenan, Y. Osakada, W. Xu, R. S. Sinit, Liang Chen, X. Zhao, J.-Y. Chen, Bianxiao Cui, and Chengbiao Wu. 2013. "Defective Axonal Transport of Rab7 GTPase Results in Dysregulated Trophic Signaling." *Journal of Neuroscience* 33 (17): 7451–62. <https://doi.org/10.1523/JNEUROSCI.4322-12.2013>.
- Zhao, Chunjie, Junko Takita, Yosuke Tanaka, Mitsutoshi Setou, Terunaga Nakagawa, Sen Takeda, Hong Wei Yang, et al. 2001. "Charcot-Marie-Tooth Disease Type 2A Caused by Mutation in a Microtubule Motor KIF1B (Gaku et al., 1994; Termed KIF1B Hereafter) That We Call KIF1B. The Two Isoforms, Splice Variants of the Same Gene Mapped on Mouse Chromosome 4E, Share the N-Terminal Motor." *Cell* 105: 587–97. <http://www>.
- Zhao, Jian, Kristy Brown, and Ronald K.H. Liem. 2017. "Abnormal Neurofilament Inclusions and Segregations in Dorsal Root Ganglia of a Charcot-Marie-Tooth Type 2E Mouse Model." *PLoS ONE* 12 (6): 1–15. <https://doi.org/10.1371/journal.pone.0180038>.

- Zhao, Jing, Yi Wang, Huan Xu, Yuan Fu, Ting Qian, Deng Bo, Yan Xin Lu, et al. 2016. "Dync1h1 Mutation Causes Proprioceptive Sensory Neuron Loss and Impaired Retrograde Axonal Transport of Dorsal Root Ganglion Neurons." *CNS Neuroscience and Therapeutics* 22 (7): 593–601. <https://doi.org/10.1111/cns.12552>.
- Zhou, Ye, Joshua R. Miles, Hagai Tavori, Min Lin, Habibeh Khoshbouei, David R. Borchelt, Hannah Bazick, et al. 2019. "PMP22 Regulates Cholesterol Trafficking and ABCA1-Mediated Cholesterol Efflux." *Journal of Neuroscience* 39 (27): 5404–18. <https://doi.org/10.1523/JNEUROSCI.2942-18.2019>.
- Züchner, Stephan, Irina V. Mersiyanova, Maria Muglia, Nisrine Bissar-Tadmouri, Julie Rochelle, Elena L. Dadali, Mario Zappia, et al. 2004. "Mutations in the Mitochondrial GTPase Mitofusin 2 Cause Charcot-Marie-Tooth Neuropathy Type 2A." *Nature Genetics* 36 (5): 449–51. <https://doi.org/10.1038/ng1341>.
- Züchner, Stephan, Maher Nouredine, Marina Kennerson, Kristien Verhoeven, Kristl Claeyls, Peter De Jonghe, John Merory, et al. 2005. "Mutations in the Pleckstrin Homology Domain of Dynamin 2 Cause Dominant Intermediate Charcot-Marie-Tooth Disease." *Nature Genetics* 37 (3): 289–94. <https://doi.org/10.1038/ng1514>.

2 SENSORY AXON GROWTH REQUIRES SPATIOTEMPORAL INTEGRATION OF CASR AND TRKB SIGNALING

In the second chapter I am looking at receptor interaction for signal diversification during development.

By facilitating a combination of primary cell culture, biochemistry, imaging techniques and chemical inhibition *in ovo*, we show that calcium sensing receptor (CaSR), a G-Protein coupled receptor (GPCR), facilitates growth in early BDNF/TrkB independent nodose neurons of the chicken. These early-stage neurons are still independent of BDNF for survival and do not express TrkB yet. In this period, CaSR induces growth by activating an Akt pathway that signals independently of Glycogen synthase kinase 3 (GSK3)/MAPK and is routed into late Rab7-positive endosomes upon activation.

We further show that CaSR enhances TrkB-mediated neurite growth at later developmental stages. When nodose neurons mature, express TrkB and become BDNF-dependent for survival, CaSR is no longer able to induce neurite growth on its own. However, CaSR does increase TrkB-induced growth by changing its downstream signalling cascade to a shared signalling node. Activation of CaSR alone in later neurons shifts its downstream target from PI3Kinase/Akt to GSK3 α on tyrosine (Tyr)279. However, this activation does not induce growth. On the other hand, BDNF induced activation of TrkB phosphorylates GSK3 α on Tyr279, but also GSK3 β on Tyr216 and serine (Ser)9. Of note, phosphorylation on tyrosine residues activates GSK3, while phosphorylation on serine deactivates GSK3. We observed that BDNF signalling increased overall growth compared to CaSR, but neurons were still much shorter than expected. When we induced co-activation of both receptors in these older neurons, we observed a really interesting mechanism of signal integration. We found that CaSR and TrkB acting together caused activation of GSK3 by phosphorylation of GSK3 α on Tyr279 and a deactivating response by phosphorylation of GSK3 β on Ser9. This “switch-on-switch-off” response regulates normal axonal outgrowth by affecting microtubule assembly and disassembly via the GSK3 downstream target Tau (Venkatramani and Panda, 2019). Our data are showing that these two different receptors can influence each other’s signaling cascade in a non-additive fashion by functioning on the same signaling node resulting in a synergistic growth effect.

ORIGINAL PUBLICATION

AUTHORS:

Markworth R, Adolfs Y, Dambeck V, Steinbeck LM, Lizé M, Pasterkamp RJ, Bähr M, Dean C, Burk K. Sensory Axon Growth Requires Spatiotemporal Integration of CaSR and TrkB Signaling. *J Neurosci*. 2019 Jul 24;39(30):5842-5860. doi: 10.1523/JNEUROSCI.0027-19.2019. Epub 2019 May 23.

Personal contribution: Performance and analysis (together with Katja Burk) of experiments shown in the following figures: Figure 1A-B,E, Figure 1F-G (together with Lars Malte Steinbeck), Figure 2E, Figure 2F-G, Figure 3A-B, Figure 4B,E, Figure 5, Figure 6, Figure 7 (together with Vivian Dambeck), Figure 8, Figure 9B,D,F, Figure 10B,D,F, Figure 11. I contributed to the figure design, and further contributed to the manuscript writing in the figure legends and methods section, as well as by editing.

Sensory Axon Growth Requires Spatiotemporal Integration of CaSR and TrkB Signaling

Ronja Markworth,^{1,2,3} Youri Adolfs,⁴ Vivian Dambeck,^{1,3} Lars M. Steinbeck,³ Muriel Lizé,¹
R. Jeroen Pasterkamp,⁴ Mathias Bähr,¹ Camin Dean,² and Katja Burk^{1,2,3}

¹Department of Neurology, University Medical Center Göttingen, 37075 Göttingen, Germany, ²European Neuroscience Institute, 37077 Göttingen, Germany, ³Center for Biostructural Imaging of Neurodegeneration, 37075 Göttingen, Germany, and ⁴Department of Translational Neuroscience, University Medical Center Utrecht, Utrecht University, 3584 CG Utrecht, The Netherlands

Neural circuit development involves the coordinated growth and guidance of axons. During this process, axons encounter many different cues, but how these cues are integrated and translated into growth is poorly understood. In this study, we report that receptor signaling does not follow a linear path but changes dependent on developmental stage and coreceptors involved. Using developing chicken embryos of both sexes, our data show that calcium-sensing receptor (CaSR), a G-protein-coupled receptor important for regulating calcium homeostasis, regulates neurite growth in two distinct ways. First, when signaling in isolation, CaSR promotes growth through the PI3-kinase-Akt pathway. At later developmental stages, CaSR enhances tropomyosin receptor kinase B (TrkB)/BDNF-mediated neurite growth. This enhancement is facilitated through a switch in the signaling cascade downstream of CaSR (i.e., from the PI3-kinase-Akt pathway to activation of GSK3 α Tyr279). TrkB and CaSR colocalize within late endosomes, cotraffic and coactivate GSK3, which serves as a shared signaling node for both receptors. Our study provides evidence that two unrelated receptors can integrate their individual signaling cascades toward a nonadditive effect and thus control neurite growth during development.

Key words: CaSR; cosignaling; GSK3; neurite growth; signal integration; TrkB

Significance Statement

This work highlights the effect of receptor coactivation and signal integration in a developmental setting. During embryonic development, neurites grow toward their targets guided by cues in the extracellular environment. These cues are sensed by receptors at the surface that trigger intracellular signaling events modulating the cytoskeleton. Emerging evidence suggests that the effects of guidance cues are diversified, therefore expanding the number of responses. Here, we show that two unrelated receptors can change the downstream signaling cascade and regulate neuronal growth through a shared signaling node. In addition to unraveling a novel signaling pathway in neurite growth, this research stresses the importance of receptor coactivation and signal integration during development of the nervous system.

Introduction

The development of the nervous system requires axons and growth cones to extend through a complex environment. This

direction-mediated process allows growth cones to find and innervate their appropriate targets and form functional synapses.

Axon pathfinding demands neurons to respond to long- and short-range signals, either repulsive or attractive (Dickson, 2002; Wen and Zheng, 2006; Bashaw and Klein, 2010) in addition to factors accelerating or inhibiting axonal extension (Filbin, 2006). Remarkably, our nervous system contains trillions of connections but only about a hundred of growth/guidance cues. Therefore, one important question is how this relatively small number of cues coordinates the wiring of a disproportionately large number of connections. Evidence is emerging that the axon growth/guidance cues are diversified and spatiotemporally controlled, expanding the number of guidance decisions they can mediate.

The signals involved for fine-tuning neuronal growth are diversified (e.g., through several ligands binding to one receptor)

Received Jan. 4, 2019; revised May 12, 2019; accepted May 15, 2019.

Author contributions: R.M., Y.A., V.D., M.L., and K.B. performed research; R.M., L.M.S., and K.B. analyzed data; R.M., M.L., R.J.P., M.B., C.D., and K.B. edited the paper; Y.A., R.J.P., and K.B. designed research; K.B. wrote the first draft of the paper; K.B. wrote the paper.

This work was supported by a Dorothea Schloerz fellowship to K.B., an International Max Planck Research School for Neurosciences stipend to R.M., the Center for Nanoscale Microscopy and Molecular Physiology of the Brain to K.B., R.M., M.L., and C.D., and The Netherlands Organization for Scientific Research to R.J.P. We thank Michael Levine for providing the GFP-CaSR full-length and GFP-R185Q constructs; Moses Chao for the TrkB-RFP construct; and Luisa Leiss for helping with image acquisition.

The authors declare no competing financial interests.

Correspondence should be addressed to Katja Burk at kburk@gwdg.de.

<https://doi.org/10.1523/JNEUROSCI.0027-19.2019>

Copyright © 2019 the authors

(Chao, 2003; Zhou et al., 2008; Dudanova and Klein, 2013) or ligands binding directly to their receptors or through a coreceptor (Chauvet et al., 2007; Bellon et al., 2010; Song et al., 2015; Mire et al., 2018), eventually leading to differential changes of the cytoskeleton (Bashaw and Klein, 2010).

Additionally, spatial and temporal expression of receptors and coreceptors modulates responses depending on developmental states (Dickson and Gilestro, 2006; Mire et al., 2012, 2018). Furthermore, several studies have reported that signaling cascades interact to generate complex cellular behaviors (Bourne and Nicoll, 1993; Cornell and Kimelman, 1994; Prehoda and Lim, 2002; McClean et al., 2007). These interactions of downstream signaling cascades are classified into two categories: additive and non-additive. Additive signaling is integrated as a sum of positive and/or negative signals. Nonadditive effects are quantitatively or qualitatively different from the sum of signals (Dudanova and Klein, 2013). These nonadditive effects can include synergistic, hierarchical, and permissive subclasses of interactions (see Morales and Kania, 2017). However, despite recent progress, our understanding of how signal integration induces growth and guidance remains incomplete.

To address these questions, we used the calcium-sensing receptor (CaSR), a G-protein-coupled receptor, monitoring extracellular free ionized calcium in organs involved in calcium homeostasis. Recently, unexpected functions of CaSR in the nervous system were found (Vizard et al., 2008; Ruat and Traiffort, 2013; Jones and Smith, 2016).

Vizard et al. (2008) reported that CaSR enhances neurotrophic-mediated growth of neurons from the mouse superior cervical ganglion (SCG). The authors used neurons of the SCG, which require NGF/TrkA signaling for growth and survival. When CaSR was activated additionally to TrkA, neurite length increased compared with TrkA activation alone.

To answer how CaSR increases neurotrophin-facilitated growth, we used the chicken nodose ganglia as a model system. During early chick development, nodose neurons do not require neurotrophins for growth and survival (Davies, 1989) but rather become dependent on BDNF-TrkB signaling upon target innervation (Vogel and Davies, 1991; Robinson et al., 1996). Early nodose neurons respond to BDNF after ~72 h in culture, which was suggested to be the time when neurons innervate their targets *in vivo* (Vogel and Davies, 1991; Robinson et al., 1996). We used this developmental switch to study CaSR signaling in the absence and presence of BDNF-TrkB signaling.

Our data show that, when CaSR signals in isolation, it routes into Rab7-positive endosomes and regulates axonal growth through activation of Akt. Later in development with expression and coactivation of TrkB, CaSR colocalizes with TrkB in Rab7-positive endosomes, cotraffics and coimmunoprecipitates with TrkB, and enhances BDNF-mediated growth through shared activation on GSK3.

In summary, this study reports several novel observations. First, CaSR regulates BDNF-independent neurite growth. Second, downstream targets shift, depending on developmental stages. Further, we show how two unrelated receptors integrate their signaling in a nonadditive manner on a shared signaling-node, namely, GSK3 α tyrosine (Tyr) 279 and GSK3 β serine (Ser) 9. Last, both receptors act on the activity state of GSK3. This activity state, in turn, affects the phosphorylation state of Tau, which modulates microtubule assembly and disassembly.

Materials and Methods

All research involving animals was approved by, and done in accordance with, the Institutional Animal Care and Ethics Committees of Göttingen University and with German animal welfare laws, and in accordance with the Animals Scientific Procedures Act of 1986 (UK). To generate mouse embryonic fibroblasts (MEFs), embryos were isolated from gestating C57BL/6N females at embryonic day E13.5 after fertilization by male C57BL/6N, minced, and taken into culture in DMEM.

Calculation of calcium concentration. DMEM (catalog #31966-021, Invitrogen) was used to culture chicken nodose neurons, which has a standard calcium concentration of 1.8 mM (details on calcium concentrations for DMEM can be found on the manufacturer's website). To increase calcium levels by 0.5 mM (1.8–2.3 mM), the amount of 1 M CaCl needed for the respective volume was calculated and added to the media. To decrease calcium levels by 1.1 mM (1.8–0.7 mM), the amount of 0.5 M EGTA needed for the respective volume used was calculated and added to the media.

Culture of chicken nodose neurons. Nodose ganglia were removed from 10–12 chicken embryos of both sexes per dissection (for immunostainings and Western blots) and transferred to ice-cold HBSS buffer and kept on ice during dissection. Nodose ganglia were then transferred into 0.25% trypsin solution and incubated for 10 min at 37°C. During the incubation, 1 ml “plating medium” (DMEM-containing glucose, pyruvate, glutamine, penicillin/streptomycin, and 10% FBS) was filled into each well of 24-well plates containing poly-L-ornithine and laminin-coated coverslips. After incubation, enzyme solution was removed and 5 ml plating medium added and incubated for 5 min at 37°C for neutralization. Plating medium was removed, and nodose ganglia were washed twice with plating medium; 2 ml plating medium was added to the dissected ganglia, and the tissue was dissociated with a 1 ml pipette; 400 μ l of cell suspension was added to each well. Neurons were then kept at 37°C, 5% CO₂ and 100% humidity in calcium concentrations specified for each experiment below.

Survival assay. Nodose neurons were dissected as described above at different developmental time points and kept in “plating medium” in 35 mm tissue culture dishes (Greiner Cellstar, catalog #M9312-100EA) coated with poly-L-ornithine and laminin at a density of ~2000 neurons per dish. After an initial count, which was performed 2 h after plating for neurons to settle on the bottom of the culture dish, half of the dishes were treated with 10 ng/ml BDNF and half of the dishes served as controls. The number of neurons within a predefined 12 \times 12 mm area in the middle of the culture dish were counted again 24 h after plating. The number of neurons surviving at these times was expressed as a percentage of the initial number of neurons. Three to five independent cultures were analyzed for all conditions, and the data shown were compiled from separate experiments.

Measuring neurite length. Nodose neurons were dissected as described above and plated on acidified glass coverslips coated with poly-L-ornithine and laminin at a density of ~5000 neurons per well and placed in 24-well tissue culture dishes (Greiner Cellstar, catalog #M9312-100EA). Neurons were grown at 5% CO₂ and 37°C for 24 h in “plating medium” adjusted to the respective calcium concentrations 0.7, 1.1, 1.3, or 2.3 mM calcium, 0.7 mM + 10 μ M CaSR agonist (R568 hydrochloride), or 2.3 mM + 10 μ M CaSR antagonist (Calhex 231 hydrochloride), respectively (for Stage 20 nodose neurons). Stage 30 nodose neurons were cultured in 10 ng/ml BDNF (R&D Systems) and the following conditions: 0.7 mM, 0.7 mM + CaSR agonist (R568 hydrochloride), 2.3 mM or 2.3 mM + CaSR antagonist (Calhex 231 hydrochloride). Inhibitors for growth pathways were used as follows: 50 μ M PI3-kinase inhibitor LY294002 (Sigma-Aldrich, catalog #L9908), 10 μ M GSK3 inhibitor BIO (Sigma-Aldrich, catalog #B1686), and 10 μ M MEK1/2 inhibitor PD98059 (Sigma-Aldrich catalog #P215). Caspase inhibitor was used at 25 μ M (caspase inhibitor III/Boc-D-FMK, Merck Millipore, catalog #218745).

After 24 h, neurons were fixed in 4% PFA, washed 3 \times in PBS, and stained with tubulin antibody as described in Immunocytochemistry or directly stained with CalceinAM (Thermo Fisher Scientific, catalog #C3100MP).

Neurite length was measured using the Fiji PlugIn Simple Neurite Tracer (RRID:SCR_016566). In early, bipolar neurons, the entire length of neurons was measured, whereas in late development we took the sum of lengths from all neurites of a neuron to stay consistent with our measuring method.

The number of branch points was measured using the Fiji PlugIn Cell Counter (RRID:SCR_002285), which was used to manually mark each branch point on a neuron.

For *in ovo* measurements, eggs were opened at Stage 18, and a 10 μ l droplet of agonist/antagonist solution (100 μ g/ μ l) or DMSO was added to the region of the node and the embryos were incubated for 24 h.

Whole-mount neurofilament staining was performed as follows: Embryos were fixed in 4% PFA for 2 h. Subsequently, embryos were washed 3 times (30 min each) in PBS containing 1% Triton-X and then blocked for 2 h in PBS containing 1% Triton-X, 10% FCS. Then, embryos were blocked overnight in PBS containing 1% Triton-X, 10% FCS, and 0.1% H₂O₂. The next day, embryos were washed 3 times in blocking solution (PBS containing 1% Triton-X, 10% FCS) and then incubated for 2 d in antineurofilament antibody (1:50, catalog #N4142, Sigma-Aldrich, RRID:AB_477272). Following this, embryos were washed 3 times for 30 min each in blocking solution and then incubated for 2 d in secondary antibody (1:250 catalog #ab6721, Abcam, RRID:AB_955447). After incubation, embryos were washed 3 times in PBS containing 1% Triton-X and then incubated in DAB substrate containing H₂O₂ (5 μ l H₂O₂ per 1 ml of DAB) until neurons were clearly visible. DAB solution was removed; embryos were washed in PBS and imaged using a light microscope. The length of nodose neurons was measured from the hindbrain to the tip of the longest neurite (using the Fiji PlugIn Simple Neurite Tracer, RRID:SCR_016566) and normalized to the circumference of the midbrain.

Transfection with Lipofectamine 2000 reagent (for neurite length measurements, TIRF microscopy, and construct expression in N1E-115 cells). RFP-tagged TrkB was obtained from Moses Chao; CaSR-WT and CaSR-DN R185Q were obtained from Michel Levine. For expression in chicken neurons, pCAG-GFP vector (Addgene, 11150) was cut with SmaI and NotI, which removed GFP from the pCAG-GFP vector, which was replaced by CaSR-eGFP (restricted from a CaSR-eGFP-N1 vector) or the R185Q-GFP via ligation. Hereby, CaSR was expressed under a β -actin promoter.

For nodose neurons, neurons were dissected at Stage 20 and kept in “plating medium” for 2 h to settle before being transfected on the day of dissection. Because neurons become dependent on BDNF when kept in culture after Stage 24, we allowed neurons to grow for 30 h in plating medium at 37°C 5% CO₂ for the constructs to be expressed. Because of the short expression time, we enhanced the GFP signal after fixation using an anti-GFP antibody (ChromoTek, catalog #3h9-100, RRID:AB_10773374; details in Immunocytochemistry).

MEFs and N1E-115 cells were transfected at 70% density, and expression was allowed for 2–3 d.

Lipofectamine transfection was performed according to the manufacturer's instructions. For Solution A, 1 μ l of Lipofectamine 2000 (Thermo Fisher Scientific) was added to 100 μ l DMEM (Invitrogen) (to be adjusted to the final volume per well, depending on the experiment) and incubated for 5 min at room temperature. For Solution B, 1 μ g of the desired plasmid was added to 100 μ l of DMEM (to be adjusted to final volume per well). Then both solutions were mixed and incubated for 20 min at room temperature. In the meantime, “plating medium” from each well was replaced by prewarmed DMEM and stored at 37°C. After the incubation time, the transfection mixture was added to each well and incubated for 75 min at 37°C. Finally, the transfection mixture was removed, and the stored “plating medium” was added back to the cultures.

TIRF microscopy. Transfected MEFs were trypsinized and replated on a MatTek 35 mm glass-bottom poly-D-lysine-coated tissue culture dish. On the day of imaging, MEFs were kept in “starving medium” (DMEM without penicillin/streptomycin and FBS), which was adjusted to 0.7 mM calcium for 20 min. Then, “starving media” was refreshed serving as a control, and MEFs were placed on an AxioObserver Z1 TIRF microscope (Carl Zeiss) with an Evolve CCD camera (Photometrics) using the 100 \times objective and imaged (5 min time-lapse recordings with pictures taken in

10 s intervals). Subsequently, after imaging control conditions, MEFs were stimulated with 10 μ M of CaSR agonist R568 hydrochloride (Tocris Bioscience), 10 ng/ml BDNF (R&D Systems), or a combination of both, and imaged during 5 min time-lapse recordings with pictures taken in 10 s intervals. From time-lapse recordings, we analyzed colocalization and generated kymographs. Colocalization was evaluated using the Fiji colocalization plugin measuring the Pearson correlation coefficient (Fiji, RRID:SCR_002285). Kymographs were generated using the Fiji PlugIn KymographBuilder (RRID for KymographBuilder PlugIn not available, for Fiji software: RRID:SCR_002285). Comovement was evaluated by quantifying the percentage of moving tracks, where moving was defined as a deflection >20 degrees from vertical for at least 30 s.

Colocalization of CaSR and TrkB with endosomes (for immunocytochemistry). Nodose neurons were dissected as described above and plated on acidified glass coverslips coated with poly-L-ornithine and laminin at a density of ~5000 neurons per well and placed in 24-well tissue culture dishes (Greiner Cellstar, catalog #M9312-100EA). Neurons were grown at 5% CO₂ and 37°C for 24 h in “plating medium” (1.8 mM calcium) and, for Stage 30 nodose neurons, in the presence of 10 ng/ml BDNF (R&D Systems). After 24 h, neurons were starved for 20 min using “starving medium” adjusted to 0.7 mM calcium. Subsequently, neurons were stimulated for 20 min with 10 μ M of CaSR agonist R568 hydrochloride or 10 ng/ml BDNF. Nonstimulated neurons in “starving medium” served as a control. Following this, neurons were fixed in 4% PFA, washed 3 times in PBS, and stained with antibodies as described in Immunocytochemistry.

Immunocytochemistry. Nodose neurons were dissected as described above and fixed on DIV2 with 4% PFA. Cells were blocked in 0.1% Triton and 2% FBS for at least 60 min on a shaker at room temperature. Cells were then incubated in primary antibody (1/1000) overnight in blocking solution at 4°C. Antibodies used include the following: anti-GFP (rat) 3h9-100 ChromoTek (RRID:AB_10773374), EEA1 (rabbit), catalog #PA5-17228 Thermo Fisher Scientific (RRID:AB_11004515); Rab5 (mouse) catalog #108001 Synaptic Systems (RRID:AB_2619777); Rab11 (rabbit) catalog #ab3612 Abcam (RRID:AB_10861613); Rab7 (rabbit) catalog #D95F2 Cell Signaling Technology (RRID:AB_1904103); Lamp1 (rabbit) catalog #9091 Cell Signaling Technology (RRID:AB_2687579); TrkB (chicken) catalog #G1561 Promega (RRID:AB_430846), CaSR (goat) catalog #F19 Santa Cruz Biotechnology (RRID:AB_2290992), and β III-tubulin (mouse) catalog #ab78078 Abcam (RRID:AB_2256751). Secondary antibodies were AlexaFluor-488 goat anti-mouse catalog #A-11001 Thermo Fisher Scientific (RRID:AB_2534069); AlexaFluor-488 goat anti-rabbit catalog #A-11008, Thermo Fisher Scientific (RRID:AB_143165); AlexaFluor-546 goat anti-mouse catalog #A-11003, Invitrogen (RRID:AB_141370); AlexaFluor-546 goat anti-rabbit catalog #A-11035 Thermo Fisher Scientific (RRID:AB_2534093); AlexaFluor-488 goat anti-chicken catalog #A-11039 Invitrogen (RRID:AB_142924); AlexaFluor-488 donkey anti-goat catalog #A-11055 Thermo Fisher Scientific (RRID:AB_2534102); and AlexaFluor-546 donkey anti-rabbit catalog #A10040 Thermo Fischer Scientific (RRID:AB_2534016).

After three washes of ~5 min with PBS, secondary antibodies were applied for 120 min at room temperature. Cells were washed three times for 10 min with PBS followed by a quick rinse in ddH₂O, and then the coverslips were immediately mounted using Mowiol 4–88. Images were acquired with the LSM710 confocal microscope (Carl Zeiss) using the 63 \times or 100 \times objective, including Z stacks. Gain was set so that there was no saturation in the images. On average, 3 optical slices were taken per image at a 1 μ m interval between slices. Average optical thickness was 0.5 μ m.

Colocalization was analyzed in single optical slices with the Fiji colocalization plugin measuring the Pearson correlation coefficient (Fiji, RRID:SCR_002285).

Transfection with calcium phosphate (for coimmunoprecipitation). HEK293 cells were transfected using a calcium phosphate protocol to receive high levels of transfection for biochemistry experiments. Transfection buffer containing 274 mM NaCl, 10 mM KCl, 1.4 mM Na₂HPO₄, 15 mM glucose, and 42 mM HEPES was added dropwise to a solution of DNA (10 μ g/10 cm dish) and 250 mM CaCl₂. The resulting mix was kept in the dark for 20 min and then added onto HEK cells and left on for 1–2 d to allow expression.

Immunoprecipitation. HEK and N1E-115 cells (plated in 10 cm culture dishes in DMEM containing 10% FBS and 1% penicillin/streptomycin) were transfected with TrkB-RFP and CaSR-GFP constructs as described above. Two days after transfection, cells were washed with ice-cold PBS and subsequently lysed using 1 ml of “lysis buffer” containing 10 mM Tris/HCl, pH 7.5, 150 mM NaCl, 0.5 mM EDTA, and 0.5% NP-40. Protease inhibitors (Sigma-Aldrich, catalog #P8340) were added just before application. RFP-Trap, GFP-Trap (ChromoTek), or control beads (coated with rabbit IgG, Sigma-Aldrich, catalog #A8914) were washed 3 times with “wash buffer” (“lysis buffer” without NP-40) before use; 60 μ l was taken from the lysate for the input control and mixed with 60 μ l of 2 \times sample buffer. The whole leftover lysate was added to the beads for 3 h, followed by removal of the lysate from the beads and recovering 60 μ l for unbound controls, mixed with 60 μ l of 2 \times sample buffer. Beads were then washed 3 times with “wash buffer.” Following washing, 100 μ l of sample buffer was added to the beads. All samples were boiled for 10 min and then loaded on a 10% SDS-PAGE gel.

Western blots. Nodose ganglia were dissected as described above and plated in high density in 96-well plates (Greiner Cellstar, catalog #M0687-100EA, ~2 ganglia per 1 well) coated with poly-L-ornithine and laminin. After allowing neurons to grow for 24 h in “plating medium” (containing 10 ng/ml BDNF for neurons after Stage 22), neurons were starved in “starving medium” adjusted to 0.7 mM calcium for 20 min. Following starvation, medium was removed (except for control) and replaced by respective stimulants, which were either 10 μ M CaSR agonist in 0.7 mM “starving medium” (R568 hydrochloride, catalog #3815, Tocris Bioscience), 10 μ M antagonist in 2.3 mM “starving medium” (Calhex 231 hydrochloride, catalog #4387, Tocris Bioscience), 10 ng/ml BDNF in 0.7 mM “starving medium” (catalog #PHC7074, Invitrogen) or 10 ng/ml BDNF and 10 μ M CaSR agonist in 0.7 mM “starving medium” for 5, 15, and 30 min. Subsequently, neurons were lysed using “lysis buffer.” Samples were prepared for SDS-PAGE by adding 2 \times sample buffer and boiling for 10 min followed by loading on a 10%, 12%, or 15% SDS-PAGE gel, depending on the target protein size. Gels were transferred and developed using following antibodies: TrkB (rabbit), catalog #AB9872, Millipore (RRID:AB_2236301); β -actin, catalog #251003, Synaptic Systems (RRID:AB_11042458); p-AKT Ser473, catalog #TA328006, Acris, β III-tubulin, catalog #ab78078, Abcam (RRID:AB_2256751); p-Y279/216-GSK3, catalog #ab68476, Abcam (RRID:AB_10013745); p-S9-GSK3, catalog #5558, Cell Signaling Technology (RRID:AB_10013750); anti-RFP 5f8-100, ChromoTek (RRID:AB_2336064), anti-GFP 3h9-100, ChromoTek (RRID:AB_10773374); p-Tau ab109390, Abcam (RRID:AB_10860822); and β -catenin, catalog #4270, Cell Signaling Technology (RRID:AB_1903918). Secondary antibodies were IRDye 800RD donkey anti-mouse, catalog #925-32210, LI-COR Biosciences (RRID:AB_2687825) and IRDye 800RD donkey anti-rabbit, catalog #925-32211, LI-COR Biosciences (RRID:AB_2651127). Image acquisition was performed using Odyssey Imaging Systems, Odyssey CLx (RRID:SCR_014579), quantification was done using CAPT (RRID:SCR_016305).

Experimental design and statistical analysis. All experiments on chicken nodose neurons were performed using chicken embryos of both sexes either at Stage 22 or Stage 30. For individual experiments, 10–12 embryos were dissected from 3–5 independent experiments as indicated below. Statistical analysis was performed by GraphPad Prism 6.0 software (RRID:SCR_002798); level of significance was set at $p < 0.05$. For multiple-comparisons, one-way ANOVAs were performed followed by *post hoc* Sidak's, Tukey's, or Dunnett's, as appropriate and indicated below and in the figure legends. Since GraphPad Prism 6.0 software does not provide exact p values under a range of $p < 0.0001$, we refer to standard p value ranges as indicated in the figure legends. Exact p values (when provided) are indicated in Results. Degrees of freedom for each experiment are indicated in the text and in the figure legends.

We performed three individual experiments for dose–response and four independent experiments for CaSR agonist and antagonist responses at Stage 22 (see Fig. 1D). At Stage 30, we performed five independent experiments for CaSR agonist and antagonist responses (see Fig. 3D). The number of neurons imaged for these experiments ranged between 25 and 60 neurons per condition and experiment. Neurite length

was measured using the Fiji PlugIn Simple Neurite Tracer (RRID:SCR_016566). Significance was determined by one-way ANOVA with *post hoc* Tukey.

Branch points were counted on images from growth experiments in either 0.7 or 2.3 mM calcium or the CaSR agonist and antagonist (see Figs. 1E, 3F). For branch point analysis, we compared two groups by Student's t test and outliers were removed using Tukey's fences.

In vitro transfection was analyzed from three individual experiments. The number of neurons imaged for these experiments ranged between 15 and 30 per condition (see Fig. 1G). Neurite length was measured using the Fiji PlugIn Simple Neurite Tracer (RRID:SCR_016566). Significance was determined by one-way ANOVA with *post hoc* Tukey.

In vivo measurements were analyzed from three individual experiments with three or four embryos being used per condition and experiment. Since neurites were on different optical planes, three or four pictures were taken of each embryo. Three or four of the longest neurites were measured per plane and condition and used for analyses (see Fig. 1I). Neurite length was measured using the Fiji PlugIn Simple Neurite Tracer (RRID:SCR_016566). Significance was determined by one-way ANOVA with *post hoc* Tukey.

For experiments in the presence of PI3-kinase, GSK3, and Mek/Erk inhibitors, we performed four individual experiments (see Figs. 2B, 4B). The number of neurons imaged for these experiments ranged between 25 and 60 neurons per condition and experiment. Significance was determined by one-way ANOVA with *post hoc* Dunnett compared with control (2.3 mM calcium).

Western blots and coimmunoprecipitation experiments were analyzed from 4–6 individual experiments (see Figs. 2C–E, 4C–F, 7A–C, 9A–G, 10A–F). Significance was determined by one-way ANOVA with *post hoc* Tukey (see Figs. 2E, 4E) or Dunnett compared with normalized control (0.7 mM calcium also normalized to each loading control).

Colocalization experiments in neurons were analyzed from three individual experiments (see Figs. 2F, G, 5A–D, 6A–F) by using 15–30 images (containing two or three optical sections) per condition and experiment. An ROI was identified in a single optical section (excluding nucleus) and measured with the Fiji PlugIn for Pearson's correlation coefficient (Fiji, RRID:SCR_002285). Significance was determined by one-way ANOVA with *post hoc* Tukey.

Neuronal survival over development was analyzed from three individual experiments per age group. Neurons were counted as described in Materials and Methods. Significance was determined by one-way ANOVA with *post hoc* Sidak compared with the no factor control of each age group (see Fig. 3C).

Kymographs were analyzed using the Fiji KymographBuilder PlugIn, using three independent experiments and 10–15 time-lapse recordings per condition. Three or four kymographs (containing between 6 and 10 tracks) per recording were generated using the Fiji PlugIn KymographBuilder (RRID for KymographBuilder PlugIn not available, for Fiji software: RRID:SCR_002285). Comovement was evaluated by quantifying the percentage of moving tracks, where moving was defined as a deflection >20 degrees from vertical for at least 30 s. Significance was determined by one-way ANOVA with *post hoc* Tukey (see Fig. 8A–D).

Results

CaSR regulates growth in early, BDNF-TrkB-independent chicken nodose neurons

To address how the CaSR is able to enhance BDNF-mediated growth, we investigated how CaSR signals in isolation. First, we verified that chicken nodose neurons express CaSR but do not express TrkB receptors at early stages of development. It is reported that TrkB levels are very low at Stage 20 to Stage 22 of the Hamburger–Hamilton stages (Hamburger and Hamilton, 1992) and increase by twofold at Stage 23 and sixfold at Stage 24 (Robinson et al., 1996). Using Stage 22 chicken nodose neurons, we found no detectable levels of TrkB in Western blots (Fig. 1A). Since our CaSR antibody did not work in Western blots, we confirmed expression by performing immunocytochemistry and found the CaSR being expressed in Stage 22 nodose neurons (Fig.

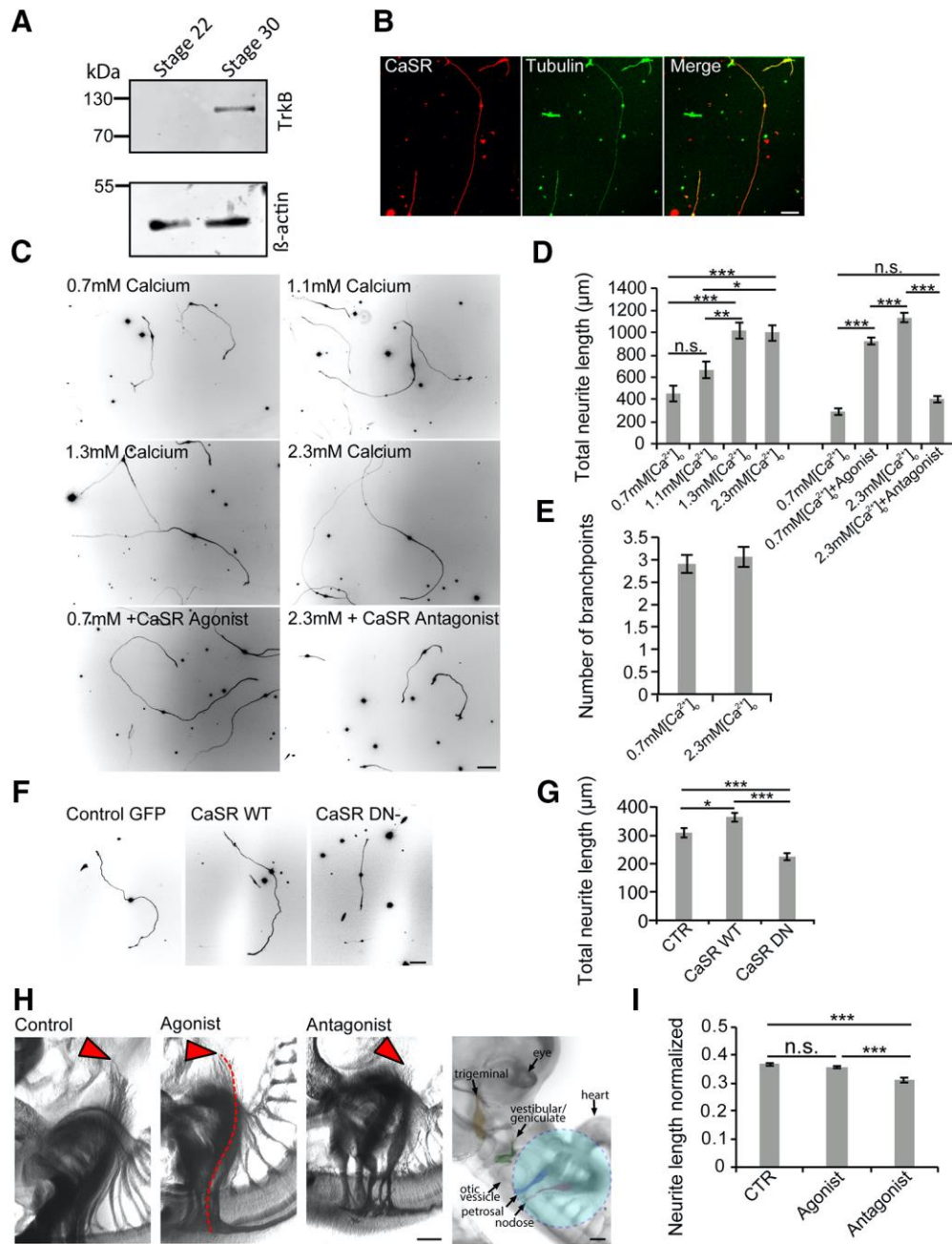


Figure 1. CaSR regulates growth in BDNF-independent nodose neurons. **A, B**, Expression of CaSR and TrkB in Stage 22 nodose neurons using Western blot and immunocytochemistry. **C–E**, Effects of high extracellular calcium, the CaSR agonist R568 hydrochloride, and the CaSR antagonist Calhex231 on neurite growth and branching in Stage 22 nodose neurons. **F, G**, *In vitro* effects of CaSR overexpression. **H, I**, Effects to the CaSR agonist R568 hydrochloride and the CaSR antagonist Calhex231 hydrochloride on neurite growth *in vivo*. Red arrows point to the end of the longest neurite of the nodose ganglion. Red dashed line indicates exemplary measurement of length. An overview of the area is given and ganglia marked in color as follows: pink represents nodose; blue represents petrosal; green represents vestibular; yellow represents trigeminal. Light blue shading represents the area of drug application. Quantification normalized to circumference of midbrain. Scale bar, 100 μm . Significance was determined by one-way ANOVA with *post hoc* Tukey. $n = 25$ –60 images per condition from three or four independent experiments (**D, G**). $Df_n = 3$, $Df_d = 641$ (**D**), $Df_n = 2$, $Df_d = 209$ (**G**). $n = 3$ or 4 embryos per condition from three independent experiments. $Df_n = 2$, $Df_d = 150$ (**I**). Branch points were analyzed using Student's *t* test to compare 0.7 mM with 2.3 mM $Df = 62$ (**E**). $n = 15$ –20 images per condition from three independent experiments. Error bar indicates SEM. * $p < 0.05$, ** $p < 0.01$, *** $p < 0.001$. Non-significant differences are indicated as n.s.

1B). Further, assessing neuronal survival during these early stages revealed that neurons do not require BDNF (see Fig. 3C).

Next, we raised the question whether CaSR can regulate axonal growth in BDNF-independent nodose neurons. Previous work reports enhanced growth of mouse SCG neurons using increased levels of extracellular calcium as well as a specific pharmacological CaSR agonist while showing reduced growth in the presence of a specific pharmacological antagonist (Vizard et al., 2008). At Stage 22, where TrkB is not expressed yet, increasing

levels of extracellular calcium enhanced neurite growth (Fig. 1C,D). We also found an increase in neurite length in the presence of 0.7 mM calcium together with the pharmacological CaSR agonist R568 hydrochloride (for calcium concentration, $F_{(3,192)} = 15.26$; for agonist and antagonist experiments, $F_{(3,641)} = 150.3$, 1.1 mM $[\text{Ca}^{2+}]_o$ vs 1.3 $[\text{Ca}^{2+}]_o$, $p = 0.007$; 1.1 mM $[\text{Ca}^{2+}]_o$ vs 2.3 $[\text{Ca}^{2+}]_o$, $p = 0.0138$; for significance, GraphPad Prism 6.0 software does not provide exact *p* values under a range of $p < 0.0001$, *post hoc* Tukey; Figure 1C,D). Further, we also found reduced

neurite length in the presence of high extracellular calcium (2.3 mM) and the pharmacological CaSR antagonist Calhex231 hydrochloride (Fig. 1C,D). Therefore, activating CaSR enhances neurite growth during early development when neurons are still independent of neurotrophic support.

To test whether CaSR activation induces branching, we quantified branch points per neuron. In all conditions, Stage 22 nodose neurons showed a bipolar morphology with an occasional branch point. We found no differences in branch points between neurons cultured in 0.7 mM calcium or in 2.3 mM calcium ($p = 0.599$, unpaired t test; Fig. 1E). To further investigate whether this is a specific response to CaSR, we transfected neurons with a CaSR-WT (referring to full-length CaSR) and a CaSR-dominant negative (DN) construct and compared neurite length to a GFP-transfected control. When transfecting *in vitro*, we found that overexpressing CaSR-WT enhanced neurite length compared with GFP control. The R185Q mutation of CaSR has been shown to attenuate the response to high extracellular calcium since the mutation resides within the extracellular domain where it modulates the affinity to extracellular calcium as well as to other agonists (Bai et al., 1996). When overexpressing the CaSR-R185Q construct in nodose neurons, we found a significant decrease in neurite length compared with control and the CaSR-WT construct ($F_{(2,209)} = 23.671$, GFP vs WT, $p = 0.0242$, GFP vs DN and WT vs DN, $p < 0.0001$, *post hoc* Tukey; Fig. 1F,G).

Next, we investigated axon growth effects *in vivo*. Because of the location of the nodose ganglia, *in ovo* electroporation proved to be technically challenging. Applying current for electroporation caused heart failure and embryonic death. Therefore, we used a different approach and applied the CaSR agonist R568 hydrochloride and the CaSR antagonist Calhex231 hydrochloride in the area of the nodose at Stage 18 and fixed the embryos at Stage 20. The area of application as well as the location of cranial neurons are shown in Figure 1H. Following whole-mount neurofilament staining, we measured the length of nodose neurons from the hindbrain to the longest neurite (method of measurement is indicated as a dashed line, arrow points to the longest neurite) and normalized the length to the circumference of the midbrain. Using this approach, we found no further increase in length using the CaSR agonist, but a significant decrease in neurite length with the CaSR antagonist ($F_{(2,150)} = 21.208$, CTR vs antagonist and agonist vs antagonist, $p < 0.0001$, *post hoc* Tukey; Fig. 1H,I).

At Stage 22, CaSR activates p-Akt and localizes to Rab7- and Lamp1-positive endosomes

Following the observation that CaSR regulates BDNF-independent neurite growth, we examined the downstream signaling pathway. Commonly described pathways in regulating axonal growth are the PI3-kinase-Akt-GSK3 pathway or the Mek-Erk pathway (Chao, 2003; Yoshimura et al., 2005; Zhou et al., 2008). Therefore, we dissected early Stage 22 chick nodose neurons, placed them in culture medium containing low (0.7 mM) and high (2.3 mM) levels of extracellular calcium in the presence of specific PI3-kinase, GSK3, and Mek inhibitors, and measured their response on neurite growth. We found that early chick nodose neurons, when cultured in 2.3 mM calcium, respond solely to the PI3-kinase inhibitor LY294002 with decreased growth but do not respond to the GSK3 and Mek inhibitors BIO and PD98059, respectively (Fig. 2A,B). Further, the CaSR was reported to signal through Mek-Erk in different cell types (Holstein et al., 2004; Brennan et al., 2013; Vizard et al., 2015; Mizumachi et al., 2017), a response we did not observe in Stage 22 chicken nodose neu-

rons. ($F_{(3,142)} = 14.262$, 2.3 mM $[Ca^{2+}]_o$ vs 2.3 mM $[Ca^{2+}]_o$ + LY $p < 0.0001$, *post hoc* Dunnett in 2.3 mM $[Ca^{2+}]_o$; Fig. 2A,B).

To confirm and to place this response specifically downstream of the CaSR, we stimulated these neurons with the allosteric CaSR agonist (in 0.7 mM calcium) and antagonist (in 2.3 mM calcium) and performed Western blots against p-Akt, p-GSK3 α Tyr279, and p-GSK3 β Tyr216 and p-GSK3 β Ser9. We found that indeed p-Akt was increased after activating CaSR but strongly decreased in the presence of the CaSR antagonist ($F_{(4,11)} = 34.708$, 0.7 mM $[Ca^{2+}]_o$ vs 15' 0.7 mM $[Ca^{2+}]_o$ + agonist and 5', 15', and 30' 2.3 mM $[Ca^{2+}]_o$ + antagonist vs 15' 0.7 mM $[Ca^{2+}]_o$ + agonist, $p < 0.0001$, *post hoc* Tukey; Fig. 2C–E). Surprisingly, but in line with the observation that the GSK3 inhibitor BIO had no effect on neurite growth, we did not find phosphorylation on GSK3 α Tyr279, p-GSK3 β Tyr216, or GSK3 β Ser9. This result was unexpected since the PI3-kinase-Akt pathway has been reported to be upstream of GSK3 β Ser9 (Yoshimura et al., 2005; Zhou et al., 2008; Bellon et al., 2010; Burk et al., 2017a), suggesting an uncoupled mechanism (Fig. 2C).

Because trafficking and signaling of receptors are tightly linked (Wu et al., 2001; Barford et al., 2017; Burk et al., 2017a), we next investigated the trafficking route of CaSR. Literature reports that CaSR is endocytosed and trafficked through Rab11-recycling endosomes, as well as being degraded through late endosomes (Holstein et al., 2004; Reyes-Ibarra et al., 2007; Zhuang et al., 2012; Ray, 2015). We performed colocalization experiments of CaSR with different endosomal compartments using antibodies against CaSR as well as EEA1, Rab11, Rab7, and Lamp1 to represent early, recycling, and late endosomes as well as lysosomes. When stimulated with the CaSR agonist in medium containing 0.7 mM calcium, we found high colocalization of activated CaSR with Rab7- and Lamp1-positive late endosomes/lysosomes ($F_{(3,588)} = 89.412$, except EEA1 vs Rab11, $p = 0.9996$, all other conditions compared in *post hoc* Tukey, $p < 0.0001$; Fig. 2F,G). In all, our data show that CaSR regulates neurotrophin-independent growth by activating Akt.

Late, BDNF-dependent neurite growth is enhanced by CaSR activation

Next, we studied the effect of CaSR activation in Stage 30 nodose neurons, which are dependent on BDNF for growth and survival (Robinson et al., 1996). In Stage 30 nodose neuron cultures, CaSR and TrkB are expressed in neurons but not in non-neuronal cells (Fig. 3A).

Further, we found that CaSR and TrkB show colocalizing puncta in nodose neurons (Fig. 3B). As previously reported (Vogel and Davies, 1991; Robinson et al., 1996), Stage 30 nodose neurons depend on BDNF for survival from Stage 24 onwards ($F_{(7,98)} = 26.336$, Stage 25 no factor vs BDNF and Stage 30 no factor vs BDNF significance under a range of $p < 0.0001$, *post hoc* Sidak; Fig. 3C). Since we found that CaSR regulates BDNF-independent growth, we raised the question whether CaSR activation could still regulate neurite growth in the absence of BDNF. To investigate this, neurons were plated in the presence of caspase inhibitors to block apoptosis (Gavaldà et al., 2009) and plated in either 0.7 mM or 2.3 mM calcium. Interestingly, at these later stages when neurons depend on BDNF for survival, CaSR activation alone failed to induce neurite growth (Fig. 3D,E). We then examined the effect of BDNF in the presence of low levels of extracellular calcium (0.7 mM) where the CaSR should be minimally active (Vizard et al., 2008). Here, BDNF-induced neurite growth significantly increased compared with neurons cultured in the presence of caspase inhibitors (Fig. 3D,E). However, plat-

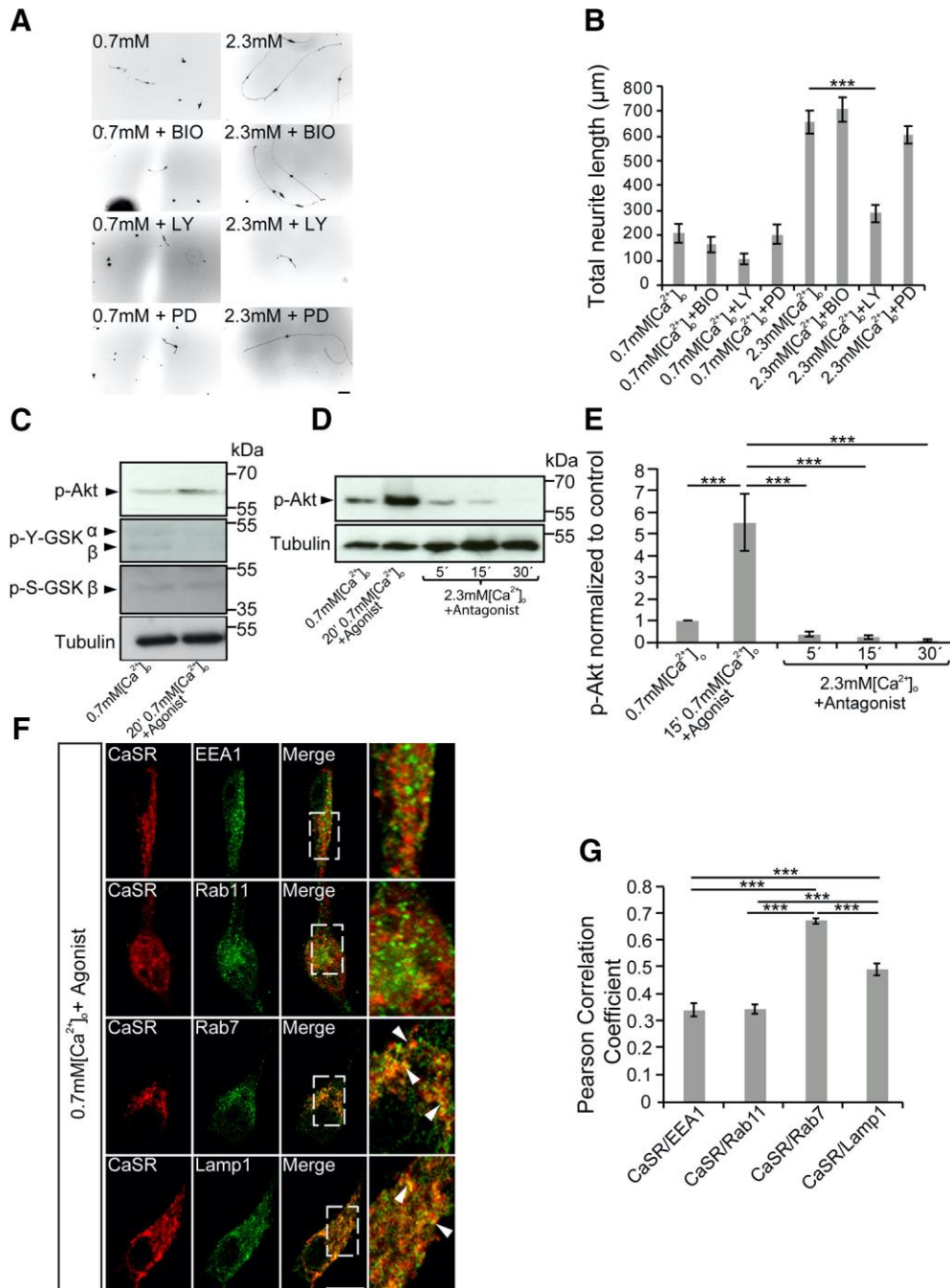


Figure 2. At Stage 22, CaSR signals through Akt and routes into late endosomes. **A, B**, Effects of inhibitors for GSK3 (BIO), PI3-kinase (LY), and Mek (PD) on neurite length in the presence of 0.7 or 2.3 mM extracellular calcium. **C, D**, Western blots for p-Akt and p-GSK3 after stimulation with the CaSR agonist and antagonist. **E**, Quantitation of p-Akt normalized to tubulin and control condition (0.7 mM calcium normalized to each loading control). **F, G**, Colocalization of CaSR with endosomal markers. Arrows point to colocalizing puncta. $n = 4–6$ independent experiments for Western blots. Scale bars: **A**, 100 μm ; **F**, 10 μm . Significance was determined by one-way ANOVA with *post hoc* Dunnett compared with control (0.7 mM calcium + agonist) (**B**) or Tukey (**E, G**). $n = 25–60$ images per condition from four independent experiments (**B, G**). $Df_n = 3$, $Df_d = 142$ (**B**), $Df_n = 3$, $Df_d = 588$ (**G**). $n =$ three independent experiments. $Df_n = 4$, $Df_d = 11$ (**E**). Error bar indicates SEM. *** $p < 0.001$.

ing neurons in the presence of BDNF together with 2.3 mM calcium or in 0.7 mM and in the CaSR agonist, further increased neurite length significantly compared with BDNF alone (Fig. 3D,E). In contrast, plating neurons in 2.3 mM calcium containing BDNF and the CaSR antagonist Calhex 231 reduced neurite length below the level of BDNF in 0.7 mM extracellular calcium ($F_{(5,10271)} = 230.187$, for 0.7 mM $[\text{Ca}^{2+}]_o$ + BDNF vs 2.3 mM $[\text{Ca}^{2+}]_o$ + antagonist, $p = 0.0009$, all other conditions compared in *post hoc* Tukey are under a range of $p < 0.0001$; Fig. 3D,E). In

addition to neurite length, we analyzed branching of these neurons. We found that Stage 30 nodose neurons, when cultured in 2.3 mM calcium and 10 ng/ml BDNF, had more branch points compared with 0.7 mM calcium control cultures containing 10 ng/ml BDNF. Also, when neurons were cultured in 2.3 mM calcium, 10 ng/ml BDNF and CaSR antagonist, branch points were significantly reduced compared with neurons cultured in 0.7 mM, calcium with 10 ng/ml BDNF and the CaSR agonist (0.7 mM $[\text{Ca}^{2+}]_o$ vs 2.3 mM $[\text{Ca}^{2+}]_o$ and 0.7 mM $[\text{Ca}^{2+}]_o$ + agonist vs 2.3

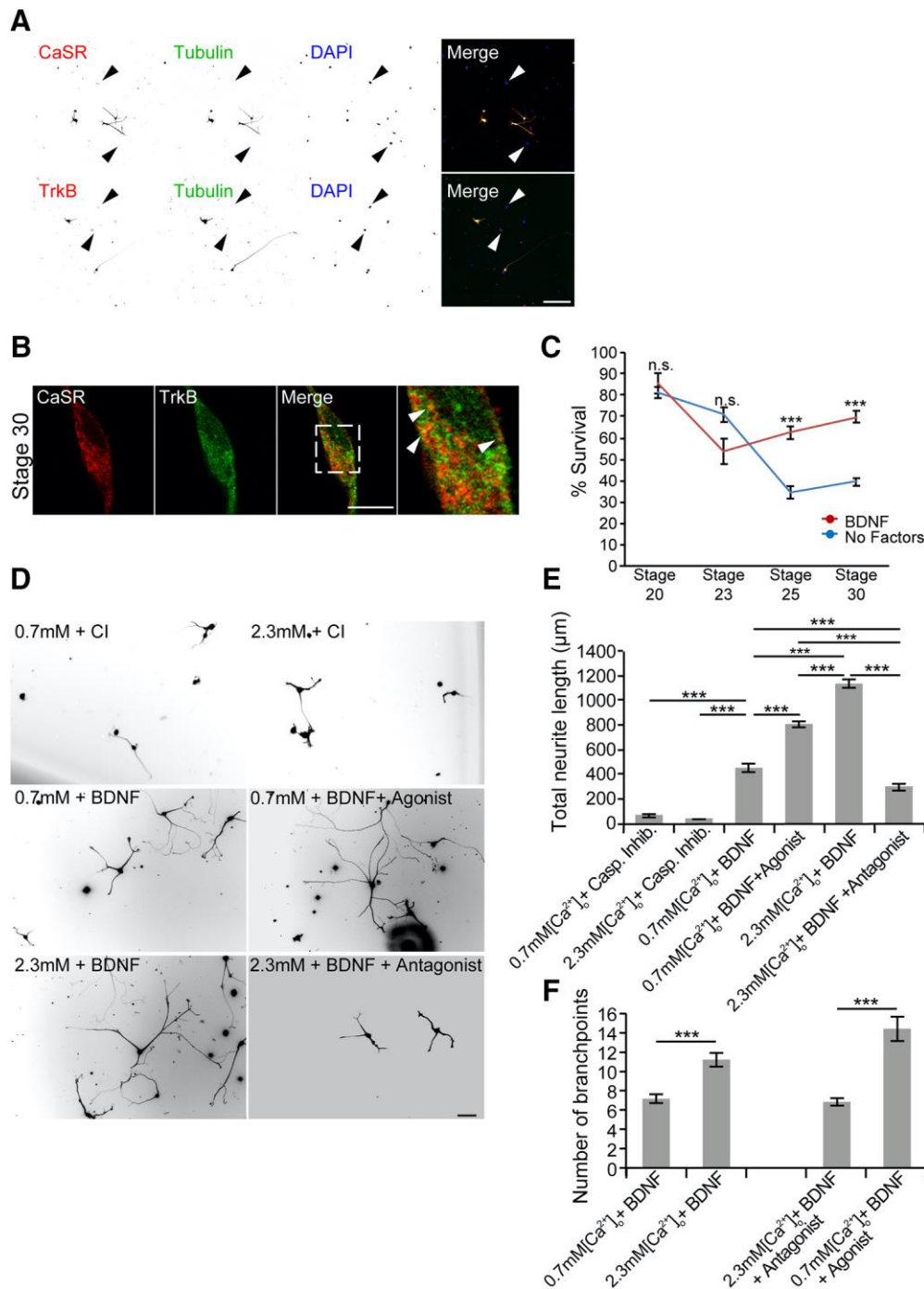


Figure 3. CaSR regulates growth in BDNF-dependent nodose neurons. **A**, Expression of CaSR and TrkB in Stage 30 nodose neurons but not in non-neuronal cells using immunocytochemistry. Arrows point to non-neuronal cells. **B**, CaSR and TrkB colocalizing in Stage 30 nodose neurons using immunocytochemistry. Arrows point to colocalizing puncta. **C**, Neuronal survival over development in the presence and absence of BDNF. **D**, Effects of high extracellular calcium, the CaSR agonist R568 hydrochloride, the CaSR antagonist Calhex231, and BDNF on neurite growth in Stage 30 nodose neurons. Cl, Caspase inhibitors. **E**, Quantitation of neuronal length as shown in **D**. **F**, Quantitation of branch points in 0.7 mM calcium, 2.3 mM calcium (together with BDNF), or with the CaSR agonist (in 0.7 mM calcium) and the CaSR antagonist (in 2.3 mM calcium, both in the presence of BDNF). Scale bars: **A, C**, 100 μm; **B**, 10 μm. Significance was determined by one-way ANOVA with *post hoc* Sidak. DFn = 7, DFd = 98 (**C**) or Tukey (**E**). *n* = 25–60 images per condition from five independent experiments. DFn = 5, DFd = 1271. Branch points were analyzed using Student’s *t* test to compare 0.7 mM with 2.3 mM and 2.3 mM + CaSR antagonist with 0.7 mM + CaSR agonist DF = 75 (**F**). Error bar indicates SEM. ****p* < 0.001. Non-significant differences are indicated as n.s.

mM [Ca²⁺]_o + antagonist *p* < 0.0001, unpaired *t* test; Fig. 3F). These results indicate that during a time point where neurons innervate their targets *in vivo* (Davies and Lindsay, 1985; Davies et al., 1986; Davies, 1989; Vogel and Davies, 1991; Robinson et al., 1996), CaSR enhances BDNF-mediated neurite length and branching from Stage 30 but fails to regulate growth when stimulated in isolation. This result is in line with previous reports by

Vizard et al. (2008) where the authors show that the CaSR enhances NGF-mediated neurite growth.

At Stage 30, CaSR activates p-tyrosine GSK3 and localizes to Rab7 and Lamp1-positive endosomes

Surprisingly, at Stage 30, we found the downstream signaling cascade of CaSR changed after the onset of BDNF dependence.

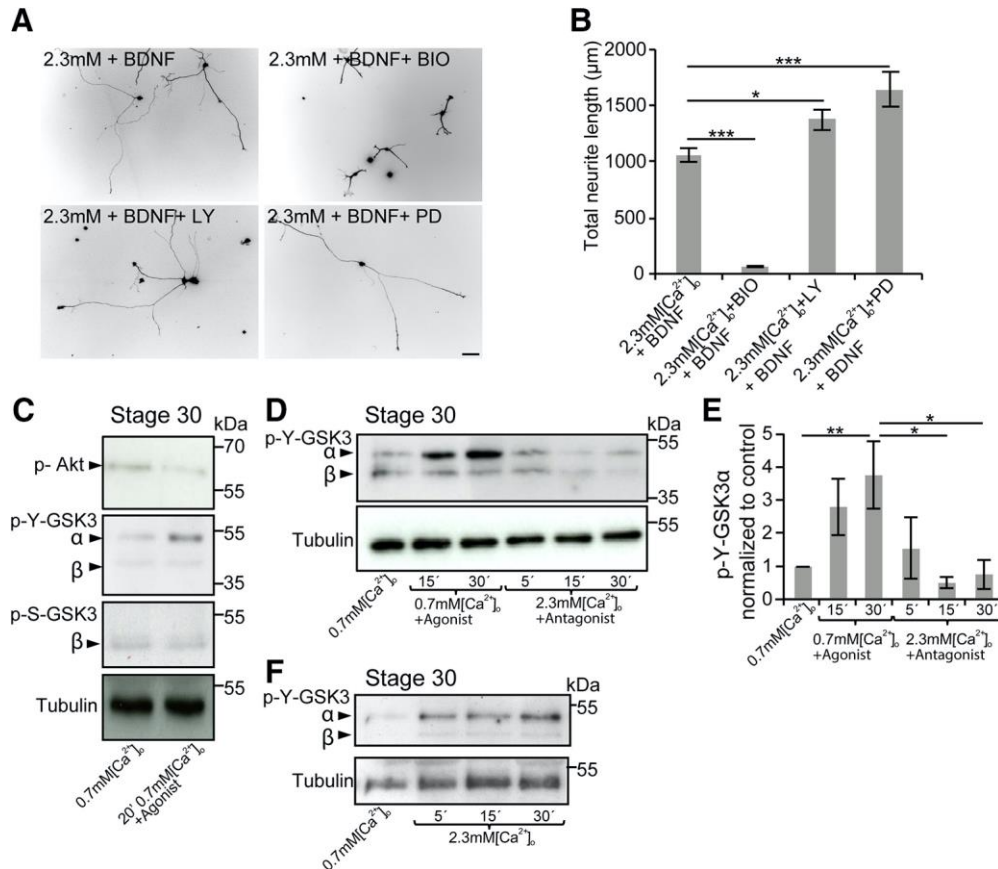


Figure 4. At Stage 30, CaSR signals through GSK3. **A, B**, Effects and quantitation of inhibitors for GSK3, PI3-kinase, and Mek (BIO, LY, and PD, respectively) on neurite length in the presence of 2.3 mM extracellular calcium. **C, D**, Western blots for p-Akt and p-GSK3 after stimulation with the CaSR agonist or antagonist. **E**, Quantitation of p-GSK3 normalized to tubulin and control condition (0.7 mM calcium normalized to each loading control). **F**, Western blot for p-GSK3 Tyr279 (α) and Tyr216 (β) after stimulation with 2.3 mM calcium. $N = 4-6$ independent experiments for Western blots. Scale bar: **A**, 100 μm . Significance was determined by one-way ANOVA with *post hoc* Tukey (**E**) or Dunnett (**B**) compared with control (2.3 mM + BDNF). $n = 25-60$ images per condition from four independent experiments. $Df_n = 3$, $Df_d = 131$ (**B**), $Df_n = 5$, $Df_d = 21$ (**E**). Error bar indicates SEM. * $p < 0.05$, ** $p < 0.01$, *** $p < 0.001$.

When plating neurons in the presence of 2.3 mM calcium containing 10 ng/ml BDNF as well as in the presence of PI3-kinase, GSK3, or Mek inhibitors, we found a different response compared with Stage 22 BDNF-independent neurons. Unlike at Stage 22, the PI3-kinase inhibitor LY294002 as well as Mek inhibition using PD98059 showed an increase on neurite growth, whereas blocking GSK3 signaling inhibited neurite growth significantly ($F_{(3,131)} = 76.104$, 2.3 mM $[\text{Ca}^{2+}]_o$ + BDNF vs 2.3 mM $[\text{Ca}^{2+}]_o$ + BDNF + LY, $p = 0.0129$, all other conditions compared with control under a range of $p < 0.0001$, *post hoc* Dunnett; Fig. 4A, B).

We confirmed this result using biochemistry. For this experiment, we grew neurons for 24 h in plating medium containing 10 ng/ml of BDNF to ensure growth and survival. The next day, neurons were starved in “starving medium” adjusted to 0.7 mM without BDNF for 20 min. Subsequently, neurons were stimulated in starving medium containing the allosteric CaSR agonist (in 0.7 mM calcium) or antagonist (in 2.3 mM calcium), and lysates were analyzed by Western blots. Stimulating Stage 30 nodose neurons with CaSR agonist did not lead to phosphorylation of Akt (Fig. 4C1). In contrast, stimulation of CaSR by the CaSR agonist as well as 2.3 mM calcium increased phosphorylation on GSK3 α Tyr279 (Fig. 4C2, E, F) but not on GSK3 β Ser9 (Fig. 4C3). This phosphorylation of Tyr279 could be reversed by adding the CaSR antagonist in the presence of 2.3 mM calcium ($F_{(5,21)} = 4.677$, 0.7 mM $[\text{Ca}^{2+}]_o$ vs 30' 0.7 mM $[\text{Ca}^{2+}]_o$ + agonist, $p = 0.0097$, 30' 0.7 mM $[\text{Ca}^{2+}]_o$ + agonist vs 15' 2.3 mM $[\text{Ca}^{2+}]_o$ +

antagonist, $p = 0.0231$, 30' 0.7 mM $[\text{Ca}^{2+}]_o$ + agonist vs 30' 2.3 mM $[\text{Ca}^{2+}]_o$ + antagonist, $p = 0.0412$, *post hoc* Tukey; Fig. 4D, E).

Because the signaling cascade completely changed in BDNF-dependent nodose neurons, we assessed whether this was linked to a change in the trafficking path of CaSR. We repeated colocalization experiments using antibodies for the CaSR and EEA1, Rab11, Rab7, and Lamp1 to represent early, recycling, and late endosomes, respectively. We found that at BDNF-dependent stages, activated CaSR still localized to late, Rab7, and Lamp-1 positive endosomes ($F_{(3,429)} = 168.384$, except for Rab7 vs Lamp1, $p = 0.9105$; all other conditions are under a range of $p < 0.0001$, *post hoc* Tukey; Fig. 5C, D) whereas in nonstimulated conditions, CaSR localized mainly to Lamp1-positive compartments ($F_{(3,86)} = 10.804$, Lamp1 vs EEA1, $p = 0.0010$, Lamp1 vs Rab11, $p = 0.0004$, Lamp1 vs Rab7, $p < 0.0001$, *post hoc* Tukey; Fig. 5A, B).

CaSR and TrkB colocalize in late Rab7-positive endosomes

Because the change in signaling was not facilitated by a change in localization of CaSR to endosomes, we wanted to determine whether the change in signaling of CaSR was dependent on TrkB. Therefore, we first investigated the localization of TrkB in Stage 30 chicken nodose neurons. We performed immunostainings and colocalization experiments using antibodies against TrkB with antibodies against EEA1, Rab11, Rab7, or Lamp1. We found

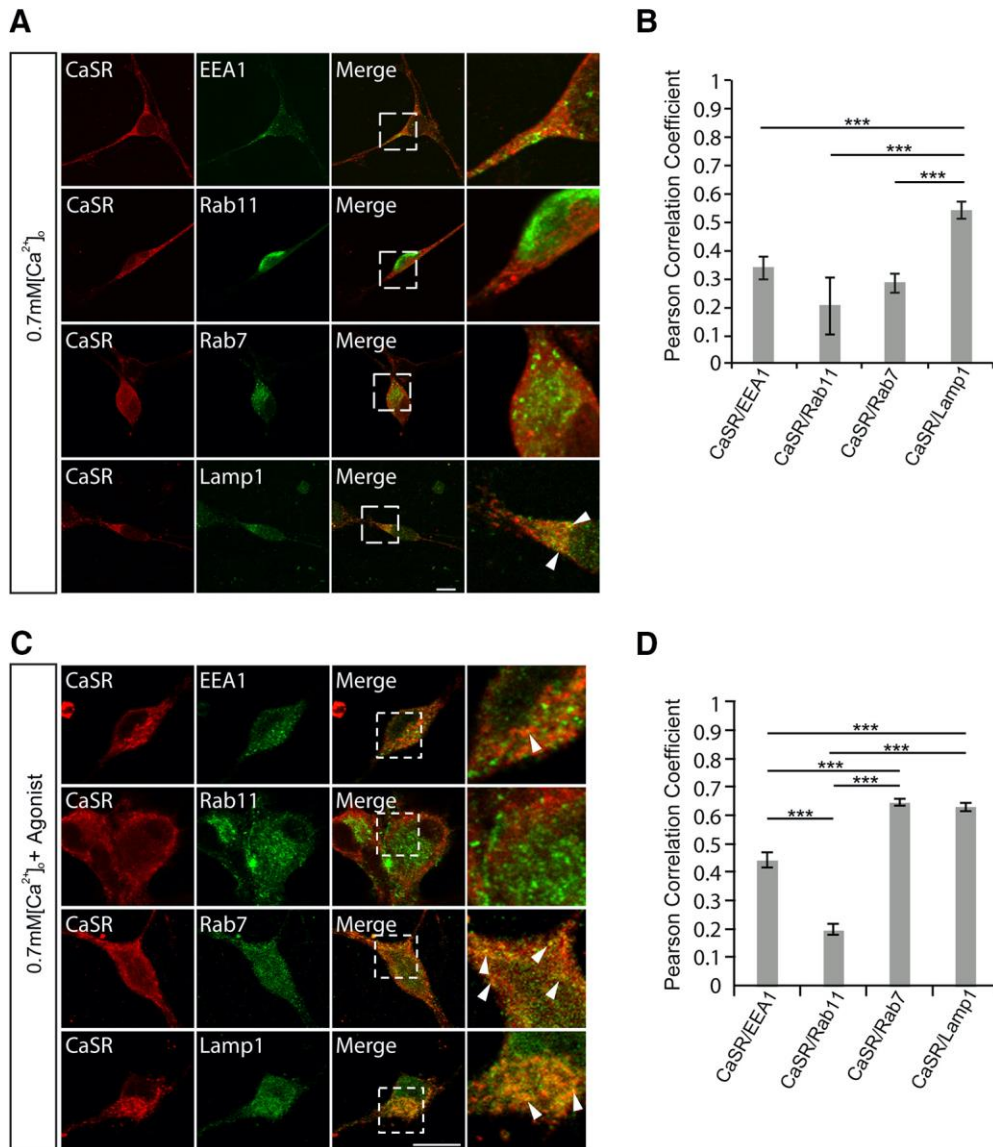


Figure 5. Activated CaSR localizes to Rab7-positive endosomes. **A, B**, Colocalization and quantitation of CaSR with endosomal markers EEA1, Rab11, Rab7, and Lamp1 in nonstimulated conditions. **C, D**, Colocalization and quantitation of CaSR with endosomal markers Rab7 and Lamp1 in the presence of the CaSR agonist. Arrows point to colocalizing puncta. Scale bar, 10 μ m. Significance was determined by one-way ANOVA with *post hoc* Tukey. $n = 15$ –30 images per condition from three independent experiments. Dfn = 3, Dfd = 86 (**B**), Dfn = 3, Dfd = 429 (**D**). Error bar indicates SEM. *** $p < 0.001$.

that, when starved of BDNF and calcium, TrkB showed low localization to all endosomal compartments but highest colocalization to recycling endosomes ($F_{(3,89)} = 15.788$, Rab11 vs all other conditions, $p < 0.0001$, *post hoc* Tukey; Fig. 6A,B). However, in the presence of BDNF in 0.7 mM calcium, TrkB routed from early into late, Rab7-positive endosomes ($F_{(3,145)} = 43.783$, EEA1 vs Lamp1, $p = 0.0104$, EEA1 vs Rab11, $p = 0.0001$, EEA1 vs Rab7, $p < 0.0001$, Rab7 vs Rab11, $p < 0.0001$ and Rab7 vs Lamp1, $p < 0.0001$, *post hoc* Tukey; Fig. 6C,D). The routing of activated TrkB into Rab7 endosomes has been reported by other groups (Kuruville et al., 2004; Deinhardt et al., 2006; Burk et al., 2017b). Further, Trk receptors start their downstream signaling from the endosomal compartment to which they localize (Wu et al., 2001; Kuruville et al., 2004; Saxena et al., 2005; Zhou et al., 2012; Barford et al., 2017). To evaluate whether CaSR and TrkB colocalize in endosomal compartments, we performed colocalization experiments between CaSR, TrkB, and the late endosomal markers Rab7 or Lamp1. We found that CaSR and TrkB show a high level

of colocalization with each other. Also, both receptors show high colocalization with Rab7-positive endosomes. However, colocalization between CaSR and Lamp1 as well as TrkB and Lamp1 was reduced compared with Rab7 ($F_{(5,180)} = 30.241$, TrkB/Rab7 vs TrkB/Lamp1 and CaSR/Rab7 vs CaSR/Lamp1, $p < 0.0001$, *post hoc* Sidak; Fig. 6E,F). These results indicate that at later developmental stages, CaSR and TrkB traffic within the same Rab7-positive endosomal compartments.

CaSR and TrkB coimmunoprecipitate and cotraffic

In an event where changes in signaling of CaSR were dependent on TrkB, we hypothesized that both receptors have to be in close proximity and physically interact. As mentioned, using immunofluorescence in Stage 30 chicken nodose neurons, we found colocalized puncta for CaSR and TrkB (Figs. 3B, 6E,F).

To determine whether both receptors interact physically, we overexpressed CaSR-WT-GFP or CaSR-DN-GFP together with either RFP or TrkB-RFP in HEK293 cells and performed RFP-

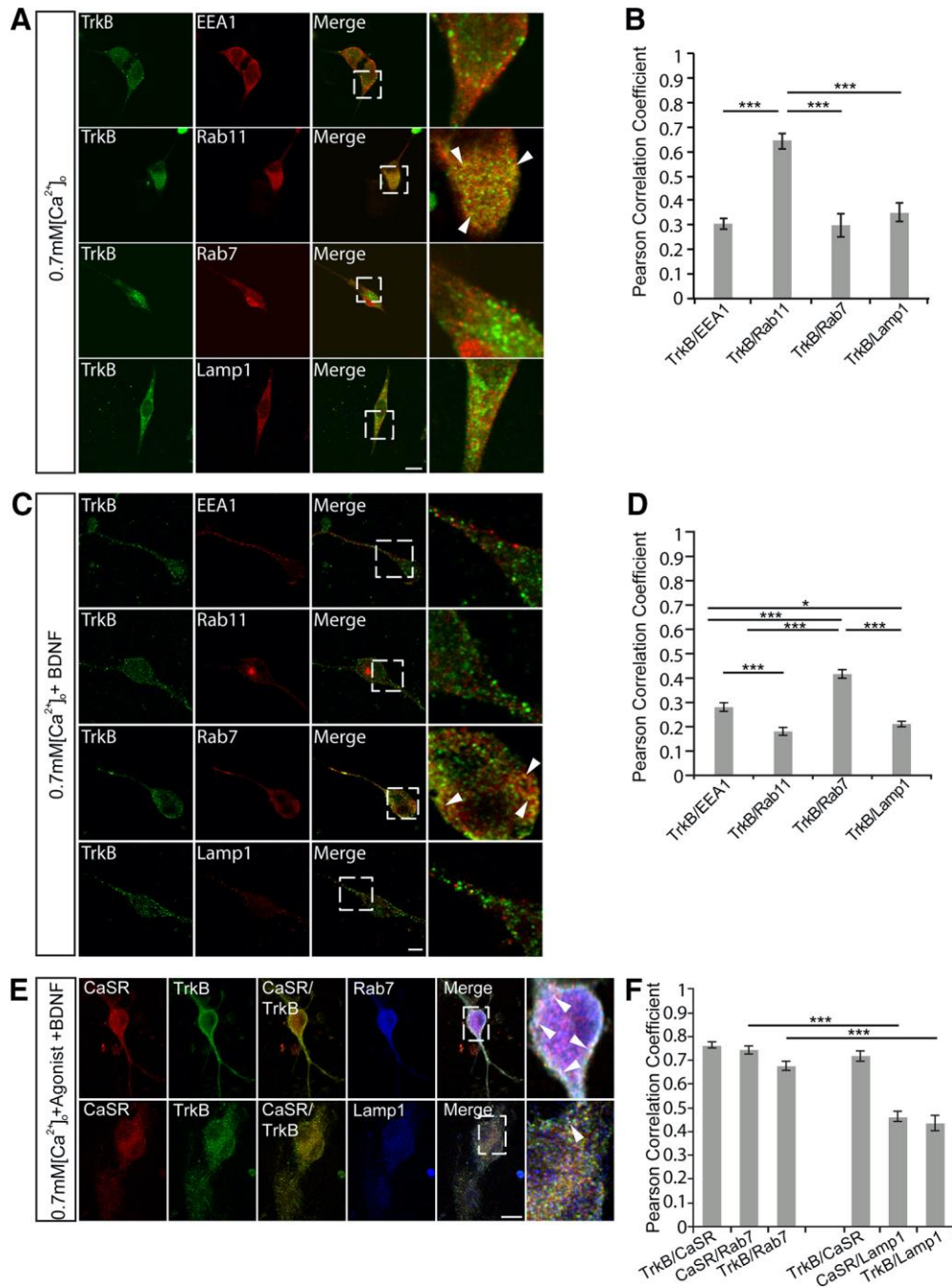


Figure 6. Activated TrkB localizes in Rab7-positive endosomes where it colocalizes with CaSR. **A, B**, Colocalization and quantitation of TrkB with endosomal markers EEA1, Rab11, Rab7, and Lamp1 in nonstimulated conditions. **C, D**, Localization and quantitation of TrkB and the endosomal markers EEA1, Rab11, Rab7, and Lamp1 in the presence of BDNF. **E, F**, Colocalization and quantitation of CaSR and TrkB as well as with endosomal markers Rab7 and Lamp1. Arrows point to colocalizing puncta. Scale bar, 10 μ m. Significance was determined by one-way ANOVA with *post hoc* Tukey test (**B, D**) or Sidak test (**F**). $n = 15$ –30 images per condition from three independent experiments. DFn = 3, Dfd = 89 (**B**), DFn = 3, Dfd = 145 (**D**), DFn = 5, Dfd = 180 (**F**). Error bar indicates SEM. * $p < 0.05$, *** $p < 0.001$.

Trap coimmunoprecipitation. Both CaSR-WT and CaSR-DN coimmunoprecipitated with TrkB but not with control (i.e., IgG-coated beads or when CaSR-GFP was coexpressed with RFP only) (Fig. 7A). The CaSR-DN construct R185Q has its mutation in the extracellular domain where it modulates the affinity to extracellular calcium as well as to other agonists, which could explain the interaction of R185Q with TrkB.

In a GFP-Trap reverse coimmunoprecipitation, we overexpressed CaSR-GFP with TrkB-RFP and tested whether interactions were ligand-dependent. We again found an interaction

between CaSR and TrkB, and this interaction was ligand-independent (Fig. 7B).

To verify the interaction in neuronal cells, we overexpressed CaSR-WT and CaSR-DN constructs in N1E-115 cells and performed RFP-Trap coimmunoprecipitation. Also, in these cells, we found interaction of TrkB with both CaSR-WT and CaSR-DN (Fig. 7C).

To investigate whether both receptors cotraffic, we overexpressed a CaSR-GFP and a TrkB-RFP construct in MEFs and kept them either in nonstimulated (0.7 mM) or stimulated conditions

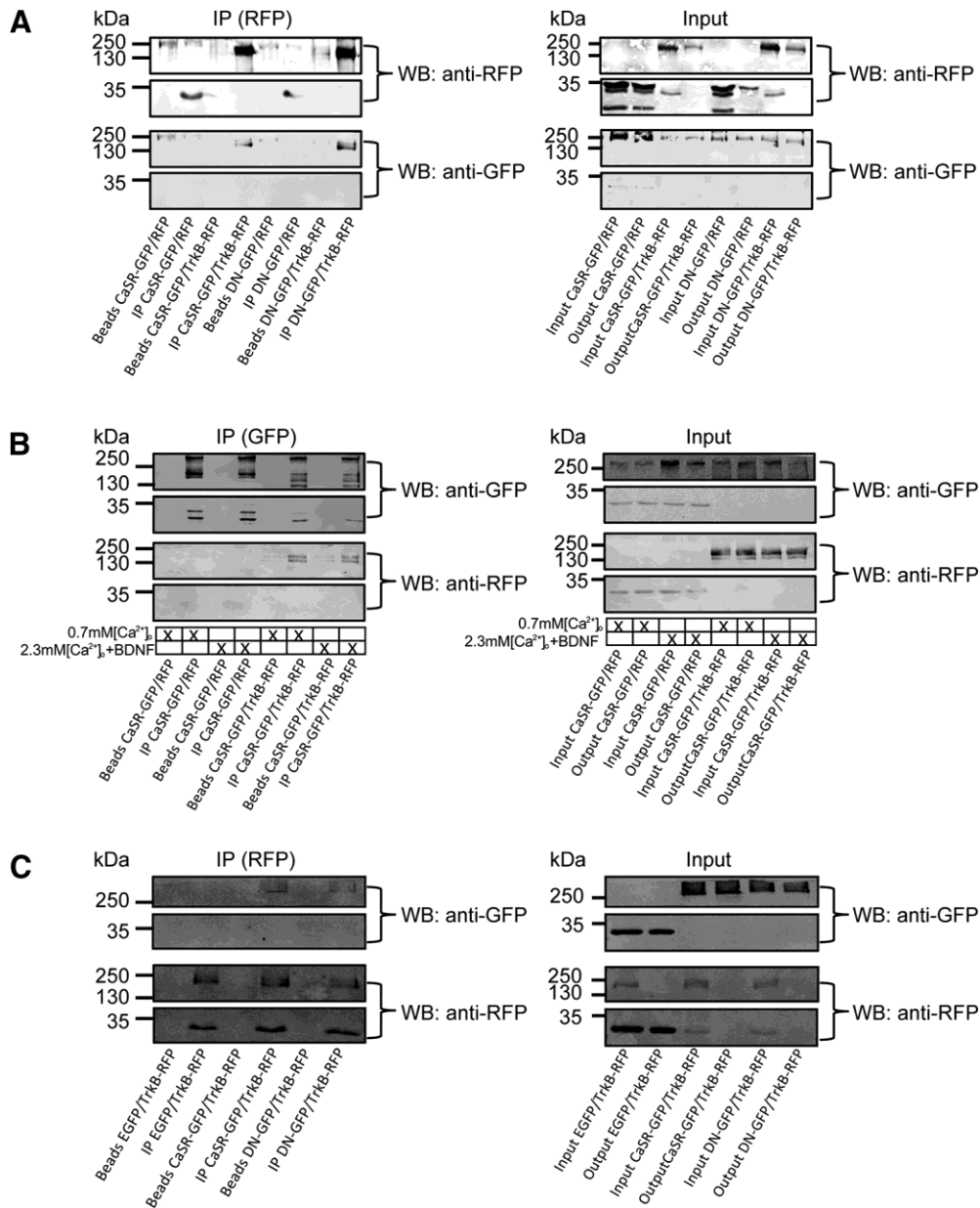


Figure 7. CaSR coimmunoprecipitates with TrkB. **A**, CaSR and CaSR DN coimmunoprecipitate with TrkB in HEK293 cells. **B**, Interaction of CaSR and TrkB is ligand-independent. **C**, CaSR and CaSR DN interact with TrkB in neuronal N1E-115 cells.

(0.7 mM calcium together with the CaSR agonist, BDNF, or both) and first performed colocalization experiments. Using this approach, we found that CaSR and TrkB colocalize in all above conditions to similar extent (ANOVA nonsignificant; Fig. 8D, Pearson’s colocalization index ranging from 0.73 to 0.8), further supporting our finding that colocalization was ligand-independent.

We then asked whether both receptors cotraffic and whether this cotrafficking was dependent on receptor activation. To test this, we performed TIRF microscopy. Our experimental set up included the following conditions: nonstimulated (0.7 mM calcium), 0.7 mM calcium + CaSR agonist R568 hydrochloride, 0.7 mM calcium + BDNF, and 0.7 mM calcium + BDNF + R568 hydrochloride.

Despite the colocalization and interaction in all conditions (Fig. 8D), we found different behaviors for cotrafficking: in control conditions (0.7 mM calcium), the CaSR and TrkB had

colocalizing tracks but minimal comovement (Fig. 8A,B). When we stimulated one of the two receptors, by either applying BDNF or the CaSR agonist R568 hydrochloride, comovement increased significantly compared with control and was equal between both receptors (Fig. 8A,B). Coactivation of both receptors by applying BDNF and CaSR agonist R568 hydrochloride further increased cotrafficking significantly compared with activation of CaSR or TrkB alone ($F_{(3,332)} = 24.1$, 0.7 mM [Ca²⁺]_o vs 0.7 mM [Ca²⁺]_o + BDNF, $p = 0.0025$, 0.7 mM [Ca²⁺]_o vs 0.7 mM [Ca²⁺]_o + agonist, $p = 0.0011$, 0.7 mM [Ca²⁺]_o vs 0.7 mM [Ca²⁺]_o + agonist + BDNF, $p < 0.0001$, 0.7 mM [Ca²⁺]_o + BDNF vs 0.7 mM [Ca²⁺]_o + agonist + BDNF, $p < 0.0001$, and 0.7 mM [Ca²⁺]_o + agonist vs 0.7 mM [Ca²⁺]_o + agonist + BDNF, $p < 0.0001$, *post hoc* Tukey; Fig. 8A,B). Next, we overexpressed the R185Q CaSR construct together with TrkB and performed cotrafficking analysis. In-

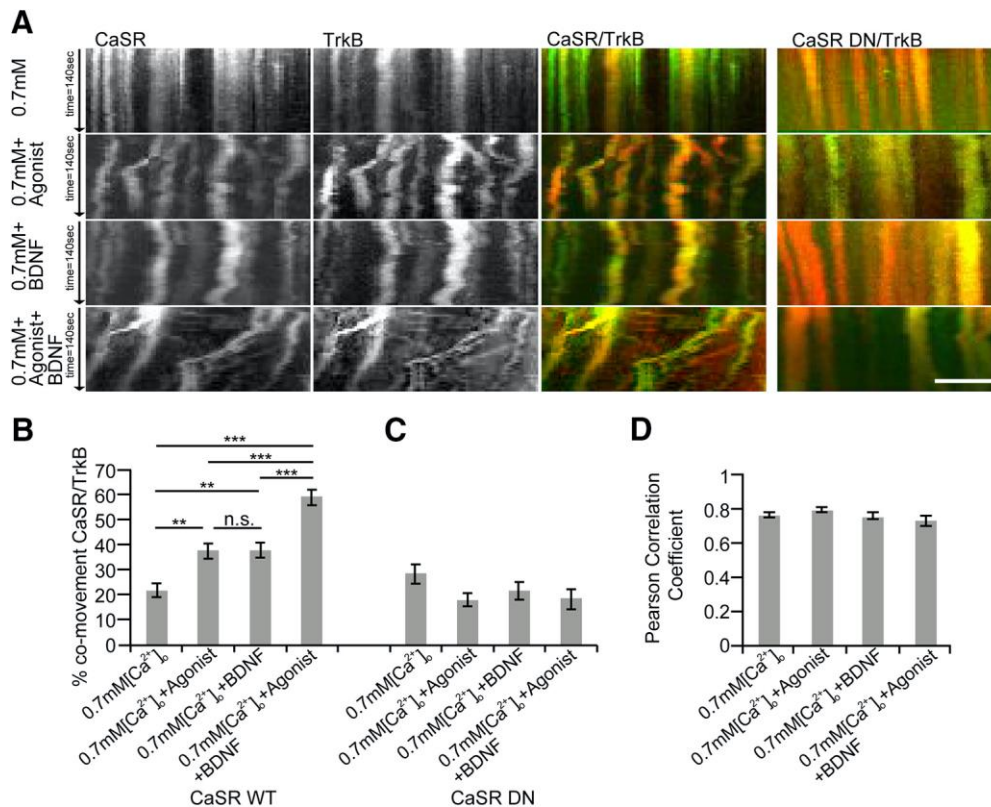


Figure 8. CaSR traffics together with TrkB. **A**, Kymographs of cotrafficking CaSR or CaSR-DN and TrkB in unstimulated and stimulated conditions from TIRF time-lapse images of MEFs cotransfected with CaSR-GFP or CaSR-DN-GFP and TrkB-RFP. **B**, Quantitation of comovement of CaSR and TrkB. Both, CaSR and TrkB when stimulated individually are able to increase comovement. This comovement further increases when both receptors are active simultaneously. **A, C**, Comovement decreases when TrkB is overexpressed with CaSR DN R185R. **D**, Colocalization of CaSR and TrkB under nonstimulated and stimulated conditions. Scale bar, 10 μ m. Significance was determined by one-way ANOVA with *post hoc* Tukey. $n = 25$ images per condition from three independent experiments. DFn = 3, Dfd = 332 (**B**), DFn = 3, Dfd = 199 (**C**). Error bar indicates SEM. ** $p < 0.01$, *** $p < 0.001$. Non-significant differences are indicated as n.s.

terestingly, using the CaSR DN construct, we did not find an increase in cotrafficking in any of the conditions (ANOVA nonsignificant; Fig. 8A, C).

CaSR and TrkB regulate growth through coactivation of GSK3

As mentioned earlier, receptor trafficking from endosomes and their downstream signaling are tightly linked (Dobrowolski and De Robertis, 2011; Pálffy et al., 2012; Harrington and Ginty, 2013). Since we found that CaSR and TrkB localize to the same endosomal compartments, coimmunoprecipitate and cotraffic, we raised the question whether enhanced neurite growth is modulated because both receptors activate the same signaling node.

In Figures 4C, D, F and 9A, B, we found that CaSR activation leads to a significant increase in phosphorylation on GSK3 α Tyr279 ($F_{(3,14)} = 3.550$, 0.7 mM [Ca²⁺]_o vs 30' 0.7 mM [Ca²⁺]_o + agonist, $p = 0.036$, *post hoc* Dunnett; Fig. 9A, B). Therefore, we tested whether TrkB activation through BDNF can also cause phosphorylation on GSK3 α Tyr279 and GSK3 β Tyr216. Interestingly, stimulation of Stage 30 nodose neurons with BDNF in 0.7 mM calcium significantly increased phosphorylation on GSK3 α Tyr279 after 30 min as well as on GSK3 β Tyr216 at 15 and 30 min ($F_{(3,12)} = 4.862$, GSK3 α Tyr279: 0.7 mM [Ca²⁺]_o vs 30' 0.7 mM [Ca²⁺]_o + BDNF, $p = 0.008$; $F_{(3,12)} = 7.984$, GSK3 β Tyr216: 0.7 mM [Ca²⁺]_o vs 15' 0.7 mM [Ca²⁺]_o + BDNF, $p = 0.0226$ and 0.7 mM [Ca²⁺]_o vs 30' 0.7 mM [Ca²⁺]_o + BDNF $p = 0.0016$, *post hoc* Dunnett; Figure 9C, D). Further, BDNF also activated the previously reported GSK3 β Ser9 pathway (Yoshimura et al., 2005),

showing that BDNF is able to target GSK3 on three phosphorylation sites in nodose neurons (Fig. 9C).

Next, we hypothesized that coactivation of CaSR and TrkB would potentially lead to an additive effect on GSK3 α Tyr279 and GSK3 β Tyr216, given the fact that both receptors phosphorylate these residues when stimulated individually. To test this, we starved Stage 30 nodose neurons in 0.7 mM calcium and applied either the CaSR agonist R568 hydrochloride or BDNF + R568 hydrochloride to cultured neurons.

When CaSR and TrkB were activated simultaneously, phosphorylation on GSK3 α Tyr279 significantly increased at 5, 15, and 30 min ($F_{(4,19)} = 3.623$, 0.7 mM [Ca²⁺]_o vs 30' 0.7 mM [Ca²⁺]_o + agonist, $p = 0.049$, 0.7 mM [Ca²⁺]_o vs 15' 0.7 mM [Ca²⁺]_o + BDNF + agonist, $p = 0.0326$, 0.7 mM [Ca²⁺]_o vs 30' 0.7 mM [Ca²⁺]_o + BDNF + agonist, $p = 0.0151$, *post hoc* Dunnett; Fig. 9E, F). However, given our hypothesis that we would potentially see an additive effect, we were surprised that there was no increase in phosphorylation on GSK3 α Tyr279 compared with agonist stimulation only and that phosphorylation on GSK3 β Tyr216 disappeared (Fig. 9E, F). To show that BDNF was added to the cultures and that it was functional, we stripped and reprobbed the membrane with an anti-GSK3 β Ser9 antibody. Control and agonist lanes confirmed the absence of BDNF while in 5, 15, and 30 min an increase in p-GSK3 Ser9 appeared due to BDNF stimulation (Fig. 9E). This result suggests that coactivation of CaSR and TrkB changes the downstream target of TrkB from GSK3 Tyr279/216 and Ser9 to GSK3 Ser9 phosphorylation only.

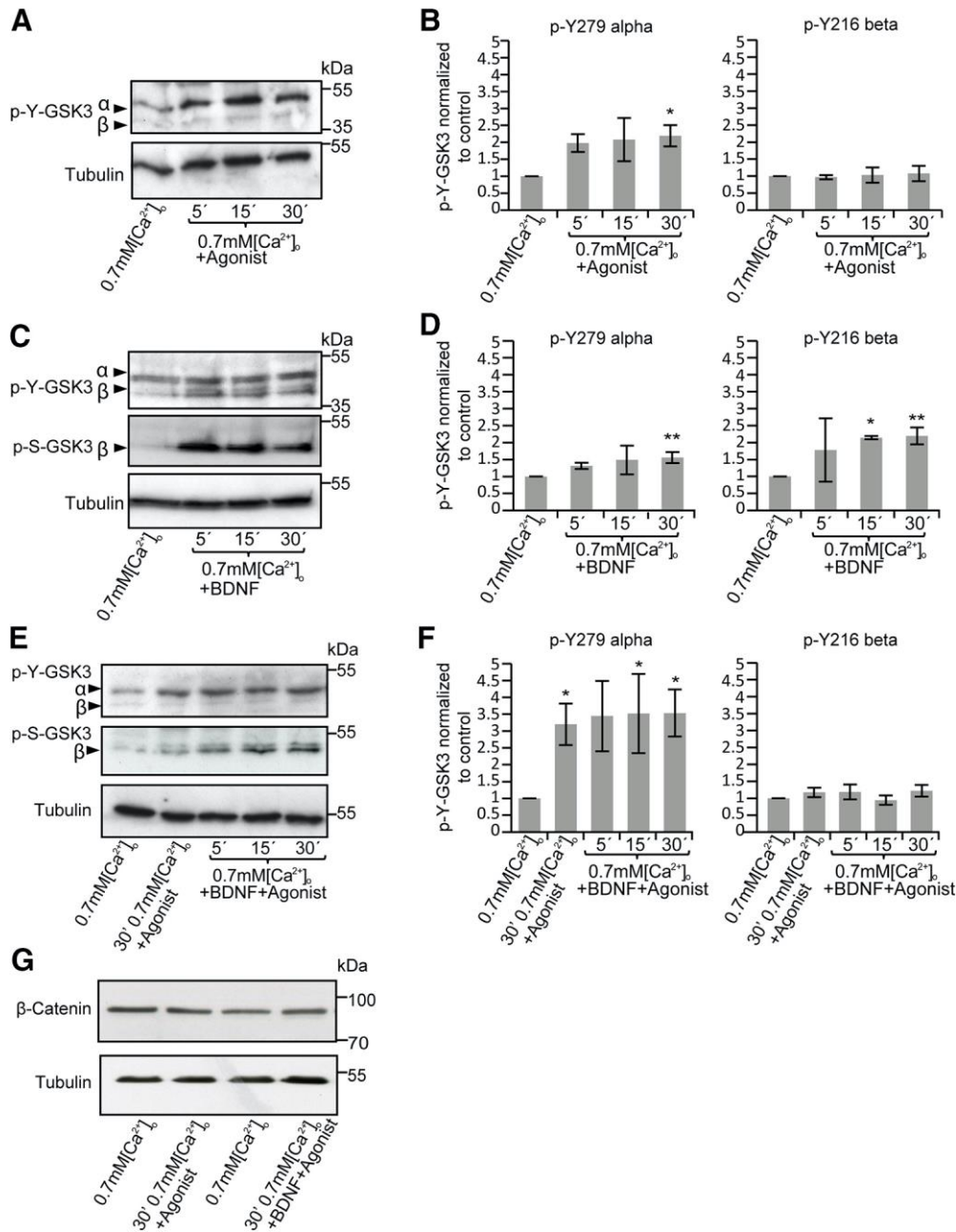


Figure 9. CaSR and TrkB activate GSK3. **A**, Western blot of p-GSK3 Tyr279 (α) and Tyr216 (β) after stimulation with the CaSR agonist R568 hydrochloride. **B**, Quantitation of p-GSK3 Tyr normalized to tubulin and 0.7 mM control. **C**, Western blot of p-GSK3 Tyr279, Tyr216, and Ser9 after stimulation with BDNF. **D**, Quantitation of p-GSK3 Tyr normalized to tubulin and 0.7 mM control. **E**, Western blot of p-GSK3 Tyr279, Tyr216, and Ser9 after stimulation with the CaSR agonist R568 hydrochloride, BDNF, or both. **F**, Quantitation of p-GSK3 Tyr normalized to tubulin and 0.7 mM control. **G**, Western blot of β -catenin after stimulation with the CaSR agonist or CaSR agonist + BDNF in 0.7 mM calcium. $N = 4-6$ independent experiments. Significance was determined by one-way ANOVA with *post hoc* Dunnett compared with control (0.7 mM calcium) $DF_n = 3$, $DF_d = 14$ (**B**), $DF_n = 3$, $DF_d = 12$ (**D**), $DF_n = 4$, $DF_d = 18$ (**F**). Error bar indicates SEM. * $p < 0.05$, ** $p < 0.01$.

Because phosphorylation on GSK3 Tyr residues has been reported to increase the activity of GSK3 and phosphorylation on GSK3 Ser9 to decrease the activity (Cross et al., 1995; Hartigan and Johnson, 1999; Lesort et al., 1999; Yoshimura et al., 2005), these results indicate that GSK3 is kept in a cycling state, which potentially affects downstream targets of GSK3.

To test whether other pathways are involved, we also tested whether the β -catenin pathway, which has been reported to interact with GSK3 and regulate axon growth (Lu et al., 2004), got activated when stimulated with the CaSR agonist and BDNF. In this experiment, we observed no changes following CaSR or TrkB

activation, suggesting no involvement of the β -catenin pathway (Fig. 9G).

Activation of GSK3 through CaSR phosphorylates Tau

To link activation of GSK3 to neurite growth, we tested whether CaSR activates Tau. To test this, we starved Stage 30 nodose neurons in 0.7 mM calcium and applied the CaSR agonist for 5 and 15 min as well as the CaSR antagonist for 5, 15, and 30 min. Western blots against p-Tau revealed a significant increase in Tau activation after 15 min of CaSR stimulation and a strong decrease in phosphorylation in the presence of CaSR antagonist ($F_{(5,26)} =$

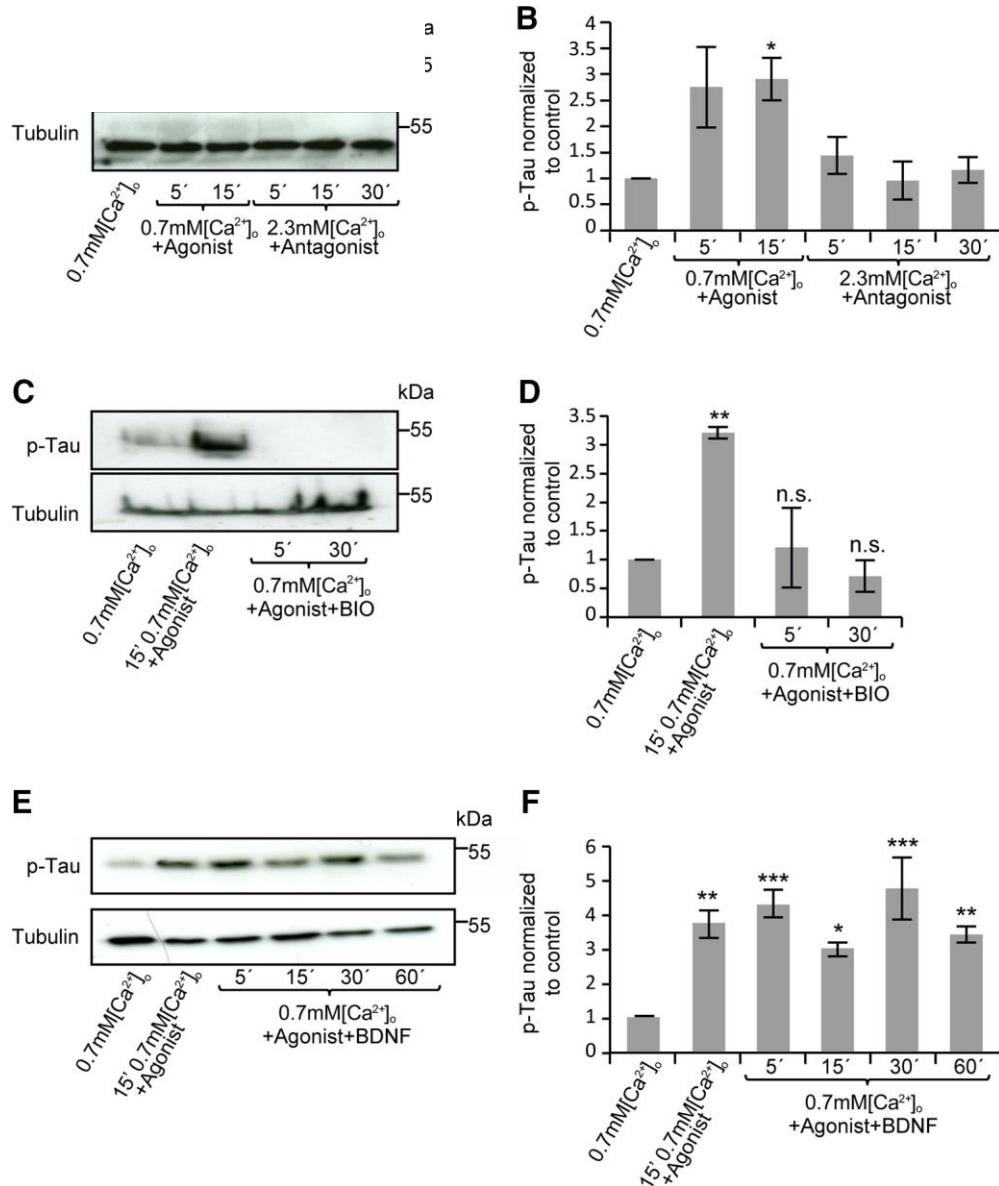


Figure 10. Coactivation of CaSR and TrkB cycles phosphorylation state of Tau. **A**, Western blot of p-Tau after stimulation with R568 hydrochloride in 0.7 mM for 5 and 15 min and Calhex231 in 2.3 mM calcium for 5, 15, and 30 min. **B**, Quantitation of p-Tau normalized to tubulin and 0.7 mM control. **C**, Western blot of p-Tau after stimulation with R568 hydrochloride in 0.7 mM calcium or R568 hydrochloride in 0.7 mM calcium + BIO (GSK3 inhibitor). **D**, Quantitation of p-Tau normalized to tubulin and 0.7 mM control. **E**, Western blot of p-Tau after a time course stimulation with the CaSR agonist R568 hydrochloride and CaSR agonist R568 + BDNF. **F**, Quantitation of p-Tau normalized to tubulin and 0.7 mM control. $N = 4-6$ independent experiments. Significance was determined by one-way ANOVA with *post hoc* Dunnett compared with control (0.7 mM calcium), $DF_n = 5$, $DF_d = 26$ (**B**), $DF_n = 3$, $DF_d = 18$ (**D**), $DF_n = 5$, $DF_d = 18$ (**F**). Error bar indicates SEM. * $p < 0.05$, ** $p < 0.01$, *** $p < 0.001$. Non-significant differences are indicated as n.s.

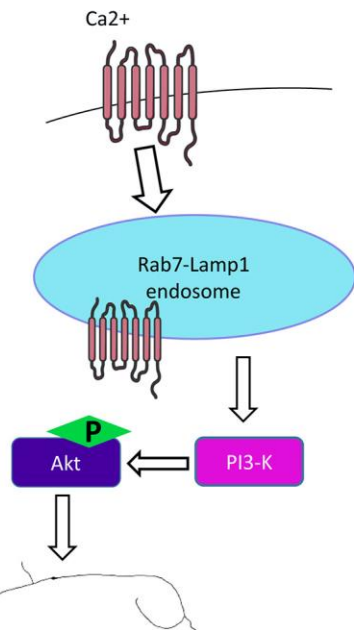
3.015, 0.7 mM $[Ca^{2+}]_o$ vs 15' 0.7 mM $[Ca^{2+}]_o$ + agonist, $p = 0.0291$, *post hoc* Dunnett; Fig. 10A,B). To verify that this activation was downstream of GSK3, we also applied the GSK3 inhibitor BIO to neurons cultured in 0.7 mM calcium plus the CaSR agonist. Indeed, we found a decrease in p-Tau after blocking GSK3 ($F_{(3,18)} = 7.112$, 0.7 mM $[Ca^{2+}]_o$ vs 15' 0.7 mM $[Ca^{2+}]_o$ + agonist, $p = 0.0015$, *post hoc* Dunnett; Fig. 10C,D). Since we hypothesized that GSK3 is regulated in a cycling way between an active and an inactive state through CaSR and TrkB, we speculated that Tau should show fluctuations in its phosphorylation state. We tested this by performing a time course on p-Tau where we used a 0.7 mM control, 0.7 mM together with R568 hydrochloride or 0.7 mM + R568 hydrochloride + BDNF for 5, 15, 30, and 60 minutes. Indeed, we found that, compared with 0.7 mM control, Tau was significantly phosphorylated, but we found a cy-

cling behavior between the stimulated conditions ($F_{(5,18)} = 8.042$, all conditions were compared with 0.7 mM $[Ca^{2+}]_o$ for 15' 0.7 mM $[Ca^{2+}]_o$ + agonist, $p = 0.0026$, 5' 0.7 mM $[Ca^{2+}]_o$ + agonist + BDNF, $p = 0.0004$, 15' 0.7 mM $[Ca^{2+}]_o$ + agonist + BDNF, $p = 0.0280$, 30' 0.7 mM $[Ca^{2+}]_o$ + agonist + BDNF $p = 0.0001$, 60' 0.7 mM $[Ca^{2+}]_o$ + agonist + BDNF $p = 0.0072$, *post hoc* Dunnett; Fig. 10E,F). These results suggest that neurite growth is regulated through the GSK3-Tau pathway following activation of CaSR.

Discussion

Neurons use different signaling systems to diversify the read-out to a limited number of guidance cues, increasing possible growth and guidance responses. However, despite recent progress, our understanding of how signal integration induces growth and

A Early development „en route“ to target



B Late development, during target innervation

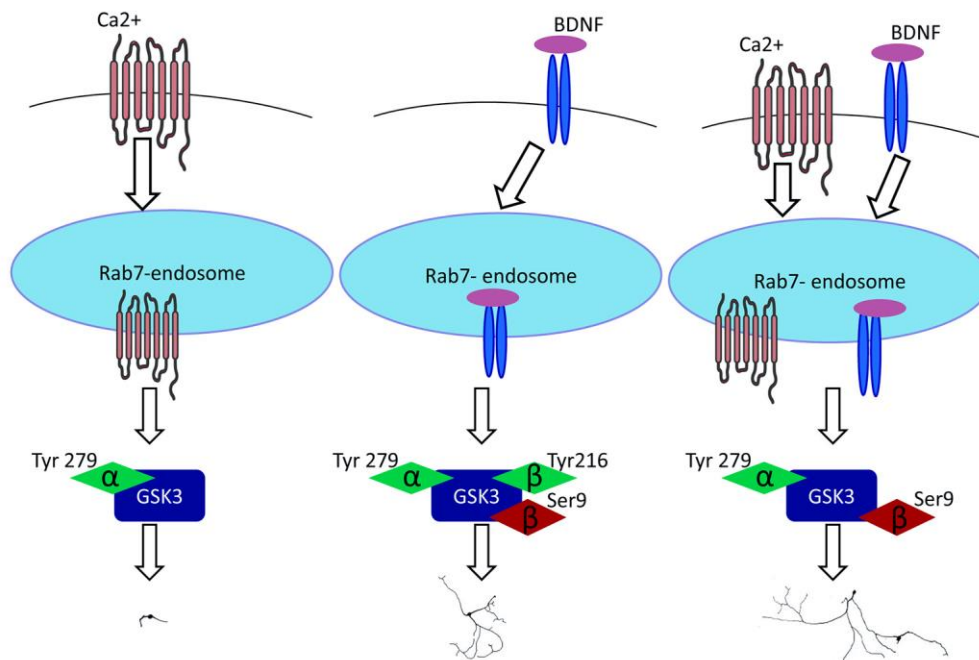


Figure 11. Summary of CaSR regulating growth in early nodose neurons and synergistic effects of CaSR/TrkB in late nodose neurons. **A**, Nodose neurons, which do not express TrkB, regulate growth by routing CaSR into Rab7 endosomes and activation of p-Akt. **B**, During target innervation, activation of CaSR leads to routing into Rab7 endosomes and phosphorylation of GSK3 α Tyr279. This phosphorylation only leads to minimal growth. Activation of TrkB leads to phosphorylation of GSK3 α Tyr279 and GSK3 β Tyr216, as well as GSK3 β Ser9. This interaction leads to an increase in growth compared with activation of CaSR alone. Activation of both CaSR and TrkB simultaneously leads to nonadditive effects by phosphorylating GSK3 α Tyr279 and GSK3 β Ser9. This coactivation significantly increases neurite growth compared with BDNF stimulation alone. Illustration of the CaSR was taken from Servier Medical Art templates, which are licensed under a Creative Commons Attribution 3.0 Unported License; <https://smart.servier.com>.

guidance remains incomplete. In this study, we show that CaSR regulates neural growth in two different ways: in isolation during early chick development and as a coreceptor of TrkB at later developmental stages. Coactivation of CaSR and TrkB leads to a change in downstream signaling of CaSR. During target innervation, CaSR and TrkB both localize to Rab7-late endosomes, coimmunoprecipitate, and phosphorylate GSK3 on specific residues, which causes GSK3 to cycle in its activity state. This change

in activity subsequently results in cycling of the phosphorylation state of Tau, potentially modulating microtubule assembly and disassembly.

Neurotrophic independence of cranial neurons

The duration of neurotrophic independence for survival and the expression of TrkB in early cranial neurons, which are *en route* to their targets, correlate with target distance and with the arrival of

axons in the vicinity of their targets (Vogel and Davies, 1991; Robinson et al., 1996).

In Figure 3C, we demonstrate that neurons become dependent on neurotrophic support for survival around Stage 24 (see also Robinson et al., 1996) and that the survival rate in absence of BDNF at Stage 30 (representing E6.5 to E7) is ~35%. Importantly, our results are in line with the observations of Vogel and Davies (1991) where the authors cultured different cranial sensory neurons in the absence of BDNF for up to 144 h and found a survival rate of ~40%.

However, why ~30%–40% of neurons survive in the absence of BDNF remains unexplained. For survival experiments, neurons were cultured in low density, and we expected neurotrophins produced by neurons themselves to be diluted in the culture medium and therefore ineffective. However, supplementary data of Vizard et al. (2008) show that cultured SCG neurons show ~20% survival in the absence of NGF and ~40% survival in the presence of only 0.1 ng/ml NGF. Therefore, it is possible that some neurons respond to very low amounts of neurotrophic factors produced by neurons themselves.

Further, nodose neurons have been found to consist of several types of neurons, which show differences in their conductance velocity and their morphological appearance (Li and Schild, 2007; Lu et al., 2013). Apart from prosurvival signaling mediated by neurotrophins, an increase in spontaneous activity is commonly associated with a decreased rate of apoptosis (Golbs et al., 2011; Murase et al., 2011; Blanquie et al., 2017). For example, adult-generated neurons from the olfactory bulb have been shown to require intrinsic electrical properties to survive before and during their integration with their synaptic targets (Lin et al., 2010).

Thus, one possible mechanism to explain higher survival rates in nodose neurons could be that these (or a subset of these) neurons show intrinsic electrical activity for a certain amount of time to increase survival before and during target innervation.

Signaling of CaSR during development

Unfortunately, not much is known about $[Ca^{2+}]_o$ in the chicken embryo. One paper reported that calcium levels in the chicken blood serum (in milligrams Ca/100 mg) rise during development (Narbaiz et al., 1973). In the rat, $[Ca^{2+}]_o$ levels of cerebrospinal fluid declines from about 1.6 mM in the fetus to 1.1 mM in adults (Jones and Keep, 1988), showing that these embryos are hypercalcemic during development. Further, it is known that in humans, the fetus is hypercalcemic in their blood calcium levels compared to the mother (Kovacs and Kronenberg, 1997). Therefore, our findings suggest that the $[Ca^{2+}]_o$, to which nodose neurons are exposed to during development, constitutively stimulate neurite and axonal growth via CaSR.

To understand how signal integration of CaSR and TrkB functions, we took advantage of the fact that nodose neurons do not express TrkB until Hamburger–Hamilton Stage 23/24. We first investigated signaling of CaSR in the absence of TrkB during early development. In the absence of TrkB at Stage 22 (Davies et al., 1986; Davies, 1989; Vogel and Davies, 1991; Robinson et al., 1996), we show that activation of CaSR regulates neurite growth *in vitro* and *in vivo*.

Because trafficking and signaling are tightly linked (Dobrowolski and De Robertis, 2011; Pálffy et al., 2012; Harrington and Ginty, 2013), we evaluated the signaling cascade of CaSR as well as its localization to endosomes. Activation of CaSR leads to localization to late endosomes and phosphorylation of Akt but does not activate GSK3 or MAPK signaling, which is interesting since

CaSR was reported to activate the Mek-Erk pathway in various cell types (Holstein et al., 2004; Reyes-Ibarra et al., 2007; Vizard et al., 2015; Mizumachi et al., 2017). However, later in development, we observed that blocking Mek with PD98059 caused neurons to grow larger compared with 2.3 mM calcium, suggesting a developmental as well as a cell-specific response.

At the time of target innervation, nodose neurons become dependent on BDNF-TrkB signaling for growth and survival (Davies and Lindsay, 1985; Lindsay et al., 1985; Vogel and Davies, 1991; Robinson et al., 1996). At Stage 30, CaSR is unable to regulate growth when activated in isolation but enhances TrkB/BDNF-mediated neurite growth. As mentioned, Trk receptors traffic in and signal from Rab7-positive endosomes (Kuruville et al., 2004; Deinhardt et al., 2006; Burk et al., 2017b). For CaSR to enhance TrkB-mediated growth, we hypothesized that both receptors need to be in close proximity to interact. The literature reports that CaSR is endocytosed and traffics through Rab11-recycling endosomes, as well as being degraded through late endosomes (Holstein et al., 2004; Reyes-Ibarra et al., 2007; Zhuang et al., 2012; Ray, 2015). Indeed, in Stage 30 nodose neurons, CaSR colocalizes in late Rab7-positive endosomes and coimmunoprecipitates to and cotraffics with TrkB. Further, at Stage 30, CaSR switches its downstream signaling from Akt to GSK3 α Tyr279, a finding we are the first to report (discussed below).

How neurons switch their downstream signaling cascades from one protein to another is still debated. Because many proteins localize to endosomal membranes and can be targeted by multiple interconnected upstream players, mechanisms must exist to “insulate” the multitude of signals received by the cell. In the example of GSK3, insulation of signaling pathways has been proposed by regulation of the kinase that is used to prime a target for GSK3-mediated phosphorylation as well as other factors, such as the relative affinity of GSK3 for various target proteins (Dobrowolski and De Robertis, 2011). Our results suggest that the switch in CaSR signaling is spatiotemporally controlled, increasing the response range to different target cues over time. Still, which players regulate response mechanisms upstream of GSK3 or Akt, or how CaSR interacts with TrkB, direct or indirect, remains unanswered and will be subject of future research.

Neurite growth regulation by GSK3 via signal integration of CaSR and TrkB

Different growth and guidance cues use the Akt-GSK3 β Ser9 pathway to regulate neurite growth (Yoshimura et al., 2005; Zhou et al., 2008; Bellon et al., 2010). However, we report, for the first time, that phosphorylation on GSK3 α Tyr279 and GSK3 β Tyr216 is also involved in regulating neurite growth, which is interesting for two reasons. First, until now, the physiological significance of tyrosine phosphorylation on GSK3 α remained unclear, especially because this phosphorylation has been reported to be constitutive (Hughes et al., 1993). This, however, could be due to the cells generally being cultured in media containing physiological levels of calcium, ranging from 1.4 to 1.8 mM. Therefore, in any experimental setup using normal cell culture medium, CaSR would be fully active, thus explaining constitutive phosphorylation on GSK3 α Tyr279. Second, phosphorylation of GSK3 on its different residues changes the activity rates of GSK3 and therefore of its downstream targets. Phosphorylation of GSK3 on its tyrosine residues has been reported to increase activity of GSK3: Insulin treatment of SH-SY5Y cells caused increased GSK3 β phosphorylation on Tyr216, increased GSK3 activity, and increased Tau phosphorylation (discussed below) (Hartigan and Johnson, 1999; Lesort et al., 1999). Therefore,

BDNF-TrkB signaling phosphorylates GSK3 α Tyr279 as well as GSK3 β Tyr216 increases the activity of GSK3. Contrarily, BDNF-induced activation of PI3-kinase/Akt results in phosphorylation of Ser9 of GSK3 β , which inhibits GSK3 activity leading to the dephosphorylation of substrates (Cross et al., 1995; Cohen et al., 1997; Yoshimura et al., 2005). In our study, we found that the Akt-GSK3 β Ser9 pathway also occurs when neurons were stimulated with BDNF, which reduces the activity of GSK3.

Therefore, our results report different “activity-increasing” and “activity-decreasing” signals, and we found that the signal integration of TrkB and CaSR on GSK3 is not a sum of all incoming signals but a synergistic effect (for summary, see Fig. 11B).

Data from another study suggest that the interaction of CaSR/Trk is a more general mechanism regulating neurite growth. Vizard et al. (2015) demonstrated that mouse SCG neurons cultured in the presence of 0.7 mM calcium containing 10 ng/ml of NGF (therefore, only activating TrkA) show low levels of p-Erk in immunostainings. Similarly, SCG neurons cultured in 2.3 mM calcium in the absence of NGF (therefore, only activating CaSR) also showed low levels of p-Erk. However, SCG neurons cultured in 2.3 mM calcium together with 10 ng/ml of NGF (therefore, TrkA and CaSR being activated simultaneously), caused a significant increase in p-Erk staining, suggesting that CaSR/Trk interaction and signaling also occur in other neurons. However, depending on neuronal subtype, downstream targets of these two receptors change: In nodose neurons, the main downstream target is GSK3, whereas in SCG neurons the Mek/Erk pathway is activated. Further, in organotypic slice cultures of mouse hippocampal neurons, transfection of CaSR-DN decreases branching of pyramidal neurons (Vizard et al., 2008). Because other studies show that the number, complexity, and length of primary dendrites in hippocampal neurons are dependent on BDNF (Ji et al., 2005; Burk et al., 2018), these findings suggest that branching of hippocampal pyramidal neurons could be facilitated by an interaction of CaSR and TrkB. Because CaSR/Trk interactions seem to be a general mechanism, we also tried to show interactions of CaSR and TrkB in mouse hippocampal neurons by overexpressing GFP-CaSR and RFP-TrkB. However, due to low transfection rates of CaSR and TrkB constructs, we did not find interaction. Performing coimmunoprecipitation from endogenous proteins was not possible because the CaSR-antibody does not work in Western blots.

Tau activity regulating neurite growth

So far, our results suggest that CaSR and TrkB regulate growth through activation and inactivation of GSK3, cycling it between activity states. This would suggest that downstream substrates, such as Tau, show cycling behavior in their phosphorylation state, which can be used as a read-out for microtubule assembly and disassembly, a key mechanism for neurite growth (Lindwall and Cole, 1984; Drechsel et al., 1992).

To link GSK3 activity to microtubule assembly, we tested whether Tau is activated downstream of CaSR when signaling in isolation as well as a coreceptor to TrkB. We found that Tau is phosphorylated downstream of CaSR and GSK3 activation and inactive in the presence of the CaSR and GSK3 antagonist Calhex 231 and Bio, respectively. In line with our hypothesis, we found that, when CaSR and TrkB are coactivated, Tau phosphorylation shows a cycling behavior, suggesting that CaSR and TrkB regulate GSK3 activity and inactivity. Thus, these results identify a novel regulatory pathway mediating neurite growth.

In conclusion, a deeper understanding of signal diversification in neurons will shed more light on neural circuit assembly

and might help to develop tools for modulating neural regeneration. In addition, the effect of CaSR on neurite growth and target innervation together with TrkB may help to explain neurological and developmental deficits of patients with mutations of CaSR (Cole et al., 1990).

References

- Bai M, Quinn S, Trivedi S, Kifor O, Pearce SH, Pollak MR, Krapcho K, Hebert SC, Brown EM (1996) Expression and characterization of inactivating and activating mutations in the human Ca²⁺ (o)-sensing receptor. *J Biol Chem* 271:19537–19545.
- Barford K, Deppmann C, Winckler B (2017) The neurotrophin receptor signaling endosome: where trafficking meets signaling. *Dev Neurobiol* 77:405–418.
- Bashaw GJ, Klein R (2010) Signaling from axon guidance receptors. *Cold Spring Harb Perspect Biol* 2:a001941.
- Bellon A, Luchino J, Haigh K, Rougon G, Haigh J, Chauvet S, Mann F (2010) VEGFR2 (KDR/Flk1) signaling mediates axon growth in response to semaphorin 3E in the developing brain. *Neuron* 66:205–219.
- Blanquie O, Yang JW, Sharopov S, Sinning A, Luhmann HJ (2017) Electrical activity controls area-specific expression of neuronal apoptosis in the mouse developing cerebral cortex. *Elife* 6:e27696.
- Bourne HR, Nicoll R (1993) Molecular machines integrate coincident synaptic signals. *Cell* 72 [Suppl]:65–75.
- Brennan SC, Thiem U, Roth S, Aggarwal A, Fetahu IS, Tennakoon S, Gomes AR, Brandi ML, Bruggeman F, Mentaverri R, Riccardi D, Kallay E (2013) Calcium sensing receptor signalling in physiology and cancer. *Biochim Biophys Acta* 1833:1732–1744.
- Burk K, Mire E, Bellon A, Hocine M, Guillot J, Moraes F, Yoshida Y, Simons M, Chauvet S, Mann F (2017a) Post-endocytic sorting of Plexin-D1 controls signal transduction and development of axonal and vascular circuits. *Nat Commun* 8:14508.
- Burk K, Murdoch JD, Freytag S, Koenig M, Bharat V, Markworth R, Burkhardt S, Fischer A, Dean C (2017b) EndophilinAs regulate endosomal sorting of BDNF-TrkB to mediate survival signaling in hippocampal neurons. *Sci Rep* 7:2149.
- Burk K, Ramachandran B, Ahmed S, Hurtado-Zavala JI, Awasthi A, Benito E, Faram R, Ahmad H, Swaminathan A, McIlhinney J, Fischer A, Perestenko P, Dean C (2018) Regulation of dendritic spine morphology in hippocampal neurons by copine-6. *Cereb Cortex* 28:1087–1104.
- Chao MV (2003) Neurotrophins and their receptors: a convergence point for many signalling pathways. *Nat Rev Neurosci* 4:299–309.
- Chauvet S, Cohen S, Yoshida Y, Fekrane L, Livet J, Gayet O, Segu L, Buhot MC, Jessell TM, Henderson CE, Mann F (2007) Gating of Sema3E/PlexinD1 signaling by neuropilin-1 switches axonal repulsion to attraction during brain development. *Neuron* 56:807–822.
- Cohen P, Alessi DR, Cross DA (1997) PDK1, one of the missing links in insulin signal transduction? *FEBS Lett* 410:3–10.
- Cole D, Forsythe CR, Dooley JM, Grantmyre EB, Salisbury SR (1990) Primary neonatal hyperparathyroidism: a devastating neurodevelopmental disorder if left untreated. *J Craniofac Genet Dev Biol* 10:205–214.
- Cornell RA, Kimelman D (1994) Combinatorial signaling in development. *BioEssays* 16:577–581.
- Cross DA, Alessi DR, Cohen P, Andjelkovich M, Hemmings BA (1995) Inhibition of glycogen synthase kinase-3 by insulin mediated by protein kinase B. *Nature* 378:785–789.
- Davies AM (1989) Intrinsic differences in the growth rate of early nerve fibres related to target distance. *Nature* 337:553–555.
- Davies AM, Lindsay RM (1985) The cranial sensory ganglia in culture: differences in the response of placode-derived and neural crest-derived neurons to nerve growth factor. *Dev Biol* 111:62–72.
- Davies AM, Thoenen H, Barde YA (1986) The response of chick sensory neurons to brain-derived neurotrophic factor. *J Neurosci* 6:1897–1904.
- Deinhardt K, Salinas S, Verastegui C, Watson R, Worth D, Hanrahan S, Bucci C, Schiavo G (2006) Rab5 and Rab7 control endocytic sorting along the axonal retrograde transport pathway. *Neuron* 52:293–305.
- Dickson BJ (2002) Molecular mechanisms of axon guidance. *Science* 298:1959–1964.
- Dickson BJ, Gilestro GF (2006) Regulation of commissural axon pathfinding by slit and its Robo receptors. *Annu Rev Cell Dev Biol* 22:651–675.
- Dobrowolski R, De Robertis EM (2011) Endocytic control of growth factor

- signalling: multivesicular bodies as signalling organelles. *Nat Rev Mol Cell Biol* 13:53–60.
- Drechsel DN, Hyman AA, Cobb MH, Kirschner MW (1992) Modulation of the dynamic instability of tubulin assembly by the microtubule-associated protein Tau. *Mol Biol Cell* 3:1141–1154.
- Dudanova I, Klein R (2013) Integration of guidance cues: Parallel signaling and crosstalk. *Trends Neurosci* 36:295–304.
- Filbin MT (2006) Recapitulate development to promote axonal regeneration: good or bad approach? *Philos Trans R Soc Lond B Biol Sci* 361:1565–1574.
- Gavaldà N, Gutierrez H, Davies AM (2009) Developmental switch in NF- κ B signalling required for neurite growth. *Development* 136:3405–3412.
- Golbs A, Nimmervoll B, Sun JJ, Sava IE, Luhmann HJ (2011) Control of programmed cell death by distinct electrical activity patterns. *Cereb Cortex* 21:1192–1202.
- Hamburger V, Hamilton HL (1992) A series of normal stages in the development of the chick embryo. *Dev Dyn* 195:231–272.
- Harrington AW, Ginty DD (2013) Long-distance retrograde neurotrophic factor signalling in neurons. *Nat Rev Neurosci* 14:177–187.
- Hartigan JA, Johnson GV (1999) Transient increases in intracellular calcium result in prolonged site-selective increases in Tau phosphorylation through a glycogen synthase kinase β -dependent pathway. *J Biol Chem* 274:21395–21401.
- Holstein DM, Berg KA, Leeb-Lundberg LM, Olson MS, Saunders C (2004) Calcium-sensing receptor-mediated ERK1/2 activation requires $G\alpha_{i2}$ coupling and dynamin-independent receptor internalization. *J Biol Chem* 279:10060–10069.
- Hughes K, Nikolakaki E, Plyte SE, Totty NF, Woodgett JR (1993) Modulation of the glycogen synthase kinase-3 family by tyrosine phosphorylation. *EMBO J* 12:803–808.
- Ji Y, Pang PT, Feng L, Lu B (2005) Cyclic AMP controls BDNF-induced TrkB phosphorylation and dendritic spine formation in mature hippocampal neurons. *Nat Neurosci* 8:164–172.
- Jones BL, Smith SM (2016) Calcium-sensing receptor: a key target for extracellular calcium signaling in neurons. *Front Physiol* 7:116.
- Jones HC, Keep RF (1988) Brain fluid calcium concentration and response to acute hypercalcaemia during development in the rat. *J Physiol* 402:579–593.
- Kovacs CS, Kronenberg HM (1997) Maternal-fetal calcium and bone metabolism during pregnancy, puerperium, and lactation. *Endocr Rev* 18:832–872.
- Kuruville R, Zweifel LS, Glebova NO, Lonze BE, Valdez G, Ye H, Ginty DD (2004) A neurotrophin signaling cascade coordinates sympathetic neuron development through differential control of TrkA trafficking and retrograde signaling. *Cell* 118:243–255.
- Lesort M, Jope RS, Johnson GV (1999) Insulin transiently increases Tau phosphorylation: involvement of glycogen synthase kinase- β and fyn tyrosine kinase. *J Neurochem* 72:576–584.
- Li BY, Schild JH (2007) Electrophysiological and pharmacological validation of vagal afferent fiber type of neurons enzymatically isolated from rat nodose ganglia. *J Neurosci Methods* 164:75–85.
- Lin CW, Sim S, Ainsworth A, Okada M, Kelsch W, Lois C (2010) Genetically increased cell-intrinsic excitability enhances neuronal integration into adult brain circuits. *Neuron* 65:32–39.
- Lindsay RM, Thoenen H, Barde YA (1985) Placode and neural crest-derived sensory neurons are responsive at early developmental stages to brain-derived neurotrophic factor. *Dev Biol* 112:319–328.
- Lindwall G, Cole RD (1984) Phosphorylation affects the ability of Tau protein to promote microtubule assembly. *J Biol Chem* 259:5301–5305.
- Lu W, Yamamoto V, Ortega B, Baltimore D (2004) Mammalian Ryk is a Wnt coreceptor required for stimulation of neurite outgrowth. *Cell* 119:97–108.
- Lu XL, Xu WX, Yan ZY, Qian Z, Xu B, Liu Y, Han LM, Gao RC, Li JN, Yuan M, Zhao CB, Qiao GF, Li BY (2013) Subtype identification in acutely dissociated rat nodose ganglion neurons based on morphologic parameters. *Int J Biol Sci* 9:716–727.
- McClellan MN, Mody A, Broach JR, Ramanathan S (2007) Cross-talk and decision making in MAP kinase pathways. *Nat Genet* 39:409–414.
- Mire E, Mezzerà C, Leyva-Díaz E, Paternain AV, Squarzone P, Bluy L, Castillo-Paterna M, López MJ, Peregrín S, Tessier-Lavigne M, Garel S, Galcerán J, Lerma J, López-Bendito G (2012) Spontaneous activity regulates Robo1 transcription to mediate a switch in thalamocortical axon growth. *Nat Neurosci* 15:1134–1143.
- Mire E, Hocine M, Bazellières E, Jungas T, Davy A, Chauvet S, Mann F (2018) Developmental upregulation of Ephrin-B1 silences *Sema3C/Neuropilin-1* signaling during post-crossing navigation of corpus callosum axons. *Curr Biol* 28:1768–1782.e4.
- Mizumachi H, Yoshida S, Tomokiyo A, Hasegawa D, Hamano S, Yuda A, Sugii H, Serita S, Mitarai H, Koori K, Wada N, Maeda H (2017) Calcium-sensing receptor-ERK signaling promotes odontoblastic differentiation of human dental pulp cells. *Bone* 101:191–201.
- Morales D, Kania A (2017) Cooperation and crosstalk in axon guidance cue integration: additivity, synergy, and fine-tuning in combinatorial signaling. *Dev Neurobiol* 77:891–904.
- Murase S, Owens DF, McKay RD (2011) In the newborn hippocampus, neurotrophin-dependent survival requires spontaneous activity and integrin signaling. *J Neurosci* 31:7791–7800.
- Pálffy M, Reményi A, Korcsmáros T (2012) Endosomal crosstalk: meeting points for signaling pathways. *Trends Cell Biol* 22:447–456.
- Prehoda KE, Lim WA (2002) How signaling proteins integrate multiple inputs: a comparison of N-WASP and Cdk2. *Curr Opin Cell Biol* 14:149–154.
- Narbaitz R, Bélanger LF, Hunt BJ (1973) Calcium regulation by the chick embryo: an experimental approach. *Calcif Tissue Res* 11:238–241.
- Ray K (2015) Calcium-sensing receptor: trafficking, endocytosis, recycling, and importance of interacting proteins. In: *Progress in molecular biology and translational science*, pp 127–150. Amsterdam: Elsevier.
- Reyes-Ibarra AP, García-Regalado A, Ramírez-Rangel I, Esparza-Silva AL, Valadez-Sánchez M, Vázquez-Prado J, Reyes-Cruz G (2007) Calcium-sensing receptor endocytosis links extracellular calcium signaling to parathyroid hormone-related peptide secretion via a Rab11a-dependent and AMSH-sensitive mechanism. *Mol Endocrinol* 21:1394–1407.
- Robinson M, Adu J, Davies AM (1996) Timing and regulation of trkB and BDNF mRNA expression in placode-derived sensory neurons and their targets. *Eur J Neurosci* 8:2399–2406.
- Ruat M, Traiffort E (2013) Roles of the calcium sensing receptor in the central nervous system. In: *Best practice and research: clinical endocrinology and metabolism*, pp 429–442. Amsterdam: Elsevier.
- Saxena S, Bucci C, Weis J, Kruttgen A (2005) The small GTPase Rab7 controls the endosomal trafficking and neurotrogenic signaling of the nerve growth factor receptor TrkA. *J Neurosci* 25:10930–10940.
- Song M, Giza J, Proenca CC, Jing D, Elliott M, Dincheva I, Shmelkov SV, Kim J, Schreiner R, Huang SH, Castrén E, Prekeris R, Hempstead BL, Chao MV, Dichtenberg JB, Rafii S, Chen ZY, Rodriguez-Boulán E, Lee FS (2015) Slitrk5 mediates BDNF-dependent TrkB receptor trafficking and signaling. *Dev Cell* 33:690–702.
- Vizard TN, O’Keefe GW, Gutierrez H, Kos CH, Riccardi D, Davies AM (2008) Regulation of axonal and dendritic growth by the extracellular calcium-sensing receptor. *Nat Neurosci* 11:285–291.
- Vizard TN, Newton M, Howard L, Wyatt S, Davies AM (2015) ERK signaling mediates CaSR-promoted axon growth. *Neurosci Lett* 603:77–83.
- Vogel KS, Davies AM (1991) The duration of neurotrophic factor independence in early sensory neurons is matched to the time course of target field innervation. *Neuron* 7:819–830.
- Wen Z, Zheng JQ (2006) Directional guidance of nerve growth cones. *Curr Opin Neurobiol* 16:52–58.
- Wu C, Lai CF, Mobley WC (2001) Nerve growth factor activates persistent Rap1 signaling in endosomes. *J Neurosci* 21:5406–5416.
- Yoshimura T, Kawano Y, Arimura N, Kawabata S, Kikuchi A, Kaibuchi K (2005) GSK-3 β regulates phosphorylation of CRMP-2 and neuronal polarity. *Cell* 120:137–149.
- Zhou B, Cai Q, Xie Y, Sheng ZH (2012) Snapin recruits dynein to BDNF-TrkB signaling endosomes for retrograde axonal transport and is essential for dendrite growth of cortical neurons. *Cell Rep* 2:42–51.
- Zhou Y, Gunput RA, Pasterkamp RJ (2008) Semaphorin signaling: progress made and promises ahead. *Trends Biochem Sci* 33:161–170.
- Zhuang X, Northup JK, Ray K (2012) Large putative PEST-like sequence motif at the carboxyl tail of human calcium receptor directs lysosomal degradation and regulates cell surface receptor level. *J Biol Chem* 287:4165–4176.

3 TUBULAR MICRODOMAINS OF RAB7-ENDOSOMES RETRIEVE TRKA, A MECHANISM DISRUPTED IN CHARCOT-MARIE-TOOTH 2B

In chapter 3, I look at the potential mechanism of receptor retrieval and its effects on receptor signalling.

As described in the introduction, neurotrophic signalling ensures axonal growth and survival. Upon activation neurotrophic receptors are endocytosed and transported retrogradely to the soma. En route, they localize within ILVs of Rab7-positive late endosomes or MVBs, which segregate Trks from the cytoplasm (Ye et al., 2018). Therefore, one long-debated question is, how neurotrophic receptors are able to signal from ILVs, given the insulating properties of these vesicles shielding neurotrophic receptors from the cytoplasm.

Our study reveals that in DRG neurons, Rab7-positive endosomes/MVBs extend tubular domains after stimulation with NGF but not epidermal growth factor (EGF). Further, we found that these tubuli are often pinched off, generating a small vesicle. Due to the small size of endosomes in neurons, we opted to further study this mechanism in mouse embryonic fibroblasts (MEFs), where we confirmed the observation that Rab7-endosomes/MVBs induce these tubuli upon NGF but not upon EGF stimulation. Further, we found that Rab7-endosomes are morphologically diverse and that TrkA and EGFR are recruited differentially upon stimulation. TrkA is recruited into larger, vacuolar-like Rab7 structures upon NGF stimulation, whereas EGFR preferentially localizes to the limiting membrane of such vacuoles. Further, we found TrkA localizing to/within the extending tubuli- an observation we did not make for EGFR.

Investigating the potential mechanism of tubuli induction and the proteins regulating this process, we found EndophilinA1, A2 and A3, three BAR-domain-containing proteins to be involved. MEFs generated from EndophilinAs triple knockout mice were unable to induce tubuli and subsequently affect the phosphorylation status of TrkA. Further, EndophilinAs show biochemical interaction with TrkA but not EGFR and EndophilinA2 co-immunoprecipitates with Rab7 and WASH1. The WASH-complex is known for its role in receptor sorting for recycling and stabilizes recycling tubuli by actin-nucleation (Seaman et al., 2013).

Lastly, we found a disrupted mechanism of creating tubular domains with the CMT2B-causing Rab7 mutants. These mutants influence the Rab7-GTPase by changing the kinetics of the GTP binding pocket (Spinosa et al., 2008). The disruption of tubuli-generation implies that Rab7-GTPase finely controls this process, as a shift in its functionality causes a great disturbance of NGF-induced tubuli. Two mutations (L129F and N161T) show an overtubulating phenotype, whereas two other mutations (K157N and V162M) show a reduction in tubulation events. This disturbance in tubuli was mirrored in the levels of pTrkA and neuronal growth: CMT2B mutants that did not tubulate showed reduced levels of pTrkA indicating signalling defects, reduced binding to EndophilinA2 and reduced neuronal growth. This study supports a novel retrieval mechanism from Rab7-endosomes/MVBs, which allows TrkA to signal.

AUTHORS:

Markworth R. ^{1,2,3}, **Dambeck V.** ^{1,3}, **Steinbeck L.M.** ^{1,3}, **Koufali A.** ^{1,3}, **Bues B.** ^{1,3}, **Dankovich T.M.** ⁴, **Wichmann C.** ^{3,5,6} and **Burk K.** ^{1,2,3}

¹Department of Neurology, University Medical Center Göttingen, Robert Koch Straße 40, 37075 Göttingen, Germany, ²European Neuroscience Institute, Grisebachstraße 5, 37077 Göttingen, Germany, ³Center for Biostructural Imaging of Neurodegeneration, Von-Siebold Straße 3A, 37075 Göttingen Germany, University Medical Center Göttingen, ⁴Institute for Neuro- and Sensory Physiology, Humboldtallee 23, 37073 Göttingen. ⁵Molecular Architecture of Synapses Group, Institute for Auditory Neuroscience and InnerEarLab, University Medical Center Göttingen, Göttingen, Germany. ⁶Collaborative Research Centers 889 "Cellular Mechanisms of Sensory Processing" and 1286 "Quantitative Synaptology", 37099 Göttingen, Germany

Personal contribution: Performance and analysis (together with Katja Burk) of experiments shown in the following figures: Figure 1A-G, Figure 1H (together with Carolin Wichmann), Figure 2A-C, E, G-K, Figure 2D, F (together with Tal Dankovich), Figure 3, Figure 4A-E, Figure 4G, H (together with Vivian Dambeck), Figure 4I (together with Tal Dankovich), Figure 5A (together with Lars Malte Steinbeck), Figure 5B-E, Figure 5G, H (together with Vivian Dambeck), Figure 5I (together with Tal Dankovich), Figure 6A, B (together with Bastian Bues and Angeliki Koufali), Figure 6C-F, Figure 7A, B, G, H, Figure 7E, F (together with Lars Malte Steinbeck), Figure 8. I contributed to the figure design, and further contributed to the manuscript writing in the figure legends and methods section, as well as by editing.

This manuscript has been submitted to Journal of Cell Science on the 16th of February 2021 and has been revised and accepted with minor changes on August 23rd 2021:

Markworth R, Dambeck V, Steinbeck LM, Koufali A, Bues B, Dankovich TM, Wichmann C, Burk K. Tubular microdomains of Rab7-endosomes retrieve TrkA, a mechanism disrupted in Charcot-Marie-Tooth 2B. *J Cell Sci.* 2021 Sep 6:jcs.258559. doi: <https://doi.org/10.1242/jcs.258559>. Epub ahead of print. PMID: 34486665.

3.1 ABSTRACT

Axonal survival and growth require signalling from tropomyosin receptor kinases (Trks). To transmit their signals, receptor-ligand complexes are endocytosed and retrogradely trafficked to the soma where downstream signalling occurs. Vesicles transporting neurotrophic receptors to the soma are reported to be Rab7-positive late endosomes/multi vesicular bodies where receptors localize within so-called intraluminal vesicles. Therefore, one challenging question is how downstream signalling is possible given the insulating properties of intraluminal vesicles. In this study, we report that Rab7-endosomes/multi vesicular bodies retrieve TrkA through tubular microdomains. Interestingly, this phenotype is absent for the EGF-receptor. Further, we found that EndophilinA1, EndophilinA2 and EndophilinA3 together with WASH1 are involved in the tubulation process. In Charcot-Marie-Tooth 2B, a neuropathy of the peripheral nervous system, this tubulating mechanism is disrupted. In addition, the ability to tubulate correlates with the phosphorylation levels of TrkA as well as with neurite length in neuronal cultures from dorsal root ganglia. Overall, we report a new retrieval mechanism of late Rab7-endosomes, which enables TrkA signalling and sheds new light onto how neurotrophic signalling is disrupted in CMT2B.

3.2 INTRODUCTION

Neurotrophic signals transmitted through tropomyosin receptor kinases (Trks) are essential for neuronal health. They are required for regulating neuronal survival, axonal growth, gene expression, sub-type specification and synapse formation (Campenot, 1977; Deinhardt et al., 2006; Harrington and Ginty, 2013; Sharma et al., 2010; Singh et al., 2008). In the last years, it has been reported that neurotrophic receptors are endocytosed after ligand binding and targeted to endosomes, from where downstream signalling is initiated while being transported to the soma (Cosker et al., 2008; Ginty and Segal, 2002; Harrington and Ginty, 2013; Ito and Enomoto, 2016; Schmieg et al., 2014).

However, the type of endosome that transports Trks retrogradely to the soma has been debated for a long time. One major model for retrograde trafficking is the signalling endosome. This model postulates that nerve growth factor (NGF)/tropomyosin receptor kinase A (TrkA) or brain-derived neurotrophic factor (BDNF)/tropomyosin receptor kinase B (TrkB) complexes are formed and endocytosed upon stimulation at the distal axon. Following endocytosis, these complexes are sorted into maturing, signalling competent endosomes, which are trafficked retrogradely to the soma in a dynein-dynactin dependent manner (Howe and Mobley, 2005; Schmieg et al., 2014; Wu et al., 2007). Some studies suggest that neurotrophic signalling occurs from early Rab5-endosomes. From these early endosomes, Trks would signal from the limiting membrane, allowing the C-terminal domain to interact with proteins in the cytoplasm (Cosker and Segal, 2014; Harrington and Ginty, 2013; Howe and Mobley, 2005).

Other studies have supported the role of late Rab7-endosomes /multi-vesicular bodies (MVBs) in retrograde transport of Trks (Weible and Hendry, 2004). MVBs occur during endosomal maturation, a process that requires an increase in intraluminal acidification, a change in the phosphoinositide (PIP) composition of the endosomal membrane as well as a switch from Rab5 to Rab7-GTPase on the endosomal membrane (Marat and Haucke, 2016; Maxfield and Yamashiro, 1987; Rink et al., 2005). In addition, intraluminal vesicles (ILVs) containing cargo are formed via inclusion from the limiting membrane on maturing endosomes (Cullen and Steinberg, 2018).

Supporting this hypothesis, several studies have reported Trks localizing to Rab7-positive endosomes. In P0 mouse hippocampal neurons, TrkB predominantly colocalizes to Rab7-positive endosomes (Burk et al., 2017a). In cultured DRG and motor neurons, internalized tetanus toxin colocalizes with TrkB-containing endosomes that are positive for Rab5 or Rab7 within axons. However, only endosomes positive for Rab7 are transported retrogradely to the soma (Deinhardt et al., 2006). When ¹²⁵I-NGF was added to distal axons of sympathetic neurons, ultrastructural analysis revealed that ¹²⁵I-NGF mainly localized to MVBs and lysosomes in cell bodies (Claude et al., 1982). Superior cervical ganglia neurons from a FLAG-TrkA knock-in mouse line revealed that the majority of retrogradely transported TrkA localized to MVBs. Of MVB-localized TrkA, approximately 70% localized to ILVs and 30% to the outer membrane of MVBs (Ye et al., 2018). Also, phosphorylated TrkA colocalizes with MVBs in axons in vivo (Bhattacharyya et al., 2002; Sandow et al., 2000).

However, the localization of TrkA/TrkB within ILVs would mean that receptors are insulated from the cytoplasm. Therefore, the key question is how Trks facilitate signalling from MVBs.

So far, some studies have shed light on how receptors could signal from MVBs. The Bronfman lab conducted a study where they followed the p75NTR receptor, a co-receptor of Trks. This study revealed that p75NTR localizes to MVBs and is released from cells in exosomes (Escudero et al., 2014). This mechanism has also been reported for Eph receptors. EphB2 has been found to be

released from exosomes that are taken up by glioblastoma cells and neurons and induce tyrosine-phosphorylation of ephrinB1 and growth cone collapse (Gonget al., 2016). In this scenario, p75NTR and EphB2 containing exosomes coming from the extracellular space would need to fuse with the plasma membrane either of the same or another cell and be re-endocytosed. On the other hand, the Deppmann lab found that once arriving at the soma, NGF/TrkA signalling endosomes interact with Coronin-1, which facilitates recycling of TrkA within recycling Rab11-endosomes (Suo et al., 2014). Further, the Ginty lab proposes that MVBs generate single-membrane vesicles from where Trks are able to start downstream signalling and avoid lysosomal degradation (Ye et al., 2018). While exosomes are ILVs released into the cytoplasm by fusion of MVBs with the plasma membrane (Kalluri and LeBleu, 2020), the other studies suggest a back-fusion of Trks from ILVs into the limiting membrane of MVBs before they are sorted into other endosomal compartments. While an LBPA/Alix-dependent back-fusion of viruses and toxins has been reported (for review see (Bissig and Gruenberg, 2014; Gruenberg, 2020)), back-fusion of neurotrophic receptors has not been shown yet. However, Tomas et al. report that epidermal growth factor receptors (EGFR) also undergo back-fusion into the limiting membrane of MVBs (Tomas et al., 2015).

In our study, we investigated retrieval of TrkA from MVBs. We performed EM and live-cell imaging using total internal reflection fluorescence (TIRF) microscopy and found that Rab7-endosomes extend tubular domains after stimulation with NGF. TrkA localized into these tubular microdomains, which were observed to be pinched off. Stimulated Emission Depletion (STED) microscopy revealed that p-TrkA then localized adjacent to small Rab7-positive endosomes. Interestingly, we did not observe a tubulation phenotype when we followed EGFR, which also signals from Rab7-endosomes (Ceresa and Bahr, 2006; Schmidt et al., 2003; Taub et al., 2007). To investigate the mechanisms inducing tubulation, we studied proteins capable of inducing membrane curvature and have been shown to sort cargo from early endosomes. We found that EndophilinA1, EndophilinA2 and EndophilinA3 (hence EndophilinAs) interact with TrkA but not with EGFR. Further, EndophilinAs interact with Rab7 and WASH1 and EndophilinAs knockout MEFs revealed an inability to tubulate Rab7-endosomes and low levels of phosphorylated TrkA.

Since the activity of Rab7-GTPase seemed to play a role, we applied our findings onto Charcot-Marie-Tooth Disease 2B (CMT2B), a neuropathy of the peripheral nervous system, caused by mutations within the Rab7-GTPase. We found that in CMT2B, Rab7-endosomes show disruptions in extending tubuli that correlate with altered phosphorylation as well as with neurite length of cultured DRG neurons. Also, EndophilinA2 showed decreased binding to most CMT2B-mutations.

3.3 RESULTS

RAB7-ENDOSOMES FORM TUBULAR MICRODOMAINS IN DRG NEURONS

In order to study mechanisms that allow signalling from late, Rab7-endosomes, we used TIRF-microscopy. When imaging DRG neurons that were transfected with RFP-Rab7 and stimulated with NGF, we noted that many Rab7-endosomes extended tubular domains while in transport (Fig. 1A-D). These tubuli also appeared to be pinched off, forming a smaller endosomal structure (Fig. 1B,C). When analysing tubulation events, we found a significant increase in tubulating Rab7-endosomes when stimulated with NGF compared to control (Fig. 1A,D). In addition to overexpression, we performed immunocytochemistry on DRG neurons and found vacuolar-structured Rab7-endosomes as well as Rab7-endosomes that extended tubular domains (Fig. 1E,F). To link TrkA to tubulating Rab7-endosomes from DRG neurons, we performed colocalization experiments of

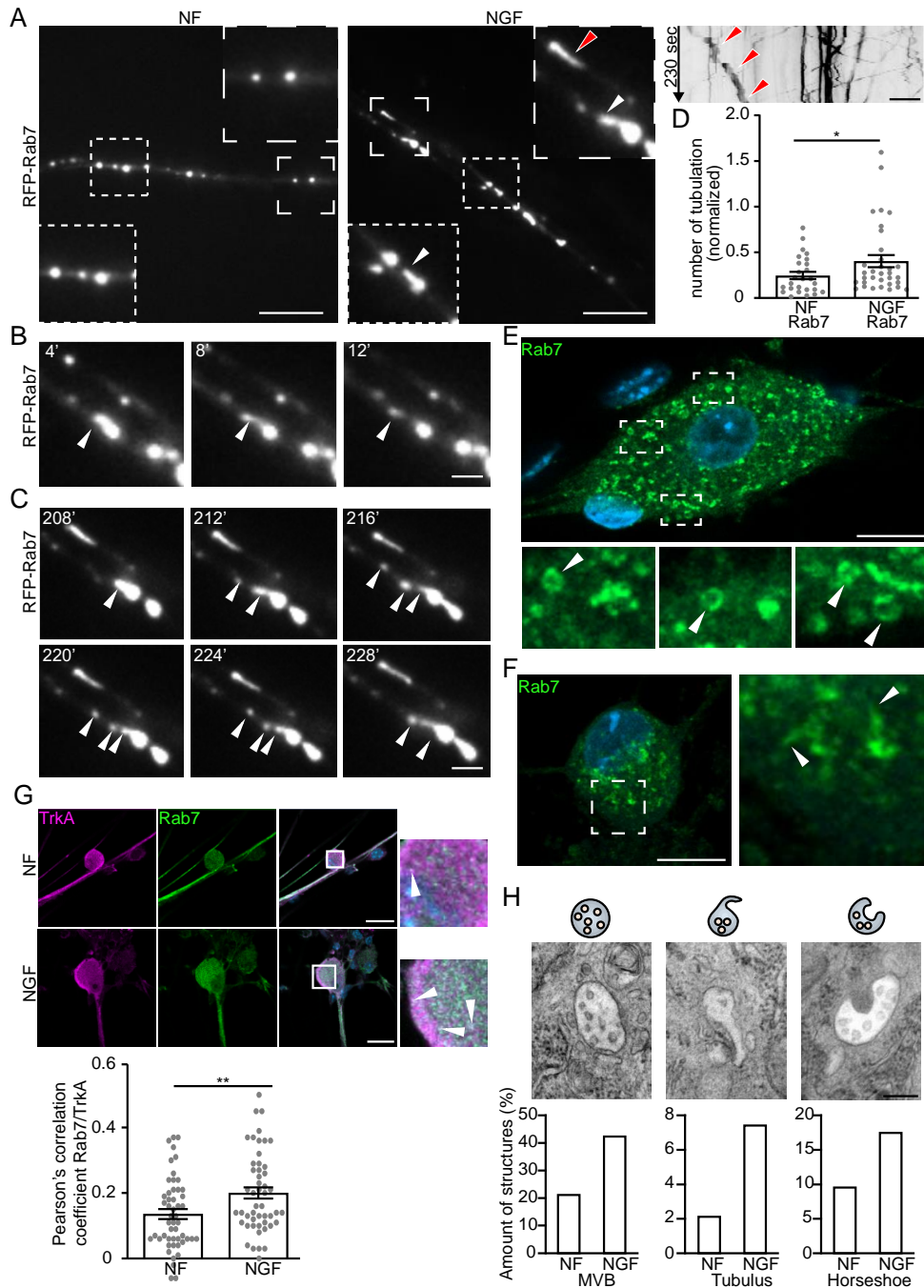


Figure 1. Rab7-endosomes extend tubular domains after stimulation with NGF in DRG neurons. (A) TIRF-microscopy images of DRG neurites transfected with RFP-Rab7 with or without 100ng/mL NGF. Arrowheads point to tubulation events; red arrowheads point to movement of endosome marked in NGF; scale bar=10 μ m. **(B,C)** Time-lapse zooms of TIRF-microscopy showing Rab7-endosomes forming tubular microdomains, pinched off over time. Time in seconds; scale bar=2 μ m. **(D)** Quantification of tubulation events per neurite, normalized to video length $p=0.05$ $df=50.77$. Significance was determined by unpaired t-test with Welch's correction, $n=30$ images per condition in three independent experiments; mean \pm SEM, * $p=0.05$. **(E,F)** Confocal images of DRG soma stained for Rab7. Arrowheads point at vacuolar structures (E) and tubular domains (F); scale bar=10 μ m. **(G)** Confocal images of DRG neurons stained against TrkA and Rab7 in unstimulated/stimulated conditions; scale bar=20 μ m. Pearson's correlation coefficient of TrkA and Rab7 in DRG soma. NF vs NGF: $p=0.006$. Significance was determined by unpaired t-test, $n=15-20$ images per condition in three independent experiments; mean \pm SEM, ** $p<0.01$. **(H)** EM images of MVBs in mouse DRGs categorized as MVB-, tubulating- or horseshoe-shaped, scale bar=0.2 μ m. Quantification presented as amounts of structures in percentage of total amount of counted structures.

endogenous Rab7 and TrkA. As reported (Saxena et al., 2005), we found an increase in colocalization of TrkA to Rab7-endosomes after stimulation with NGF, suggesting that tubulating Rab7-endosomes contain TrkA (Fig. 1G).

To determine if tubulating structures are MVBs, we performed EM of non-stimulated and stimulated DRGs. We distinguished MVBs into three different shapes, round, tubulating and curved/horseshoe-shaped (Fig. 1H). Of all found MVBs, from both conditions, ~21% of non-stimulated and ~42% of stimulated conditions were categorized as normal round-shaped MVBs. This suggests that MVBs develop, as reported, during inclusion of cargo (Cullen and Steinberg, 2018). Further, ~2% of MVBs were categorized as tubulating in non-stimulated and ~7% in stimulated conditions, which is in line with tubulating endosomes from our live-cell imaging approach. Lastly, to distinguish tubulating MVBs from elongated, curved MVBs, we added another category “horseshoe” as shown in Fig. 1H. Approximately 9% of MVBs classified as elongated, curved MVBs in non-stimulated and ~17% in stimulated conditions.

However, neuronal endosomes are rather small; the average size of endosomes we found was approximately 0.5 μm . This size and the resolution-limit of TIRF and confocal microscopy makes it hard to study such dynamics in neurons. To overcome this technical limitation, we used mouse embryonic fibroblasts (MEFs), in which we overexpressed GFP-Rab7. MEFs express TrkB mRNA, the neurotrophic receptor for BDNF, both full length and the truncated T1 form. This mRNA is translated into protein and functional TrkB receptors, shown by increased phosphorylation of TrkB following BDNF stimulation (Burk, et al., 2017a).

First, we tested if, apart from TrkB, MEFs also express TrkA and EGFR using Western Blot and immunocytochemistry (Fig. S1A,A',B). To ensure these receptors are functional and the downstream machinery is present, we tested for TrkA and EGFR phosphorylation upon stimulation (Fig. S1C,D).

In the next step, we tested if Rab7-endosomes also extend tubular domains following neurotrophic stimulation as observed in DRG neurons. Therefore, we expressed GFP-Rab7 in MEFs and followed their dynamics in non-stimulated and stimulated conditions. Fig. 2A shows a zoom of individual Rab7-endosomes illustrating their dynamics. In non-stimulated conditions, Rab7-endosomes remained round endosomal vesicles that were not very mobile. However, upon stimulation with NGF, Rab7-endosomes extended tubular microdomains as described for early endosomal sorting platforms (Jovic et al., 2010; Seaman, 2012a; Seaman et al., 2013) and for MVBs (Cooney et al., 2002; Inoue et al., 2015; Woodman and Futter, 2008). Interestingly, these tubular domains were not induced following EGF stimulation (Fig. 2A lowest panel).

NGF-INDUCED TUBULATING RAB7-ENDOSOMES ARE MORPHOLOGICALLY DIVERSE

Following transfection of GFP-Rab7-WT into MEFs, we noted that tubulating Rab7-endosomes appeared in different sizes and shapes. We found round structures between the sizes of 0.1-1 μm and vacuolar-shaped structures in a size range of 1->2 μm (Fig. 2B upper panel, C). To exclude that these shapes are artefacts due to overexpression, we stained for endogenous Rab7 and found the same distribution of endosomal sizes and shapes (Fig. 2B lower panel, C). Using STED-microscopy, we found that Rab7-endosomes contain small, intra-endosomal vesicles, which are also positive for Rab7 (Fig. 2D). In TIRF live-imaging, where we overexpressed GFP-Rab7 together with TrkA-RFP, we also found GFP-positive small vesicles inside the vacuolar structures (Fig. 2E), which moved around

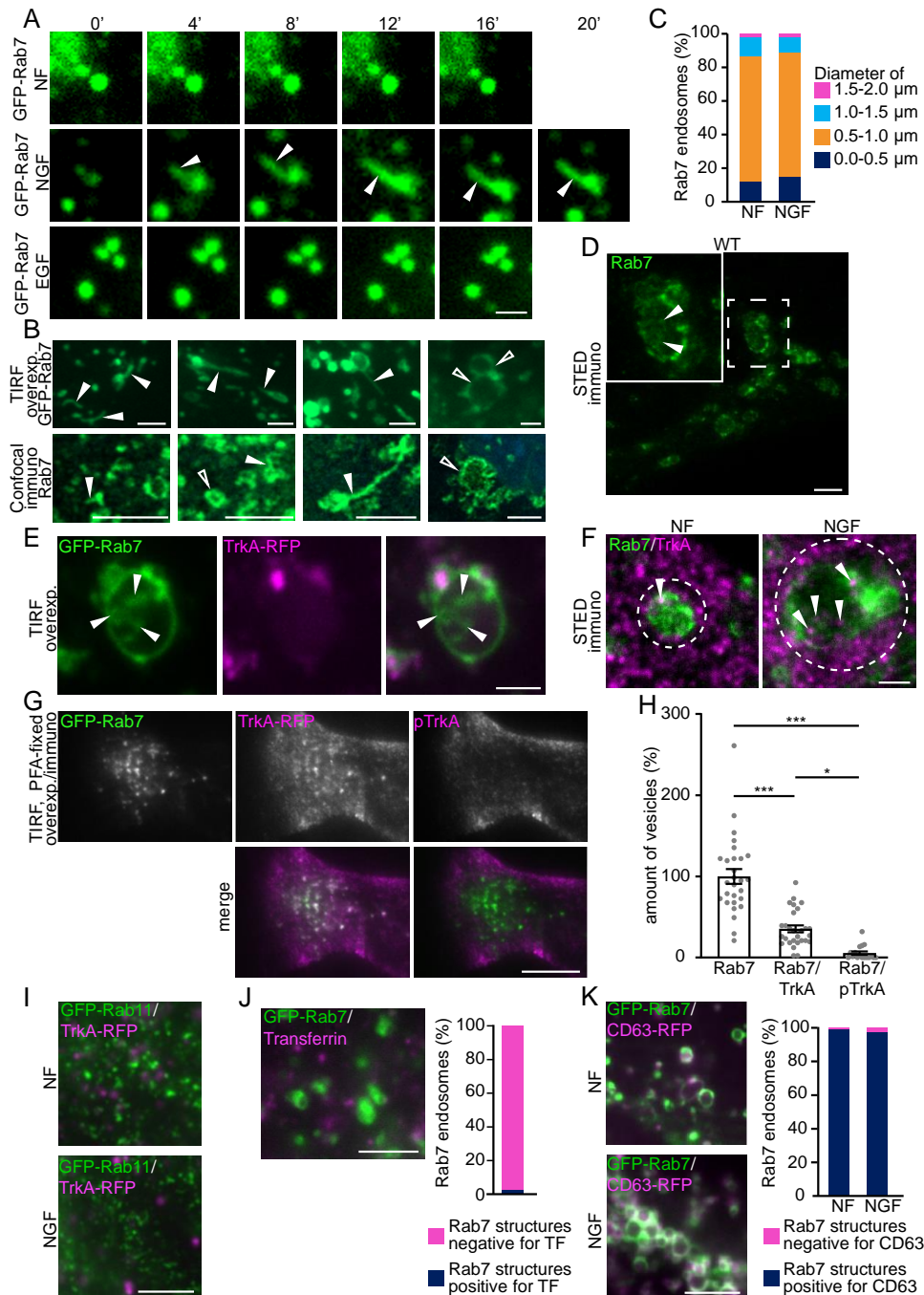


Figure 2. Rab7-endosomes show diverse vacuolar morphology and tubulation dynamics. (A) Zoom time-lapse TIRF-microscopy images of MEFs transfected with GFP-tagged Rab7, in the presence/absence of stimulants as indicated. Arrowheads indicate tubulation events. Time in seconds; scale bar=2 μ m. (B) Images of TIRF-microscopy showing overexpressed GFP-Rab7 and confocal images stained against endogenous Rab7. Filled arrowheads point at tubulation events, empty arrowheads at vacuolar structures; scale bar=2 μ m for TIRF images and 0.5 μ m for confocal images. (C) Quantification of proportion of Rab7 vacuoles by size in stimulated/unstimulated conditions. (D) STED image of a MEF stained against Rab7, arrow heads point to ILVs, scale bar=2.5 μ m. (E) MVB as seen in live TIRF-microscopy in MEFs overexpressing GFP-Rab7 and TrkA-RFP; arrows point at ILVs, scale bar=2 μ m. (F) STED image of an MVB stained against Rab7 and TrkA, arrows point at TrkA within vacuolar structure, scale bar=1 μ m. (G) TIRF images of PFA-fixed MEF overexpressing GFP-Rab7, TrkA-RFP stained against pTrkA, scale bar=10 μ m. (H) Quantification of Rab7 vesicles positive for TrkA or pTrkA. Significance was determined by one-way ANOVA with post-hoc Tukey's mean \pm SEM, * p <0.05, ** p <0.001. (I) MEFs overexpressing GFP-Rab11 and TrkA-RFP in non-stimulated/stimulated condition. Images show no colocalizing punctae; scale bar=5 μ m (J) Representative image and quantified proportion of MEFs overexpressing GFP-Rab7 that do not colocalize with Alexa-Fluor 647 tagged Transferrin. Scale bar=5 μ m. (K)

Representative images and quantified proportions of MEFs transfected with GFP-tagged Rab7 and RFP-tagged CD63, with or without NGF; scale bar=5 μ m.

(Suppl. video 1). We also performed STED microscopy to decipher if the small intra-endosomal vesicles contain TrkA. While we did see TrkA inside vacuolar Rab7-endosomes, compared to live-imaging, PFA-fixed cells revealed abundant TrkA outside of Rab7-endosomes, which did not appear in overexpression (compare Fig. 2F to 2E, and Fig. 2G to S2A showing MEFs from the same experiments imaged live (Fig. S2A) and afterwards fixed with 4% PFA (Fig. 2G)). GFP-Rab7 and TrkA-RFP revealed a 35% co-localization (Fig. 2G,H). Interestingly, we found only 5% of immunostained p-TrkA co-localizing with Rab7-endosomes, suggesting that p-TrkA follows a distinct route (Fig. 2G,H). Since tubulating endosomes have been associated with the recycling pathway (Jovic et al., 2010; Naslavsky and Caplan, 2018) we tested if TrkA localizes to recycling Rab11-endosomes in NGF-stimulated conditions. Almost no TrkA localized to Rab11-endosomes (Fig. 2I). Additionally, we tested if Transferrin, another marker of the recycling pathway, localizes to our overexpressed Rab7-positive endosomes and found hardly any colocalizing punctae. (Fig. 2J). Next, we tested if vacuolar Rab7-structures are positive for the MVB-marker CD63 (Fernandez-Borja et al., 1999) and found that almost all Rab7-vacuolar structures are positive (Fig. 2K). Taken together, tubulating Rab7 structures are late endosomes/MVBs and not part of the recycling pathway.

Next, we tested if TrkA and EGF-receptors localize to Rab7-endosomes in MEFs as shown in Fig. 1G and described for neurons (Ceresa and Bahr, 2006; Ye et al., 2018). Therefore, we co-expressed GFP-Rab7 (both WT and the constitutively active form Q67L) together with TrkA-RFP or EGFR-RFP and analysed their localization and dynamics using TIRF microscopy. Intriguingly, we observed various localizations, depending on the shape of Rab7-endosomes as well as the receptor present. On first observation, we noted that TrkA localized to the limiting membrane of small round structures (Fig. 3A,C). In vacuolar structures, TrkA was found enclosed within the vacuole (Fig. 3A,B), and rarely localized to the limiting membrane of the vacuole (Fig. 3A,D).

To further decipher the localization of TrkA, we analysed the distribution of TrkA to Rab7-endosomes upon stimulation. In unstimulated conditions, TrkA mainly localized to small round structures and rarely to vacuolar structures, which enclosed TrkA. Upon stimulation, however, the localization of TrkA shifted from small Rab7-positive structures to the much larger ring-like structures enclosing TrkA (approx. 85% of small structures in unstimulated conditions to ~57% in NGF-stimulated conditions and approximately 10% of TrkA localizing to ring-like structures in unstimulated conditions to ~40% in stimulated conditions, Fig. 3B,C,D). The amount of TrkA localizing to the limiting membrane of Rab7-vacuolar structures was very low, approximately 1.3% in non-stimulated and 1.8% in stimulated conditions (Fig. 3A,D). Using overexpression, the overall percentage of vacuolar structures did not change with TrkA shifting its localization (Fig. 3E).

Interestingly, EGFR showed different localizations compared to TrkA. When EGFR was overexpressed with Rab7, EGFR mainly localized to small round Rab7-positive structures (~70% in both unstimulated and EGF-stimulated conditions, Fig. 3F,H). EGFR localized to much higher amounts to the limiting membrane of vacuolar ring-like structures compared to TrkA (~18% in control and 13% in EGF-stimulated conditions, Fig. 3F,I). The numbers of enclosed EGFR within vacuoles, both in unstimulated and stimulated conditions were much lower compared to TrkA (~5% in unstimulated conditions and 13% in EGF-stimulated conditions Fig. 3F,G).

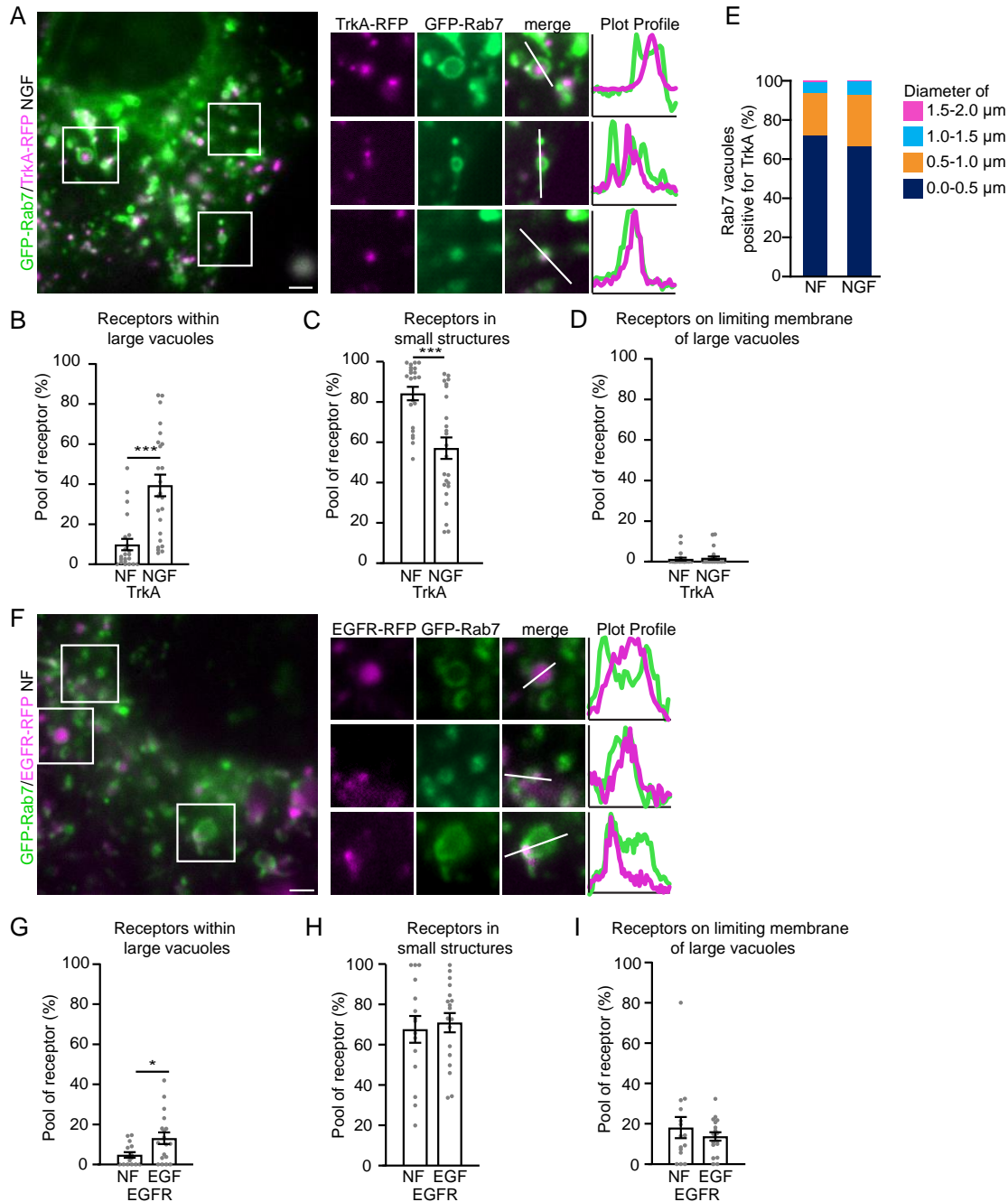


Figure 3. Trk receptors localize within ring-like Rab7-endosomes. (A) TIRF-microscopy images of MEFs co-transfected with GFP-Rab7 and TrkA-RFP. Line histograms show TrkA within or on the rim of Rab7-vacuoles and on top of small Rab7-structures; scale bar=2 μ m. (B) Quantification of proportion of TrkA localized within large vacuolar Rab7-structures. NF vs NGF: $p < 0.0001$. (C) Proportion of TrkA localized to small structures. NF vs NGF: $p = 0.0001$. (D) Proportion of receptors localized on the limiting membrane of large vacuolar Rab7-structures. NF vs NGF: $p = 0.6472$. (E) Proportion of Rab7-vacuoles positive for TrkA by size in stimulated/unstimulated conditions. (F) TIRF-microscopy images of MEFs with GFP-Rab7 and EGFR-RFP. Line histograms show EGFR within or on the rim of Rab7 vacuoles and on the rim of small Rab7-structures; scale bar=2 μ m. (G) Proportion of EGFR localized within large vacuolar Rab7-structures. NF vs EGF: $p < 0.0219$. (H) Proportion of EGFR localized to small structures. NF vs EGF: $p = 0.6830$. (I) Proportion of receptors localized on the limiting membrane of large vacuolar Rab7-structures. NF vs EGF: $p = 0.4152$. Significance was determined by unpaired t-test; $n = 7$ videos per condition in three independent experiments, $n = 10-15$ images per condition in three independent experiments (F); mean \pm SEM, * $p < 0.05$, ** $p < 0.01$, *** $p < 0.001$.

To test if the localization of TrkA or EGFR to or within the different structures depends on the Rab7-GTPase activity, we overexpressed its constitutively active form Q67L. In co-expression with TrkA, we found large amounts of TrkA within large vacuoles in unstimulated conditions, which did not further increase following NGF stimulation (approx. 45% in control and NGF-stimulated conditions Fig. S3A,C). Additionally, the number of TrkA localizing to small round structures in unstimulated and stimulated conditions resembled Rab7-WT stimulation with NGF (Fig. S3A,D, ~52% in both conditions for Q67L compared to 85% in control and 57% in WT (Fig. 3A,C)). Localization of TrkA to the limiting membrane of vacuolar structures remained low (Fig. S3A,E). This observation suggests that active Rab7-GTPase facilitates localization of TrkA to large, vacuolar structures.

In contrast, overexpression of Q67L with EGFR showed low amount of EGFR enclosed within ring-like structures in both unstimulated (~5%) and EGF-stimulated conditions (~10%) as observed in Rab7-WT co-expression experiments (Fig. S3B,C). Also, for Rab7-Q67L, we found a significant increase in localization to the limiting membrane of ring-like structures in unstimulated and stimulated conditions compared to Trks (approx. 5% in control and 10% in EGF-stimulated conditions, (Fig. S3B,E). Further, Q67L revealed no increase for EGFR within small structures in control or EGF-stimulated conditions (Fig. S3B,D). Studies on several receptors including Trks have shown that their activation changes the activity of GTPases localizing to the endosomal compartment the receptor is transported in (Deininger et al., 2008; Wu et al., 2014; Burk et al., 2017b). Our findings suggest that activation of Rab7-GTPase favours the localization of TrkA to vacuolar structures.

TRKA BUT NOT EGFR LOCALIZE WITHIN TUBULAR DOMAINS OF RAB7-ENDOSOMES

So far, we observed two new phenotypes- Rab7-endosomes tubulate upon stimulation with NGF but not EGF. Also, following stimulation, the localization of TrkA shifts from small Rab7-positive structures to be enclosed within larger vacuolar structures, positive for MVB-marker CD63.

To study this tubulation phenotype in more detail, we over-expressed Rab7-constructs together with TrkA and EGFR in MEFs and observed their dynamics in non-stimulated and stimulated conditions.

Co-expression of TrkA or EGFR with Rab7-WT revealed two findings: First, the number of tubulations per frame increased significantly upon stimulation with NGF (Fig. 4A,B, Suppl. Videos 2 and 3) but not with EGF (Fig. 4C,B). Second, TrkA localized within the tubular domains of Rab7-endosomes (Fig. 4E). We did not observe this localization for EGFR (Fig. 4E).

Co-expression with Rab7-Q67L revealed induced tubulation already in unstimulated conditions (Fig. 4A,D). On the other hand, Rab7-endosomes containing EGFR showed a low number of tubulation events, which did not increase following EGF stimulation - neither in Rab7-WT nor in Q67L (Fig. 4B,C,D). This observation suggests that the enclosed receptor and the GTPase activity are involved in tubulation events of Rab7-endosomes. As a control for GTPase activity, we also overexpressed the dominant-negative Rab7-T22N construct to see if, and how, this affects endosomal structures and tubulation. As reported previously, T22N localizes mainly to the cytosol and not to endosomal membranes (Bucci et al., 2000). Therefore, we analysed the number of tubulating TrkA structures, which we included in a separate panel (Fig. 4A,D second panel).

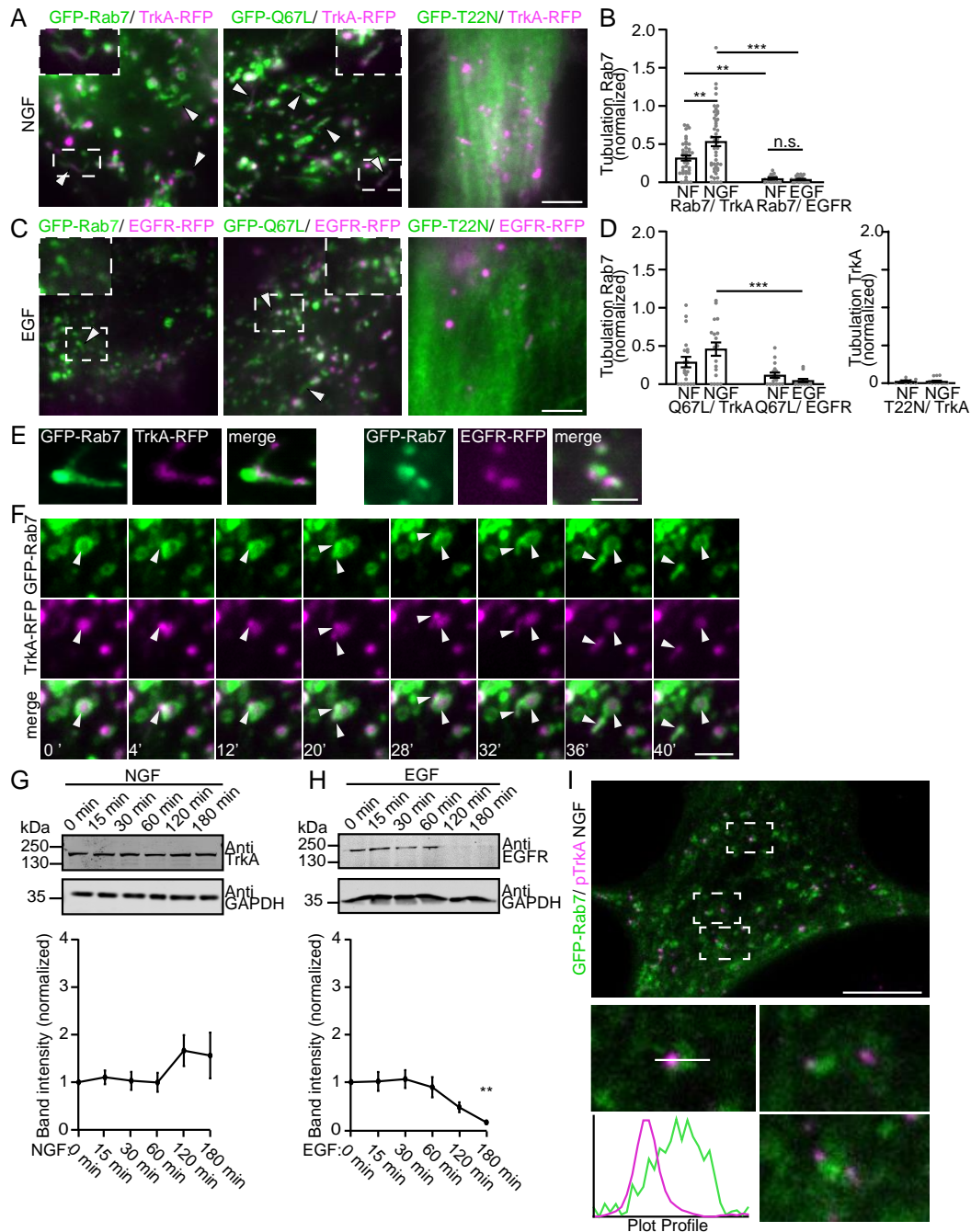


Figure 4. Rab7-endosomes induce tubulation after NGF-stimulation and these tubuli contain TrkA. (A) TIRF-microscopy of MEFs with GFP-Rab7 (WT, Q67L or T22N) and TrkA-RFP, with 100ng/mL NGF, scale bar=5 μ m. (B) Quantification of tubulation events of Rab7-WT normalized to video length. TrkA NF vs NGF p=0.0025; TrkA NF vs EGFR NF: p=0.0081; TrkA NGF vs EGFR EGF: p<0.0001 (C) TIRF-microscopy images of MEFs with GFP-Rab7 (WT, Q67L or T22N) and EGFR-RFP, with 100ng/mL EGF, scale bar=5 μ m. (D) Quantification of tubulation events of Rab7-Q67L normalized to video length or of TrkA when co-expressed with Rab7-T22N. TrkA NGF vs EGFR EGF: p=0.0003. Significance was determined by one-way ANOVA with post-hoc Sidak's; n=7 videos per condition in three independent experiments. (E) Zoomed TIRF images of TrkA in Rab7-tubuli and EGFR localized to Rab7 puncta, scale bar=2 μ m (F) Zoom time-lapse TIRF-microscopy images of MEFs transfected with GFP-Rab7, with or without stimulants as indicated. Arrowheads indicate TrkA leaving the endosome via a tubulus, time in seconds; scale bar=2 μ m. (G,H) Degradation assay of TrkA in MEFs after stimulation with NGF (G) or EGF (H), band intensities were quantified and normalized to GAPDH and timepoint 0. EGF 0 min vs EGF 180 min p=0.0016. Significance was determined by one-way ANOVA with post-hoc Dunnett's. (I) STED image of MEF overexpressing GFP-Rab7 stained for pTrkA, stimulated with NGF, scale bar=5 μ m, mean \pm SEM, **p<0.01, ***p<0.001.

During analysis of time-lapse videos, we observed tubuli being pinched off, generating small structures positive for Rab7 and TrkA. The time-lapse in Fig. 4F shows such a pinch-off: At first, it appears as a confined accumulation of TrkA localized within the vacuolar structure of Rab7 (Fig. 4F timepoint 0'). Subsequently, the accumulation of TrkA divides (Fig. 4F timepoint 4' and 12'). Next, accumulated TrkA elongates (Fig. 4F timepoint 20' and 28) and localizes to a Rab7-positive tubulus (Fig. 4F timepoint 32'). Following elongation, this tubulus is pinched off (Fig. 4F timepoint 36' and 40').

The observation that TrkA but not EGFR localizes to tubular microdomains that are pinched off, let us speculate if this mechanism leads to decreased TrkA, but not EGFR, degradation. To test this, we performed time-course stimulation with NGF and EGF and Western Blots. TrkA levels remained relatively stable (Fig. 4G). EGFR levels, however, degraded over time (Fig. 4H as reported in (Bakker et al., 2017)). We then hypothesized that retrieval of TrkA allows TrkA to signal (as observed using EM in (Ye et al., 2018)). To test this, we used STED microscopy, and found that the C-terminal domain of p-TrkA localizes adjacent to small, round Rab7-endosomes, suggesting that the C-terminal domain is exposed to the cytoplasm (Fig. 4I). Taken together, our results suggest TrkA retrieval from Rab7-endosomes via tubular microdomains, allowing TrkA to signal.

ENDOPHILINAS INTERACT WITH TRKA, RAB7 AND WASH1

So far, our results indicate that late, Rab7-endosomes tubulate upon stimulation with NGF and release TrkA. While retrieval of the cation-independent mannose-6-phosphate receptor (CI-M6PR) is facilitated by Rab7, Sorting Nexins (SNxs) and Vacuolar protein sorting-associated protein (VPS) proteins (Guerra and Bucci, 2016); recycling events through tubular domains on endosomes have been described on early endosomes (Jovic et al., 2010; Seaman, 2012a; Seaman et al., 2013).

Interestingly, EndophilinAs are similar in structure to SNxs and are also capable to induce membrane curvature. EndophilinAs were initially discovered by screening tissues for SH3 domain-containing transcripts. Three EndophilinAs (EndophilinA1-3 or SH3GL1-3) were identified, all exhibiting transcripts in the central nervous system (Giachino et al., 1997). EndophilinAs play a crucial role in the process of endocytosis (Milosevic et al., 2011). Additionally to their SH3 domains, which allow them to recruit proteins with prolin-rich domains (PRD), e.g. Dynamin (Meinecke et al., 2013), EndophilinAs also carry BAR domains, by which they can function as membrane benders (Bai et al., 2010; Gallop et al., 2006) similar to SNxs 1, 2, 5, and 6. Several recent studies have shown that EndophilinAs play a role within the endosomal system. They transiently localize to autophagosomes and triple *EndophilinA1^{-/-};A2^{-/-};A3^{-/-}* (TKO) mice showed less LC3 (a marker for autophagosomes) in brain lysates (Murdoch et al., 2016). In line with this, EndophilinAs are involved in autophagosome formation at synapses (Soukup et al., 2016). In our previous study, we reported that EndophilinAs increase tubulation on endosomes after stimulation with BDNF and interact with TrkB (Burk, et al., 2017a). Therefore, we raised the question if EndophilinAs are a modulator of the retrieval of TrkA from Rab7-endosomes.

To link EndophilinAs to cargo retrieval, we tested if EndophilinAs interact with Rab7 by co-immunoprecipitation. By overexpressing Rab7-WT, Q67L and T22N we found that upon stimulation with NGF, EndophilinA2 interacts with Rab7-WT and Q67L but only in limited amounts with T22N (Fig. 5A). This interaction is not occurring in the absence of NGF (Fig. S4A). Additionally, we used live-TIRF imaging to study the localization of EndophilinAs. We found EndophilinA2 localizing to Rab7-endosomes, upon exogenous expression (Fig. 5B). To validate these findings, we used MEFs

from TKO mice (Burk et al., 2017a). While genotyping has been published (Burk et al., 2017a), we also validated these MEFs using antibodies against EndophilinA1, EndophilinA2 and EndophilinA3 in control and TKO-MEFs. Staining of EndophilinAs in TKO-MEFs was significantly reduced compared to wild-type controls (Fig. S5A,B). Next, we evaluated if Rab7-endosomes in EndophilinA TKOs extend tubular microdomains after stimulation with NGF. As reported in Fig. 4A,B, WT-MEFs extended tubular domains upon stimulation with NGF. In TKO-MEFs, however, Rab7-endosomes failed to extend tubular domains following NGF stimulation (Fig. 5C,D). Following this result, we expected the phosphorylation of TrkA to be reduced in TKO-MEFs. Staining for p-TrkA in WT-MEFs following NGF stimulation showed an increase in p-TrkA intensity compared to non-stimulated control, which we did not find in MEFs from EndophilinA TKOs (Fig. 5E,F). Interestingly, TrkA does not undergo degradation as we suspected given the lack of retrieval. When performing time-course experiments as described for Figure 4 G,H, we found that TrkA remained relatively stable until 60 minutes of stimulation and then significantly increased expression levels at 120 and 180 minutes (Fig. 5G). EGFR, on the other hand, degraded faster compared to WT-control (significant decrease already at 60 minutes of EGF stimulation compared to 180 minutes in WT-control Fig. 5H). Lastly, overall morphology of Rab7-endosomes in TKO-MEFs resembled morphology of Rab7-endosomes in WT-MEFs. Using STED microscopy, we found round, vacuolar structures containing smaller intraluminal vacuoles that are positive for Rab7 (Fig. 5I).

Next, we tested if EndophilinAs interact with proteins of the endosomal sorting machinery. It has been shown that EndophilinAs interact with Dynamin-2 (Ross et al., 2011) and that Dynamin-2 is recruited by the WASH-complex (Nicoziani et al., 2000; Derivery et al. 2010; Ross et al., 2011). Given that we found Rab7-endosomes tubulating in the presence of NGF but not EGF, We performed co-immunoprecipitation experiments and found that EndophilinAs interact with TrkA but not with EGFR (Fig. 6A,B). To ensure specific binding, we added two controls: co-expression of TrkA with GFP as well as incubating the lysate to IgG beads (Fig. 6A and Fig. S4B). Next, we performed immunostainings of WASH1 and Rab7 in MEFs and found that plot profiles showed overlaps in the presence of NGF but not EGF (Fig. 6C,D). When performing immunocytochemistry in DRG neurons, colocalization of WASH1 and Rab7 significantly increased in the presence of NGF (Fig. 6E). To address interaction biochemically, we overexpressed WASH1-RFP together with EndophilinA1-, A2- and A3-GFP in HEK293 cells and tested their interaction by co-immunoprecipitation. All three EndophilinAs co-immunoprecipitated with WASH1, with the strongest interaction for A2 and the weakest for A3 (Fig. 6F).

In the next step, we asked if EndophilinAs interact with SNxs, given their structural similarity. We tested all three EndophilinAs with SNx1, SNx2, SNx5 and SNx6 but found no interaction (Fig. S6A-D).

Finally, we examined whether EndophilinAs interact with proteins of the retromer-complex. Therefore, we overexpressed VPS26, VPS29 and VPS35 with EndophilinAs. These approaches did not show interaction of EndophilinAs with VPS proteins (Fig. S7A-C). Taken together, our microscopy and biochemical results suggest that EndophilinAs interact with TrkA and WASH1 but not with SNxs or VPS26/29/35.

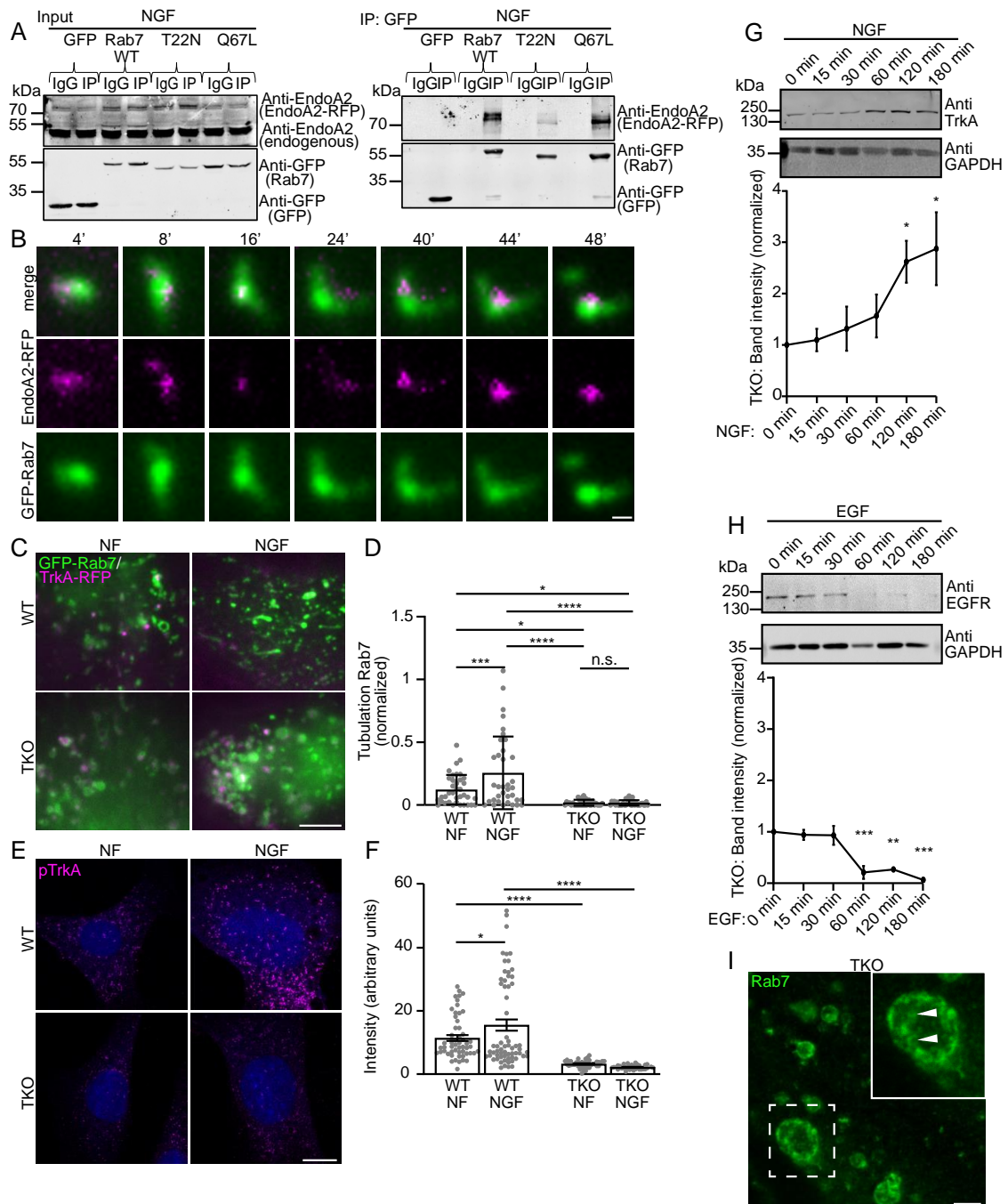


Figure 5. EndophilinA2 associates with late, tubulating Rab7-endosome complexes. (A) GFP-conjugated beads (or IgG control beads) were used to pull down GFP-Rab7 (WT, T22N, Q67L) showing interaction with EndophilinA2-RFP in with NGF-treated Hek293 cells (Input on the left, IP on the right). (B) Time-lapse TIRF-microscopy images of MEFs with EndophilinA2-RFP and GFP-Rab7. Time in seconds, scale bar=0.5 μm. (C) TIRF-microscopy images of WT or EndophilinA2-TKO-MEFs c with GFP-Rab7 and TrkA-RFP, with or without 100 ng/mL NGF, scale bar=5 μm. (D) Tubulation events of Rab7 in WT- and TKO-MEFs normalized to video length. WT NF vs NGF p=0.0022; WT NF vs TKO NF p=0.0033; WT NF vs TKO NGF p=0.0256; WT NGF vs TKO NF p<0.0001; WT NGF vs TKO NGF p<0.0001. (E) Confocal images of WT- and TKO-MEFs stained for pTrkA in unstimulated/stimulated conditions, scale bar=10 μm. (F) Signal intensity of pTrkA in different conditions. Statistical significance was determined by one-way ANOVA with post-hoc Sidak's WT NF vs WT NGF p=0.0498, WT NF vs TKO NF p<0.0001, WT NGF vs TKO NGF p<0.0001. (G,H) Degradation assay of TrkA in EndophilinA2 TKO-MEFs after stimulation with NGF (G) or EGF (H), band intensities were quantified and normalized to GAPDH and timepoint 0 min. NGF 120 min p=0.0492, NGF 180 min p=0.0191, EGF 60 min p=0.005, EGF 120 min p=0.001, EGF 180 min p=0.0001. Significance was determined by one-way ANOVA with post-hoc Dunnett's. (I) STED image of EndophilinA2 TKO-MEF stained against Rab7, scale bar=2.5 μm, mean±SEM, *p<0.05, **p<0.01, ***p<0.001.

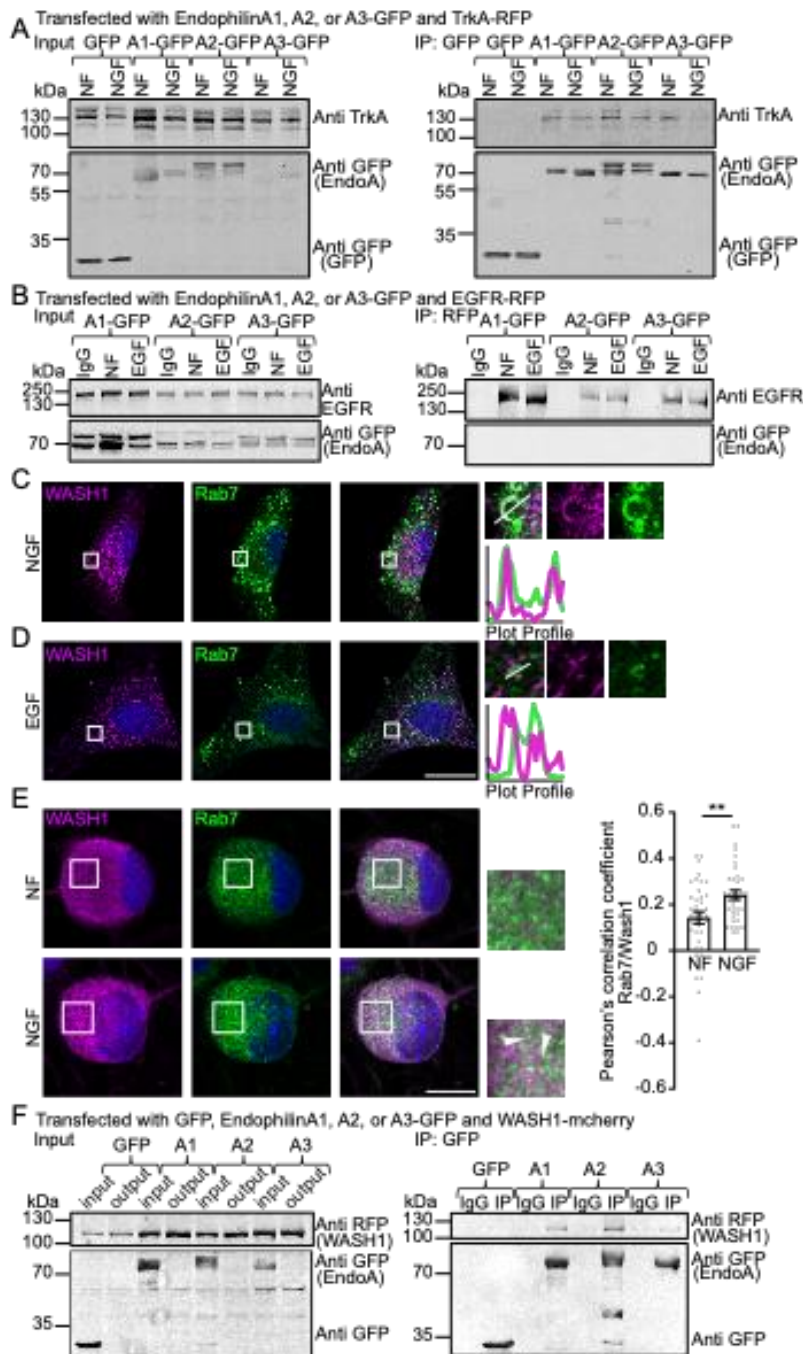


Figure 6. WASH1 is involved in late receptor tubulations. (A) GFP-conjugated beads were used to pull down GFP, EndophilinA1, A2, or A3-GFP in with TrkA-RFP co-transfected Hek293 cells (Input on the left, IP on the right) in the presence/absence 100 ng/mL NGF. (B) Anti-RFP-conjugated beads (or IgG control beads) were used to pull down EGFR-RFP in with EndophilinA1, A2, or A3-GFP co-transfected Hek293 cells in the presence/absence of 100 ng/mL EGF. (C) Immunostaining of MEFs showing WASH1 on the rim of late Rab7 vacuoles when stimulated with NGF; scale bar=20 μ m. (D) Immunostaining of MEFs showing WASH1 not localizing to late Rab7 vacuoles when stimulated with EGF; scale bar=20 μ m. (E) Colocalization of stained WASH1 and Rab7 increases in DRGs upon stimulation with NGF. Quantified with Pearson's Correlation Coefficient. Statistical significance was determined using unpaired t-test $p=0.0046$, $n=10-15$ images were taken per condition, the experiment was performed three times, scale bar=10 μ m. (F) EndophilinAs co-immunoprecipitate with WASH1 in co-transfected HEK293 cells.

RAB7-CMT2B MUTATIONS CAUSE DISRUPTED TUBULATION EVENTS, DEFECTS IN TRK-RECEPTOR SIGNALLING, DECREASED BINDING TO ENDOPHILINA2 AND REDUCED NEURITE LENGTH OF SENSORY NEURONS

CMT2B disease, a neuropathy of the peripheral nervous system affecting sensory and motor neurons, is caused by six missense mutations in the Rab7-GTPase (Auer-Grumbach et al., 2000; De Jonghe et al., 1997; De Luca et al., 2008; Houlden et al., 2004; Meggouh et al., 2006; Saveri et al., 2020; Verhoeven et al., 2003; Wang et al., 2014). Studies on CMT2B reported disrupted sorting of EGFR, fewer EGFRs in late endosomal compartments and disrupted EGFR downstream signalling (BasuRay et al., 2013). Additionally, Rab7-CMT2B mutants showed prolonged phosphorylation of TrkA and EGFR compared to Rab7-WT (Basuray et al., 2010; BasuRay et al., 2013), suggesting disrupted receptor sorting. To link TrkA-receptor retrieval from Rab7-endosomes via tubulation to CMT2B, we overexpressed Rab7-WT and the four best-characterized Rab7-CMT2B mutations in MEFs and studied their ability to induce tubulation in the presence and absence of NGF. All tested CMT2B constructs showed alterations in their ability to tubulate. Rab7-K157N is unable to induce tubular events- unstimulated tubulation is even lower than in Rab7-WT control and there is no increase after stimulation with NGF (Fig. 7A,B). Both, Rab7-L129F and -N161T seem to „overtubulate“. Here, tubulation events are increased compared to control but with no increase in tubulation following NGF stimulation (Fig. 7A,B). Finally, Rab7-V162M shows tubulation events close to unstimulated control, which also do not increase following NGF stimulation (Fig. 7A,B). Next, we tested how tubulation relates to signalling of TrkA. As shown in Fig. 4F, tubular domains are pinched off, generating a new vesicle. Ye et al. reported in their study that single membrane vesicles, which are generated from MVBs in sensory neurons, contain signalling-competent TrkA (Ye et al., 2018). In Fig. 4I, we found p-TrkA adjacent to small Rab7-positive structures. If defects in tubulation affect the generation of signalling competent TrkA vesicles, then CMT2B constructs that show an inability to form tubular domains should affect the phosphorylation of TrkA. To test this, we expressed TrkA-, GFP- and Rab7 constructs (WT-Rab7 and CMT2B-Rab7 constructs) in HEK293 cells. Interestingly, the overexpression of Rab7 together with TrkA increased the basal phosphorylation of TrkA (Fig. 7C, compare lane 1 and 2 (GFP) to lanes 3 and 4 (GFP-Rab7)). This suggests that not only receptors are able to change the activity of GTPases on endosomes (compare Fig. 3B to Fig. S3C) (Deininger et al., 2008; Wu et al., 2014; Burk et al., 2017b) but that Rab-GTPases also affect the activity state of receptors. Further, we found that tubulation events of Rab7 constructs reflect the levels of phosphorylated TrkA in Western Blots from HEK293 cells. We normalized p-TrkA to Rab7, given that these were the two proteins overexpressed (e.g. low levels of Rab7 could affect phosphorylation state of TrkA). However, total TrkA remains stable (Fig. 7C). As with tubulation events, Rab7-WT showed a significant increase in p-TrkA after stimulation with NGF. Rab7-L129F and -N161T revealed overall higher p-TrkA, which did not increase in stimulated conditions. Rab7-K157N and -V162M revealed lower levels of p-TrkA, however, Rab7-V162M showed a significant increase following stimulation with NGF, which did not occur for K157N (Fig. 7C,D).

Since we found EndophilinAs being recruited to Rab7-endosomes (Fig. 5A,B), we tested if EndophilinA2 binds to Rab7-CMT2B constructs. Overexpressing CMT2B constructs Rab7-L129F, -K157N, -N161T and -V162M together with EndophilinA2 revealed that EndophilinA2 does not bind in unstimulated conditions (Fig. S8). In NGF-stimulated conditions, EndophilinA2 bound to Rab7-WT

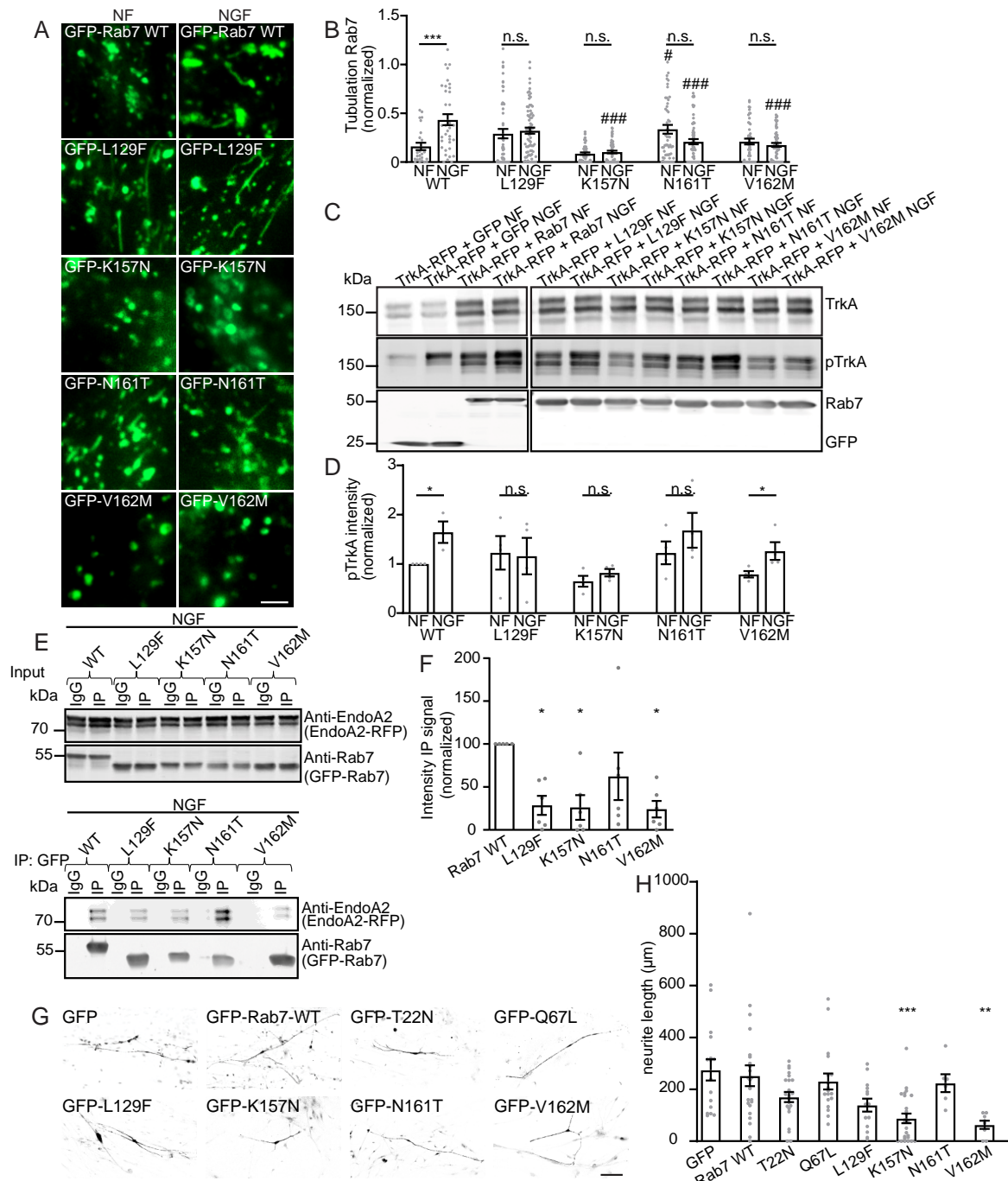


Figure 7. CMT2B-Rab7 mutations show abnormal tubulation phenotypes. (A) TIRF-microscopy images of MEFs with GFP-Rab7 (WT or CMT2B mutants) with or without 100ng/mL NGF, scale bar=2 μ m. (B) Tubulation events normalized to video length (n=7 videos per condition in six independent experiments). *p<0.05, ***p<0.001 (significance between each NF/NGF condition), #p<0.05, ###p<0.001 (significance between each condition with its respective WT control). (C) Western Blot of HEK293 lysate co-expressing TrkA-RFP and GFP-Rab7-constructs in unstimulated/stimulated conditions. (D) pTrkA band intensity normalized to Rab7 band intensity and to WT NF. WT NF vs NGF p=0.0169; Rab7-V162M NF vs NGF: p=0.0494. (n=4 independent experiments) (E) GFP-conjugated beads (or IgG control beads) were used to pull down GFP-Rab7-WT and the CMT2B mutants L129F, K157N, N161T, V162M with EndophilinA2-RFP in stimulated Hek293 cells. (Input on top, IP on bottom.) (F) EndophilinA2-RFP IP band-intensity from six independent experiments, normalized to Rab7 band-intensity. Rab7-WT vs L129F p=0.0164, Rab7-WT vs K157N p=0.0130, Rab7-WT vs V162M p=0.0105. (G) DRGs transfected with GFP-Rab7 (WT, T22N, Q67L and CMT2B mutants, or GFP) stained for β III-tubulin show decreased neurite length in CMT2B mutants at DIV15, scale bar=100 μ m. (H) Quantification of neurite length. WT vs K157N: p=0.0002; WT vs V162M p=0.0034 (3-10 images per condition, the experiment was performed three times). Significance was determined by one-way-ANOVA with post-hoc

Sidak's (B), Dunnett's (F, H), or unpaired t-tests between each unstimulated and stimulated condition (D); mean±SEM, *p<0.05, **p<0.01, ***p<0.001.

as shown before (Fig. 5A) but showed significantly reduced binding to three CMT2B constructs; Rab7-L129F, -K157N and -V162M (Fig. 7E,F).

To test if the defects observed in phosphorylation of TrkA lead to effects in neurons, we overexpressed GFP, Rab7-WT, -Q67L and -T22N, as controls, as well as CMT2B constructs in adult mouse DRG neurons. On day *in vitro* (DIV) 15, Rab7-K157N and -V162M, where tubulation and phosphorylation of TrkA was decreased, led to significantly decreased neurite length (Fig. 7G,H). Such decrease was not observed for Rab7-L129F and Rab7-N161T, which were able to tubulate and phosphorylate TrkA.

Taken together, Rab7-endosomes are able to retrieve TrkA. In CMT2B mutations, which show defects in tubular domain formation, we found a decrease in phosphorylation of TrkA and consequently, a decrease in neurite length over time (Fig. 8A,B,C).

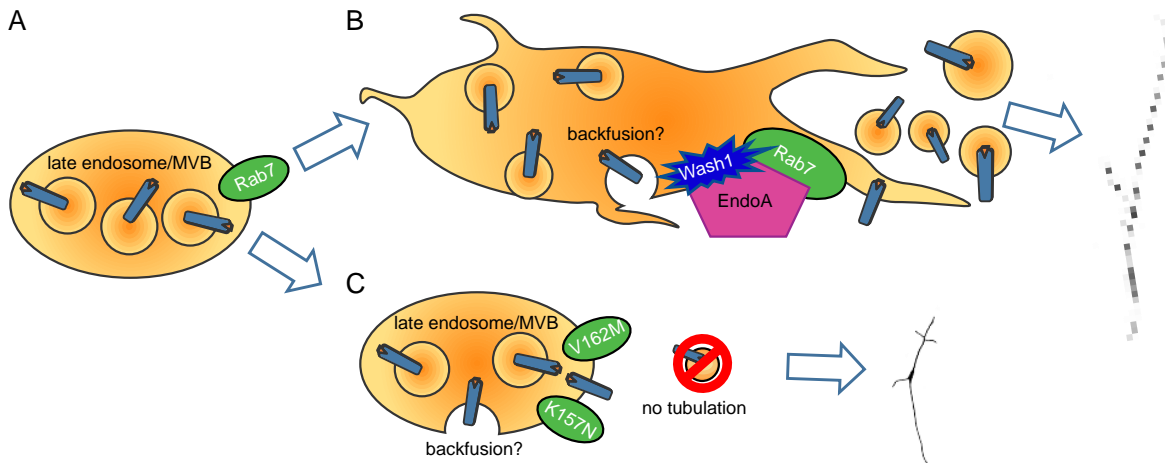


Figure 8. Model of TrkA retrieval from Rab7-endosomes. (A) Rab7-endosomes/MVBs with TrkA within ILVs. **(B)** Proposed retrieval of TrkA via tubuli in an EndophilinAs/WASH1/Rab7-dependent manner. TrkA may undergo back-fusion to the limiting membrane. **(C)** CMT2B-mutants K157N and V162M do not retrieve TrkA via tubuli, leading to shorter neurite length. This figure was created using Servier Medical Art templates, licensed under a Creative Commons Attribution 3.0 Unported License; <https://smart.servier.com/CMT2B>.

3.4 DISCUSSION

In this study, we report a retrieval mechanism of TrkA from late Rab7-endosomes. Using TIRF, STED and EM, we analysed Rab7-endosomes in the presence and absence of NGF and EGF. We found that TrkA localizes to or within Rab7-endosomes of various sizes while EGFR localized more to the limiting membrane of Rab7-endosomes. When stimulated with NGF but not EGF, Rab7-endosomes extend tubular domains, in which TrkA localizes and subsequently is pinched off. This tubulation event correlated with the phosphorylation status of TrkA. Additionally, TrkA remained stable in time-course Western Blot experiments while EGFR levels decreased over time. In peripheral neuropathy CMT2B tubulation events were disrupted. Disrupted tubulation events in CMT2B correlated with phosphorylation of TrkA and with DRG neurite length.

IDENTIFICATION OF TRK-CONTAINING RAB7-ENDOSOMES

MVBs are generally categorized using ultrastructural analysis, which allows categorization for appearance or density (Klumperman and Raposo, 2014). Therefore, in order to determine if tubulating, vacuolar Rab7-structures are indeed late endosomes/MVBs, we examined non-stimulated and NGF-stimulated DRGs using EM, revealing an increase in number of MVBs upon stimulation-that we also found tubulating. Additionally, co-expression of Rab7 together with CD63, a marker for ILV/MVBs (Bebelman et al., 2020; Fernandez-Borja et al., 1999) revealed colocalization. Using STED microscopy on Rab7-endosomes, we found vacuolar structures that contained small ILVs, positive for Rab7. Since ILVs are formed by inward budding from the limiting endosomal membrane (Cullen and Steinberg, 2018), it is not surprising to find these ILVs positive for Rab7. Lastly, these Rab7-positive structures were negative for Transferrin, indicating that they are not part of the recycling pathway, despite them inducing tubular domains (Mayle, Le and Kamei, 2013). However, pinpointing the exact identity of endosomes has been a challenge for decades and for this study. While overexpressing Rab-GTPases often causes secondary effects such as mis-localization or effects on the cells' physiology, antibody stainings provide the challenge that Rab-GTPase recruitment to endosomes has overlapping dynamics (Rink et al., 2005; Humphries et al., 2011), making it difficult to determine the exact identity of an endosome. Further, about 70% of all endo-lysosomal structures are positive for Rab7 and Lysosomal-associated membrane protein 1 (Lamp1) (Humphries et al., 2011). When using ultrastructural analysis, dynamics in live cells cannot be observed and classifying maturing endosomes on their intraluminal acidity proves to be difficult. Therefore, our approach may also involve endosomes on the switch between Rab5 and Rab7 as well as Rab7/Lamp1-positive endolysosomes. Nevertheless, in our study, TrkA shows no evidence to be part of the recycling pathway as observed in (Suo et al., 2014).

RELEASE OF TRKA FROM RAB7-ENDOSOMES

The first receptor to be reported to shuttle from the trans-golgi network (TGN) to endosomes and back was CI-M6PR. CI-M6PR-ligand complexes exit the TGN through clathrin-coated vesicles, which subsequently fuse with endosomal structures. Because of the low pH in late endosomes, the ligand dissociates from CI-M6PR, allowing CI-M6PR to shuttle back to the TGN (Braulke and Bonifacio, 2009). Related to the current study, Ye et al. showed sorting of TrkA from late, Rab7-endosomes. Here, the kinase activity of TrkA changes the dynamics of MVBs by generating single-membrane vesicles containing p-TrkA, which avoid degradation (Ye et al., 2018), but how these vesicles evolve remains unresolved. The evolution of new vesicles has been shown on early endosomal sorting into the recycling pathway via tubular microdomains. In short, early endosomes extend tubular domains, into which cargo is routed. Several proteins such as the WASH-complex, SNxs 1, 2 and 5, 6, VPS 26, 29 and 35 facilitate cargo sorting. The trimeric VPS26,29,35 retromer subdomain forms the core functional component (cargo selective complex, CSC) (Fjorback et al., 2012; Norwood et al., 2011; Nothwehr et al., 2000; Seaman, 2012b).

SNxs carry a BAR domain, which can sense and induce membrane curvature (Carlton et al., 2004; Frost et al., 2009; Peter et al., 2004; Van Weering et al., 2012). They also contain a phosphoinositide 3-kinase (PI3K) homologous domain (PX) that binds to PI(3)P (Ellson et al., 2002). The WASH-complex facilitates a dense branched actin network, which generates a pulling force on the membrane and leads to the formation of tubuli. WASH's interaction with Dynamin finally leads to tubulus fission of the sorted cargo in its newly-formed endosomal subdomain (Derivery et al., 2009; Duleh et al., 2010; Seaman, 2012b; Seaman et al., 2013).

In our previous study, we found that EndophilinAs are recruited to endosomal compartments upon BDNF-stimulation, co-traffic with endosomes and induce the formation of tubuli (Burk et al., 2017a). EndophilinAs possess an SH3 domain, allowing recruitment of PRD containing proteins such as Dynamin (Meinecke et al., 2013). In addition, EndophilinAs contain a BAR domain, which induces and senses membrane curvature (Bai et al., 2010; Gallop et al., 2006). Therefore, we speculated cargo retrieval from late endosomes via EndophilinA-induced tubular domains. Interestingly, we did not find such a phenotype for EGFR. EGFR has been reported to localize to Rab7-endosomes from where it signals (BasuRay et al., 2013; Ceresa and Bahr, 2006; Cullen and Steinberg, 2018). This signalling cascade is terminated by degradation of the receptor, which is achieved by the fusion of late, Rab7-endosomes with lysosomes (Bakker et al., 2017; BasuRay et al., 2013). Our observations suggest that indeed EGFR remains in Rab7-endosomes to undergo degradation. However, in order to signal, EGFR should localize to the limiting membrane of Rab7-endosomes and evidence from Tomas et al indicates that EGFR undergoes back-fusion into the limiting membrane of MVBs (Tomas et al., 2015). Nevertheless, EGFR has also been reported to localize to ILVs, requiring a precise spatiotemporal regulation of EGFR localization (Cullen and Steinberg, 2018).

We observed that EndophilinA is recruited to Rab7-endosomes and interacts biochemically with TrkA but not EGFR. The absence of EndophilinAs abolishes tubulation of Rab7-endosomes as well as phosphorylation of TrkA. Interaction of EndophilinAs with TrkB and EGFR have previously been shown (Schmidt et al., 2003; Burk et al., 2017a). In contrast, our co-immunoprecipitation experiments did not show interaction of EGFR with all three EndophilinAs, which is not in line with (Schmidt et al., 2003). Schmidt et al. found interaction of EGFR with EndophilinA1 in HEK293 cells while studying the role of EndophilinA1 in EGFR endocytosis. However, giving the finding that Rab7-endosomes containing EGFR do not induce tubulation, our result of no interaction fits with the hypothesis that EndophilinAs retrieve Trks but not EGFR via the formation of tubular microdomains.

In order to link EndophilinAs to cargo retrieval, we tested interactions with the known components of the endosomal sorting machinery, such as VPS-, SNx- proteins and the WASH-complex. We found that all three EndophilinAs interact with WASH1. In terms of tubular fission, this result fits with previous reports that WASH1 and EndophilinAs recruit and interact with Dynamin-2 (Derivery et al., 2009; Ross et al., 2011). Interestingly, cells lacking the WASH-complex sustain a collapse of the endolysosomal system (Derivery et al. 2010) and lack of all three EndophilinAs leads to an increase in Rab7-protein and an accumulation of TrkB in Rab7-endosomes (Burk et al., 2017a).

Shuttling of cargo also involves the endoplasmic reticulum (ER) (Wu et al., 2018). Endosome fission occurs on ER-endosome contact sites and is important for recycling of cargoes and endosome maturation. ER tubuli and endosomes establish contacts, which are also positive for Coronin-1 and FAM21, a subunit of the WASH-complex (Rowland et al., 2014). The study of (Suo et al., 2014) reported an interaction of TrkA and Coronin-1, a modulator in ER-endosome fission. This interaction leads to recycling of TrkA via Rab11-endosomes. Since we find Rab7-endosomes extending tubuli, it is possible that this involves contact sites with the ER. However, we did not find TrkA localizing to Rab11-endosomes, suggesting that the retrieval mechanism we observe is independent of ER-endosome contact sites.

NGF INDUCED EXPRESSION OF TRKA IN ENDOPHILINA TKO-MEFs

Since TKO-MEFs failed to extend tubular domains following NGF-stimulation, we expected TrkA to undergo degradation as EGFR. However, TrkA levels significantly increased at 120 minutes of NGF stimulation (by 3-fold). Since we did not observe increased p-TrkA in NGF-stimulated TKO-MEFs compared to control (Fig. 5E,F), this observation could result from a compensatory mechanism for lack of TrkA retrieval. Increase of TrkB mRNA levels following exposure to BDNF in placode-derived sensory neurons has been reported previously (Robinson, 1996), suggesting that this increase could result from a positive feedback-loop. However, another possibility is a compensatory mechanism on neuronal survival. Hippocampal neurons of EndophilinA TKO mice die faster in culture compared to control and are not rescued by BDNF administration, suggesting a disruption in the mediation of the survival signalling cascade (Burk, et al., 2017a). Therefore, increase in TrkA expression could result from the inability to retrieve TrkA and mediate signalling.

TRKA RETRIEVAL IN CHARCOT-MARIE-TOOTH-DISEASE

Subsequent to our results indicating defective neurotrophic receptor retrieval, our focus shifted to CMT2B. Several studies have linked CMT2B to impairments in growth-factor receptor endocytosis and signalling (Basuray et al., 2010; BasuRay et al., 2013; Cogli et al., 2010; Zhang et al., 2013). Here, we report that four different Rab7-mutations causing CMT2B show different phenotypes after stimulation with NGF, we found changes in p-TrkA and growth defects. In addition, three out of four CMT2B constructs showed decreased interaction with EndophilinA2. Interestingly, in 2009, Seaman et al. linked retromer-dependent sorting to CMT2B. In this study, the authors overexpressed Rab7-WT and Rab7-CMT2B constructs together with VPS35. The authors found that Rab7-K157N was unable to bind to VPS35 (Seaman et al., 2009). In addition, Rab7-V162M showed no binding to VPS35, however, expression of Rab7-V162M was much lower compared to other CMT2B constructs and excluded from analysis. While we did not find EndophilinAs binding to VPS proteins, defects in tubular formation could be caused by reduced binding of EndophilinAs to CMT2B-Rab7 in addition to the inability of VPS35 binding to Rab7-K157N and -potentially Rab7-V162M.

In conclusion, Rab7-endosomes are able to retrieve or maintain specific cargo and therefore facilitate spatial and temporal signalling cascades. Further studies on these findings will help to shed light on stabilizing neural circuits. In addition, understanding these mechanisms may help to elucidate the pathogenic mechanisms leading to CMT2B.

3.5 MATERIAL AND METHODS

All research involving animals was approved by, and done in accordance with, the Institutional Animal Care and Ethics Committees of Göttingen University (T1714) and with German animal welfare laws, and in accordance with the Animals Scientific Procedures Act of 1986 (UK).

Cell Culture (MEFs): To generate mouse embryonic fibroblasts (MEFs), embryos were isolated from gestating *mus musculus* C57BL/6N females at embryonic day E13.5 after fertilization by male C57BL/6N, minced, and taken into culture in complete DMEM with 10% FBS and 1% penicillin/streptomycin at 37°C, 5% CO₂. Endophilin KO MEFs (from Burk et al., 2017a) were provided by Ira Milosevic (European Neuroscience Institute, Goettingen).

(HEK293) (from Burk et al., 2017a): HEK 293 cells were plated in complete DMEM medium containing 10% FBS and 1% penicillin/streptomycin and cultivated at 37 °C, 5% CO₂.

Primary dorsal root ganglia (DRG) cell culture: Cover slips coated with Poly-L-Lysine and Laminin. DRG neurons were isolated from adult BL6 mice and incubated with collagenase solution (200U/ml) for 1 h at 37 °C. Tubes were shaken every 15 minutes. Following the collagenase treatment, a Papain-enzyme solution was added and neurons incubated for 30 minutes at 37 °C, shaking the tubes every 15 minutes. Eventually, the solution was exchanged by pre-warmed plating medium (F12/DMEM, 1% penicillin/streptomycin, 10% horse serum) and 100µL of the suspension were plated on the prepared cover slips to incubate for 1h at 37 °C, 5% CO₂. Afterwards, wells were filled with an additional 400µL pre-warmed plating medium and left to incubate overnight at 37 °C, 5% CO₂.

For TIRF microscopy, neurons were plated on Matek dishes and medium was exchanged on DIV1 to neuronal medium (F12/DMEM 0.5% pen/Strep, 1%Glutamax, 2%B27). DRG neurons were transfected with lipofectamine on DIV 6 and imaged on DIV9. Cells were starved with DMEM/F12 only and subsequently stimulated with 100 ng/mL NGF.

For neurite length measurements, neurons were transfected on DIV1 with lipofectamine and endotoxin free plasmids. After transfection the medium was replaced with pre-warmed neuronal medium. At DIV15 DRG neurons were fixed in 4% PFA for 10 min and stained. Images were acquired on a Zeiss LSM800.

Plasmids: The eGFP-Rab7-WT plasmid was generated by subcloning Rab7-WT from an mRFP-Rab7-WT plasmid (from Barbara Flix) into a pEGFP-C1 plasmid (GFP-Rab7-Q67L gift from Reinhard Jahn, Göttingen) by HindIII and MfeI. This eGFP-Rab7-WT plasmid was cut with AflIII and KpnI to replace the Rab7-WT with Rab7-T22N or Rab7-Q67L from mRFP-Rab7-T22N / mRFP-Rab7-Q67L both obtained from Barbara Flix. TrkA-RFP was a gift from Moses Chao (Addgene plasmid # 24093 ; <http://n2t.net/addgene:24093>; RRID:Addgene_24093). EGFR-RFP was a gift from Philippe Bastiaens. EndophilinA1-GFP, EndophilinA2-GFP and EndophilinA3-GFP were obtained from I. Milosevic/P. De Camilli (Cao, M., Milosevic, I., Giovedi, S. & De Camilli, P. Upregulation of Parkin in Endophilin mutant mice. *J. Neurosci.* 34, 16544–9, doi:10.1523/JNEUROSCI.1710-14.2014). mCherry-WASH1-N-18 was a gift from Michael Davidson (Addgene plasmid # 55163; <http://n2t.net/addgene:55163>; RRID:Addgene_55163). SNx1-mCherry, SNx2-mCherry, SNx5-mCherry, SNx6-mCherry, VPS26-GFP, VPS-29-GFP, and VPS35-GFP were gifts from Pete Cullen. GFP-Rab7-K157N and GFP-N161T were kind gifts from Cecilia Bucci, (Spinosa et al., 2008). GFP-Rab7-L129F and GFP-V162M were gifts from Angela Wandinger-Ness, (BasuRay, Mukherjee, Romero, Seaman, & Wandinger-Ness, 2013).

Lipofectamine transfection (for TIRF in DRGs and MEFs or neurite length measurements in DRGs). Cells were transfected using the Lipofectamine 2000 reagent (Thermo Fisher Scientific Inc., #11668030) according to manufacturer's instructions. Briefly, 1µl of Lipofectamine 2000 was mixed with 100 µl DMEM (solution A, RPMI for DRGs), while in another reaction tube 1 µg of the plasmid of interest was added to 100 µl of DMEM (solution B, RPMI for DRGs). Following 5 min of incubation of solution A at room temperature, it was mixed with solution B and the mix was incubated at 37°C for one hour. Culture media were aspirated and replaced with pre-warmed DMEM (RPMI for DRGs). The transfection mix was added to each well and the cells were placed back to the incubator for 75

min. Finally, the transfection mix was replaced with culture medium and expression was allowed for 2-3 days (15 days for DRGs).

TIRF microscopy. Transfected MEFs were trypsinized and replated on MaTek 35mm glass-bottom poly-d-lysine-coated tissue culture dishes. On the day of imaging, MEFs were placed in non-supplemented DMEM on an AxioObserver Z1 TIRF microscope (Carl Zeiss) with an Evolve CCD camera (Photometrics) using the 100X objective and imaged (5 min time-lapse recordings with pictures taken in 4 s intervals). Subsequently, after imaging control conditions, MEFs were stimulated with 100 ng/mL NGF or EGF, and imaged during 5 min time-lapse recordings with pictures taken in 4s intervals. From time-lapse recordings, we analyzed tubulation and localization. For figures, images have been adjusted to improve visualization.

Immunocytochemistry. MEFs and DRGs were fixed with 4%PFA and incubated in blocking solution (10%NHS, 5%BSA, 0.3% Triton, 25mM Glycine in PBS) for 1 h. Cells were then incubated overnight in primary antibody (1:1000 unless otherwise indicated) in blocking solution at 4°C. Cells were subsequently washed three times in PBS and 1:1000 dilution of secondary antibody was applied for 2 h at room temperature. After washing with PBS, cells were stained with 0.5 µg/mL DAPI in PBS for 10 min, consequently washed with PBS, shortly rinsed with ddH₂O and then mounted on a coverslip using Mowiol 4-88. Immunofluorescence was performed using the following antibodies: TrkA polyclonal rabbit antibody (Millipore, cat# 06-574), EGFR (A-10) mouse monoclonal antibody (Santa Cruz, cat# sc-373746), pTrkA Y794 polyclonal rabbit antibody (Millipore, cat# ABN1383), pEGFR Y1068 monoclonal rabbit antibody (CellSignaling Technologies, cat# 3777), betaIII-Tubulin mouse monoclonal antibody (abcam, cat# ab78078), WASH1 polyclonal rabbit antibody (Sigma, cat# SAB4200372), EndophilinA1 mouse monoclonal antibody (Santa Cruz, cat# sc-374279), EndophilinA2 mouse monoclonal antibody (Santa Cruz, cat# sc-365704), EndophilinA2 rabbit polyclonal antibody (Proteintech, cat# 27014-1-AP), EndophilinA3 mouse monoclonal antibody (Santa Cruz, cat# sc-376592), Rab7 mouse monoclonal antibody (Cell Signaling Technologies, cat# 95746), Rab7 polyclonal rabbit antibody (Synaptic Systems, cat# 320 003). Secondary antibodies were Alexa Fluor 546 goat anti-mouse (Thermo Fisher Scientific, cat# A11003), Alexa Fluor 546 goat anti-rabbit (Thermo Fisher Scientific, cat# A11035), Alexa Fluor 488 goat anti-mouse (Thermo Fisher Scientific, cat# A11001) and Alexa Fluor 488 goat anti rabbit (Thermo Fisher Scientific, cat# A-11008). For STED, secondary labels were Abberior STAR635P anti-mouse nanobodies (Nanotag, catalog#N1202) and Abberior STAR580 goat anti-rabbit antibodies (Abberior, catalog#ST580-1002). For confocal, images were acquired with a Zeiss LSM 800 Airyscan confocal microscope with Zen acquisition software. STED images were taken on an Abberior QUAD scan STED microscope (Abberior instruments GmbH, Germany) with pulsed STED lines at 775nm and 595 nm, and excitation lasers at 485 nm, 580 nm and 640 nm. Pixel size was set to 25nm. Images were acquired with a 100x/1.4 NA magnification oil immersion lens and processed with Imspector (Abberior Instruments GmbH, Germany) and FIJI (<https://fiji.sc/>).

Electron Microscopy. DRGs were isolated from adult BL6 mice. Following a 30 min starvation period in F12/DMEM, DRGs of the left side were stimulated with 200 ng/mL NGF, whereas DRGs of the right side were simulated with PBS containing 0.1%BSA. DRGs were then fixed with 4% paraformaldehyde and 0.5% glutaraldehyde in PBS (pH 7.4) for 1 h and further fixed overnight with 2% glutaraldehyde in 0.1 M sodium cacodylate buffer (pH 7.2). Subsequently, samples were washed in 0.1 M sodium cacodylate buffer and treated with 1% osmium tetroxide (v/v in 0.1 M sodium cacodylate buffer) for 1 h and after incubation washed twice in 0.1 M sodium cacodylate buffer for

10 min, respectively, and further in distilled water (three times for 5 min each). Next, en bloc staining with 1% uranyl acetate (v/v in distilled water) was performed for 1 h and samples were briefly washed three times in distilled water. This was followed by the dehydration in an ascending concentration series of ethanol, infiltrated and embedded in epoxy resin (AGAR-100, Plano, Germany). The steps were as followed: 5 min in 30% ethanol/distilled water (v/v), 5 min in 50% ethanol/distilled water (v/v), 10 min in 70% ethanol/distilled water (v/v), 10 min in 95% ethanol/distilled water (v/v), exchanged once and incubated another 10 min in 95% ethanol/distilled water (v/v). Afterwards the samples were incubated 3x 10 min in 100% ethanol (waterfree). All steps were performed on ice. Subsequently, infiltration started at room temperature (RT) with 100% ethanol (waterfree)/epoxy resin (50:50) on a turning wheel for 30 min, followed by another incubation in fresh 100% ethanol (waterfree)/epoxy resin (50:50) for 90 min. Samples were transferred to fresh 100% epoxy resin and incubated at RT overnight on a slowly turning wheel. On the next day, the 100% epoxy resin was exchanged once, and after 6 h of incubation the DRGs were placed in flat embedding moulds and polymerized for 48 h at 70°C. From the cured resin blocks, DRGs were approached with a file for ultrathin sectioning. Ultrathin sections (70-75 nm) were cut with an UC7 ultramicrotome (Leica Microsystems, Germany) using a 35° diamond knife (Diatome AG, Switzerland), mounted on 1% formvar-coated (w/v in water-free chloroform) copper slot grids (ATHENE, 3.05 mm Ø, 1 mm x 2 mm; Plano, Germany) and counterstained with Uranylless solution (EMS, Science Services GmbH, Germany). Thereafter, sections were examined at 80 kV using a JEM1011 transmission electron microscope (JEOL GmbH, Freising, Germany) and micrographs were acquired at 6,000-x magnification with a Gatan Orius 1200A camera (GATAN GmbH, Munich, Germany, using the Digital Micrograph software package). The DRGs were cut, and images acquired, and subsequently cut again to a deeper region of the DRGs for another round of image acquisition. Grids from different DRGs were analysed blindly. The number of MVBs per condition was counted and MVBs sorted into one of three categories depending on appearance: round structures were categorized as MVBS; round structures with an extension were categorized as MVBs with tubulus; curved MVBs were categorized as horseshoe-shaped MVBs (see Fig. 1H for examples).

Western Blots: Before lysis, cultured cells were starved in non-supplemented DMEM for 20 minutes followed by a 20 minute stimulation with the factor indicated (NGF or EGF) before being lysed with “lysis buffer” containing 10 mM Tris/HCl, pH 7.5, 150 mM NaCl, 0.5 mM EDTA, and 0.5% NP-40. Protease and phosphatase inhibitors (Sigma-Aldrich, catalog #P8340) were added just prior to application. Whole brain, liver, or cultured embryonic DRGs served as control tissues. Brain and liver were dissected from adult BL6 mice, minced and lysed in lysis buffer. For degradation assays, MEFs were plated onto 6 well dishes and starved in non-supplemented DMEM for 30 minutes followed by a stimulation with either 100 ng/mL EGF or 100 ng/mL NGF for 15, 30, 60, 120, or 180 minutes. Cells were then washed with cold glucose and lysed with lysis buffer supplemented with proteinase inhibitor and phosphor-stop. Sample concentration was quantified with a BCA kit to determine protein levels. Samples were prepared for SDS-PAGE by adding 2x sample buffer, boiled for 10 min and loaded on a 10% SDS-PAGE gel for Western Blotting. Gels were transferred and developed using the antibodies listed below. Image acquisition was performed using the Odyssey CLx infrared scanner (Odyssey Imaging Systems, RRID: SCR_014579) and the software LI-COR® Image Studio™ (LI-COR, Inc.). Antibodies used for Western Blotting: Rab7a polyclonal rabbit antibody (Synaptic Systems, cat# 320 003), SNx1 monoclonal mouse Antibody (51) (Santa Cruz Biotechnology, cat# sc-136247), SNx2 monoclonal mouse Antibody (13) (Santa Cruz Biotechnology,

cat# sc-136072), SNx5 monoclonal mouse Antibody (F-11) (Santa Cruz Biotechnology, cat# sc-515215), SNx6 monoclonal mouse Antibody (D-1) (Santa Cruz Biotechnology, cat# sc-365795), Endophilin I monoclonal mouse Antibody (B-1) (Santa Cruz Biotechnology, cat# sc-374279), Endophilin II monoclonal mouse Antibody (A-11) (Santa Cruz Biotechnology, cat# sc-365704), Endophilin III monoclonal mouse Antibody (F-4) (Santa Cruz Biotechnology, cat# sc-376592), EGFR (A-10) ms mAb (Santa Cruz Biotechnology, cat# sc-373746), GFP (pabg1-10) rabbit pAb (Chromotek, cat# pabg1), RFP ms mAb (Chromotek, cat# 6G6), TrkA rabbit pAb (Millipore, cat# 06-574), GAPDH ms mAb (HyTest, cat# 5G4). Secondary antibodies were IRDye 800RD donkey anti-mouse, cat #925-32210, LI-COR Biosciences (RRID: AB_2687825) and IRDye 800RD donkey anti-rabbit, cat #925-32211, LI-COR Biosciences (RRID: AB_2651127).

Transfection with calcium phosphate (for coimmunoprecipitation). HEK293 cells were transfected using a calcium phosphate protocol. A transfection buffer (274.0 mM NaCl, 10.0 mM KCl, 1.4 mM Na₂HPO₄, 15.0 mM Glucose) was used to prepare the transfection mix (1035 μL transfection buffer, 129 μL CaCl₂, 20 μg DNA, add ddH₂O to total volume of 2070 μL). It was left to incubate at room temperature for 20 minutes, before being added to the culture dish dropwise. Cells were incubated to allow for protein expression for 24-48h at 37 °C, 5% CO₂.

Co-Immunoprecipitation. HEK293 cells were transfected with RFP or GFP-tagged DNA constructs as described above. Culture medium was aspirated and replaced with serum-free medium (incubation for 20 min at 37°C, 5% CO₂) prior to stimulation with receptor specific ligands (100 ng/ mL NGF or EGF; incubation for 20 min at 37°C, 5% CO₂). Cells were subsequently washed once with DPBS and lysed using 1 mL lysis buffer (10 mM Tris/ HCl pH 7.5, 150 mM NaCl, 0.5 mM EDTA, 0.5% Nonidet P-40). Protease inhibitors (Sigma-Aldrich, catalog #P8340) were added just before application. RFP-Trap, GFP-Trap (ChromoTek), Protein-G-coated agarose beads incubated overnight with antibodies as indicated, or control beads (coated with rabbit IgG, Sigma-Aldrich, catalog #A8914) were washed 3 times with “wash buffer” (“lysis buffer” without NP-40) and blocked with blocking buffer (1% w/v BSA in wash buffer) at 4°C for 1 h. Before use, lysate was taken and mixed with sample buffer for the input control. The leftover lysate was added to the beads for 3 h at 4°C. The beads were spun down and lysate was mixed with sample buffer as output control. The beads were washed 3 times using wash buffer and mixed with sample buffer. All samples were boiled for 10 min before being loaded on a 10% SDS-PAGE gel.

Experimental setup/statistical analysis. Statistical analysis was performed by GraphPad Prism 8.4.3 software, level of significance was set at p<0.5. For multiple-comparisons, one-way ANOVAs were performed followed by *post-hoc* Sidak's, Dunnett's or Tukey's as appropriate and indicated below.

Tubulations in DRG neurons were counted manually over the course of the time-lapse and normalized to the length of the recording. 5-8 videos were taken per condition and the experiment was repeated three times (p=0.05 df=50.77 unpaired t-test with Welsh's correction).

The colocalization of TrkA and Rab7 staining in DRG neurons was determined by FIJI-coloc 2 with Pearson's Correlation Coefficient in a region of interest defined within the soma excluding the nucleus. Statistical significance was determined by an unpaired t-test, comparing non-stimulated and NGF-stimulated condition (df=99 p=0.006), 15-20 images were taken per condition and the experiment was performed three times.

The MVBs were counted and classified as described above. The numbers were normalized to the total amount of MVBs counted. 2 stimulated and 3 non stimulated DRGs from one mouse were imaged, between 4 and 31 images were taken per DRG. No statistical analysis was performed as all DRGs were from the same animal.

The intensity of the immunostaining (in Fig. S1C,D) was measured with FIJI as mean intensity of the soma chosen as a region of interest. The intensity was normalized to the intensity of the non-stimulated condition of each experiment, 30 pictures were taken per condition per experiment and the experiment was repeated three times in total (pTrkA NF vs NGF: $df=254$; pEGFR NF vs EGF: $df=108$, $p<0.0001$).

The diameter of the Rab7-positive vacuoles was measured in the TIRF images and clustered by size. The amounts are shown as percentage of the total number of Rab7 vacuoles counted per condition.

The amount of vesicles positive for Rab7, for Rab7 and TrkA, and for Rab7 and pTrkA was counted and normalized to the average number of Rab7 vesicles. 28 pictures were taken and analysed. Statistical significance was determined by one-way ANOVA ($p<0.0001$, $DFn=2$, $DFd=70$) with post-hoc Tukey's (Rab7 vs Rab7/TrkA: $p<0.0001$, Rab7 vs Rab7/p-TrkA: $p<0.0001$, Rab7/TrkA vs Rab7/p-TrkA: $p=0.0125$).

The vacuolar structures of Rab7 positive for Transferrin or CD63 were counted and are portrayed as percentages of the total number of Rab7 vacuoles.

Receptors within large vacuolar structures were categorized as ring or vacuolar structures that were positive for the receptors. Receptors localizing to small structures were categorized as receptors localizing to small Rab7 puncta that did not show a ring/vacuolar structure. Receptors localizing to the limiting membrane of large vacuoles were categorized as receptors localizing to the outside of large vacuolar Rab7 structures. The localization of the receptors was assessed in one frame per video by counting the localization of the receptor according to the categorization in a non-stimulated condition and when stimulated with the respective ligand and normalizing it to the total number of receptor puncta per image, presented as percentage. Seven videos were imaged per condition, each experiment was repeated three times. Statistical significance was determined by unpaired t-test between each unstimulated and stimulated condition. Receptors within large Rab7 vacuoles: TrkA NF vs NGF ($df=44$, $p<0.0001$); EGFR NF vs EGF ($df=31$, $p=0.0219$). Receptors within small Rab7-WT structures: TrkA NF vs NGF ($df=44$, $p=0.0001$); EGFR NF vs EGF ($df=31$, $p=0.6830$). Receptors on limiting membrane of large Rab7-WT vacuolar structures: TrkA NF vs NGF ($df=44$, $p=0.6472$); EGFR NF vs EGF ($df=31$, $p=0.4152$).

The quantification of receptors within large Rab7-Q67L vacuolar structures was performed as for Rab7-WT as described above. Statistical significance was determined by unpaired one-way ANOVA with post-hoc Sidak's ($DFn=3$, $DFd=57$, TrkA NF vs NGF: $p=0.9921$; EGFR NF vs EGF: $p=0.9716$; TrkA NF vs EGFR NF: $p<0.0001$; TrkA NGF vs EGFR EGF: $p=0.0001$).

The diameters of the Rab7 vacuoles positive for TrkA were measured in the TIRF images and clustered by size. The amounts are shown as percentages of the total number of Rab7 vacuoles counted per condition.

Receptors within small Rab7-Q67L structures ($DFn=3$, $DFd=57$, TrkA NF vs NGF: $p=0.9986$; EGFR NF vs EGF: $p=0.9998$; TrkA NF vs EGFR NF: $p=1535$; TrkA NGF vs EGFR EGF: $p=02034$).

Receptors on limiting membrane of large Rab7-Q67L vacuolar structures (DFn=3, DFd=57, TrkA NF vs NGF: p=0.9951; EGFR NF vs EGF: p=0.8260; TrkA NF vs EGFR NF: p=0.0022; TrkA NGF vs EGFR EGF: p=0.0058)

To investigate the ability of Rab7-endosomes to tubulate we overexpressed WT GFP-Rab7, dominant negative GFP-T22N, or constitutively active GFP-Q67L together with TrkA-RFP, EGFR-RFP in MEFs and did live cell imaging in starving medium (DMEM only) or under the addition of the ligands (NGF or EGF) as indicated. Tubulation events were counted manually over the course of the time-lapse and normalized to the length of the recording for Rab7-WT and Rab7-Q67L. As Rab7-T22N appeared cytoplasmic tubulation events were counted in the TrkA-RFP channel. Seven videos per condition were imaged and analyzed in three biological repeats. Outliers were taken out by ROUT (Q=1%); Statistical significance was determined by one-way ANOVA with post-hoc Sidak's between each unstimulated and stimulated condition, as well as each receptor in its unstimulated or stimulated condition. For tubulation events of Rab7-WT (DFn=3, DFd=119, TrkA NF vs NGF p=0.0025; EGFR NF vs EGF: p>0.9999; TrkA NF vs EGFR NF: p=0.0081; TrkA NGF vs EGFR EGF: p<0.0001).

For tubulation events of Rab7-Q67L (DFn=3, DFd=65, TrkA NF vs NGF p=0.1887; EGFR NF vs EGF: p=0.9240; TrkA NF vs EGFR NF: p=0.2078; TrkA NGF vs EGFR EGF: p=0.0003).

For the degradation blots in WT-MEFs, intensities of the bands were measured from three individual experiments with technical repeats with FIJI (<https://fiji.sc/>) and normalized to GAPDH intensity and to 0min. For statistical analysis a one-way ANOVA with post-hoc Dunnett's was performed comparing each stimulated condition to 0min. For the degradation blot of TrkA (DFn=5, DFd=77, p=0.2888). For the degradation blot of EGFR (DFn=5, DFd=30, p=0.0005, 0 min vs 15 min p>0.999, 0 min vs 30 min p=0.9981, 0 min vs 60 min p=0.9805, 0 min vs 120 min p=0.0675, 0 min vs 180 min p=0.0016).

For the statistical analysis of Rab7 tubulation events in WT-MEFs in comparison to the EndophilinA triple knock out MEFs a one-way ANOVA with post-hoc Tukey's was performed. (DFn=3, DFd=140). Seven videos per condition were imaged of three experiments. Outliers were taken out by ROUT (Q=1%). (WT NF vs NGF p=0.0022; WT NF vs TKO NF p=0.0033; WT NF vs TKO NGF p=0.0256; WT NGF vs TKO NF p<0.0001; WT NGF vs TKO NGF p<0.0001; TKO NF vs TKO NGF p>0.9999).

The intensity of the pTrkA immunostaining was measured with FIJI as mean intensity of the soma chosen as a region of interest excluding the nucleus. 30 pictures were taken per condition per experiment and the experiment was repeated three times in total using the same microscopy settings For statistical analysis a one-way ANOVA was performed with post-hoc Sidak's, outliers were taken out by ROUT (Q=1%). (DFn=3, DFd=188, p<0.0001, WT NF vs WT NGF p=0.0498, TKO NF vs TKO NGF p=0.9769, WT NF vs TKO NF p<0.0001, WT NGF vs TKO NGF p<0.0001).

Intensities of the bands of the TKO-degradation blots were measured from three individual experiments with technical repeats with FIJI (<https://fiji.sc/>) and normalized to GAPDH intensity and to 0min. For statistical analysis, a one-way ANOVA with post-hoc Dunnett's was performed comparing each stimulated condition to 0min. For the degradation blot of TrkA (DFn=5, DFd=24, p=0.0143, 0 min vs 15 min p=0.9997, 0 min vs 30 min p=0.9773, 0 min vs 60 min p=0.8090, 0 min vs 120 min p=0.0492, 0 min vs 180 min p=0.0191). For the degradation blot of EGFR (DFn=5,

DFd=12, $p < 0.0001$, 0 min vs 15 min $p = 0.9910$, 0 min vs 30 min $p = 0.9828$, 0 min vs 60 min $p = 0.0005$, 0 min vs 120 min $p = 0.0010$, 0 min vs 180 min $p = 0.0001$).

The colocalization of WASH1 and Rab7 in DRG neurons was determined by FIJI-coloc 2 with Pearson's Correlation Coefficient in a region of interest defined within the soma excluding the nucleus. Statistical significance was determined by an unpaired t-test, comparing non-stimulated and NGF-stimulated condition ($df = 74$, $p = 0.0046$), 10-15 images were taken per condition and the experiment was performed three times.

For the statistical analysis of tubulation events in Rab7-WT in comparison to the CMT2B mutants a one-way ANOVA with post-hoc Sidak's was performed, testing each NF to NGF condition as well as each CMT2B condition to its respective WT control ($DFn = 9$, $DFd = 506$). Seven videos per condition were imaged and analysed in six biological repeats. Outliers were taken out by ROUT ($Q = 1\%$). (Rab7-WT NF vs NGF $p = 0.0003$; L129F NF vs NGF $p = 0.9998$; K157N NF vs NGF $p > 0.9999$; N161T NF vs NGF $p = 0.0508$; V162M NF vs NGF $p = 0.9997$; Rab7 WT NF vs L129F NF $p = 0.3115$; Rab7 WT NF vs K157N NF $p = 0.9615$; Rab7 WT NF vs N161T NF $p = 0.037$; Rab7 WT NF vs V162M NF $p = 0.999$; Rab7 WT NGF vs L129F NGF $p = 0.2812$; Rab7 WT NGF vs K157N NGF $p < 0.0001$; Rab7 WT NGF vs N161T NGF $p = 0.0002$; Rab7 WT NGF vs V162M NGF $p < 0.0001$)

Western Blots were analyzed from four individual experiments, with technical repeats. Band intensity was measured with EvolutionCapt and normalized to the band intensity of the overexpressed Rab7 protein and to the WT NF condition. Significance was determined with unpaired t-tests between each unstimulated and stimulated condition. (Rab7-WT NF vs NGF: $df = 5$, $p = 0.0169$; Rab7-L129F NF vs NGF: $df = 6$, $p = 0.8966$; Rab7-K157N NF vs NGF: $df = 6$, $p = 0.2464$; Rab7-N161T NF vs NGF: $df = 6$, $p = 0.3189$; Rab7-V162M NF vs NGF: $df = 6$, $p = 0.0494$).

Co-Immunoprecipitation was quantified from six individual experiments by measuring the band intensity of EndophilinA2 and normalizing it to the band intensity of each Rab7 band in the IP. Significance was determined by one-way ANOVA with post-hoc Dunnett's comparing each condition to Rab7-WT ($DFn = 4$, $DFd = 24$) Rab7-WT vs L129F $p = 0.0164$; Rab7-WT vs K157N $p = 0.0130$; Rab7-WT vs N161T $p = 0.3028$; Rab7-WT vs V162M $p = 0.0105$)

The *in vitro* effect of the CMT2B mutants in mouse DRG neurons was determined by measuring the longest neurite of a transfected neuron using the Fiji PlugIn Simple Neurite Tracer in three independent experiments. Outliers were removed by ROUT ($Q = 0.1\%$) and statistical significance was determined by one-way ANOVA with post-hoc Dunnett's ($DFn = 7$, $DFd = 124$) compared with Rab7-WT (Rab7-WT vs GFP: $p = 0.9949$; Rab7-WT vs T22N: $p = 0.1856$; Rab7-WT vs Q67L: $p = 0.9947$; Rab7-WT vs L129F: $p = 0.0642$; Rab7-WT vs K157N: $p = 0.0002$; Rab7-WT vs N161T: $p = 0.9974$; Rab7-WT vs V162M $p = 0.0034$).

ACKNOWLEDGEMENTS

We thank Prof. Mathias Bähr for support and hosting of our lab and Dr. Camin Dean for providing us with the live-imaging set-up. We thank Anna J. Goldak und Sina Langer for excellent technical support for EM experiments. We thank Prof. Silvio Rizzoli for providing us with the STED microscope and for critically reading the manuscript. We thank Prof. Peter Schu, and Prof. Jeroen Pasterkamp for critically reading this manuscript.

FUNDING

This work was funded by the Deutsche Forschungsgemeinschaft (DFG) Grant No. 427899738, the Forschungsförderung of the University Medical Center Göttingen to KB and the Center for Nanoscale Microscopy and Molecular Physiology of the Brain (CNMPB) to KB and RM. RM received a stipend from the International Max Planck Research School (IMPRS) Neuroscience. TMD received funding from the DFG, RI 1967/11-1. CW received funding from the Collaborative Research Center 889 (A07 to CW) and the Collaborative Research Center 1286 (A04 to CW).

AUTHOR CONTRIBUTIONS

RM: Software, validation, formal analysis, investigation, writing-review and editing, visualization. VD: Validation, formal analysis, investigation, writing-review and editing LMS: Software, validation, formal analysis, investigation, AK: Validation, formal analysis, investigation, BB: Software, validation, formal analysis, investigation, TMD: STED microscopy, CW: EM microscopy, KB: Conceptualization, methodology, formal analysis, investigation, writing original draft, writing-review and editing, supervision, project administration and funding acquisition.

CONFLICT OF INTEREST

The authors declare no conflict of interest

3.6 REFERENCES

- Auer-Grumbach, M., De Jonghe, P., Wagner, K., Verhoeven, K., Hartung, H.-P. and Timmerman, V. (2000). Phenotype-genotype correlations in a CMT2B family with refined 3q13-q22 locus. *Neurology* **55**, 1552–1557.
- Bai, J., Hu, Z., Dittman, J. S., Pym, E. C. G. and Kaplan, J. M. (2010). Endophilin functions as a membrane-bending molecule and is delivered to endocytic zones by exocytosis. *Cell* **143**, 430–441.
- Bakker, J., Spits, M., Neefjes, J. and Berlin, I. (2017). The EGFR odyssey - from activation to destruction in space and time. *J. Cell Sci.*
- Basuray, S., Mukherjee, S., Romero, E., Wilson, M. C. and Wandinger-Ness, A. (2010). Rab7 mutants associated with charcot-Marie-tooth disease exhibit enhanced NGF-stimulated signaling. *PLoS One* **5**.
- BasuRay, S., Mukherjee, S., Romero, E. G., Seaman, M. N. J. and Wandinger-Ness, A. (2013). Rab7 mutants associated with Charcot-Marie-Tooth disease cause delayed growth factor receptor transport and altered endosomal and nuclear signaling. *J. Biol. Chem.* **288**, 1135–1149.
- Bebelman, M. P., Bun, P., Huveneers, S., van Niel, G., Pegtel, D. M. and Verweij, F. J. (2020). Real-time imaging of multivesicular body–plasma membrane fusion to quantify exosome release from single cells. *Nat. Protoc.*
- Bhattacharyya, A., Watson, F. L., Pomeroy, S. L., Zhang, Y. Z., Stiles, C. D. and Segal, R. A. (2002). High-resolution imaging demonstrates dynein-based vesicular transport of activated Trk receptors. *J. Neurobiol.* **51**, 302–312.
- Bissig, C. and Gruenberg, J. (2014). ALIX and the multivesicular endosome: ALIX in Wonderland. *Trends Cell Biol.*
- Braulke, T. and Bonifacio, J. S. (2009). Sorting of lysosomal proteins. *Biochim. Biophys. Acta - Mol. Cell Res.* **1793**, 605–614.
- Bucci, C., Thomsen, P., Nicoziani, P., McCarthy, J. and Van Deurs, B. (2000). Rab7: A key to lysosome biogenesis. *Mol. Biol. Cell.*
- Burk, K., Murdoch, J. D., Freytag, S., Koenig, M., Bharat, V., Markworth, R., Burkhardt, S., Fischer, A. and Dean, C. (2017a). EndophilinAs regulate endosomal sorting of BDNF-TrkB to mediate survival signaling in hippocampal neurons. *Sci. Rep.* **7**, 2149.
- Burk, K., Mire, E., Bellon, A., Hocine, M., Guillot, J., Moraes, F., Yoshida, Y., Simons, M., Chauvet, S. and Mann, F. (2017b). Post-endocytic sorting of Plexin-D1 controls signal transduction and development of axonal and vascular circuits. *Nat. Commun.* **8**, 14508.

- Campenot, R. B.** (1977). Local control of neurite development by nerve growth factor. *Proc. Natl. Acad. Sci.* **74**, 4516–4519.
- Carlton, J., Bujny, M., Peter, B. J., Oorschot, V. M. J., Rutherford, A., Mellor, H., Klumperman, J., McMahon, H. T. and Cullen, P. J.** (2004). Sorting nexin-1 mediates tubular endosome-to-TGN transport through coincidence sensing of high-curvature membranes and 3-phosphoinositides. *Curr. Biol.*
- Ceresa, B. P. and Bahr, S. J.** (2006). rab7 activity affects epidermal growth factor: Epidermal growth factor receptor degradation by regulating endocytic trafficking from the late endosome. *J. Biol. Chem.* **281**, 1099–1106.
- Claude, P., Hawrot, E., Dunis, D. A. and Campenot, R. B.** (1982). Binding, internalization, and retrograde transport of 125I-nerve growth factor in cultured rat sympathetic neurons. *J. Neurosci.*
- Cogli, L., Progida, C., Lecci, R., Bramato, R., Krüttgen, A. and Bucci, C.** (2010). CMT2B-associated Rab7 mutants inhibit neurite outgrowth. *Acta Neuropathol.* **120**, 491–501.
- Cooney, J. R., Hurlburt, J. L., Selig, D. K., Harris, K. M. and Fiala, J. C.** (2002). Endosomal compartments serve multiple hippocampal dendritic spines from a widespread rather than a local store of recycling membrane. *J. Neurosci.*
- Cosker, K. E. and Segal, R. A.** (2014). Neuronal signaling through endocytosis. *Cold Spring Harb. Perspect. Biol.* **6**.
- Cosker, K. E., Courchesne, S. L. and Segal, R. A.** (2008). Action in the axon: generation and transport of signaling endosomes. *Curr. Opin. Neurobiol.*
- Cullen, P. J. and Steinberg, F.** (2018). To degrade or not to degrade: mechanisms and significance of endocytic recycling. *Nat. Rev. Mol. Cell Biol.*
- De Jonghe, P., Timmerman, V., FitzPatrick, D., Spoelers, P., Martin, J. J. and Van Broeckhoven, C.** (1997). Mutilating neuropathic ulcerations in a chromosome 3q13-q22 linked Charcot-Marie-Tooth disease type 2B family. *J. Neurol. Neurosurg. Psychiatry* **62**, 570–3.
- De Luca, A., Progida, C., Spinosa, M. R., Alifano, P. and Bucci, C.** (2008). Characterization of the Rab7K157N mutant protein associated with Charcot-Marie-Tooth type 2B. *Biochem. Biophys. Res. Commun.* **372**, 283–287.
- Deinhardt, K., Salinas, S., Verastegui, C., Watson, R., Worth, D., Hanrahan, S., Bucci, C. and Schiavo, G.** (2006). Rab5 and Rab7 Control Endocytic Sorting along the Axonal Retrograde Transport Pathway. *Neuron* **52**, 293–305.
- Deininger, K., Eder, M., Kramer, E. R., Zieglgänsberger, W., Dodt, H. U., Dornmair, K., Colicelli, J. and Klein, R.** (2008). The Rab5 guanylate exchange factor Rin1 regulates endocytosis of the EphA4 receptor in mature excitatory neurons. *Proc. Natl. Acad. Sci. U. S. A.*
- Derivery, E., Sousa, C., Gautier, J.J., Lombard, B., Loew, D., Gautreau, A.** (2009). The Arp2/3 activator WASH controls the fission of endosomes through a large multiprotein complex. *Dev Cell* **17**, 712–723.
- Duleh, S.N., Welch, M. D.** (2010). WASH and the Arp2/3 complex regulate endosome shape and trafficking. *Cytoskeleton*. **67**, 193–206.
- Ellson, C. D., Andrews, S., Stephens, L. R. and Hawkins, P. T.** (2002). The PX domain: A new phosphoinositide-binding module. *J. Cell Sci.*
- Escudero, C. A., Lazo, O. M., Galleguillos, C., Parraguez, J. I., Lopez-Verrilli, M. A., Cabeza, C., Leon, L., Saeed, U., Retamal, C., Gonzalez, A., et al.** (2014). The p75 neurotrophin receptor evades the endolysosomal route in neuronal cells, favouring multivesicular bodies specialised for exosomal release. *J. Cell Sci.*
- Fernandez-Borja, M., Wubbolts, R., Calafat, J., Janssen, H., Divecha, N., Dusseljee, S. and Neefjes, J.** (1999). Multivesicular body morphogenesis requires phosphatidylinositol 3-kinase activity. *Curr. Biol.*
- Fjorback, A. W., Seaman, M., Gustafsen, C., Mehmedbasic, A., Gokool, S., Wu, C., Militz, D., Schmidt, V., Madsen, P., Nyengaard, J. R., et al.** (2012). Retromer binds the FANSHY sorting motif in sorLA to regulate amyloid precursor protein sorting and processing. *J. Neurosci.*
- Frost, A., Unger, V. M. and De Camilli, P.** (2009). The BAR Domain Superfamily: Membrane-Molding Macromolecules. *Cell.*
- Gallop, J. L., Jao, C. C., Kent, H. M., Butler, P. J. G., Evans, P. R., Langen, R. and McMahon, H. T.** (2006). Mechanism of endophilin N-BAR domain-mediated membrane curvature. *EMBO J.* **25**, 2898–2910.
- Giachino, C., Lantelme, E., Lanzetti, L., Saccone, S., Bella Valle, G. and Migone, N.** (1997). A novel SH3-containing human gene family preferentially expressed in the central nervous system. *Genomics* **41**, 427–434.
- Ginty, D. D. and Segal, R. A.** (2002). Retrograde neurotrophin signaling: Trk-ing along the axon. *Curr. Opin. Neurobiol.* **12**, 268–274.
- Gong, J., Körner, R., Gaitanos, L. and Klein, R.** (2016). Exosomes mediate cell contact-independent ephrin-Eph signaling during axon guidance. *J. Cell Biol.*

- Gruenberg, J.** (2020). Life in the lumen: The multivesicular endosome. *Traffic*.
- Guerra, F. and Bucci, C.** (2016). Multiple Roles of the Small GTPase Rab7. *Cells*.
- Harrington, A. W. and Ginty, D. D.** (2013). Long-distance retrograde neurotrophic factor signalling in neurons. *Nat Rev Neurosci* **14**, 177–187.
- Houlden, H., King, R. H. M., Muddle, J. R., Warner, T. T., Reilly, M. M., Orrell, R. W. and Ginsberg, L.** (2004). A novel RAB7 mutation associated with ulcero-mutilating neuropathy. *Ann. Neurol.* **56**, 586–590.
- Howe, C. L. and Mobley, W. C.** (2005). Long-distance retrograde neurotrophic signaling. *Curr. Opin. Neurobiol.*
- Humphries, W. H., Szymanski, C. J. and Payne, C. K.** (2011). Endo-lysosomal vesicles positive for rab7 and lamp1 are terminal vesicles for the transport of dextran. *PLoS One* **6**,.
- Inoue, J., Krueger, E. W., Chen, J., Cao, H., Ninomiya, M. and McNiven, M. A.** (2015). HBV secretion is regulated through the activation of endocytic and autophagic compartments mediated by Rab7 stimulation. *J. Cell Sci.*
- Ito, K. and Enomoto, H.** (2016). Retrograde transport of neurotrophic factor signaling: implications in neuronal development and pathogenesis. *J. Biochem.*
- Jovic, M., Sharma, M., Rahajeng, J. and Caplan, S.** (2010). The early endosome: A busy sorting station for proteins at the crossroads. *Histol. Histopathol.* **25**, 99–112.
- Kalluri, R. and LeBleu, V. S.** (2020). The biology, function, and biomedical applications of exosomes. *Science* (80-).
- Klumperman, J. and Raposo, G.** (2014). The complex ultrastructure of the endolysosomal system. *Cold Spring Harb. Perspect. Biol.*
- Marat, A. L. and Haucke, V.** (2016). Phosphatidylinositol 3-phosphates—at the interface between cell signalling and membrane traffic. *EMBO J.* **35**, 561–579.
- Matthew N. J. Seaman, Michael E. Harbour, Daniel Tattersall, Eliot Read, N. B., Seaman, M. N. J., Harbour, M. E., Tattersall, D., Read, E., Bright, N. and Matthew N. J. Seaman, Michael E. Harbour, Daniel Tattersall, Eliot Read, and N. B.** (2009). Membrane recruitment of the cargo-selective retromer subcomplex is catalysed by the small GTPase Rab7 and inhibited by the Rab-GAP TBC1D5. *J. Cell Sci* **122**, 2371–2382.
- Maxfield, F. R. and Yamashiro, D. J.** (1987). Endosome acidification and the pathways of receptor-mediated endocytosis. *Adv. Exp. Med. Biol.*
- Mayle, KM; Le AM, and Kamei, D.** (2013). The Intracellular Trafficking Pathway of Transferrin. *Biochim Biophys Acta.* **1820**, 264–281.
- Meggouh, F., Bienfait, H. M. E., Weterman, M. A. J., De Visser, M. and Baas, F.** (2006). Charcot-Marie-tooth disease due to a de novo mutation of the RAB7 gene. *Neurology* **67**, 1476–1478.
- Meinecke, M., Boucrot, E., Camdere, G., Hon, W. C., Mittal, R. and McMahon, H. T.** (2013). Cooperative recruitment of dynamin and BIN/Amphiphysin/Rvs (BAR) domain-containing proteins leads to GTP-dependent membrane scission. *J. Biol. Chem.*
- Milosevic, I., Giovedi, S., Lou, X., Raimondi, A., Collesi, C., Shen, H., Paradise, S., O’Toole, E., Ferguson, S., Cremona, O., et al.** (2011). Recruitment of endophilin to clathrin-coated pit necks is required for efficient vesicle uncoating after fission. *Neuron* **72**, 587–601.
- Murdoch, J. D., Rostosky, C. M., Gowrisankaran, S., Arora, A. S., Soukup, S. F., Vidal, R., Capece, V., Freytag, S., Fischer, A., Verstreken, P., et al.** (2016). Endophilin-A Deficiency Induces the Foxo3a-Fbxo32 Network in the Brain and Causes Dysregulation of Autophagy and the Ubiquitin-Proteasome System. *Cell Rep.* **17**, 1071–1086.
- Naslavsky, N. and Caplan, S.** (2018). The enigmatic endosome - Sorting the ins and outs of endocytic trafficking. *J. Cell Sci.*
- Nicoziani, P., Vilhardt, F., Llorente, A., Hilout, L., Courtoy, P. J., Sandvig, K. and van Deurs, B.** (2000). Role for dynamin in late endosome dynamics and trafficking of the cation-independent mannose 6-phosphate receptor. *Mol. Biol. Cell* **11**, 481–495.
- Nonis, D., Schmidt, M. H. H. H., van de Loo, S., Eich, F., Dikic, I., Nowock, J. and Auburger, G.** (2008). Ataxin-2 associates with the endocytosis complex and affects EGF receptor trafficking. *Cell. Signal.* **20**, 1725–1739.
- Norwood, S. J., Shaw, D. J., Cowieson, N. P., Owen, D. J., Teasdale, R. D. and Collins, B. M.** (2011). Assembly and solution structure of the core retromer protein complex. *Traffic*.
- Nothwehr, S. F., Ha, S. A. and Bruinsma, P.** (2000). Sorting of yeast membrane proteins into an endosome-to-Golgi pathway involves direct interaction of their cytosolic domains with Vps35p. *J. Cell Biol.*
- Peter, B. J., Kent, H. M., Mills, I. G., Vallis, Y., Butler, P. J. G., Evans, P. R. and McMahon, H. T.** (2004). BAR Domains as Sensors of Membrane Curvature: The Amphiphysin BAR Structure. *Science* (80-).

- Rink, J., Ghigo, E., Kalaidzidis, Y. and Zerial, M. (2005). Rab conversion as a mechanism of progression from early to late endosomes. *Cell*.
- Robinson, M. (1996). Timing and regulation of trkB and BDNF mRNA expression in placode-derived sensory neurons and their targets. *Eur. J. Neurosci.* **8**, 2399–2406.
- Ross, J. A., Chen, Y., Müller, J., Barylko, B., Wang, L., Banks, H. B., Albanesi, J. P. and Jameson, D. M. (2011). Dimeric endophilin A2 stimulates assembly and GTPase activity of dynamin 2. *Biophys. J.* **100**, 729–737.
- Rowland, A. A., Chitwood, P. J., Phillips, M. J. and Voeltz, G. K. (2014). ER contact sites define the position and timing of endosome fission. *Cell*.
- Sandow, S. L., Heydon, K., Weible, M. W., Reynolds, A. J., Bartlett, S. E. and Hendry, I. A. (2000). Signalling organelle for retrograde axonal transport of internalized neurotrophins from the nerve terminal. In *Immunology and Cell Biology*, .
- Saveri, P., De Luca, M., Nisi, V., Pisciotto, C., Romano, R., Piscoquito, G., Reilly, M. M., Polke, J. M., Cavallaro, T., Fabrizi, G. M., et al. (2020). Charcot-Marie-Tooth Type 2B: A New Phenotype Associated with a Novel RAB7A Mutation and Inhibited EGFR Degradation. *Cells*.
- Saxena, S., Bucci, C., Weis, J. and Kruttgen, A. (2005). The small GTPase Rab7 controls the endosomal trafficking and neuritogenic signaling of the nerve growth factor receptor TrkA. *J. Neurosci.* **25**, 10930–10940.
- Schmidt, M. H. H., Furnari, F. B., Cavenee, W. K. and Bogler, O. (2003). Epidermal growth factor receptor signaling intensity determines intracellular protein interactions, ubiquitination, and internalization. *Proc. Natl. Acad. Sci.*
- Schmieg, N., Menendez, G., Schiavo, G. and Terenzio, M. (2014). Signalling endosomes in axonal transport: Travel updates on the molecular highway. *Semin. Cell Dev. Biol.*
- Seaman, M. N. J. (2012a). The retromer complex - endosomal protein recycling and beyond. *J. Cell Sci.* **125**, 4693–702.
- Seaman, M. N. J. (2012b). The retromer complex-endosomal protein recycling and beyond. *J. Cell Sci.*
- Seaman, M. N. J., Gautreau, A. and Billadeau, D. D. (2013). Retromer-mediated endosomal protein sorting: All WASHed up! *Trends Cell Biol.* **23**, 522–528.
- Sharma, N., Deppmann, C. D., Harrington, A. W., St. Hillaire, C., Chen, Z. Y., Lee, F. S. and Ginty, D. D. (2010). Long-Distance Control of Synapse Assembly by Target-Derived NGF. *Neuron* **67**, 422–434.
- Singh, K. K., Park, K. J., Hong, E. J., Kramer, B. M., Greenberg, M. E., Kaplan, D. R. and Miller, F. D. (2008). Developmental axon pruning mediated by BDNF-p75NTR-dependent axon degeneration. *Nat. Neurosci.* **11**, 649–658.
- Soukup, S. F., Kuenen, S., Vanhauwaert, R., Manetsberger, J., Hernández-Díaz, S., Swerts, J., Schoovaerts, N., Vilain, S., Gounko, N. V., Vints, K., et al. (2016). A LRRK2-Dependent EndophilinA Phosphoswitch Is Critical for Macroautophagy at Presynaptic Terminals. *Neuron* **92**, 829–844.
- Suo, D., Park, J., Harrington, A. W., Zweifel, L. S., Mihalas, S. and Deppmann, C. D. (2014). Coronin-1 is a neurotrophin endosomal effector that is required for developmental competition for survival. *Nat. Neurosci.*
- Taub, N., Teis, D., Ebner, H. L., Hess, M. W., Huber, L. A. and N. Taub, D. Teis, H. L. Ebner, M. W. Hess, and L. A. H. (2007). Late endosomal traffic of the epidermal growth factor receptor ensures spatial and temporal fidelity of mitogen-activated protein kinase signaling. *Mol. Biol. Cell* **18**, 4698–4710.
- Tomas, A., Vaughan, S. O., Burgoyne, T., Sorkin, A., Hartley, J. A., Hochhauser, D. and Futter, C. E. (2015). WASH and Tsg101/ALIX-dependent diversion of stress-internalized EGFR from the canonical endocytic pathway. *Nat. Commun.*
- Van Weering, J. R. T., Sessions, R. B., Traer, C. J., Kloer, D. P., Bhatia, V. K., Stamou, D., Carlsson, S. R., Hurley, J. H. and Cullen, P. J. (2012). Molecular basis for SNX-BAR-mediated assembly of distinct endosomal sorting tubules. *EMBO J.*
- Verhoeven, K., De Jonghe, P., Coen, K., Verpoorten, N., Auer-Grumbach, M., Kwon, J. M., FitzPatrick, D., Schmedding, E., De Vriendt, E., Jacobs, A., et al. (2003). Mutations in the small GTP-ase late endosomal protein RAB7 cause Charcot-Marie-Tooth type 2B neuropathy. *Am J Hum Genet* **72**, 722–727.
- Wang, X., Han, C., Liu, W., Wang, P. and Zhang, X. (2014). A novel RAB7 mutation in a Chinese family with Charcot-Marie-Tooth type 2B disease. *Gene* **534**, 431–434.
- Weible, M. W. and Hendry, I. A. (2004). What is the Importance of Multivesicular Bodies in Retrograde Axonal Transport In Vivo? *J. Neurobiol.*
- Woodman, P. G. and Futter, C. E. (2008). Multivesicular bodies: co-ordinated progression to maturity. *Curr. Opin. Cell Biol.*
- Wu, C., Ramirez, A., Cui, B., Ding, J., Delcroix, J. D. M., Valletta, J. S., Liu, J. J., Yang, Y., Chu, S. and Mobley, W. C. (2007). A functional dynein-microtubule network is required for NGF signaling through the

Rap1/MAPK pathway. *Traffic*.

Wu, K. Y., He, M., Hou, Q. Q., Sheng, A. L., Yuan, L., Liu, F., Liu, W. W., Li, G., Jiang, X. Y. and Luo, Z. G. (2014). Semaphorin 3A activates the guanosine triphosphatase Rab5 to promote growth cone collapse and organize callosal axon projections. *Sci. Signal*.

Wu, H., Carvalho, P. and Voeltz, G. K. (2018). Here, there, and everywhere: The importance of ER membrane contact sites. *Science* (80-).

Ye, M., Lehigh, K. M. and Ginty, D. D. (2018). Multivesicular bodies mediate long-range retrograde NGF-TrkA signaling. *Elife* 7,.

Zhang, K., Fishel Ben Kenan, R., Osakada, Y., Xu, W., Sinit, R. S., Chen, L., Zhao, X., Chen, J.-Y., Cui, B. and Wu, C. (2013). Defective Axonal Transport of Rab7 GTPase Results in Dysregulated Trophic Signaling. *J. Neurosci.* 33, 7451–7462.

3.7 SUPPLEMENTARY DATA

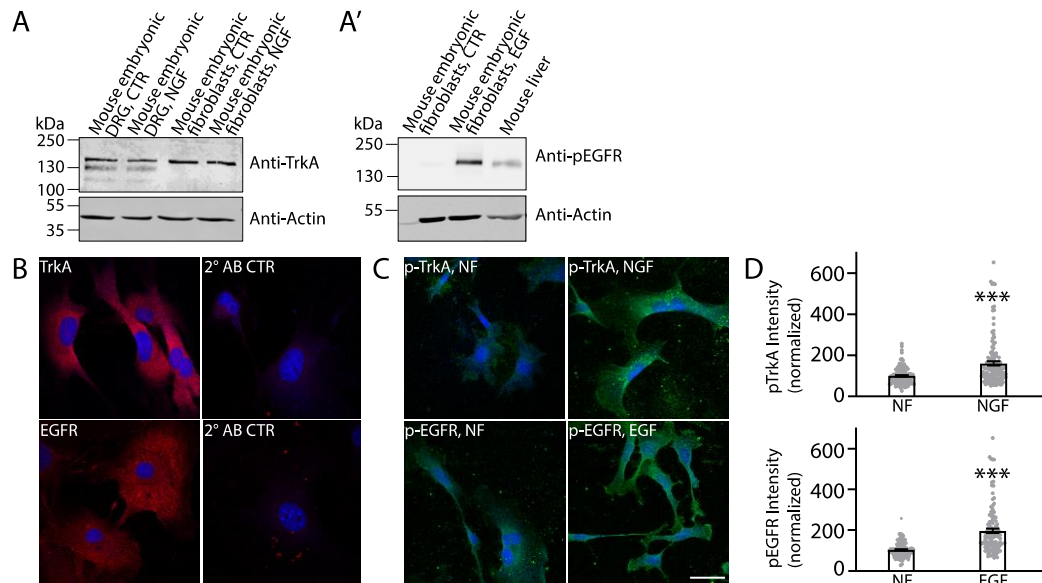


Fig. S1. Trk and EGFR expression and functionality in MEFs. (A, A') Expression of TrkA and EGFR in MEFs using Western Blot. (B) Expression of TrkA and EGFR in MEFs using immunocytochemistry. (C) Images of pTrkA, and pEGFR immunostaining in cultured MEFs in “no factor” (NF) untreated conditions and following treatment with respective ligand (100ng/ml NGF or EGF) for 20 minutes; scale bar=40 μm. (D) Quantification of pTrkA and pEGFR signal in MEFs in NF and ligand stimulated conditions, normalized to NF. pTrkA NF vs NGF: df=254, p<0.0001; pEGFR NF vs EGF: df=108, p<0.0001. Significance was determined by Student’s t-test, n=30 images per condition in three independent experiments; error=SEM, ***p<0.001.

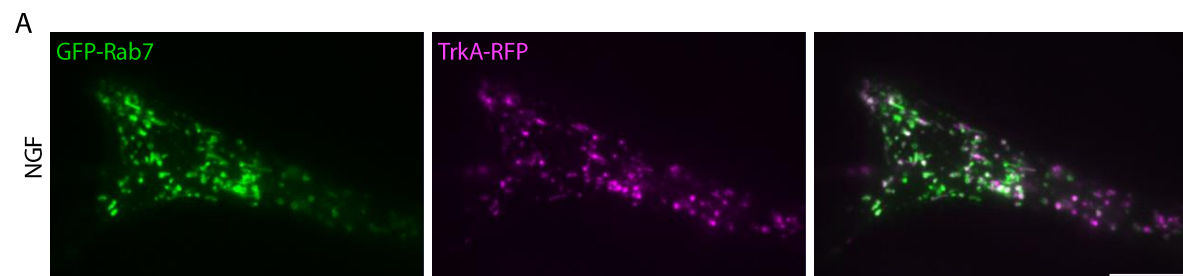


Fig. S2. TrkA-RFP expression in MEFs in live-TIRF. (A,) Representative TIRF microscopy images of MEFs co-transfected with GFP-tagged Rab7 and RFP-tagged TrkA in the presence of NGF from the same culture as images in Figure 2G; scale bar=10μm.

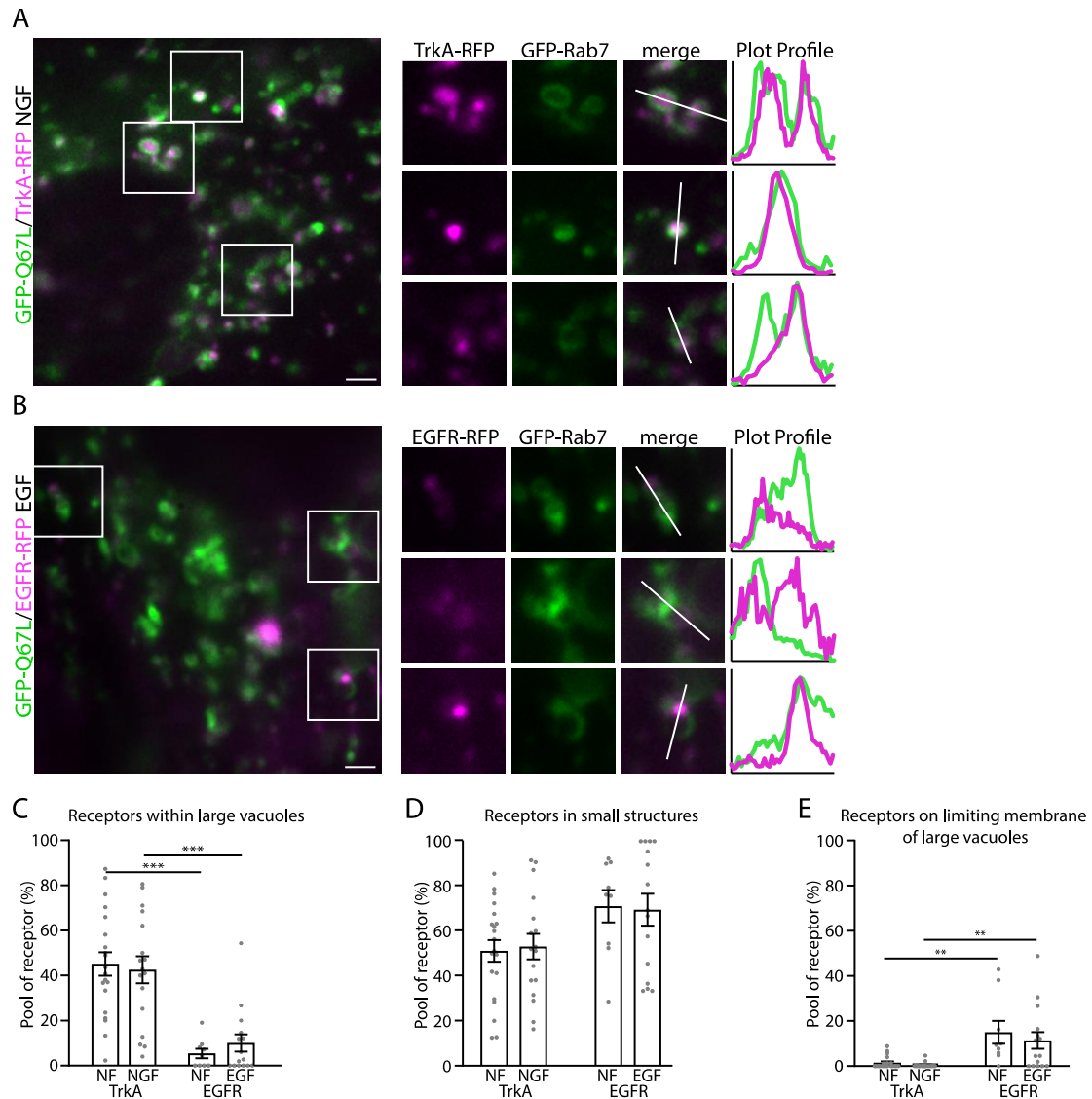


Fig. S3. Q67L induces TrkA localization within large vacuolar structures. (A, B) Representative TIRF microscopy images of MEFs co-transfected with GFP-tagged Rab7 Q67L and RFP-tagged receptor (TrkA or EGFR), in the presence or absence of its respective ligand (100ng/ml NGF, EGF). Line histograms show receptors being localized within Rab7 vacuoles, on the rim of Rab7 vacuoles and on small Rab7 structures; scale bar=2 μ m. (C) Quantification of proportion of receptors (TrkA, EGFR) localized within large vacuolar Rab7-Q67L structures. TrkA NF vs EGFR NF: $p < 0.0001$; TrkA NGF vs EGFR EGF: $p = 0.0001$. (D) Quantification of proportion of receptors (TrkA, EGFR) localized to small structures. (E) Quantification of proportion of receptors localized on the limiting membrane of large vacuolar Rab7 structures. TrkA NF vs EGFR NF: $p = 0.0022$; TrkA NGF vs EGFR EGF: $p = 0.0058$. Significance was determined by one-way ANOVA with post hoc Sidak's; $n = 7$ videos per condition in three independent experiments; error= SEM, ** $p < 0.01$, *** $p < 0.001$.

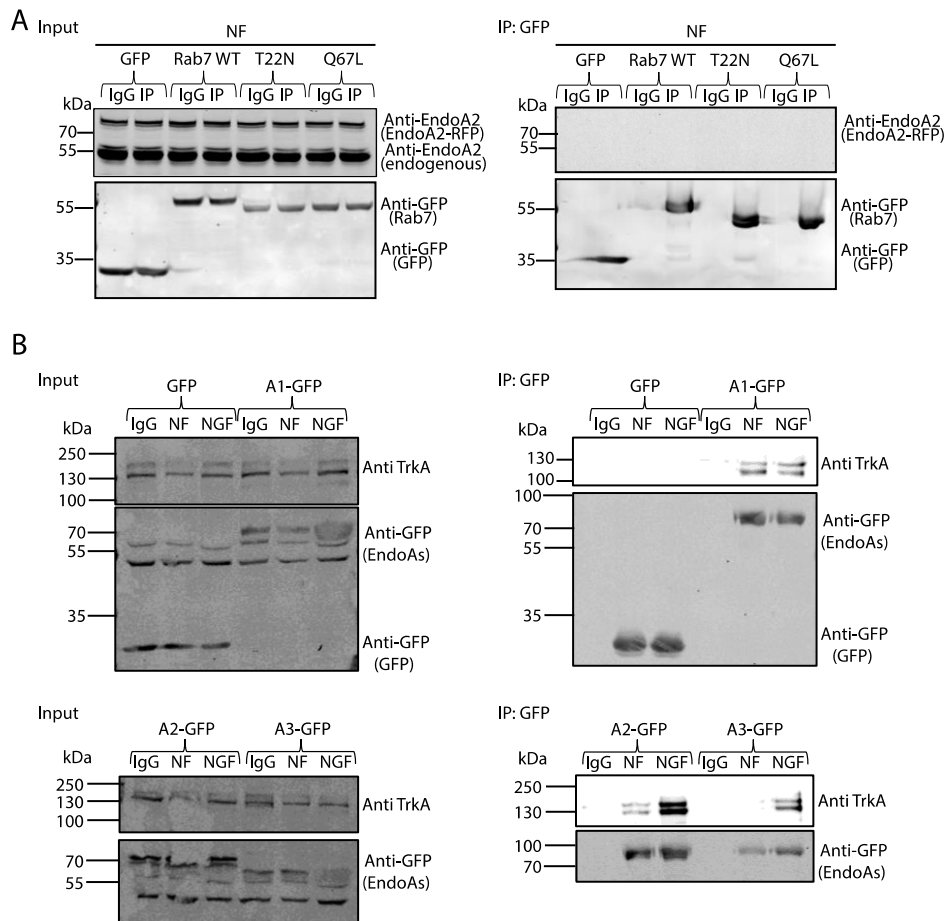


Fig. S4. EndophilinA2 does not associate with late Rab7 in non-stimulated conditions. (A) Input is shown on the left, IP on the right. GFP-conjugated beads (or IgG control beads) were used to pull down GFP-Rab7 (WT, T22N, Q67L) showing no interaction with EndophilinA2-RFP in non-stimulated Hek293 cells. (B) GFP-conjugated beads (or IgG control beads) were used to pull down GFP, EndophilinA1, A2, or A3-GFP in with TrkA-RFP co-transfected Hek293 cells (Input is shown on the left, IP on the right) in the presence or absence 100 ng/ml NGF.

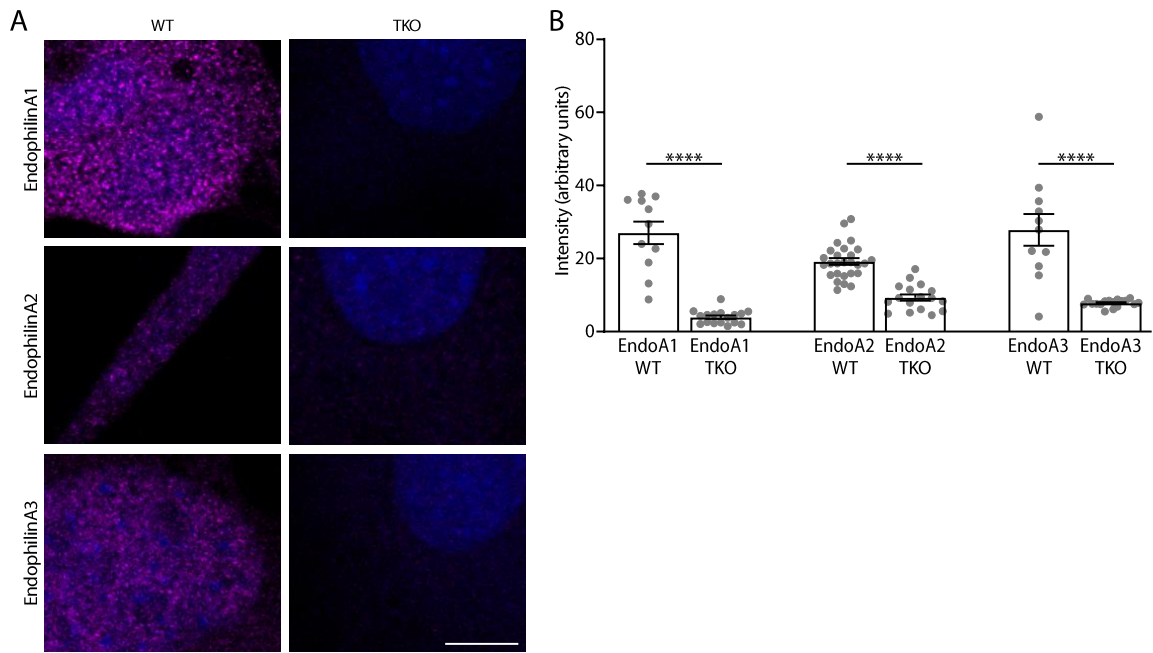


Fig. S5. EndophilinA TKO MEFs do not stain for EndophilinAs. (A) WT and EndophilinA TKO MEFs stained against EndophilinA1,2, and 3, scale bar= 10 μ m. (B) Quantification of staining intensity in WT and TKO MEFs. Significance was determined by student's t-test, **** p <0.0001.

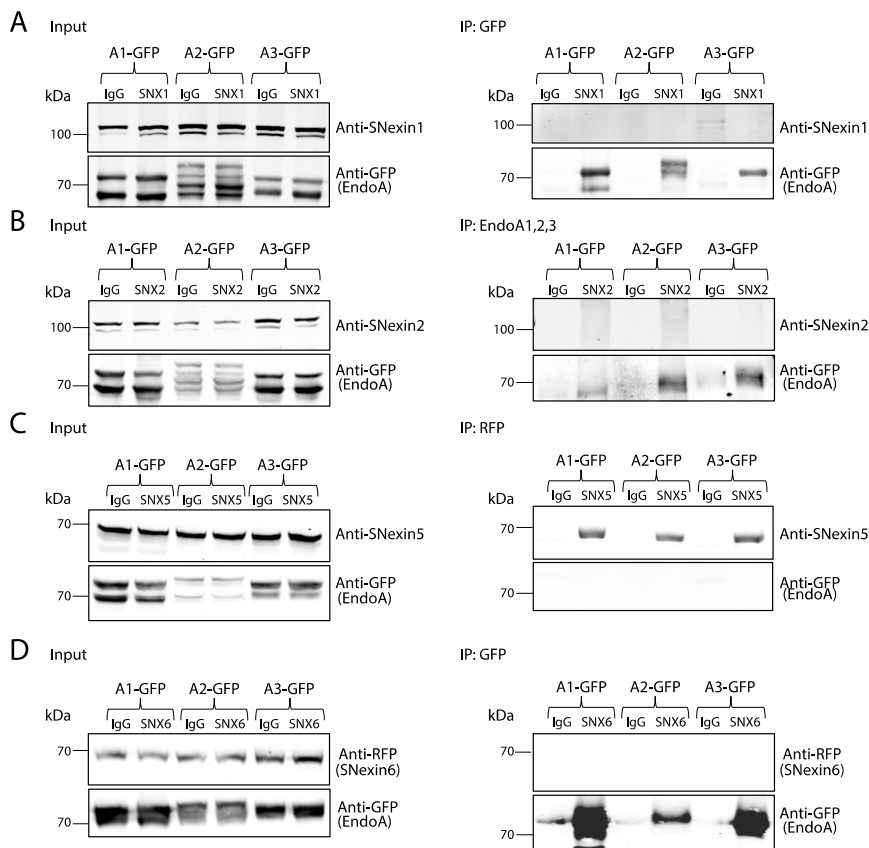


Fig. S6. EndophilinAs do not bind Snxs of retromer complex co-transfected in HEK293 cells. (A) EndophilinAs do not co-immunoprecipitate with Snx1. (B) EndophilinAs do not co-immunoprecipitate with Snx2. (C) EndophilinAs do not co-immunoprecipitate with Snx5. (D) EndophilinAs do not co-immunoprecipitate with Snx6.

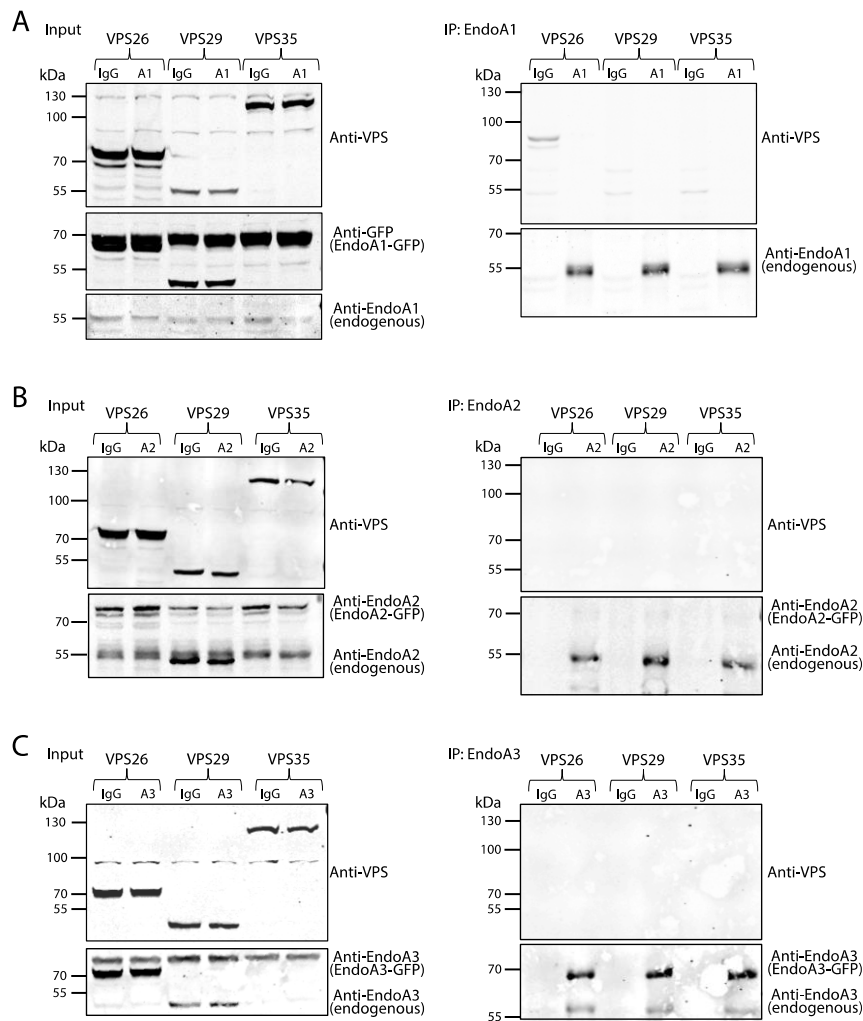


Fig. S7. EndophilinAs do not bind the cargo recognition unit of retromer complex co-transfected in HEK293 cells. (A) EndophilinAs do not co-immunoprecipitate with VPS26. (B) EndophilinAs do not co-immunoprecipitate with VPS29. (C) EndophilinAs do not co-immunoprecipitate with VPS35.

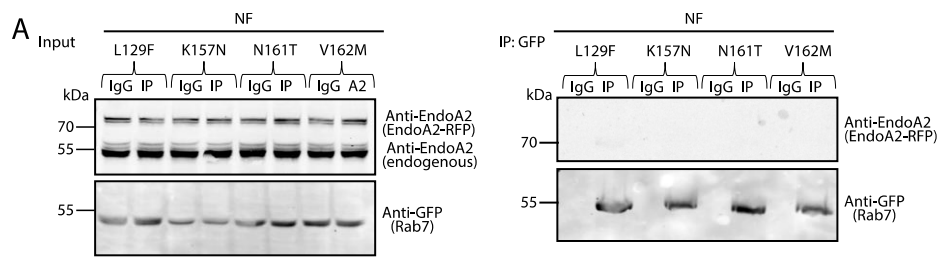


Fig. S8. CMT2B-Rab7 mutations do not bind EndophilinA2 in non-stimulated HEK cells. (A) GFP-conjugated beads (or IgG control beads) were used to pull down GFP-Rab7 WT and the CMT2B mutants L129F, K157N, N161T, V162M with EndophilinA2-RFP in non-stimulated Hek293 cells. Input is shown on the left, IP on the right.

4 DISCUSSION

The overall topic of my thesis is how the endosomal system regulates receptor signalling in axonal growth and degeneration. In my first project, we investigated how a few guidance cues and receptors are able to facilitate trillions of connections. In part, we answered this by the concept of signal integration. Here, we investigated how two unrelated receptors stimulated by two different ligands localize to the same endosomes and spatiotemporally integrate their signal to induce neuronal growth during development. In my second project, we have shown that TrkA is retrieved from vacuolar late endosomes by tubular microdomains enabling proper signalling in sensory neurons. Both of these studies highlight the importance of receptor signalling from endosomes and the receptor's location being tightly controlled. The need for spatiotemporal fine-tuning of signalling is apparent when looking at the limited number of guidance cues in the developing nervous system that elicit a highly complex and specific variety of responses.

4.1 SIGNAL INTEGRATION

The complexity of the nervous system is directed by growth and guidance cues coordinating axons to their targets. Though many such cues have been identified and their pathways characterized, the majority was analyzed in isolation, looking at each cue/receptor pair individually. However, due to the limited number of guidance cues regulating the immense amount of distinct paths an axon can take, the principle of signal crosstalk emerged. This allows a tight control over the directional fate of the growth cone by timing, expression and localization of guidance cues and receptors. The localization of receptors and their intracellular transport paths upon activation into different endosomal pathways offers an extra layer of spatiotemporal control. We show that two unrelated receptors can end up on the same endosome and influence each other's signalling cascade via a shared signalling node, which ends in a response greater than the simple addition of the two individual pathways. This signal integration can be classified as synergistic signalling and has been shown for several other unrelated receptors indicating that this is a common phenomenon often overlooked in result analysis and interpretation.

4.1.1 SIGNALLING NODES

Receptor crosstalk and signal integration at a shared intermediate is a common theme in developmental signalling. Multiple guidance pathways for example involve the activity of Src family kinase (SFK), including Sonic hedgehog (Shh), Netrin-1 signalling, as well as Vascular endothelial growth factor (VEGF) and Semaphorin 3B signalling (Morales and Kania, 2017). Netrin-1 and Shh signal via their respective receptors Deleted in Colorectal Cancer (DCC) and Brother of CDO (BOC). Each guidance cue alone can elicit a response if its fractional change in concentration is high enough. However, at gradients too shallow to result in a response for each guidance cue alone, activating both guidance cues results in a response of growth cone turning. This synergistic response is mediated by the shared signalling on downstream signalling molecule SFK: at concentration gradients too shallow to elicit a response of either receptor alone the combined activation lead to pSFK polarization at the growth cone, a critical step for directional growth (Sloan et al., 2015). Therefore, signals are integrated to a synergistic response. Signal integration may happen at the level of the signalling node or already at the level of receptors upstream of SFK, as we see it for CaSR and TrkB.

We propose GSK3 as the signalling node of CaSR and TrkB mediated signalling for neuronal growth in development. For GSK3 to function as such a critical signalling node, its regulation has to be finely tuned and activated differentially by different inputs. Indeed, GSK3 signalling has been shown to be finely tuned and quite complex itself, interacting with several receptor-coupled proteins including β -arrestins and G-proteins (Beurel et al., 2015). Dopamine-responsive GPCR D2 activation, for example, leads to initial cAMP production, which is followed by β arrestin recruiting Akt and GSK3 to protein phosphatase 2A. This phosphatase then dephosphorylates Akt and GSK3, thus deactivating Akt and activating GSK3 by dephosphorylation. GSK3 drives the formation of this complex, therefore acting in a feed-forward mechanism favoring its own activation (Beurel et al., 2015; O'Brien et al., 2011).

On the contrary, in the sustained Wnt pathway GSK3 signalling is sequestered within multi-vesicular endosomes (Taelman et al., 2010) showing the importance of GSK3's localization for its signalling. Overall, GSK3 shows enough complexity in response to different cellular signals to function as a signal integration node, combining two pathways synergistically. However, many studies neglect to look at tyrosine phosphorylation and the different paralogues of GSK3 namely α and β , leading to oversimplified interpretations of data.

4.2 THE ENDOSOMAL SYSTEM AS A SIGNAL DIVERSIFIER

As the case of GSK3 demonstrates, for signal integration to result in signal diversification, a tightly controlled intracellular mechanism has to be in place. This mechanism needs to keep signalling paths distinct from one another avoiding a melting pot of downstream signalling. Such a mechanism can be achieved by insulating downstream signalling to distinct organelles. The endosomal system is already known to be of critical importance when it comes to signal differentiation and regulation. Its function as a signalling regulator is most often demonstrated by receptor endocytosis from the plasma membrane, by receptor re-insertion via recycling endosomes regulating signal sensitivity, or by signal termination due to receptor degradation in the late endosomal/lysosomal pathway (Zastrow and Sorokin, 2007). However, the endosomal system has recently been shown to be critical for signal regulation by additional pathways, as initiation and signalling from endosomes has provided another level of spatial control as discussed below (Irannejad and Von Zastrow, 2014; Scott-Solomon and Kuruvilla, 2018).

4.2.1 RECEPTOR LOCALIZATION TO DISTINCT ENDOSOMAL POPULATIONS

Many receptors have a preferred trafficking pathway, e.g. Plexins have mainly been found in the recycling pathway (Pasterkamp and Burk, 2020). Recycling of receptors is initiated on early endosomes from where some receptors (such as TfR) are recycled based on geometric tubule recycling. Other receptors are distinctly sorted based on a specific sorting sequence, localized in the C-Terminal domain of the receptor. This sorting sequence allows binding to specific scaffold proteins, which help routing the receptors into their required pathways. In "sorted" recycling pathways, the sorting sequence initiates recycling through a protein complex called retromer (Seaman, 2012). Retromer recognizes the cargo by its recycling sequence and leads to the sorting of the receptor into recycling endosomes in an actin/Snx/retromer tubule-dependent fashion and then into Rab4 or Rab11 positive recycling endosomes (Cullen and Steinberg, 2018). Multiple distinct recycling sequences have been found that recruit distinct components of the retromer complex leading to differential sorting of these receptors. Without these C-terminal domains receptors remain within endosomes, which undergo endosomal maturation and degradation (Burk

et al., 2017c; Cullen and Steinberg, 2018). However, not only the sorting sequence regulates the trafficking pathway of receptors, but also the proteins binding to such as demonstrated in the example of TrkB during neurite growth and synapse formation: Developing hippocampal neurons that are growing towards their targets are dependent on BDNF for survival. Activation of TrkB by BDNF initiates localization of TrkB to late Rab7 endosomes (Burk et al., 2017a). Once neurons arrive at their targets, synaptic connections are formed. In order to generate mature synaptic spines, TrkB changes its trafficking route from the late endosomal pathway into the recycling pathway. This is facilitated through binding to a small scaffold protein called Copine6, which starts to be expressed at the time of synapse formation. Copine6 then binds to TrkB, facilitates recycling of TrkB to the plasma membrane and ensures re-activation of the TrkB signalling cascade. Via stable activation of ERK, synaptic spines mature (Burk et al., 2017b). This example shows that the sorting of receptors into distinct pathways can depend on several factors: its sorting sequence, but also the presence of adaptor proteins that can be differentially expressed leading to a wide variety of trafficking routes.

4.2.2 RECEPTOR SIGNALLING FROM DISTINCT SUBCELLULAR LOCATIONS

The fact that receptors can initiate their signalling cascade from endosomes has been shown for several receptors; both TrkA and TrkB, but also GPCRs were proven signalling-competent on endosomes, as well as on the plasma membrane (Deinhardt et al., 2006; Irannejad et al., 2013; Ye et al., 2018). The signalling outcome has been shown to be different depending on the location of the receptor, underlining the importance of regulated localization of the receptor to subcellular compartments (Burk et al., 2017c; Zhang et al., 2000).

CaSR has been shown to interact with cytoskeletal scaffold protein FilaminA increasing its localization to the plasma membrane and attenuating its degradation. Further, the presence of filaminA is required for the activation of the MAPK signalling cascade in HEK cells (Zhang and Breitwieser, 2005). FilaminA, an actin-cross-linking protein, binds directly to the C-terminal tail of CaSR and binds MAPK components activated by CaSR therefore bringing them into close proximity and establishing a connected signalling unit (Hjälml et al., 2001).

In parathyroid chief cells, CaSR has been reported to be predominantly located in caveolae, thought to serve as message centers by concentrating signalling molecules, including tyrosine kinases like EGFR and platelet-derived growth factor receptor (PDGFR), as well as downstream signalling molecules like Ras and Raf-1 of the MAPK pathway (Kifor et al., 1998; Schlegel et al., 1998). Whether these signalling caveolae are also interconnected by Filamin-A is plausible but needs confirmation considering the wide variety of possible interactions and cell type specificity.

In the nervous system, several members of the GPCR family C have been found to interact with Homer1 (Ronesi and Huber, 2008; Rong et al., 2003). In osteoblasts, CaSR colocalizes and associates with Homer1 in an activity dependent fashion. The Homer1/CaSR complex also binds to mTOR Complex 2 (mTORC2), a protein kinase that activates Akt Ser/Thr kinase by phosphorylation at Ser473. The interaction of Homer1 and CaSR is essential for activation of the Akt pathway by extracellular calcium, probably by bringing mTORC2 into spatial proximity, thus enabling signalling. The formation of the Homer1/CaSR complex was also required for extracellular calcium mediated signalling for survival and β -catenin stabilization, as well as differentiation in these osteoblasts (Rybchyn et al., 2019). This demonstrates that the location of CaSR and therefore the proximity and availability of interaction partners is critical for its signalling cascade.

4.2.3 RECEPTOR RE-ROUTING

The signal specificity seen depending on the receptor's location is an exciting regulator of the downstream signalling cascade, as re-routing of receptors can lead to a change in downstream signalling. As mentioned above adaptor proteins can lead to a re-localization of receptors. One adaptor protein that is heavily involved in the sorting and signalling of activated receptors is GIPC1. Luteinizing hormone receptor (LHR) and β 2-adrenergic receptor (β 2AR) for example undergo distinct trafficking to separate endosomal compartments in *Drosophila*. While β 2AR traffics via early endosomes, LHR is sorted into pre-early endosomes and recycled from there. This sorting depends on its C-terminal interaction with the PDZ protein GIPC1 that inhibits LHR sorting to early endosomes. When this interaction is disturbed, LHR is routed into early endosomes altering its downstream MAPK signalling, whereas its G protein dependent cAMP signalling is not altered (Jean-Alphonse et al., 2014). This highlights the significance of two processes: First, adaptor proteins need to be available in the cell in a spatiotemporally regulated manner and second, the signalling competencies of receptors when signalling from endosomes, as LHR's downstream signalling is changed upon relocation.

Interestingly, GIPC1 has also been shown to be important for receptor sorting and signalling as it facilitates the recycling of Plexin-D1. When localizing to recycling endosomes Plexin-D1 is in close proximity to R-Ras leading to signalling. Upon the loss of GIPC1, however, Plexin-D1 is misrouted, causing a loss of its signalling activity and therefore defects in axonal guidance and blood vessel development in mice (Burk et al., 2017c).

Further, GIPC1 has also been implicated in GPCR and RTK crosstalk. PDZ binding proteins are known to spatially cluster cytosolic proteins into protein complexes. GIPC1 has been shown to interact with TrkA as well as with G alpha interacting protein (GAIP), a regulator of G-protein signalling protein, bringing them into close proximity for possible interactions (Lou et al., 2001). The overexpression of GIPC1 in PC12 cells leads to a decrease in NGF induced MAPK signalling, indicating that GIPC1 is involved in the downstream signalling cascade of TrkA. The nature of this involvement remains to be shown but its colocalization with pTrkA within intracellular vesicles suggests an effect during retrograde transport (Lou et al., 2001). The mechanism, how these interactions affect NGF mediated signalling is not known. While we have not investigated a possible involvement of GIPC1 in signal integration of CaSR and TrkB, it is an interesting candidate worth investigating.

What we also found in our signal-integration project was co-trafficking of CaSR and TrkB upon co-activation. This indicates another pathway: signal integration by shared translocation. TrkA and Lysophosphatidic acid receptor 1 (LPA1) receptor synergistically activate MAPK in PC12 cells and induce translocation of TrkA and LPA1 receptor to the nucleus (Moughal et al., 2004). This interaction involves the classical GPCR pathway, as it is decreased upon treatment with pertussis toxin, which inactivates G-proteins $G_{i/o}$. Nonetheless, how G-proteins lead to the translocation of both receptors and whether these two receptors also interacted directly was not demonstrated. The idea that G-proteins can influence the trafficking paths of receptors offers a novel regulation mechanism diversifying possible signalling outcomes.

4.2.4 ENDOSOMAL REGULATION OF LOCAL TRANSLATION

The endosomal system also allows for signal diversification and distinct regulation by its involvement in local translation. Local translation plays an important role in axonal maintenance and synapse formation by regulating the axonal proteome. In retinal ganglion cells, it has been shown that RNA granules associate with Rab7-endosomes. These RNA carrying endosomes also associate with ribosomes and are sites of local protein synthesis, e.g. translating proteins important for mitochondrial function. Interestingly, this local synthesis is disrupted by CMT2B-causing Rab7 mutations (Cioni et al., 2019). In fungal cells, the transport of septin CDC3 encoding mRNA hitches a ride on Rab5-positive endosomes that interact directly with kinesin (Baumann et al., 2014). The mRNA is trafficked in a complex with the RNA-binding protein RRM4 and the adaptor protein UPA1 (Pohlmann et al., 2015). Ribosomes localizing to these endosomes translate all four septin mRNAs that build macromolecular complexes on these endosomes (Zander et al., 2016). This local translation provides a mechanism for distinct intracellular signalling as protein expression can be differentially facilitated by the endosomal identity.

4.2.5 SIGNALLING INSULATION BY LOCATION

As described above, intracellular organelles can also function as signal insulators as described for GSK3 in MVBs, where GSK3 is localized into ILVs of MVBs thus isolated from the cytoplasm and sequestering its signalling potential (Taelman et al., 2010). Similarly, MVB formation was shown to be involved in the NF- κ B signalling in *Drosophila melanogaster* (Huang et al., 2010). Endocytosis and MVB formation was shown to be required for the activation of Toll signalling, possibly by sequestration of Cactus, a negative regulator that inhibits Toll translocation to the nucleus. Funnily enough, the insulating properties of MVBs and their ILVs that allow distinct GSK3 and NF- κ B signalling, as described above, raise a critical question in the Trk signalling field at the moment. (see below)

4.2.6 ENDOSOMAL SIGNALLING OF TRK RECEPTORS

Trk receptors are described to undergo several distinct trafficking events in neurons. First, at the soma, Trk receptors are endocytosed and recycled constitutively, in the absence of neurotrophins. Upon stimulation, these Trk receptors are internalized and trafficked anterogradely to the axon in a positive feedback loop (Ascaño et al., 2009). Second, Trk receptors localized at the distal end of the axon are internalized upon neurotrophin stimulation. Following endocytosis, Trk localizes to endosomes and traffics retrogradely to the soma (Howe et al., 2001; Ye et al., 2003). Lastly, Trk receptors localizing within transport-organelles can be sorted into signalling endosomes, recycled or degraded (Suo et al., 2014; Ye et al., 2018). Importantly, signalling of Trk has been found to be different from the plasma membrane and from endosomal compartments (Zhang et al., 2000). However, despite it being studied abundantly, answers to the question whether and how endosomal sorting, trafficking and maturation influence Trk signalling as well as the identity of functionally distinct sets of endosomes involved are still controversial. For example, in sympathetic neurons survival, axonal extension and synapse formation are all NGF/TrkA dependent. How are these distinct outcomes signalled for by the same ligand/receptor pair? Do they underlie distinct trafficking and therefore signalling pathways of Trk?

When looking at the retrograde signalling pathway of Trks, studies have shown that the internalization in the distal axon and the retrograde transport are necessary for neuronal survival and neurite outgrowth. However, the identity of the retrogradely transported signalling endosome

harboring active, ligand-bound Trks remains controversial despite it being the focus of many studies. Rab5 and Rab7 positive endosomes as well as MVBs are currently favored to deliver NGF/TrkA to the soma, a combination of all three is possible (Delcroix et al., 2003; Ye et al., 2018; Zhang et al., 2013). Lately, MVBs have been shifted back into focus to be the Trk delivering compartment to the soma. After its first proposal as the transporting organelle by Claude et al. it was heavily debated (Claude et al., 1982). For example, the group of von Bartheld argued that due to their size and low numbers in axons, MVBs are probably not the trafficking organelles (Altick et al., 2009). However, it is also important to point out, that the definition of what is considered an MVB changes slightly between studies. Altick et al. categorized organelles smaller than 250nm in diameter as “MVB-like” organelles, of which many more underwent retrograde signalling. The recent study of the Ginty lab, however, showed Rab7-positive endosomes to be the main trafficking compartment of activated TrkA in sympathetic neurons *in vitro* and then confirmed in EM that TrkA localized to MVBs. Further, the authors showed that the majority of Flag-tagged TrkA is transported within intraluminal vesicles of MVBs along the axon in sympathetic neurons (Ye et al., 2018). Within these MVBs, Trk would be insulated from the cytoplasm and therefore not signalling competent. At the soma single membrane vesicles with signalling competent Trk were reported, however how these vesicles are generated is not known. We propose a retrieval mechanism of TrkA from late endosomes to allow for Trk signalling.

4.2.7 RETRIEVAL OF TRK RECEPTORS

Retrieval of neurotrophic receptors has been proposed by other groups before by several different mechanisms. One such mechanism is via retrograde transcytosis, which describes the recycling and reinternalization of a receptor at the soma. Other mechanisms include the release of receptors in exosomes (ILVs released into the extracellular space following fusion of MVBs with the plasma membrane). Following exosome release, receptors are then re-inserted into the plasma membrane (Escudero et al., 2014; Suo et al., 2014).

One important aspect within the process of retrieval is the orientation of the receptor’s signalling domain to the cytoplasm. In the study of Ye et al. the authors nicely show that the majority of TrkA localizes to ILVs, the signalling domain is insulated within the MVBs, therefore preventing access to downstream signalling proteins. However, when TrkA was found in single membrane vesicles that were derived from MVBs once arriving at the soma, TrkA is oriented with its signalling domain towards the cytoplasm, making it signalling competent (Ye et al., 2018). This observation suggests the need for a back-fusion mechanism of TrkA-positive ILVs with the limiting membrane of the MVB and a subsequent budding off of the new signalling endosome to ensure TrkA’s proper orientation. As discussed in Chapter 3, back-fusion of Trk receptors has not been shown yet and only been suggested for EGFR (Tomas et al., 2015). Interestingly, TrkA harboring single vesicles are reported to colocalize with retromer component VPS35, which is involved in the recycling from MVBs/late endosomes to the Golgi (Seaman et al., 2009; Ye et al., 2018).

We show by the tubulating phenotypes after NGF stimulation that late endosomes, likely MVBs, behave similarly to recycling endosomes, offering a mechanism of TrkA retrieval into small endosomes facilitating signalling and evasion of lysosomal degradation. We also propose the involvement of WASH1 and EndophilinAs in this process. EndophilinAs are mostly known for their role in endocytosis but have been implicated in the endosomal pathway before and even show a role in the regulation of exocytosis in chromaffin cells (Burk et al., 2017a; Gowrisankaran et al., 2020).

4.3 DIVERSITY OF RAB-GTPASES

Even though only few Rab-GTPases are mentioned in the above section, the mammalian genome actually offers over 50 Rab-GTPases with many having unknown functions (Barford et al., 2017). The most studied Rab-GTPases have been inspected in fibroblasts. While those Rab-GTPases have shown to be similar in neuronal cell bodies, there are distinct differences to endosomes in axons. For example, in somatic and dendritic early endosomes, Rab5 and its effector EEA1 are present. However, in axons, Rab5 is associated with endosomes but without its effector EEA1 (Wilson et al., 2000). How this change in endosome associated protein composition affects their function is not known. Nevertheless, it has been shown that every Rab-GTPase has their distinct pool of effector proteins, which they can associate with. This association then leads to a distinct set of signalling endosomes depending on the Rab-GTPase attached to it. Therefore, the Rab-GTPase identity of an endosome is a critical step in diversifying the pool of signalling endosomes. Rab-effectors cover a wide range of endosomal functions including the tethering and fusion with other organelles, the recruitment of cargo sorting complexes and motor proteins for the endosomal transport, as well as regulation of the cytoskeleton (Guerra and Bucci, 2016). Therefore, the endosomal identity defined by the associated Rab-GTPases and their interacting effectors, is a crucial determinant for the cargo sorting into specific carriers, the budding off and fusion with other organelles, the recycling or degradation of cargo and its translocation to different intracellular compartments. That the identity of the Rab-effectors plays an equally important role in the endosomal identity is shown for example by the ability of both Rab5 and Rab7 to interact with retrograde dynein motors as well as with anterograde kinesin motors, depending on the set of adaptor proteins available (Zhen and Stenmark, 2015).

In addition, the fluidity of the system challenges any interpretation based on the observation of one marked Rab-GTPase alone. It is well established that maturing endosomes undergo a so called Rab-switch, where Rab5 is replaced by Rab7 leading to endosomes carrying both Rab5 and Rab7 (Rink et al., 2005). In a study by Shearer and Petersen it was shown that organelles are often marked by several markers. Rab5 and Rab7 showed an overlap of around 50%. Of those endosomes positive for Rab5 32% were further positive for Lamp1, whereas those positive for Rab7 also stained for Lamp1 in 74% of the cases (Shearer and Petersen, 2019). In cases of double overexpression of Rab5 and Rab7 constructs, an overlap in 14.6% of the Rab5-endosomes was reported (Vonderheit and Helenius, 2005). However, overexpression of Rab7 and Lamp1 resulted in more than 80% colocalization (Humphries et al., 2011). To add additional challenges, antibodies for endogenous Rab-GTPases are of very mixed quality, whereas overexpression of Rab-GTPases flushes the system, potentially altering many regulatory mechanisms. Both of these caveats urge to caution when categorizing endosomal compartments.

4.4 THE ENDOSOMAL SYSTEM IN A DISEASE CONTEXT

The importance of the endolysosomal system has recently been shifted into focus in a disease context. Many genetic neurodegenerative disorders show mutations in proteins associated with the endosomal system. These observations suggest a common denominator in these disorders and highlights the importance of a properly functioning endosomal system (Burk and Pasterkamp, 2019). For example, mutations in Rab18 that cause Warburg Micro syndrome were shown to be phenotypically very similar to CMT2B mutations in Rab7. Upon closer investigation, it was shown

that Rab18 and Rab7 co-immunoprecipitate and are both associated with Lamp1-positive lysosomes. Further, it was reported that they influence each other genetically: Rab7 expression is upregulated upon loss of Rab18, potentially in a compensatory fashion, suggesting a shared pathomechanism for the two disorders (Nian et al., 2019).

On the other hand, one mutated GTPase such as the CMT2B mutated Rab7, reveals the diverse effects one malfunctioning protein can have (Liu and Wu, 2017). These diverse effects demonstrate that a small shift in functionality in a complex, dynamic, fine-tuned system can lead to a detrimental outcome. Studies investigating CMT2B-Rab7 have shown altered functions in receptor signalling, transport and degradation, mitochondrial transport, autophagy, cytoskeletal binding, and lipid metabolism (Basuray et al., 2010; BasuRay et al., 2013; Giudetti et al., 2020; Ponomareva et al., 2016; Romano et al., 2020). This reiterates many of the studies at present have a scope too limited to grasp the effect of the individual components and that more repetitive studies will be needed in the future to cover the range of effects of all the players involved.

4.5 CONCLUSION

As discussed above, signal integration can lead to signal diversification if tightly controlled by an intracellular mechanism that keeps signalling pathways distinct from one another, avoiding a melting pot of signal convergence. This tight control can be achieved by the endosomal system. The endosomal system regulates signalling on a crude level by receptor internalization and recycling to determine signal sensitivity as well as receptor degradation for signal termination and receptor downregulation. However, it also offers more fine-tuning mechanisms to regulate compartmentalized signalling by restricted localization to subcellular organelles leading to a distinct set of interacting proteins, it also allows for restricted local translation and differential transport. Overall, the endosomal system has been established as a critical determinant in many signalling pathways. However, due to its complexity and fluidity we are still miles away from understanding and detangling its many mechanisms.

5 REFERENCES

- Albers, K. M., Wright, D. E. and Davis, B. M. (1994). Overexpression of nerve growth factor in epidermis of transgenic mice causes hypertrophy of the peripheral nervous system. *J. Neurosci.* **14**, 1422–1432.
- Altick, A. L., Baryshnikova, L. M., Vu, T. Q. and Von Bartheld, C. S. (2009). Quantitative Analysis of Multivesicular Bodies (MVBs) in the Hypoglossal Nerve: Evidence that Neurotrophic Factors do not use MVBs for Retrograde Axonal Transport. *J Comp Neurol.* **514**, 641–657.
- Ascaño, M., Richmond, A., Borden, P. and Kuruvilla, R. (2009). Axonal Targeting of Trk Receptors via Transcytosis Regulates Sensitivity to Neurotrophin Responses. *J. Neurosci.* **29**, 11674 LP – 11685.
- Barde, Y. A. (1989). Trophic factors and neuronal survival. *Neuron* **2**, 1525–1534.
- Barde, Y. A. (1990). The nerve growth factor family. *Prog. Growth Factor Res.* **2**, 237–248.
- Barford, K., Deppmann, C. and Winckler, B. (2017). The neurotrophin receptor signaling endosome: Where trafficking meets signaling. *Dev. Neurobiol.* **77**, 405–418.
- Basuray, S., Mukherjee, S., Romero, E., Wilson, M. C. and Wandinger-ness, A. (2010). Rab7 mutants associated with charcot-Marie-tooth disease exhibit enhanced NGF-stimulated signaling. *PLoS One* **5**.
- BasuRay, S., Mukherjee, S., Romero, E. G., Seaman, M. N. J. and Wandinger-Ness, A. (2013). Rab7 mutants associated with Charcot-Marie-Tooth disease cause delayed growth factor receptor transport and altered endosomal and nuclear signaling. *J. Biol. Chem.* **288**, 1135–49.
- Baumann, S., Ko'ning, J., Koepke, J. and Feldbru'gge, M. (2014). Endosomal transport of septin mRNA and protein indicates local translation on endosomes and is required for correct septin filamentation. *EMBO Rep.* **15**, 94–102.
- Beurel, E., Grieco, S. F. and Jope, R. S. (2015). *Glycogen synthase kinase-3 (GSK3): regulation, actions, and diseases.*
- Bhattacharyya, A., Watson, F. L., Bradlee, T. A., Pomeroy, S. L., Stiles, C. D. and Segal, R. A. (1997). Trk receptors function as rapid retrograde signal carriers in the adult nervous system. *J. Neurosci.* **17**, 7007–7016.
- Bhattacharyya, A., Watson, F. L., Pomeroy, S. L., Zhang, Y. Z., Stiles, C. D. and Segal, R. A. (2002). High-resolution imaging demonstrates dynein-based vesicular transport of activated Trk receptors. *J. Neurobiol.* **51**, 302–312.
- Buchman, V. L. and Davies, A. M. (1993). Different neurotrophins are expressed and act in a developmental sequence to promote the survival of embryonic sensory neurons. *Development* **118**, 989–1001.
- Burk, K. (2009). The Role of the CaSR During Development of Cranial Sensory Neurons.
- Burk, K. and Pasterkamp, R. J. (2019). Disrupted neuronal trafficking in amyotrophic lateral sclerosis. *Acta Neuropathol.* **137**, 859–877.
- Burk, K., Murdoch, J. D., Freytag, S., Koenig, M., Bharat, V., Markworth, R., Burkhardt, S., Fischer, A. and Dean, C. (2017a). EndophilinAs regulate endosomal sorting of BDNF-TrkB to mediate survival signaling in hippocampal neurons. *Sci. Rep.* **7**, 2149.
- Burk, K., Ramachandran, B., Ahmed, S., Hurtado-Zavala, J. I., Awasthi, A., Benito, E., Faram, R., Ahmad, H., Swaminathan, A., McIlhinney, J., et al. (2017b). Regulation of Dendritic Spine Morphology in Hippocampal Neurons by Copine-6. *Cereb. Cortex* **1**–18.
- Burk, K., Mire, E., Bellon, A., Hocine, M., Guillot, J., Moraes, F., Yoshida, Y., Simons, M., Chauvet, S. and Mann, F. (2017c). Post-endocytic sorting of Plexin-D1 controls signal transduction and development of axonal and vascular circuits. *Nat. Commun.* **8**, 14508.
- Campenot, R. B. (1977). Local control of neurite development by nerve growth factor. *Proc. Natl. Acad. Sci. U. S. A.* **74**, 4516–4519.
- Campenot, R. B. (1982). Development of sympathetic neurons in compartmentalized cultures. *Dev. Biol.* **93**, 13–21.
- Cioni, J. M., Lin, J. Q., Holtermann, A. V., Koppers, M., Jakobs, M. A. H., Azizi, A., Turner-Bridger, B., Shigeoka, T., Franze, K., Harris, W. A., et al. (2019). Late Endosomes Act as mRNA Translation Platforms and Sustain Mitochondria in Axons. *Cell* **176**, 56–72.e15.
- Claude, P., Hawrot, E., Dunis, D. A. and Campenot, R. B. (1982). Binding, internalization, and retrograde transport of 125I-nerve growth factor in cultured rat sympathetic neurons. *J. Neurosci.* **2**, 431–442.
- Cohen, S., Levi-Montalcini, R. and Hamburger, V. (1954). A Nerve Growth-Stimulating Factor Isolated From Sarcomas 37 and 180. *Proc. Natl. Acad. Sci.* **40**, 1014–1018.
- Crowley, C., Spencer, S. D., Nishimura, M. C., Chen, K. S., Pitts-Meek, S., Armanini, M. P., Ling, L. H.,

- McMahon, S. B., Shelton, D. L., Levinson, A. D., et al.** (1994). Mice lacking nerve growth factor display perinatal loss of sensory and sympathetic neurons yet develop basal forebrain cholinergic neurons. *Cell* **76**, 1001–1011.
- Cullen, P. J. and Steinberg, F.** (2018). To degrade or not to degrade: mechanisms and significance of endocytic recycling. *Nat. Rev. Mol. Cell Biol.* **19**, 679–696.
- Davies, A. M.** (1989). Intrinsic differences in the growth rate of early nerve fibres related to target distance. *Nature* **337**, 553–555.
- Davies, A. M., Thoenen, H. and Barde, Y. A.** (1986). The response of chick sensory neurons to brain-derived neurotrophic factor. *J. Neurosci.* **6**, 1897–1904.
- Davies, A. M., Bandtlow, C., Heumann, R., Korsching, S., Rohrer, H. and Thoenen, H.** (1987). Timing and site of nerve growth factor synthesis in developing skin in relation to innervation and expression of the receptor. *Nature* **326**, 353–358.
- Deinhardt, K., Salinas, S., Verastegui, C., Watson, R., Worth, D., Hanrahan, S., Bucci, C. and Schiavo, G.** (2006). Rab5 and Rab7 Control Endocytic Sorting along the Axonal Retrograde Transport Pathway. *Neuron* **52**, 293–305.
- Delcroix, J. D., Valletta, J. S., Wu, C., Hunt, S. J., Kowal, A. S. and Mobley, W. C.** (2003). NGF signaling in sensory neurons: Evidence that early endosomes carry NGF retrograde signals. *Neuron* **39**, 69–84.
- Deppmann, C. D., Mihalas, S., Sharma, N., Lonze, B. E., Niebur, E. and Ginty, D. D.** (2008). A model for neuronal competition during development. *Science* **320**, 369–373.
- Dudanova, I. and Klein, R.** (2013). Integration of guidance cues: Parallel signaling and crosstalk. *Trends Neurosci.* **36**, 295–304.
- Ehlers, M. D., Kaplan, D. R., Price, D. L., Koliatsos, V. E., Price, I. D. L. and Koliatsos, V. E.** (1995). NGF-stimulated retrograde transport of trkA in the mammalian nervous system. *J. Cell Biol.* **130**, 149–156.
- Escudero, C. A., Lazo, O. M., Galleguillos, C., Parraguez, J. I., Lopez-Verrilli, M. A., Cabeza, C., Leon, L., Saeed, U., Retamal, C., Gonzalez, A., et al.** (2014). The p75 neurotrophin receptor evades the endolysosomal route in neuronal cells, favouring multivesicular bodies specialised for exosomal release. *J. Cell Sci.* **127**, 1966–1979.
- Giudetti, A. M., Guerra, F., Longo, S., Beli, R., Romano, R., Manganelli, F., Nolano, M., Mangini, V., Santoro, L. and Bucci, C.** (2020). An altered lipid metabolism characterizes Charcot-Marie-Tooth type 2B peripheral neuropathy. *Biochim. Biophys. Acta - Mol. Cell Biol. Lipids* **1865**.
- Glebova, N. O. and Ginty, D. D.** (2004). Heterogeneous Requirement of NGF for Sympathetic Target Innervation In Vivo. *J. Neurosci.* **24**, 743–751.
- Gowrisankaran, S., Houy, S., Peña, J. G., Steubler, V., Gelker, M., Kroll, J., Pinheiro, P. S., Schwitters, D., Halbsgut, N., Pechstein, A., et al.** (2020). Endophilin-A coordinates priming and fusion of neurosecretory vesicles via intersectin. *Nat. Commun.*
- Grimes, M. L., Zhou, J., Beattie, E. C., Yuen, E. C., Hall, D. E., Valletta, J. S., Topp, K. S., LaVail, J. H., Bunnett, N. W. and Mobley, W. C.** (1996). Endocytosis of activated trkA: Evidence that nerve growth factor induces formation of signaling endosomes. *J. Neurosci.* **16**, 7950–7964.
- Grimes, M. L., Beattie, E. and Mobley, W. C.** (1997). A signaling organelle containing the nerve growth factor-activated receptor tyrosine kinase, TrkA. *Proc. Natl. Acad. Sci. U. S. A.* **94**, 9909–9914.
- Guerra, F. and Bucci, C.** (2016). Multiple Roles of the Small GTPase Rab7. *Cells* **5**, 34.
- Hamburger, V.** (1934). The effects of wing bud extirpation on the development of the central nervous system in chick embryos. *J. Exp. Zool.* **68**, 449–494.
- Hamburger, V.** (1939). Motor and Sensory Hyperplasia following Limb-Bud Transplantations in Chick Embryos. *Physiol. Zool.* **12**, 268–284.
- Harrington, A. W. and Ginty, D. D.** (2013). Long-distance retrograde neurotrophic factor signalling in neurons. *Nat Rev Neurosci* **14**, 177–187.
- Henderson, T. A., Johnson, E. M., Osborne, P. A. and Jacquin, M. F.** (1994). Fetal NGF augmentation preserves excess trigeminal ganglion cells and interrupts whisker-related pattern formation. *J. Neurosci.* **14**, 3389 LP – 3403.
- Hendry, I. A. and Campbell, J.** (1976). Morphometric analysis of rat superior cervical ganglion after axotomy and nerve growth factor treatment. *J. Neurocytol.* **5**, 351–360.
- Hendry, I. A., Stöckel, K., Thoenen, H. and Iversen, L. L.** (1974). The retrograde axonal transport of nerve growth factor. *Brain Res.* **68**, 103–121.
- Hjälml, G., MacLeod, R. J., Kifor, O., Chattopadhyay, N. and Brown, E. M.** (2001). Filamin-A Binds to the Carboxyl-terminal Tail of the Calcium-sensing Receptor, an Interaction that Participates in CaR-mediated Activation of Mitogen-activated Protein Kinase. *J. Biol. Chem.* **276**, 34880–34887.
- Howe, C. L., Valletta, J. S., Rusnak, A. S. and Mobley, W. C.** (2001). NGF signaling from clathrin-coated

- vesicles: Evidence that signaling endosomes serve as a platform for the Ras-MAPK pathway. *Neuron* **32**, 801–814.
- Huang, H. R., Chen, Z. J., Kunes, S., Chang, G. D. and Maniatis, T.** (2010). Endocytic pathway is required for Drosophila Toll innate immune signaling. *Proc. Natl. Acad. Sci. U. S. A.* **107**, 8322–8327.
- Humphries, W. H., Szymanski, C. J. and Payne, C. K.** (2011). Endo-lysosomal vesicles positive for rab7 and lamp1 are terminal vesicles for the transport of dextran. *PLoS One* **6**,.
- Irannejad, R. and Von Zastrow, M.** (2014). GPCR signaling along the endocytic pathway. *Curr. Opin. Cell Biol.* **27**, 109–116.
- Irannejad, R., Tomshine, J. R. J. C. J. R., Tomshine, J. R. J. C. J. R., Chevalier, M., Mahoney, J. P., Steyaert, J., Rasmussen, S. G. F. F., Sunahara, R. K., El-Samad, H., Huang, B., et al.** (2013). Conformational biosensors reveal GPCR signalling from endosomes. *Nature* **495**, 534–538.
- Jean-Alphonse, F., Bowersox, S., Chen, S., Beard, G., Puthenveedu, M. A. and Hanyaloglu, A. C.** (2014). Spatially restricted G protein-coupled receptor activity via divergent endocytic compartments. *J. Biol. Chem.* **289**, 3960–3977.
- Jidigam, V. K. and Gunhaga, L.** (2013). Development of cranial placodes: Insights from studies in chick. *Dev. Growth Differ.* **55**, 79–95.
- Jones, K. R., Fariñas, I., Backus, C. and Reichardt, L. F.** (1994). Targeted disruption of the BDNF gene perturbs brain and sensory neuron development but not motor neuron development. *Cell* **76**, 989–999.
- Jullien, J., Guili, V., Derrington, E. A., Darlix, J. L., Reichardt, L. F. and Rudkin, B. B.** (2003). Trafficking of TrkA-green fluorescent protein chimerae during nerve growth factor-induced differentiation. *J. Biol. Chem.* **278**, 8706–8716.
- Kifor, O., Diaz, R., Butters, R., Kifor, I. and Brown, E. M.** (1998). The calcium-sensing receptor is localized in caveolin-rich plasma membrane domains of bovine parathyroid cells. *J. Biol. Chem.* **273**, 21708–21713.
- Klein, R., Smeyne, R. J., Wurst, W., Long, L. K., Auerbach, B. A., Joyner, A. L. and Barbacid, M.** (1993). Targeted disruption of the trkB neurotrophin receptor gene results in nervous system lesions and neonatal death. *Cell* **75**, 113–122.
- Klein, R., Silos-Santiago, I., Smeyne, R. J., Lira, S. A., Brambilla, R., Bryant, S., Zhang, L., Snider, W. D. and Barbacid, M.** (1994). Disruption of the neurotrophin-3 receptor gene trkC eliminates Ia muscle afferents and results in abnormal movements. *Nature* **368**, 249–251.
- Kononenko, N. L., Claßen, G. A., Kuijpers, M., Puchkov, D., Maritzen, T., Tempes, A., Malik, A. R., Skalecka, A., Bera, S., Jaworski, J., et al.** (2017). Retrograde transport of TrkB-containing autophagosomes via the adaptor AP-2 mediates neuronal complexity and prevents neurodegeneration. *Nat. Commun.* **8**, 14819.
- Kruttgen, A., Saxena, S., Evangelopoulos, M. E. and Weis, J.** (2003). Neurotrophins and neurodegenerative diseases: Receptors stuck in traffic? *J. Neuropathol. Exp. Neurol.* **62**, 340–350.
- Kuruvilla, R., Zweifel, L. S., Glebova, N. O., Lonze, B. E., Valdez, G., Ye, H. and Ginty, D. D.** (2004). A neurotrophin signaling cascade coordinates sympathetic neuron development through differential control of TrkA trafficking and retrograde signaling. *Cell* **118**, 243–55.
- LeMaster, A. M., Krimm, R. F., Davis, B. M., Noel, T., Forbes, M. E., Johnson, J. E. and Albers, K. M.** (1999). Overexpression of brain-derived neurotrophic factor enhances sensory innervation and selectively increases neuron number. *J. Neurosci.* **19**, 5919–5931.
- Levi-Montalcini, R.** (1987). The Nerve Growth Factor 35 Years Later. *Science (80-)*. **237**, 1154–1162.
- Levi-Montalcini, R. and Booker, B.** (1960). Destruction of the Sympathetic Ganglia in Mammals By an Antiserum To a Nerve-Growth Protein. *Proc. Natl. Acad. Sci. U. S. A.* **46**, 384–391.
- Levi-Montalcini, R. and Levi, G.** (1942). Les conséquences de la destruction d'un territoire d'innervation périphérique sur le développement des centres nerveux correspondants dans l'embryon de Poulet. *Arch Biol* **53**, 537–545.
- Lindsay, R. M., Barde, Y. A., Davies, A. M. and Rohrer, H.** (1985a). Differences and similarities in the neurotrophic growth factor requirements of sensory neurons derived from neural crest and neural placode. *J. Cell Sci. Suppl.* **3**, 115–129.
- Lindsay, R. M., Thoenen, H. and Barde, Y.** (1985b). Placode and neural crest-derived sensory neurons are responsive at early developmental stages to brain-derived neurotrophic factor. *Dev Biol.* **112**, 319–28.
- Liu, H. and Wu, C.** (2017). Charcot marie tooth 2B peripheral sensory neuropathy: How Rab7 mutations impact NGF signaling? *Int. J. Mol. Sci.* **18**,.
- Lou, X., Yano, H., Lee, F., Chao, M. V. and Farquhar, M. G.** (2001). GIPC and GAIP form a complex with TrkA: A putative link between G protein and receptor tyrosine kinase pathways. *Mol. Biol. Cell* **12**, 615–627.

- Lowery, L. A. and Vactor, D. Van** (2009). The trip of the tip: understanding the growth cone machinery. *Nat. Rev. Mol. Cell Biol.* **10**, 332–343.
- Maday, S., Wallace, K. E. and Holzbaur, E. L. F.** (2012). Autophagosomes initiated distally and mature during transport toward the cell soma in primary neurons. *J. Cell Biol.* **196**, 407–417.
- Markworth, R., Adolfs, Y., Dambeck, V., Steinbeck, L. M., Lizé, M., Pasterkamp, R. J., Bähr, M., Dean, D. and Burk, K.** (2019). Sensory Axon Growth Requires Spatiotemporal Integration of CaSR and TrkB Signaling. *J. Neurosci.* **39**, 5842–60. <https://doi.org/10.1523/JNEUROSCI.0027-19.2019>.
- Markworth, R., Bähr, M., and Burk, K.** (2021). Held Up in Traffic—Defects in the Trafficking Machinery in Charcot-Marie-Tooth Disease. *Front. Mol. Neurosci.* **14**, 167. Available at: <https://www.frontiersin.org/article/10.3389/fnmol.2021.695294>.
- Markworth, R., Dambeck, V., Steinbeck, L. M., Koufali, A., Bues, B., Dankovich, T. M., Wichmann, C., Burk, K.** (2021). Tubular microdomains of Rab7-endosomes retrieve TrkA, a mechanism disrupted in Charcot-Marie-Tooth 2B. *J. Cell Sci.* jcs.258559. doi: <https://doi.org/10.1242/jcs.258559>
- Morales, D. and Kania, A.** (2017). Cooperation and crosstalk in axon guidance cue integration: additivity, synergy, and fine-tuning in combinatorial signalling. *Dev. Neurobiol.* **77**, 891–904.
- Moughal, N. A., Waters, C., Sambhi, B., Pyne, S. and Pyne, N. J.** (2004). Nerve growth factor signaling involves interaction between the Trk A receptor and lysophosphatidate receptor 1 systems: Nuclear translocation of the lysophosphatidate receptor 1 and Trk A receptors in pheochromocytoma 12 cells. *Cell. Signal.* **16**, 127–136.
- Nian, F. S., Li, L. L., Cheng, C. Y., Wu, P. C., Lin, Y. T., Tang, C. Y., Ren, B. S., Tai, C. Y., Fann, M. J., Kao, L. Sen, et al.** (2019). Rab18 Collaborates with Rab7 to Modulate Lysosomal and Autophagy Activities in the Nervous System: an Overlapping Mechanism for Warburg Micro Syndrome and Charcot-Marie-Tooth Neuropathy Type 2B. *Mol. Neurobiol.* **56**, 6095–6105.
- Nomura, M., Nagai, T., Harada, Y. and Tani, T.** (2011). Facilitated intracellular transport of TrkA by an interaction with nerve growth factor. *Dev. Neurobiol.* **71**, 634–649.
- O'Brien, W. T., Huang, J., Buccafusca, R., Garskof, J., Valvezan, A. J., Berry, G. T. and Klein, P. S.** (2011). Glycogen synthase kinase-3 is essential for β -arrestin-2 complex formation and lithium-sensitive behaviors in mice. *J. Clin. Invest.* **121**, 3756–3762.
- Oppenheim, R. W.** (1989). The neurotrophic theory and naturally occurring motoneuron death. *Trends Neurosci.* **12**, 252–255.
- Orike, N., Thrasivoulou, C., Wrigley, A. and Cowen, T.** (2001). Differential regulation of survival and growth in adult sympathetic neurons: an in vitro study of neurotrophin responsiveness. *J. Neurobiol.* **47**, 295–305.
- Pasterkamp, R. J. and Burk, K.** (2020). Axon guidance receptors: Endocytosis, trafficking and downstream signaling from endosomes. *Prog. Neurobiol.* 101916.
- Patel, T. D., Jackman, A., Rice, F. L., Kucera, J. and Snider, W. D.** (2000). Development of sensory neurons in the absence of NGF/TrkA signaling in vivo. *Neuron* **25**, 345–357.
- Patel, T. D., Kramer, I., Kucera, J., Niederkofler, V., Jessell, T. M., Arber, S. and Snider, W. D.** (2003). Peripheral NT3 signaling is required for ETS protein expression and central patterning of proprioceptive sensory afferents. *Neuron* **38**, 403–416.
- Pla, P. and Monsoro-Burq, A. H.** (2018). The neural border: Induction, specification and maturation of the territory that generates neural crest cells. *Dev. Biol.* **444**, S36–S46.
- Pohlmann, T., Baumann, S., Haag, C., Albrecht, M. and Feldbrügge, M.** (2015). A FYVE zinc finger domain protein specifically links mRNA transport to endosome trafficking. *Elife* **4**, 1–27.
- Ponomareva, O. Y., Eliceiri, K. W. and Halloran, M. C.** (2016). Charcot-Marie-Tooth 2b associated Rab7 mutations cause axon growth and guidance defects during vertebrate sensory neuron development. *Neural Dev.* **11**, 2.
- Prior, R., Van Helleputte, L., Benoy, V. and Van Den Bosch, L.** (2017). Defective axonal transport: A common pathological mechanism in inherited and acquired peripheral neuropathies. *Neurobiol. Dis.* **105**, 300–320.
- Purves, D.** (1980). Neuronal competition. *Nature* **287**, 585–586.
- Reichardt, L. F.** (2006). Neurotrophin-regulated signalling pathways. *Philos. Trans. R. Soc. B Biol. Sci.* **361**, 1545–1564.
- Riccio, A., Pierchala, B. A., Ciarallo, C. L. and Ginty, D. D.** (1997). An NGF-TrkA-Mediated Retrograde Signal to Transcription Factor CREB in sympathetic Neurons. *Science (80-.)*, **2**, 1097–1100.
- Rink, J., Ghigo, E., Kalaidzidis, Y. and Zerial, M.** (2005). Rab conversion as a mechanism of progression from early to late endosomes. *Cell* **122**, 735–749.
- Robinson, M., Adu, J. and Davies, A. M.** (1996). Timing and Regulation of trkB and BDNF mRNA Expression

- in Placode-derived Sensorv Neurons and their Targets. **8**, 2399–2406.
- Rohrer, H., Heumann, R. and Thoenen, H.** (1988). The synthesis of nerve growth factor (NGF) in developing skin is independent of innervation. *Dev. Biol.* **128**, 240–244.
- Romano, R., Rivellini, C., De Luca, M., Tonlorenzi, R., Beli, R., Manganelli, F., Nolano, M., Santoro, L., Eskelinen, E. L., Previtali, S. C., et al.** (2020). Alteration of the late endocytic pathway in Charcot–Marie–Tooth type 2B disease. *Cell. Mol. Life Sci.* **78**, 351–372.
- Ronesi, J. A. and Huber, K. M.** (2008). Homer interactions are necessary for metabotropic glutamate receptor-induced long-term depression and translational activation. *J. Neurosci.* **28**, 543–547.
- Rong, R., Ahn, J.-Y., Huang, H., Nagata, E., Kalman, D., Kapp, J. A., Tu, J., Worley, P. F., Snyder, S. H. and Ye, K.** (2003). PI3 kinase enhancer-Homer complex couples mGluR1 to PI3 kinase, preventing neuronal apoptosis. *Nat. Neurosci.* **6**, 1153–1161.
- Rybczyn, M. S., Islam, K. S., Brennan-Speranza, T. C., Cheng, Z., Brennan, S. C., Chang, W., Mason, R. S. and Conigrave, A. D.** (2019). Homer1 mediates CaSR-dependent activation of mTOR complex 2 and initiates a novel pathway for AKT-dependent β -catenin stabilization in osteoblasts. *J. Biol. Chem.* **294**, 16337–16350.
- Sandow, S. L., Heydon, K., Weible II, M., Reynolds, A. J., Bartlett, S. E. and Hendry, I. A.** (2000). Signalling organelle for retrograde axonal transport of internalized neurotrophins from the nerve terminal. *Immunol. Cell Biol.* **78**, 430–435.
- Schlegel, A., Volonté, D., Engelman, J. A., Galbiati, F., Mehta, P., Zhang, X. L., Scherer, P. E. and Lisanti, M. P.** (1998). Crowded little caves: Structure and function of caveolae. *Cell. Signal.* **10**, 457–463.
- Scott-Solomon, E. and Kuruvilla, R.** (2018). Mechanisms of neurotrophin trafficking via Trk receptors. *Mol. Cell. Neurosci.* **91**, 25–33.
- Seaman, M. N. J.** (2012). The retromer complex-endosomal protein recycling and beyond. *J. Cell Sci.* **125**, 4693–4702.
- Seaman, M. N. J., Harbour, M. E., Tattersall, D., Read, E. and Bright, N.** (2009). Membrane recruitment of the cargo-selective retromer subcomplex is catalysed by the small GTPase Rab7 and inhibited by the Rab-GAP TBC1D5. *J. Cell Sci.* **122**, 2371–2382.
- Seaman, M. N. J., Gautreau, A. and Billadeau, D. D.** (2013). Retromer-mediated endosomal protein sorting: All WASHed up! *Trends Cell Biol.* **23**, 522–528.
- Shearer, L. J. and Petersen, N. O.** (2019). Distribution and Co-localization of endosome markers in cells. *Heliyon* **5**, e02375.
- Skaper, S. D.** (2018). Neurotrophic factors: An overview. *Methods Mol. Biol.* **1727**, 1–17.
- Sloan, T. F. W., Qasaimeh, M. A., Juncker, D., Yam, P. T. and Charron, F.** (2015). Integration of Shh and Netrin-1 Guides Commissural Axons. *PLoS Biol.* **13**, 1–24.
- Smeyne, R. J., Klein, R., Schnapp, A., Long, L. K., Bryant, S., Lewin, A., Lira, S. A. and Barbacid, M.** (1994). Severe sensory and sympathetic neuropathies in mice carrying a disrupted Trk/NGF receptor gene. *Nature* **368**, 246–249.
- Spinosa, M. R., Progida, C., De Luca, A., Colucci, A. M. R., Alifano, P. and Bucci, C.** (2008). Functional characterization of Rab7 mutant proteins associated with Charcot–Marie–Tooth type 2B disease. *J. Neurosci.* **28**, 1640–1648.
- Suo, D., Park, J., Harrington, A. W., Zweifel, L. S., Mihalas, S. and Deppmann, C. D.** (2014). Coronin-1 is a neurotrophin endosomal effector that is required for developmental competition for survival. *Nat. Neurosci.* **17**, 36–45.
- Taelman, V. F., Dobrowolski, R., Plouhinec, J. L., Fuentealba, L. C., Vorwald, P. P., Gumper, I., Sabatini, D. D. and De Robertis, E. M.** (2010). Wnt signaling requires sequestration of Glycogen Synthase Kinase 3 inside multivesicular endosomes. *Cell* **143**, 1136–1148.
- Tomas, A., Vaughan, S. O., Burgoyne, T., Sorkin, A., Hartley, J. A., Hochhauser, D. and Futter, C. E.** (2015). WASH and Tsg101/ALIX-dependent diversion of stress-internalized EGFR from the canonical endocytic pathway. *Nat. Commun.* **6**, 7324.
- Tsui-Pierchala, B. A. and Ginty, D. D.** (1999). Characterization of an NGF-P-TrkA retrograde-signaling complex and age-dependent regulation of TrkA phosphorylation in sympathetic neurons. *J. Neurosci.* **19**, 8207–8218.
- Venkatramani, A. and Panda, D.** (2019). Regulation of neuronal microtubule dynamics by tau: Implications for tauopathies. *Int. J. Biol. Macromol.* **133**, 473–483.
- Vogel, K. S. and Davies, A. M.** (1991). The duration of neurotrophic factor independence in early sensory neurons is matched to the time course of target field innervation. *Neuron* **7**, 819–830.
- Vonderheit, A. and Helenius, A.** (2005). Rab7 associates with early endosomes to mediate sorting and transport of Semliki forest virus to late endosomes. *PLoS Biol.* **3**, 1225–1238.

- Watson, F. L., Heerssen, H. M., Moheban, D. B., Lin, M. Z., Sauvageot, C. M., Bhattacharyya, A., Pomeroy, S. L. and Segal, R. A.** (1999). Rapid Nuclear Responses to Target-Derived Neurotrophins Require Retrograde Transport of Ligand – Receptor Complex. *J. Neurosci.* **19**, 7889–7900.
- Weible, M. W. and Hendry, I. A.** (2004). What is the Importance of Multivesicular Bodies in Retrograde Axonal Transport In Vivo? *J. Neurobiol.* **58**, 230–243.
- White, F. A., Keller-Peck, C. R., Knudson, C. M., Korsmeyer, S. J. and Snider, W. D.** (1998). Widespread elimination of naturally occurring neuronal death in Bax-deficient mice. *J. Neurosci.* **18**, 1428–1439.
- Wilson, J. M., de Hoop, M., Zorzi, N., Toh, B. H., Dotti, C. G. and Parton, R. G.** (2000). EEA1, a tethering protein of the early sorting endosome, shows a polarized distribution in hippocampal neurons, epithelial cells, and fibroblasts. *Mol. Biol. Cell* **11**, 2657–2671.
- Yano, H., Lee, F. S., Kong, H., Chuang, J., Arevalo, J., Perez, P., Sung, C. and Chao, M. V.** (2001). Association of Trk neurotrophin receptors with components of the cytoplasmic dynein motor. *J. Neurosci.* **21**, 1–7.
- Ye, H., Kuruvilla, R., Zweifel, L. S. and Ginty, D. D.** (2003). Evidence in Support of Signaling Endosome-Based Retrograde Survival of Sympathetic Neurons. **39**, 57–68.
- Ye, M., Lehigh, K. M. and Ginty, D. D.** (2018). Multivesicular bodies mediate long-range retrograde NGF-TrkA signaling. *Elife* **7**, 1–29.
- Zander, S., Baumann, S., Weidtkamp-Peters, S. and Feldbrügge, M.** (2016). Endosomal assembly and transport of heteromeric septin complexes promote septin cytoskeleton formation. *J. Cell Sci.* **129**, 2778–2792.
- Zastrow, M. Von and Sorkin, A.** (2007). Signaling on the endocytic pathway. *Curr. Opin. Cell Biol.* **19**, 436–445.
- Zhang, M. and Breitwieser, G. E.** (2005). High affinity interaction with filamin A protects against calcium-sensing receptor degradation. *J. Biol. Chem.* **280**, 11140–11146.
- Zhang, Y., Moheban, D. B., Conway, B. R., Bhattacharyya, A. and Segal, R. A.** (2000). Cell surface Trk receptors mediate NGF-induced survival while internalized receptors regulate NGF-induced differentiation. *J. Neurosci.* **20**, 5671–8.
- Zhang, K., Fishel Ben Kenan, R., Osakada, Y., Xu, W., Sinit, R. S., Chen, L., Zhao, X., Cui, B., Wu, C., Chen, J.-Y., et al.** (2013). Defective Axonal Transport of Rab7 GTPase Results in Dysregulated Trophic Signaling. *J. Neurosci.* **33**, 7451–7462.
- Zhen, Y. and Stenmark, H.** (2015). Cellular functions of Rab GTPases at a glance. *J. Cell Sci.* **128**, 3171–3176.

LIST OF ABBREVIATIONS

AP2	Adaptor protein 2
BDNF	Brain-derived neurotrophic factor
BMP	Bone morphogenetic protein
BOC	Brother of CDO
cAMP	cyclic AMP
CaSR	Extracellular calcium-sensing receptor
CIMPR	Cation-independent mannose 6-phosphate receptor
CMT	Charcot-Marie-Tooth disease
CNS	Central nervous system
CREB	Cyclic AMP-responsive element-binding protein
CSC	Cargo selective complex
DCC	Deleted in Colorectal Cancer
DI-CMT	Dominant-intermediate CMT
DIV	Day <i>in vitro</i>
DRG	Dorsal root ganglia
DYNC1H1	Dynein cytoplasmic 1 heavy chain 1
EEA1	Early endosome antigen 1
EGF	Epidermal growth factor
EGFR	EGF receptor
EM	Electron microscopy
ENS	Enteric nervous system
ER	Endoplasmic reticulum
ERK	Extracellular signal-regulated kinase
ESCRT	Endosomal sorting complexes required for transport
FGD4	FYVE, RhoGEF and PH domain-containing protein 4
FGF	Fibroblast growth factor
FIG4	FIG4 phosphoinositide 5-phosphatase
FRS2	Fibroblast growth factor receptor substrate 2
GAIP	G alpha interacting protein
GARP	Golgi-associated retrograde protein complex
GEF	Guanine nucleotide exchange factor
GJB1	Gap junction beta 1 protein
GlyRS	Glycyl-tRNA synthetase
GPCR	G-protein coupled receptor
GSK3	Glycogen synthase kinase 3
HDAC6	Histone deacetylase 6
Hrs	Hepatocyte growth factor-regulated tyrosine kinase substrate
HSPB1	Heat shock protein family B (small) member 1
IGF	Insulin like growth factor
IGRF	IGF receptor
ILVs	Intra-luminal vesicles
Lamp1	Lysosomal-associated membrane protein 1
LC3	Microtubule-associated protein light chain 3
LDL	Low density lipoprotein
LHR	Luteinizing hormone receptor
LITAF	Lipopolysaccharide-induced tumor necrosis factor-alpha factor
LPA1	Lysophosphatidic acid receptor 1
LRSAM1	Leucine rich and sterile alpha motif containing
MAPK	Mitogen-activated protein kinase
MEFs	Mouse embryonic fibroblasts

MFN2	Mitofusin 2
MTMR	Myotubularin-related protein
mTORC2	mTOR complex 2
MVBs	Multi-vesicular bodies
NDRG1	N-myc downstream regulated 1
NEFL	Neurofilament light polypeptide
NEFM	Neurofilament medium polypeptide
NGF	Neurotrophic growth factor
NT	Neurotrophin
PDGFR	Platelet-derived growth factor receptor
PI	Phosphatidylinositol
PI3K	Phosphoinositide 3-kinase
PIKFYVE	1-phosphatidylinositol 3-phosphate 5-kinase
PKC	Protein kinase C
PLC	Phospholipase C
PMP22	Peripheral myelin protein 22
PNS	Peripheral nervous system
PRA1	Rab Acceptor 1 protein
PRD	Prolin-rich domain
PTEN	Phosphatase and tensin homolog
PX	Phox homologous domain
RBPs	RNA-binding proteins
RILP	Rab-interacting lysosomal protein
RNPs	Ribonucleoprotein particles
SCG	Superior cervical ganglion
Ser	Serine
SFK	Src family kinase
Shc	Src homology and collagen homology
Shh	Sonic hedgehog
SNx	Sorting nexin
STED	Stimulated Emission Depletion
SV2	Synaptic vesicle protein 2
TfR	Transferrin receptor
TGN	Trans golgi network
TIRF	Total internal reflection fluorescence
TKO	Triple <i>EndophilinA1</i> ^{-/-} ; <i>A2</i> ^{-/-} ; <i>A3</i> ^{-/-}
TNF	Tumor necrosis factor
Trk	Tropomyosin receptor kinase
Tyr	Tyrosine
VEGFR	Vascular endothelial growth factor receptor
VPS	Vacuolar protein sorting- associated protein
β2AR	β2-adrenergic receptor

ACKNOWLEDGEMENTS

I would like to thank the following people for their support during the past 4 years, for which I am truly grateful.

First, and foremost: Thank you Katja for your supervision, your endless encouragements and motivation, your appreciation of my work, for making work such an enjoyable place and last but not least for all the ice cream and chocolate. I could not have asked for a better supervisor.

I would also like to thank the lab members of the AG Receptor Dynamics in Development and Disease: Vivian, I can't express enough how grateful I am that you joined our group, one Vivian-appreciation day was not enough. Thank you for all your support and especially for caring about the people you work with. Minions (Lars, Basti, Angeliki and Anna), thank you for making the lab a fun space and for wholeheartedly embracing our unique group, your presence contributed greatly to the spirit of the lab.

I would like to thank my thesis committee advisors Reinhard and Silvio: Thank you for giving me feedback, for teaching me, when I didn't know something and for creating an atmosphere that allowed me to ask "dumb questions". Thank you, Mathias Bähr, for being on my committee during the first two years and for employing us in your department.

Thank you to the coordination office of the IMPRS neuroscience Sandra Drube, Michael Hörner, Jonas Barth and Franziska Kühne by accepting me into the program you have introduced me to a family I didn't know I had.

This leads me to thank the ladies from O&W: Linda, Tal, Ali and Myrto, you quickly became my Göttinger family and I am extremely grateful for it. Meeting all of you extraordinary women was a dream come true experience.

And lastly, I would like to thank my parents, who would have been proud of me even if I had failed at this: Danke.